REPORT NO. FRA/ORD-78/56
FRA 78-6

PB

THE APPLICATION OF QUASI-LINEARIZATION TECHNIQUES TO RAIL VEHICLE DYNAMIC ANALYSES

NOVEMBER 1978
FINAL REPORT

Prepared for

U.S. DEPARTMENT OF TRANSPORTATION
FEDERAL RAILROAD ADMINISTRATION
Office of Research and Development
Washington, D.C. 20590

Technical Report Documentation Page

1. Report No.	2. Government Accession No.	3. Recipient's Catalog No.
FRA/ORD-78/56		

4. Title and Subtitle	5. Report Date
THE APPLICATION OF QUASI-LINEARIZATION TECHNIQUES TO RAIL VEHICLE DYNAMIC ANALYSES	November 1978
	6. Performing Organization Code
7. Author(s) J.K. Hedrick, N.K. Cooperrider, E.H. Law	8. Performing Organization Report No. DOT-TSC-FRA-78-6
9. Performing Organization Name and Address Mass. Inst. of Technology, Cambridge MA* Arizona State University, Tempe AZ* Clemson University, Clemson SC*	10. Work Unit No. (TRAIS) RR719/R7318
	11. Contract or Grant No. DOT-TSC-902
12. Sponsoring Agency Name and Address U.S. Department of Transportation Federal Railroad Administration Office of Research and Development Washington DC 20590	13. Type of Report and Period Covered Final Report Sept. 1975 - Feb. 1977
	14. Sponsoring Agency Code

15. Supplementary Notes

*Under contract to: U.S. Department of Transportation Transportation Systems Center Kendall Square Cambridge MA 02142

16. Abstract

The objective of the work reported here was to define methods for applying the describing function technique to realistic models of nonlinear rail cars. The describing function method offers a compromise between the accuracy of nonlinear digital simulation and the computational efficiency of linear methods. This work entailed the development of realistic describing function representations for nonlinearities such as the wheel/rail contact interaction and the development of algorithms for using these describing functions to predict the occurrence and stability of hunting and the forced response of rail vehicles to sinusoidal and statistical track irregularities. This report explains the describing function technique, demonstrates how it can be applied to nonlinear rail vehicle dynamics problems, describes algorithms that can be used for such problems, and presents results for typical nonlinear problems, including wheel profile and suspension nonlinearities.

17. Key Words	18. Distribution Statement
Rail Vehicle Dynamics, Quasi-Linearization, Describing Function Analysis	DOCUMENT IS AVAILABLE TO THE U.S. PUBLIC THROUGH THE NATIONAL TECHNICAL INFORMATION SERVICE, SPRINGFIELD, VIRGINIA 22161

19. Security Classif. (of this report)	20. Security Classif. (of this page)	21. No. of Pages	22. Price
Unclassified	Unclassified	228	

Form DOT F 1700.7 (8-72) Reproduction of completed page authorized

PREFACE

The research described in this report, undertaken at Arizona State University and the Massachusetts Institute of Technology was performed in part by Research Assistants Russell Hull (A.S.U.) and David Hannebrink (M.I.T.). The material in Sections 4 and 5 is also described in their respective master's theses.

The authors wish to acknowledge the technical contribution of H. Weinstock of the Transportation Systems Center, Cambridge, Massachusetts.

METRIC CONVERSION FACTORS

Approximate Conversions to Metric Measures

Symbol	When You Know	Multiply by	To Find	Symbol
		LENGTH		
in	inches	2.5	centimeters	cm
ft	feet	30	centimeters	cm
yd	yards	0.9	meters	m
mi	miles	1.6	kilometers	km
		AREA		
in^2	square inches	6.5	square centimeters	cm^2
ft^2	square feet	0.09	square meters	m^2
yd^2	square yards	0.8	square meters	m^2
mi^2	square miles	2.6	square kilometers	km^2
	acres	0.4	hectares	ha
		MASS (weight)		
oz	ounces	28	grams	g
lb	pounds	0.45	kilograms	kg
	short tons (2000 lb)	0.9	tonnes	t
		VOLUME		
tsp	teaspoons	5	milliliters	ml
Tbsp	tablespoons	15	milliliters	ml
fl oz	fluid ounces	30	milliliters	ml
c	cups	0.24	liters	l
pt	pints	0.47	liters	l
qt	quarts	0.95	liters	l
gal	gallons	3.8	liters	l
ft^3	cubic feet	0.03	cubic meters	m^3
yd^3	cubic yards	0.76	cubic meters	m^3
		TEMPERATURE (exact)		
°F	Fahrenheit temperature	5/9 (after subtracting 32)	Celsius temperature	°C

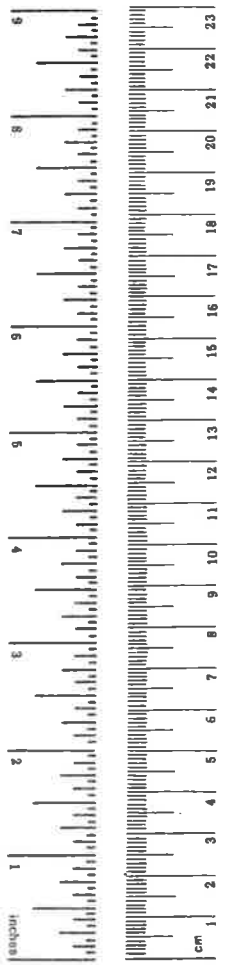

Approximate Conversions from Metric Measures

Symbol	When You Know	Multiply by	To Find	Symbol
		LENGTH		
mm	millimeters	0.04	inches	in
cm	centimeters	0.4	inches	in
m	meters	3.3	feet	ft
m	meters	1.1	yards	yd
km	kilometers	0.6	miles	mi
		AREA		
cm^2	square centimeters	0.16	square inches	in^2
m^2	square meters	1.2	square yards	yd^2
km^2	square kilometers	0.4	square miles	mi^2
ha	hectares (10,000 m^2)	2.5	acres	
		MASS (weight)		
g	grams	0.036	ounces	oz
kg	kilograms	2.2	pounds	lb
t	tonnes (1000 kg)	1.1	short tons	
		VOLUME		
ml	milliliters	0.03	fluid ounces	fl oz
l	liters	2.1	pints	pt
l	liters	1.06	quarts	qt
l	liters	0.26	gallons	gal
m^3	cubic meters	35	cubic feet	ft^3
m^3	cubic meters	1.3	cubic yards	yd^3
		TEMPERATURE (exact)		
°C	Celsius temperature	9/5 (then add 32)	Fahrenheit temperature	°F

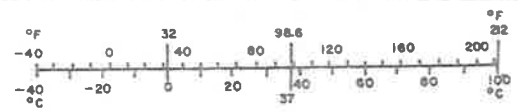

CONTENTS

CONTENTS (Cont.)

CONTENTS (Cont.)

Section | Page

CONTENTS (Cont.)

LIST OF ILLUSTRATIONS

LIST OF ILLUSTRATIONS (Cont.)

LIST OF ILLUSTRATIONS (Cont.)

LIST OF ILLUSTRATIONS (Cont.)

LIST OF TABLES

EXECUTIVE SUMMARY

The purpose of this work is to define methods for applying the describing function (quasi-linearization) technique to realistic, nonlinear dynamic rail vehicle models in order to predict important performance indices such as critical speeds and the car vibration environment. In order to predict these performance indices quantitatively it is necessary to include the effects of important nonlinearities such as wheel/rail profile geometry and suspension properties. The describing function technique enables the analyst to include the effects of nonlinearities in the analysis while avoiding the expense and complexity of nonlinear digital simulations.

Quasi-linearization techniques offer the promise, in some applications, of relieving the shortcomings of numerical integration without sacrificing the fidelity of the simulation. De Pater and his students van Bommel and Stassen used the method of Krylov and Bogoliubov (K and B) and statistical linearization to investigate the behavior of a two degree of freedom representation of a rigid dual axle truck with several nonlinearities. Law , and Law and Brand used the K and B method to study the limit cycle behavior of a single wheelset with curved wheel profiles and flange contact.

These applications of quasi-linearization to simple vehicle models demonstrated the feasibility of using such an approach for rail vehicle dynamics study, and suggested that the use of such techniques with more realistic models should be pursued. A pilot study

was conducted by Garg to evaluate the feasibility of applying describing function techniques, a generalized quasi-linearization method, to the analysis of the limit cycle behavior of rail cars.

The objective of this research is to explain the describing function technique, demonstrate how it can be applied to nonlinear rail vehicle dynamic problems, describe algorithms that can be used for such problems, and present results for typical nonlinear problems, including wheel profile and suspension nonlinearities.

The nonlinearities that are encountered in rail vehicles are described in Section 2 along with equations of motion for some typical rail vehicle models that include these nonlinearities. In Section 3, describing functions are defined and developed for many nonlinearities of interest in rail vehicle dynamics.

Algorithms were developed to use the describing function technique to find limit cycle behavior, forced sinusoidal response, and forced statistical response of complex rail vehicle models. The theory for each of these three situations is presented in Section 3 with simple examples. The algorithms for limit cycles are discussed in Section 4, those for forced sinusoidal response in Section 6, and statistical response in Section 7. Results of the application of the limit cycle technique to study rail vehicle hunting are presented and discussed in Section 5.

This report has demonstrated that describing function analysis can be successfully applied to rail vehicle analysis and design. The results indicate that:

1. Quasi-linearization permits application of linear frequency domain, eigenvalue/vector, and state space methods for nonlinear rail system dynamics problems.

2. There are significant computational advantages to be gained using quasi-linearization both for simple (e.g. wheelset) and higher order (e.g. nine D.O.F. Freight Car) dynamic models.

3. The parametric studies indicate that the wheel/rail profile and suspension nonlinearities must be included for analyzing medium-to-large amplitude rail vehicle performance.

4. Quasi-linearization computational algorithms for predicting rail vehicle hunting, forced sinusoidal response, and forced statistical response can be formulated and applied both for simple and higher order rail vehicle dynamic models.

The success of these preliminary investigations points to the need for further research and development in the following areas:

1. Improvement of the coding of these algorithms, and packaging them in a form that would be convenient to a wide range of industrial users.

2. Further validation and definition of the range of application of the quasi-linearization results by a direct comparison with nonlinear digital simulations of rail vehicle hunting, forced sinusoidal and statistical response.

3. The application of parametric studies on higher order dynamic models to determine the influence of wheel profile, axle-load, gauge, and suspension parameters on general primary and secondary suspension design.

1. INTRODUCTION

1.1 BACKGROUND

Linear analyses of rail vehicle dynamics have provided approximations for the critical speeds of hunting, values for the frequency and mode shape of vehicle response at speeds below the critical speed of hunting, and estimates for accelerations and force levels that can be expected in response to deterministic and random roadbed irregularities at sub-critical speeds. Such analyses are invaluable in understanding the nature of the influences of the various vehicle parameters on the hunting stability and forced response of rail vehicles.

However, nonlinear characteristics must be considered to study the behavior of any rail vehicle completely. The wheel flanges, for example, introduce a nonlinearity that must be considered for large amplitudes of wheelset motion. In many cases, the vehicle behavior may be approximated by linear characteristics for small motions of the vehicle components, and the nonlinear need only be considered for larger amplitude motions. However, for some vehicles, such as the North American freight car with its three piece trucks, the nonlinear characteristics can be important in all ranges of motion.

Nonlinear characteristics that are important in rail vehicle behavior include dry friction, suspension clearances and stops, rocking on the center plate, curved wheel and rail profiles, and nonlinear creep forces. With few exceptions nonlinear rail vehicle

studies have utilized analog or digital computers to integrate the equations of motion. Matsudaira [2] and Cooperrider [3] have employed numerical integration to find the influence of nonlinearities on hunting stability. Gilchrist et al. [4], Law [5], and Sauvage [6] studied the forced response of nonlinear rail vehicles by numerical integration. Tse and Martin [7], Healey [8], Wiebe [9], and B.E. Platin et al. [10] have applied numerical integration to the freight car rock rock and roll problem.

Although very complete simulations of complex systems are possible with this approach, the practicality of such simulations is severely limited by the high computation cost associated with direct numerical integration. In addition, to understand the system behavior thoroughly one must simulate the response to a wide variety of initial conditions because the nonlinear behavior depends on the motion amplitudes. In practice, the high cost of numerical integration usually limits its application to highly simplified models or restricted exploration of more complex models.

Quasi-linearization techniques offer the promise, in some applications, of relieving the shortcomings of numerical integration without sacrificing the fidelity of the simulation. De Pater [11] and his students van Bommel [12] and Stassen [13] used the method of Krylov and Bogoliubov (K and B) and statistical linearization to investigate the behavior of a two degree of freedom representation of a rigid dual axle truck with several nonlinearities. Law [14], and Law and Brand [15] used the K and B method to study the limit cycle

behavior of a single wheelset with curved wheel profiles and flange contact.

These applications of quasi-linearization to simple vehicle models demonstrated the feasibility of using such an approach for rail vehicle dynamics study, and suggested that the use of such techniques with more realistic models should be pursued. A pilot study was conducted by Garg [16] to evaluate the feasibility of applying describing function techniques, a generalized quasi-linearization method, to the analysis of the limit cycle behavior of rail cars.

1.2 OBJECTIVE

The objective of the work reported here was to develop methods of applying the describing function technique to realistic models of nonlinear rail cars. This work entailed the development of realistic describing function representations for nonlinearities such as the wheel/rail contact interaction and the development of algorithms for using the describing functions to predict the occurence and stability of limit cycles and the forced response of a rail vehicle to sinusoidal and statistical track irregularities.

This report explains the describing function technique, demonstrates how it can be applied to nonlinear rail vehicle dynamics problems, describes algorithms that can be used for such problems, and presents results for typical nonlinear problems, including wheel profile and suspension nonlinearities.

1.3 APPROACH

The nonlinearities that are encountered in rail vehicles are described in the following chapter along with equations of motion for some typical rail vehicle models that include these nonlinearities. In Section 3, describing functions are defined and developed for many nonlinearities of interest in rail vehicle dynamics.

Algorithms were developed to use the describing function technique to find limit cycle behavior, forced sinusoidal response, and forced statistical response of complex rail vehicle models. The theory for each of these three situations is presented in Section 3 with simple examples. The algorithms for limit cycles are discussed in Section 4, those for forced sinusoidal response in Section 6, and statistical response in Section 7. Results of the application of the limit cycle technique to study rail vehicle hunting are presented and discussed in Section 5.

2. RAIL VEHICLE NONLINEARITIES

2.1 INTRODUCTION

Mathematical analysis of rail vehicle dynamics requires the development of an abstract model to represent the actual rail vehicle. The assumptions, approximations, and restrictions that are made in the mathematical description of the vehicle dynamic behavior limit the fidelity of the abstract model. In most cases, a tradeoff exists between the fidelity of the model and the ease and cost of solving the equations that describe the behavior of the model. The balance point in this tradeoff, for any specific case, depends on the intended use of the results, and on the resources available for the analysis.

Mathematical analyses of rail vehicle dynamics are undertaken to determine the stability of the vehicle motion and the accelerations and forces that may arise in response to irregularities in the roadbed and track. It is common to represent the vehicle by lumped parameters that lead to a description of the vehicle dynamics by ordinary differential equations. The discussion in this report deals with models of this type.

The objective of this study was to investigate the feasibility of and demonstrate the methods of applying, quasi-linearization techniques to solve nonlinear rail vehicle dynamics problems. This was done because the quasi-linearization method appeared to provide greater fidelity in the rail vehicle model, in the form of nonlinear characteristics, without as large a penalty as other methods in difficulty or cost of solving the resutling nonlinear equations of motion.

In the following sections of this chapter, the subject of rail vehicle modeling is taken up, including a description of the nonlinear behavior found in rail vehicles and a presentation of some exaple of rail vehicle models and equations of motion. Succeeding chapters deal with the quasi-linear representations of the nonlinear effects and the solution of the quasi-linear equations of motion.

2.2 RAIL VEHICLE MODELING

Typical examples of rail passenger and freight trucks are shown in Figure 2-1. A lumped parameter model of such vehicles requires division of the vehicle into discrete components that can be treated as rigid bodies or flexible body modes in a mathematical analysis. The number of subdivisions needed depends on the desired level of accuracy and the intended use of the analysis resuts. An analysis of the shock environment of the axle roller bearings, for example, requires a model with more subdivisions than an analysis of the ride quality in the vehicle body.

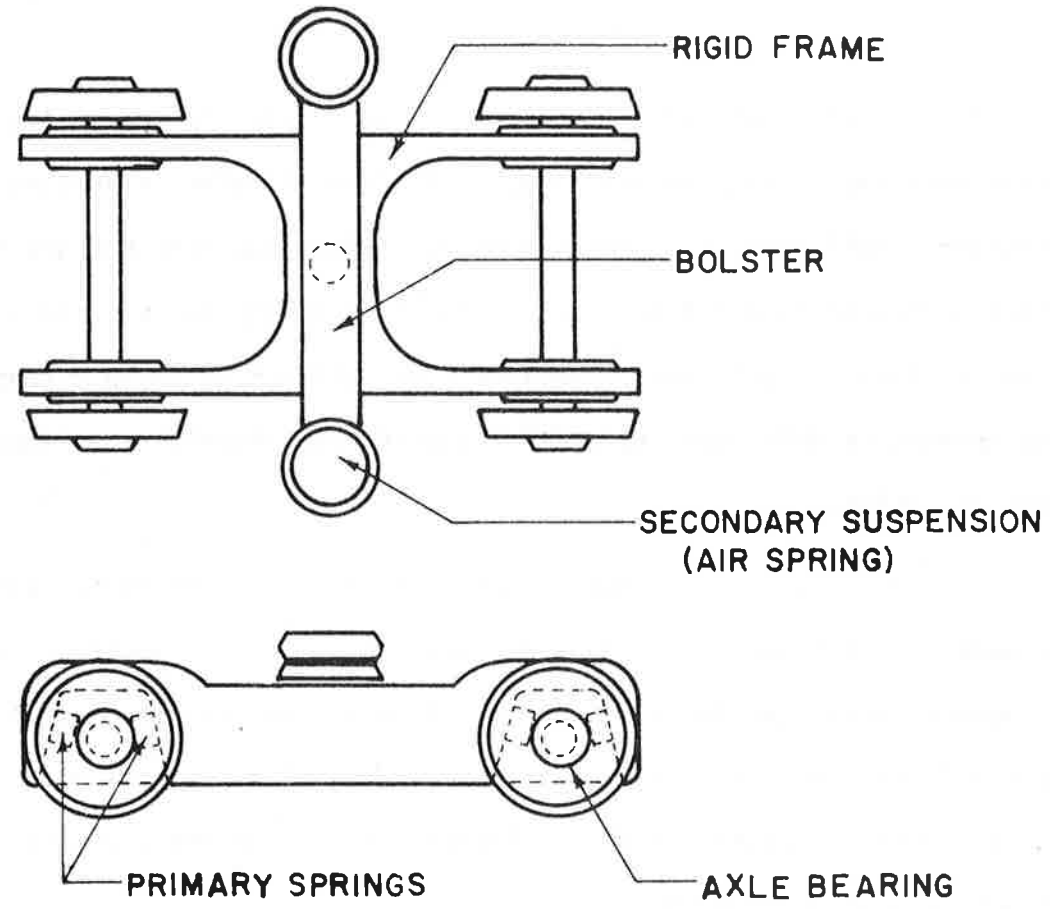

Schematic of Transit Truck

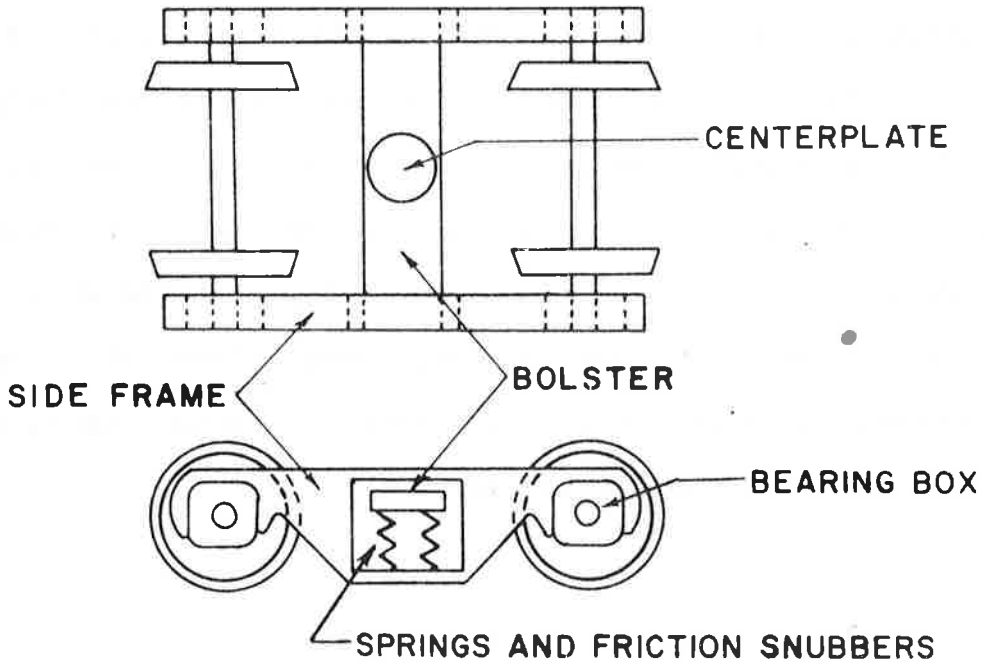

Schematic of Typical Freight Truck

FIGURE 2-1. RAIL PASSENGER AND FREIGHT TRUCKS

The forces and moments acting on the components or subdivisions of the model are determined in the second modeling step. Often these forces and moments can be described in terms of the relative displacements and velocities between components. The suspension system forces and moments, for example, are described in terms of displacements across springs and velocities across friction snubbers or viscous dampers. These forces, due to relative motion, ususally include terms that account for deformation of the components. For example, the lateral bending of the truck sideframe may be included in the lateral suspension sitffness terms.

Additional forces and moments due to interaction of the vehicle components with outside bodies or elements must also be described. The most important of these forces and moments for rail vehicle dynamic analysis are those acting at the wheel/rail contact surfaces.

The discussion below will first describe the typical suspension forces, then the wheel/rail contact forces. This discussion focuses on presentation of the nonlinear effects that may be found in conventional passenger and freight rail cars. At the close of this chapter, equations of motion are presented for models that are used in illustrative examples in Section 3-7.

2.3 SUSPENSION NONLINEARITIES

Suspensions are made up of restoring force elements providing stiffness and energy absorbing elements providing damping. When these elements are linear springs and dampers the forces or moments are described quite simply. However, for many rail vehicles these forces and moments either cannot be described by linear relationships at all, or the motion does not remain within a limited range where linear description holds.

Nearly all the nonlinearities found in rail car suspensions may be described by combinations of the following three nonlinearities.

1. Deadband spring:

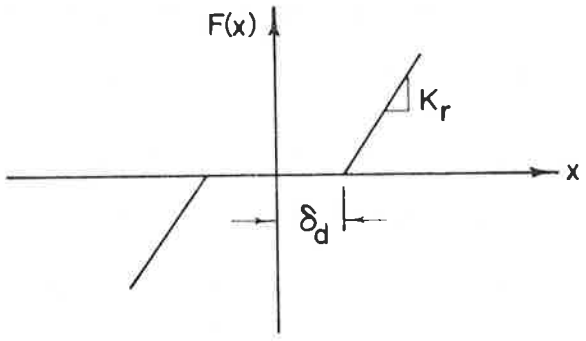

Where: δ_d - one half the deadband region

K_r - spring rate

x - spring displacement

F(x) - spring force or moment

FIGURE 2-2. DEAD BAND SPRING

2. Hardening/Softening Spring

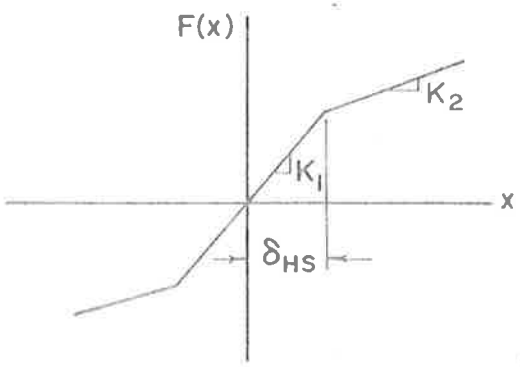

Where: δ_{Hs} - One half the range of spring, K_1

K_1, K_2 - Spring rates

x - Spring displacement

F(x) - Spring force or moment

FIGURE 2-3. HARDENING/SOFTENING SPRING

3. Coulumb Friction:

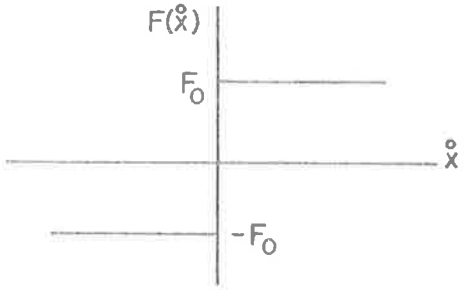

Where: F_o - Breakout friction force or moment

i.e. $\dot{x}$ - Velocity

$F(\dot{x})$ - Friction force or moment

FIGURE 2-4. COULOMB OR DRY FRICTION

Several combinations of these elements that are frequently encountered in rail car suspension modeling are described below.

2.3.1 Suspension Stops

The travel in nearly all suspensions is limited by stops. The suspension stop does not completely restrict suspension travel because once the stop is engaged, further increase in force causes deflection of the stop and the structure supporting it. Thus the stop may be represented by a stiff spring, and the overall suspension stiffness by a hardening spring:

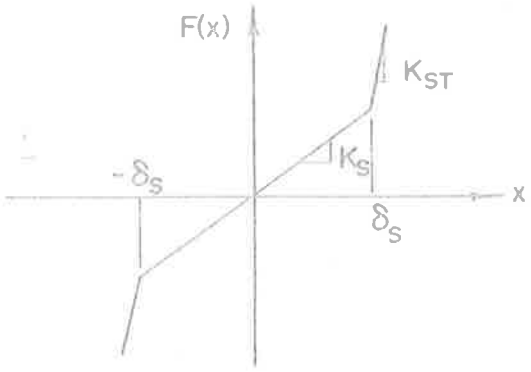

Where:

δ_X -Limit of linear displacement

K_S -Nominal suspension stiffness

K_{st} -Stop stiffness

FIGURE 2-5. SUSPENSION STOP CHARACTERISTIC

The physical stops may be rubber pads, as often found in rail passenger truck suspensions, spring bottoming, as occurs with coil springs or metal-to-metal contact, as are the gibs on the freight truck bolster.

2.3.2 Truck/Car Body Relative Yaw

The yaw motion of the truck relative to the car body almost universally allows the possibility of sliding motion between the truck and car body. In many designs this sliding occurs at a centerplate,

other designs provide for sliding on bearing pads outboard on the trucks. In either case, this sliding motion is resisted by friction that is usually best represented by the Coulomb friction characteristic.

In many cases, there is enough flexibility in the supports or connections to the sliding surfaces that significant relative yaw deflection occurs before sliding begins. One common passenger truck design, for example, connects the truck bolster to the car body through longitudinal rods with rubber bushings. The flexibility of the rubber bushings in this truck allows relative yaw displacements. This situation can be modeled by a linear spring in series with a Coulomb friction element. The behavior of this combined characteristic is shown in Figure 2-6.

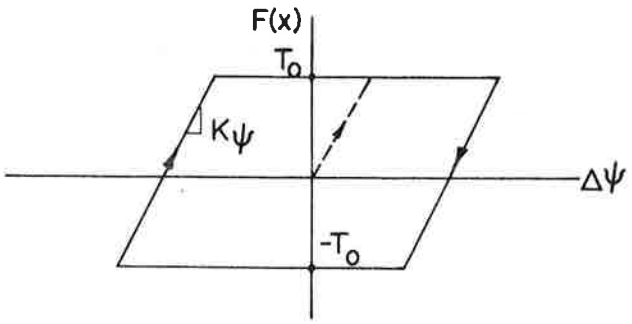

Where: T_o - Break out friction torque

K_ψ - Yaw stiffness

$\Delta\psi$ - Relative yaw displacement

FIGURE 2-6. SERIES COULOMB FRICTION-SPRING CHARACTERISTIC

Note that this combination exhibits hysteretic behavior where the torque generated by the components depends on the previous motions.

2.3.3 Freight Car Lateral and Vertical Suspension

In the conventional freight truck, the only intentional suspension components are in the connection between the bolster and the sideframes. This connection consists of the coil springs and friction wedges shown schematically in Figure 2-7(a). This suspension connection has been modeled [17] by the three parallel elements shown schematically in Figure 2-7(b): a linear spring, a linear spring with deadband, and a series combination of spring and friction element. The vertical spring rate is the spring rate of the coil springs, and the lateral spring rate is the softer, shear stiffness of the spring groups. The friction level is the same in the lateral and vertical directions.

2.3.4 Freight Truck Bolster/Centerplate/Sideframe System

The nonlinear characteristics of the bolster/centerplate/sideframe of a conventional freight truck are of interest in studying problems such as the "rock and roll" phemomena. When the car body rocks it can assume eight positions relative to the bolster:

1. Distributed contact across the center plate (one position),
2. Single point contact on the left or right edge of the centerplate (two positions),
3. Two point contact on the left or right edge of the centerplate and the sidebearing on the same side (two positions),
4. Single point contact on the left or right sidebearing (two positions), and
5. Complete separation between truck and car body (one position).

Four of the eight positions are shown in Figure 2-8.

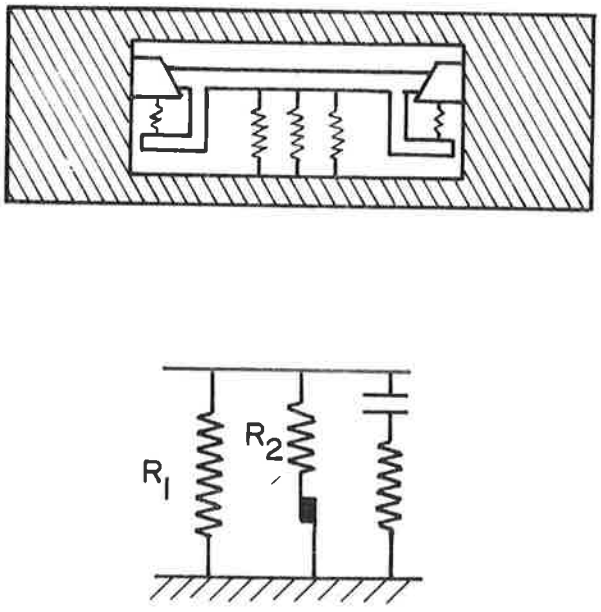

FIGURE 2-7. FREIGHT TRUCK SUSPENSION

The behavior of this connection can be represented by nonlinear springs arranged as shown in Figure 2-9. The characteristics of the three nonlinear springs are shown in Figure 2-10.

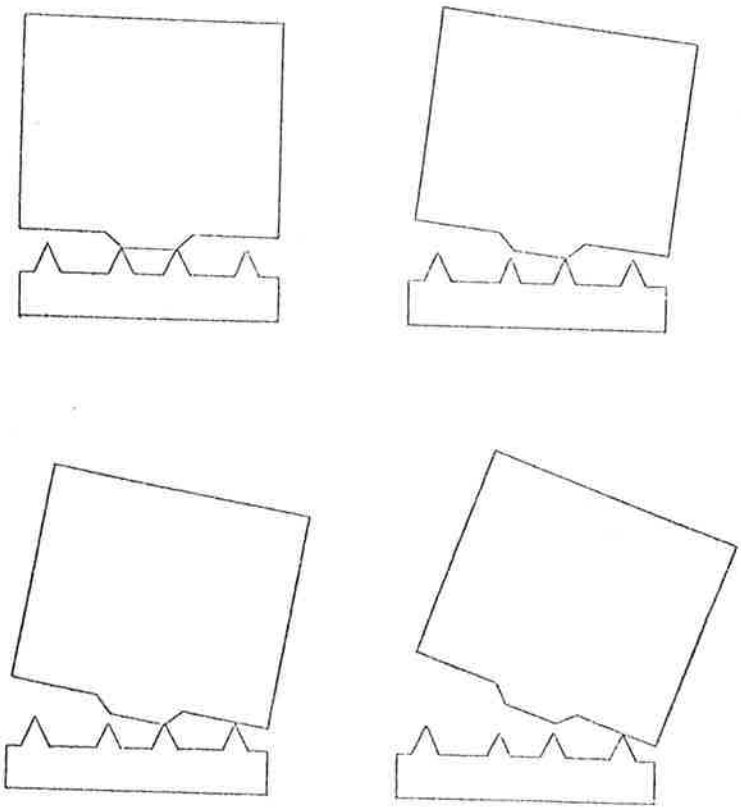

FIGURE 2-8. FOUR BASIC CAR BODY-BOLSTER RELATIVE POSITIONS CORRESPONDING TO DIFFERENT ROCKING CONDITIONS

Coefficients for the parameters of this model have been obtained from tests of two types of freight trucks [17], [18].

2.4 WHEEL/RAIL GEOMETRY NONLINEARITIES

The nature of the forces exerted between the wheel and rail, both in the plane of contact and normal to it, is determined by the geometry of the wheel and rail. Railway wheelsets, as they roll along the track, are constrained to move laterally and vertically in prescribed space

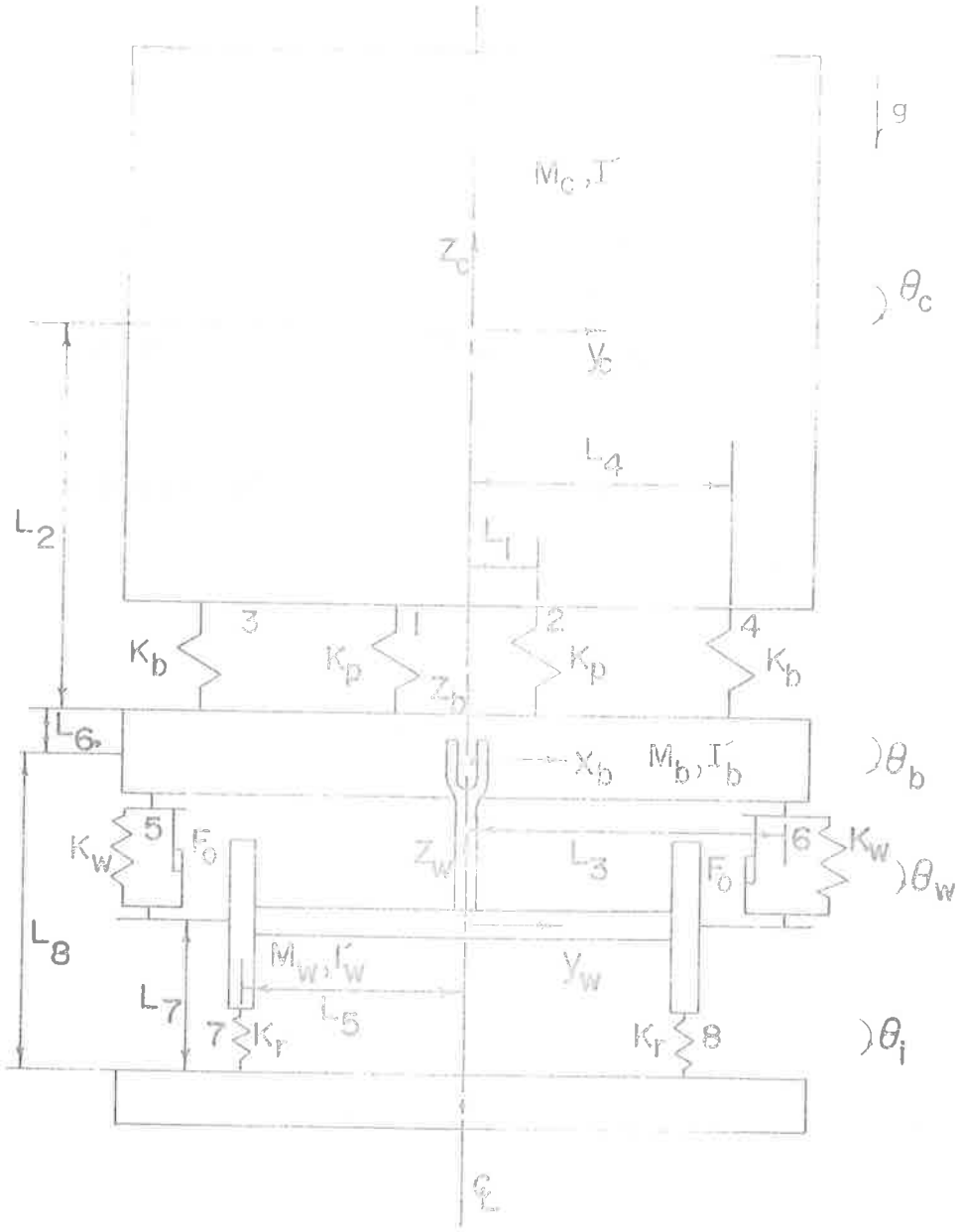

FIGURE 2-9. FREIGHT TRUCK BOLSTER/CENTERPLATE/SIDEFRAME MODEL

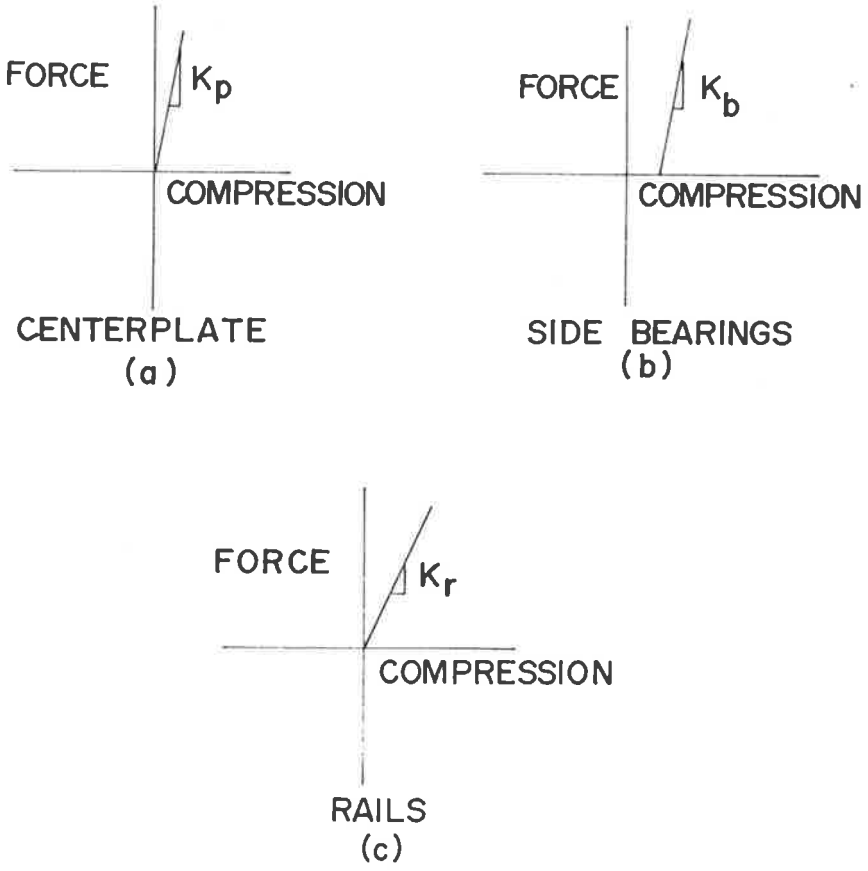

FIGURE 2-10. CENTERPLATE BOLSTER AND RAIL NONLINEAR SPRINGS

determined by the geometry of the wheels, rails, and track structure. The wheelset position may be described by two independent variables, the lateral position of its geometric center relative to the track centerline, y_w , and the angular rotation of the wheelset about a vertical axis, θ_w. The remaining motions of the wheelset, such as roll or vertical movement, are determined by the geometric constraints.

To study the lateral dynamics of rail vehicles, the following information is required as a function of the independent variables, y_w and θ_w :

r_L - instantaneous rolling radius of the left wheel

r_R - instantaneous rolling radius of the right wheel

Z_L - instantaneous height of contact point on the left rail

Z_R - instantaneous height of contact point on the right rail

δ_L - angle between the contact plane on the left wheel and the axle centerline

δ_R - angle between the contact plane on the right wheel and the axle centerline

ϕ_w - roll angle of the wheelset with respect to the plane of the rails.

These constrained variables, corresponding coordinate systems, and contact point definitions are illustrated in Figures 2-11 and 2-12.

The rolling radii constraints enter the wheelset equations of motion as the difference between the rolling radii at the two wheels of the wheelset. When the wheelset is displaced from a centered position between the rails the difference between the rolling radii at the left

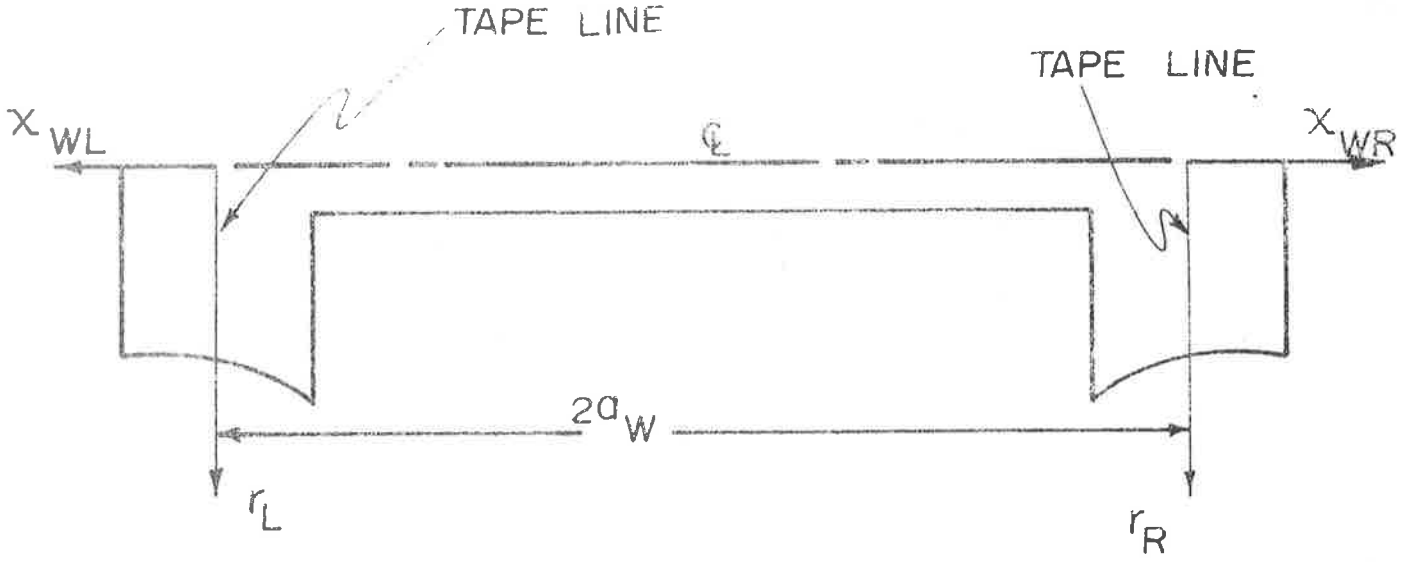

A - WHEEL COORDINATE SYSTEMS
REAR VIEW

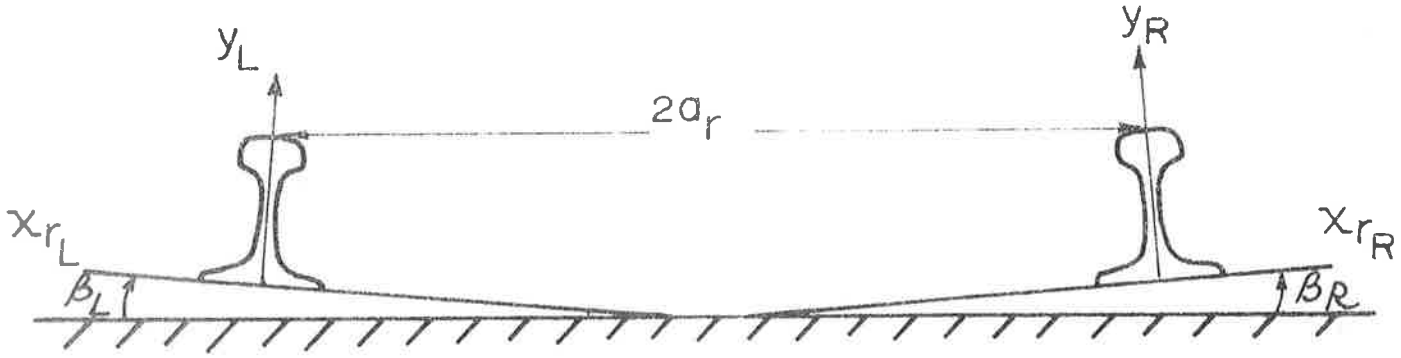

B - RAIL COORDINATE SYSTEMS
REAR VIEW

FIGURE 2-11. WHEEL/RAIL COORDINATE SYSTEMS

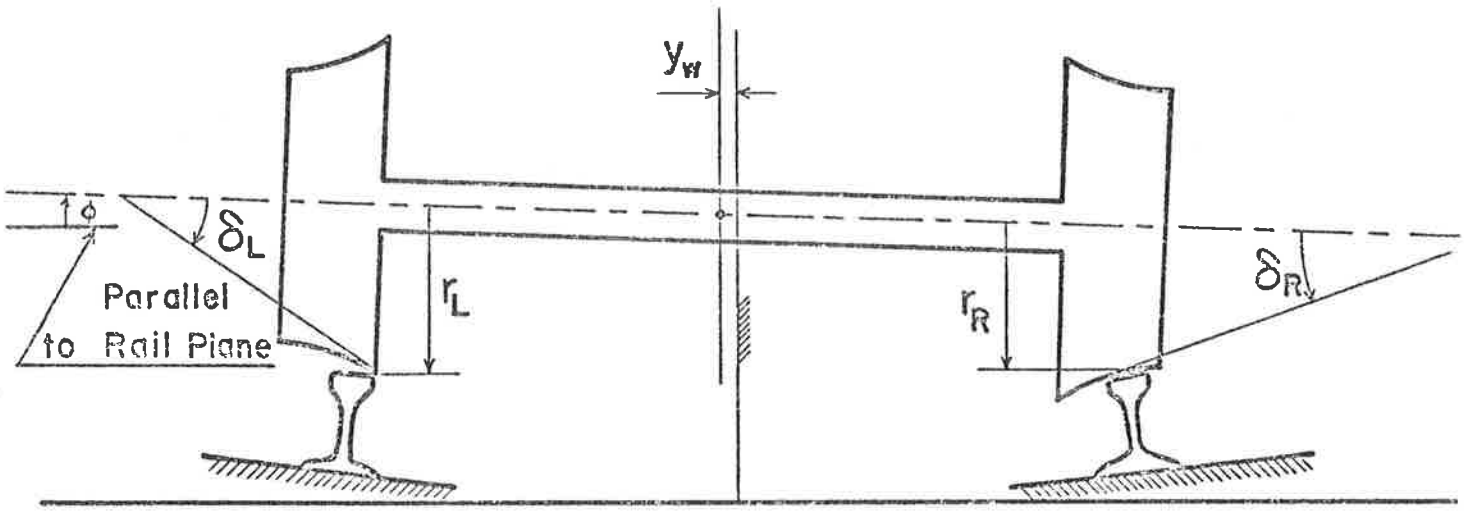

FIGURE 2-12. WHEEL/RAIL PARAMETERS

and right wheels requires that the velocities of the two wheels at their contact points differ. The result is partial slip, or creep, at the wheel/rail interface giving rise to a moment which results from the tangential or creep forces at the wheel/rail interfaces. This moment tends, in most cases, to steer the wheelset towards the centered position of the rails.

It is useful, in studying rail vehicle dynamics, to examine the rolling radii difference function, $\frac{r_L(y_w) - r_R(y_w)}{2a}$. The nature of this relationship between rolling radii difference and wheelset lateral position varies widely. For a new wheel with a conical taper, the normalized difference in rolling radii depends linearly on the wheelset lateral displacement, y_w, until flange contact is made. The constant of proportionality, called the wheelset conicity, is the wheel profile taper (usually 1/20 or 0.05). As the wheels wear, the change in rolling radii difference with wheelset lateral displacement becomes more nonlinear, and over certain ranges, ismuch greater than the rolling radii differences for new wheels.

The contact angle constraints enter the rail vehicle equations of motion in the description of the magnitude and direction of the contact forces between the wheel and rail. The contact angles for new wheels when centered are, of course, the angles of the wheel tread taper. The angle of contact with respect to the axle remains at this value until the wheelset is shifted laterally far enough for the contact point to move to the flange. For worn wheels, the contact angles usually vary continuously as the wheelset moves laterally.

The third geometrically constrained variable on the equations of motion describes the roll of the wheelset about a longitudinal axis. This variable also enters the description of the contact forces between wheel and rail.

Solutions for the wheel/rail geometric constraint functions can be obtained numerically by the technique described in reference [19]. A typical result for a wheelset with new wheels on worn rails is shown in Figure 2-13. One function, in addition to the rolling radii, contact angle, roll angle, and normalized rolling radii difference is, plotted in Figure 2-13. This function,

$$\frac{\delta_L(y_w) - \delta_R(y_w)}{2},$$

is used to compute the "gravitational stiffness" forces acting between wheel and rail, as discussed later in this Section. The highly nonlinear character of these functions is evident in these plots.

The wheel/rail geometry nonlinearities enter the rail vehicle dynamics through the expressions for the contact forces between the wheel and rail. The role of the wheel/rail geometry in determining these forces is explained in the next section.

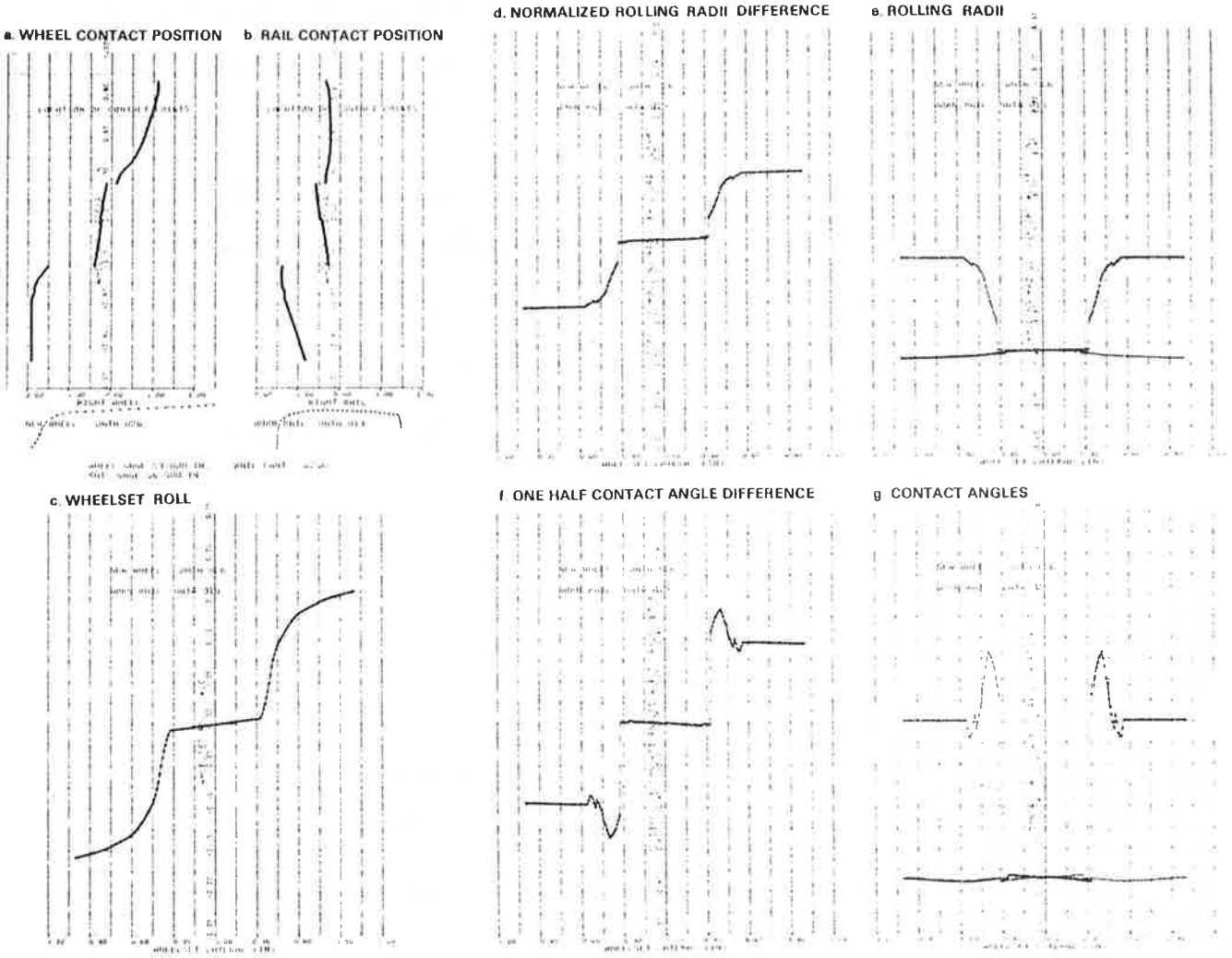

FIGURE 2-13. WHEEL/RAIL GEOMETRIC CONSTRAINT FUNCTIONS

2.5 CREEP FORCES AND MOMENT NONLINEARITIES

The creep forces and moments are exerted between the wheel and rail in the plane of contact due to a difference in the strain rates of the two bodies in the contact region. Although these forces and moments are not uniformly distributed over the contact region, and the relative strain between the two bodies also varies over the plane of contact, this situation can be modeled as a point contact problem where the creep forces and moments are expressed as functions of the strain rate, for creepage between the wheel and rail at the point of contact. The theory used to develop these characteristics must, of course, deal with the actual, distributed contact problem.

In general, two elastic bodies in rolling contact may both have a relative translational creepage and a relative spin creepage. For the wheel/rail contact problem, the translational creepage is the relative sliding velocity of the wheel over rail divided by the forward velocity of the wheel, and the spin creepage is the component of the wheelset angular velocity normal to the wheel/rail contact plane divided by the wheel forward velocity.

The relationships between the creep forces and moments and the creepages are nonlinear, due primarily to the limitation imposed by the available adhesion between wheel and rail. At present, the available theory [20] to deal with this nonlinear problem requires an iterative solution technique that must be implemented on a digital computer. The problem can be simplified by neglecting the effects of spin creepage. This step is reasonable when the contact angles between the wheel and rail are small, but may introduce serious errors when the contact angles are large.

The creepages for the wheel/rail problem depend on the wheelset variables and the wheel/rail contact geometry. Under the usual, small motion assumptions the translational creepages for a single symetric wheelset with only track alignment irregularities are given by the following relationships:

$$\xi_{yR} = \xi_{yL} = \frac{\dot{y}_w}{V} - \psi_w \qquad (2\text{-}1)$$

$$\xi_{zR} = -\xi_{zL} = -\frac{a\dot{\psi}_w}{V} - \frac{r_L (y_w - y_R) - r_R (y_w - y_R)}{2 r_o} \qquad (2\text{-}2)$$

Where a - One-half the rail gauge

r_R, r_L - Rolling radii

r_o - Centered rolling radius

V - Forward velocity

ξ_{yR}, ξ_{yL}, ξ_{zR}, ξ_{zL} - Creepages.

The spin creepage is the component of the wheelset angular velocity that is normal to the wheel/rail contact plane divided by the wheelset forward velocity. For a single,symmetric wheelset, the spin creepages at the left and right wheels are given by the following expressions:

$$\xi_{\theta_R} = \frac{\delta_R}{r_o} + \frac{\dot{\psi}_w}{V} \qquad (2\text{-}3)$$

$$\xi_{\theta_L} = \frac{\delta_L}{r_o} + \frac{\dot{\psi}_w}{V} \qquad (2\text{-}4)$$

Note that the nonlinear geometric constraint functions for the wheel rolling radii, $r_L(y_w)$ and $r_R(y_w)$, enter the equations of motion through the longitudinal creepage terms. The contact angle functions enter in the spin creepage as well as in the graviational stiffness terms described later in this Section.

For small values of the creepages the creep forces may be approximated by linear relationships where the constants of proportionality are referred to as the creep coefficients. These expressions for the forces on the right wheel are given below.

$$F_{YR} = f_{11}\xi_{YR} + f_{12}\xi_{\psi R} \tag{2-5}$$

$$F_{XR} = f_{33}\xi_{XR} \tag{2-6}$$

$$M_{\psi R} = f_{22}\xi_{\psi R} - f_{12}\xi_{YR} \tag{2-7}$$

Where:

f_{11} - Lateral creep coefficient

f_{12} - Lateral/spin creep coefficient

f_{22} - Spin creep coefficient

f_{33} - Longitudinal creep coefficient

F_{YR} - Lateral creep force

F_{XR} - Longitudinal creep force

$M_{\psi R}$ - Spin creep moment

The creep coefficients depend on the wheel and rail geometry, wheel and rail materials, and the normal force between the two bodies. The theory developed by Kalker [21] is generally used to compute these coefficients.

When the spin creepage is neglected, the creep force characteristic

has the form as shown in figure 2-14a, where the creepage is the resultant creepage between the two bodies and the creep force the resultant creep force. Johnson [22] in his theoretical treatment of this situation developed the cubic expression shown in figure 2-14 relating the resultant creepage and resultant creep force. In general, the resultant force may not be in the same direction as the resultant creepage. For the wheel/rail contact problem at small contact angles, the two are nearly coincident, and the difference can be ignored. Relationship of Figure 2-14a applies to the resultant force and resultant creepage where these resultants are related to the linear components by the following relationships:

$$\xi_R = \sqrt{\xi_x^2 + \xi_y^2} \tag{2-8}$$

$$F_R = \sqrt{F_x^2 + F_y^2} \tag{2-9}$$

However, functions of this nature complicate the quasi-linearization problem. The complications, in obtaining the quasi-linear representation of the functions above may be avoided by assuming that the lateral and longitudinal creepages would not be large at the same time. This allows application of the saturation function of figure 2-14b to the lateral and longitudinal creepages individually. This assumption can be justified on the basis that y_w and ψ_w are usually 90° out of phase, and consequently the lateral creepage (that depends on $\dot{y}_w$ and ψ_w) and the longitudinal creepage (that depends on y_w and $\dot{\psi}_w$) are also 90° out of phase.

To further simplify the creep force computation, the saturation effect can be modeled by the piecewise linear characterization shown in figure 2-14b. This assumption allows use of a readily available

a.

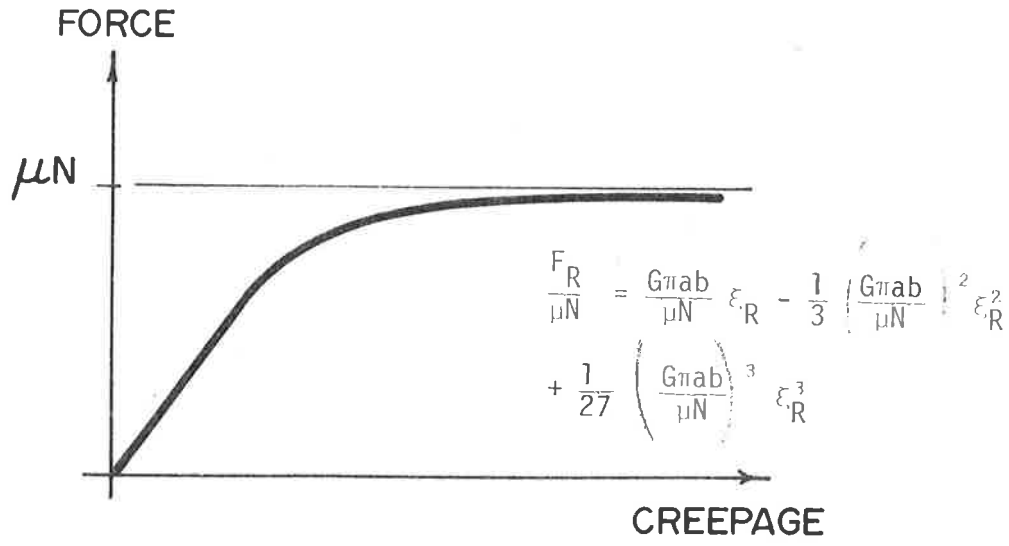

b.

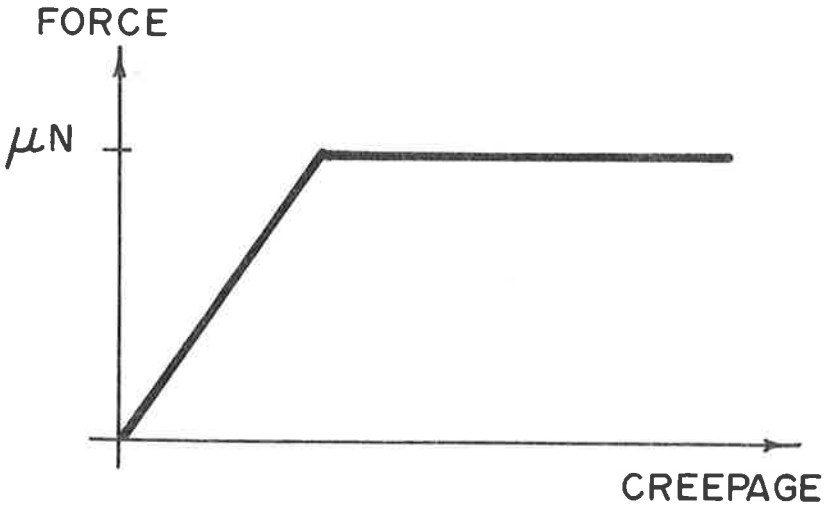

FIGURE 2-14. NONLINEAR CREEP FORCE CHARACTERISTICS

describing function for the force creepage relationship.

To summarize, the creep forces, neglecting spin effects, are represented by the following functions:

$$F_x = \begin{cases} \mu N & \xi_x > \frac{\mu N}{f_{33}} \\ f_{33}\,\xi_x - \frac{\mu N}{f_{33}} \leq \xi & \leq \frac{\mu N}{f_{33}} \\ \mu N & \xi_x < -\frac{\mu N}{f_{33}} \end{cases} \qquad (2\text{-}10)$$

$$F_y = \begin{cases} \mu N & \xi_y > \frac{\mu N}{f_{11}} \\ f_{11}\,\xi_y - \frac{\mu N}{f_{11}} \leq \xi_y & \leq \frac{\mu N}{f_{11}} \\ \mu N & \xi_y < -\frac{\mu N}{f_{11}} \end{cases} \qquad (2\text{-}11)$$

Where: f_{11} - Lateral creep coefficient

f_{33} - Longitudinal creep coefficient

N - Normal wheel load

μ - Adhesion coefficient.

2.6 FLANGE CONTACT AND GRAVITATIONAL STIFFNESS NONLINEARITIES

The remaining contact forces between the wheel and the rail are the normal forces exerted in a direction perpendicular to the plane of contact. When a symmetric wheelset is centered on a symmetric track, the normal forces on left and right wheels will be equal in magnitude and slightly inclined inward from the vertical. The sum of the vertical components of the two normal forces will equal the axle load and the lateral components will be oppostie in sign with a zero resultant lateral force on the wheelset. The angle of the contact plane is determined by the wheel and rail profiles.

In general, the contact angle of the contact plane with respect to the axle centerline will vary as the wheelset moves laterally and will be different on the left and right wheels. An example of how these angles vary for a wheelset with new wheels on worn rails is shown in Figure 2-13(g).

The magnitude of the lateral component of the normal force is determined by the magnitude of the vertical force at the contact and by the angle of the contact plane. One usually assumes, in analyzing vehicle behavior on tangent track, that the weight of the vehicle components is equally distributed among the wheels at all times. Variations in vertical forces at the wheel contact due to vertical vehicle dynamics are also small enough to be neglected. With these assumptions, the vertical component of the normal forces at all wheels are equal, and equal to the proportionate share of the vehicle weight.

The lateral resultant of the normal contact forces on the wheelset is given by the expression

$$N_{yR} + N_{yL} = \frac{W}{2}[\tan(\delta_R + \phi_w) - \tan(\delta_L - \phi_w)] \qquad (2\text{-}12)$$

Where: W - Axle load

N_{yR} - Lateral component of contact force at right wheel

N_{yL} - Lateral component of contact force at left wheel.

When the wheelset motion does not involve flange contact, the small angle approximations can be made. Then the expression above reduces to:

$$N_{yR} + N_{yL} = - W(\frac{\delta_L - \delta_R}{2} + \phi_w). \qquad (2\text{-}13)$$

This term is often called the gravitational stiffness.

A typical example of the $\frac{\delta_L - \delta_R}{2}$ function is shown in Figure 2-13. Note that the contact angle difference is nearly zero until the flange contacts the rail. This is characteristic of new wheel profiles. More

hollowed wheel profiles have a discernible slope at the origin.

For wheelsets with new wheels, the gravitational stiffness has been approximated by a deadband spring [3] with the characteristic shown in figure 2-15. This characteristic,

$$F_{rail} = \begin{cases} K_R(y_w - y_r) & (y_w - y_r) > \delta_c \\ 0 & -\delta_c \leq (y_w - y_r) \leq \delta_c \\ -K_R(y_w - y_r) & (y_w - y_r) < -\delta_c \end{cases} \quad (2\text{-}14)$$

has been used in many nonlinear rail vehicle dynamics studies.

2.7 TYPICAL NONLINEAR EQUATIONS OF MOTION

Nonlinear equations of motion are presented below for several models that include combinations of the nonlinear characteristics discussed in the preceding sections. These nonlinear equations are used in later examples that illustrate the quasi-linear solution techniques.

2.7.1 Single Wheelset with Deadband Rail Spring

Considerable insight into the dynamic behavior of rail vehicles can be gained by studying the behavior of a single wheelset. The lateral dynamics of a single wheelset, such as that shown in Figure 2-16, may be described by two degrees of freedom:

y_w - Wheelset lateral displacement,

ψ_w - Wheelset yaw displacement.

In the simplest case, one neglects the track flexibility and assumes

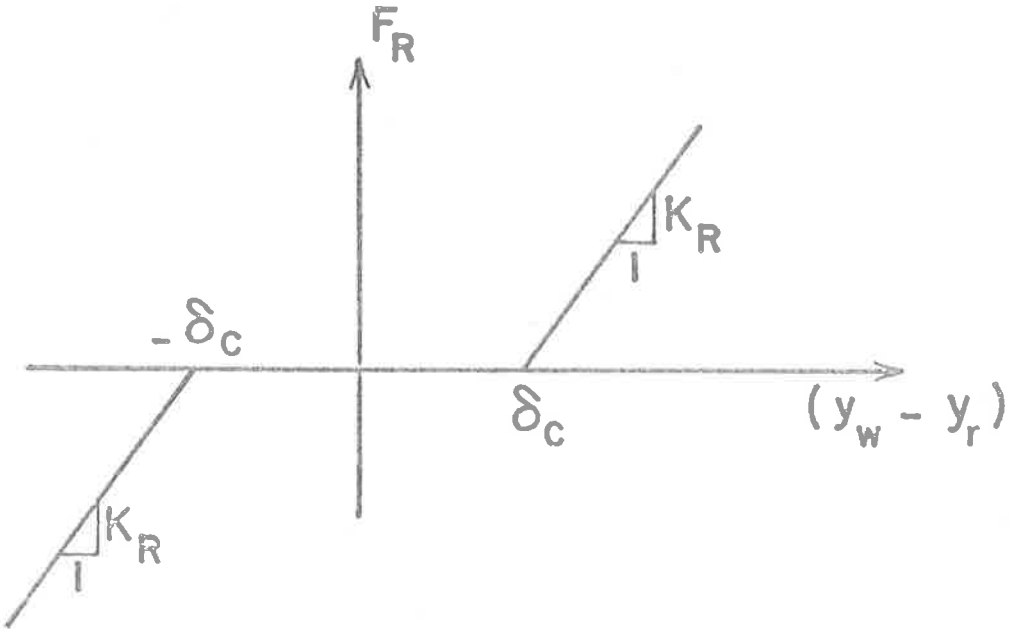

FIGURE 2-15. DEADBAND RAIL SPRING

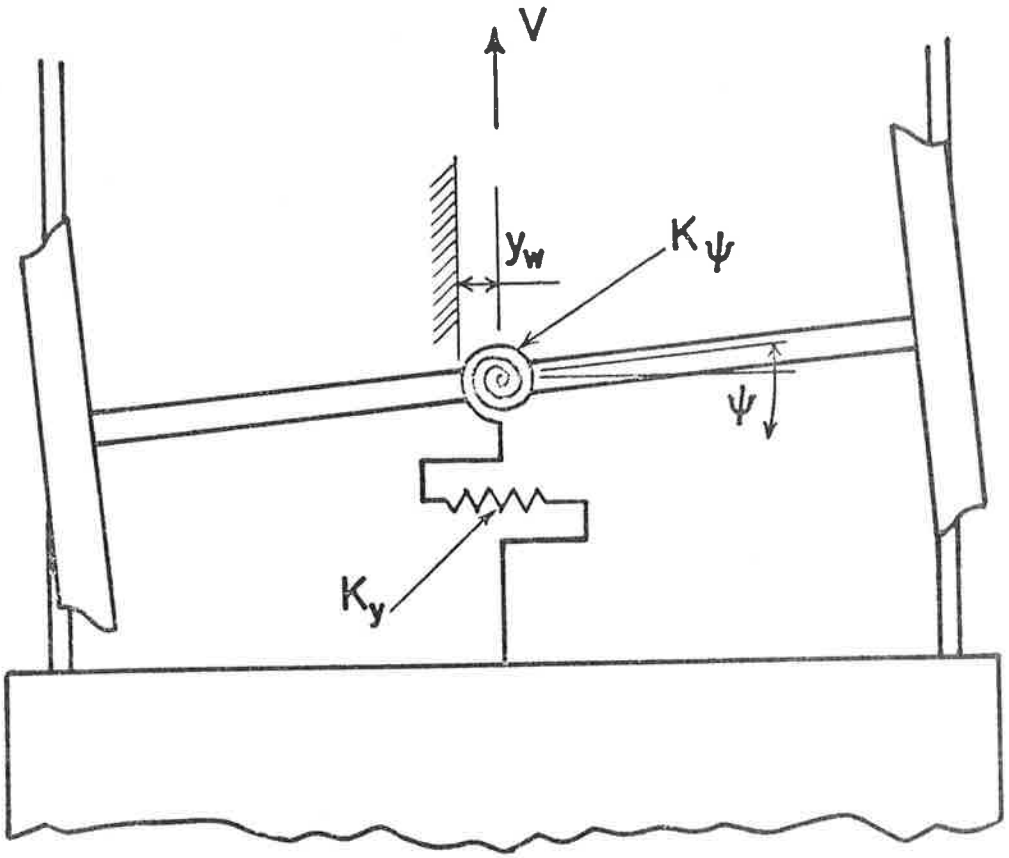

FIGURE 2-16. SINGLE WHEELSET MODEL

that the wheelset reacts to lateral track alignment irregularities described by the variable, y_R.

In order to include the suspension forces, one assumes that the wheelset is connected through a suspension system to a moving reference that travels along the track at a constant velocity, V, without lateral or vertical deviations. To represent several types of vehicles with a single wheelset model the possibility of Coulomb friction can be incorporated in both the lateral and yaw suspension connections as follows. The lateral suspension consists of a linear spring, K_y, connected in parallel with a Coulomb friction element with breakout force F_{oy}. The composite force characteristic F_{ys} for this connection is shown in Figure 2-17(a). The yaw connection is a linear spring, K_ψ in series with a Coulomb friction element with a breakout angle, ψ_o. Figure 2-17(b) illustrates the composite yaw suspension characteristics, $M_{\psi s}$.

To complete this simple wheelset model, the creep forces and wheel/rail constraints are represented with linear functions while a deadband spring represents the effect of flange contact with the rail.

The equations of motion for this simple wheelset model follow:

$$m_w \ddot{y}_w + \frac{2f_{11}}{V} \dot{y}_w + \frac{W(\Delta_1 + a_1)}{a} y_w - 2f_{11} \psi_w + F_{ys} + F_{rail} = \frac{W(\Delta_1 + a_1)}{a} y_R \qquad (2\text{-}15)$$

$$I_{wz}\ddot{\psi}_w + \frac{2f_{33}}{V} a^2\dot{\psi}_w - W \delta_o a\psi_w + 2f_{33} \frac{a}{r} \lambda y_w + M_{\psi s} = 2f_{33} \frac{a}{r} \lambda y_R \qquad (2\text{-}16)$$

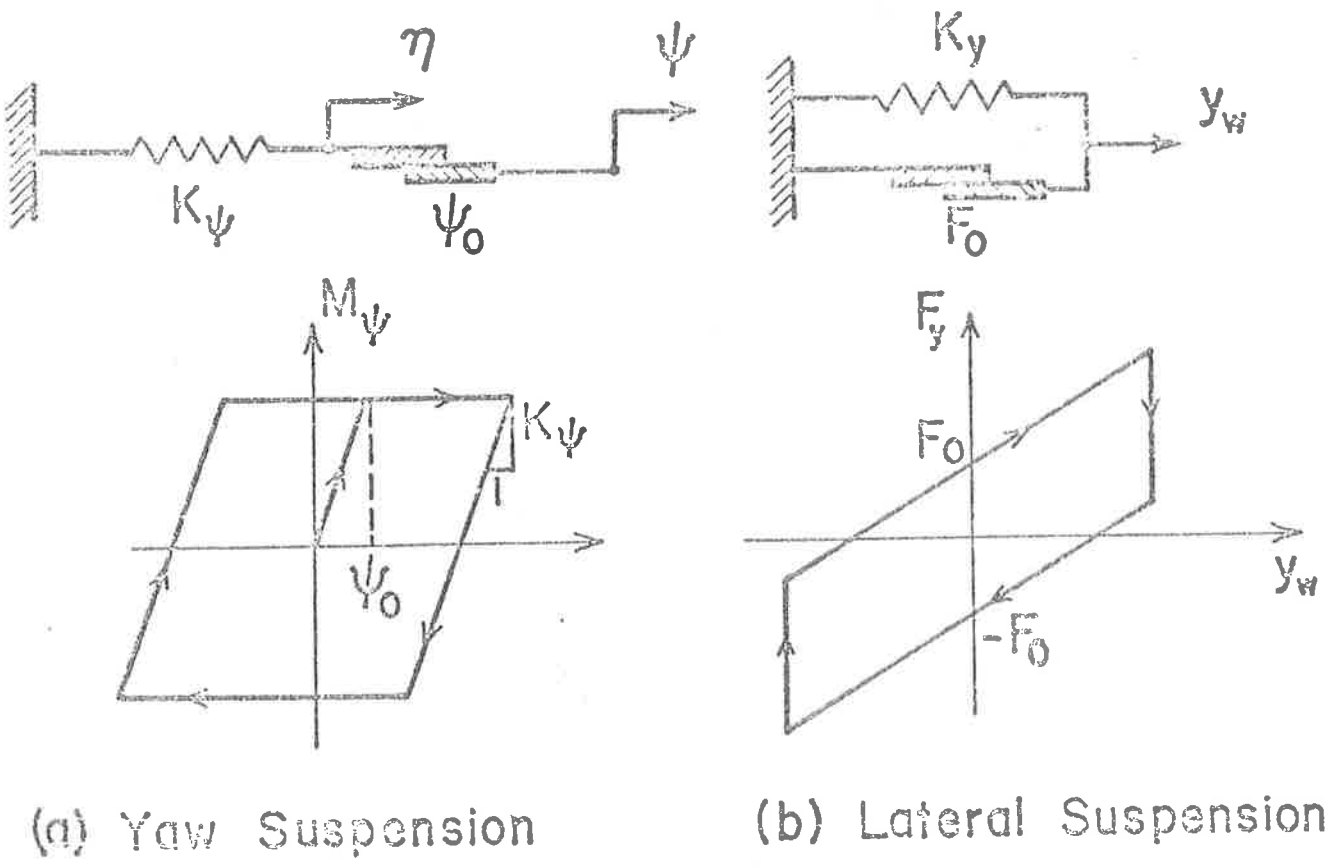

FIGURE 2-17. WHEELSET SUSPENSION NONLINEARITIES

Where:

- a - One-half the rail gauge
- a_1 - Coefficient of y_w in linearized expression for $\phi_w (y_w)$
- f_{11} - Lateral creep coefficient
- f_{33} - Longitudinal creep coefficient
- I_{wz} - Wheelset yaw moment of inertia
- M_w - Wheelset mass
- M_{fs} - Yaw suspension characteristic shown in Figure 2-
- V - Forward velocity
- W - Axle load
- δ_o - Wheel/rail contact angle when wheelset is centered
- Δ_1 - Coefficient of $\frac{y_w}{a}$ in linearized expression for $1/2(\delta_L(y_w) - \delta_R(y_w))$
- λ - coefficient of $\frac{y_w}{a}$ in linearized expression for $1/2(r_L(y_w) - r_R(y_w)) / a$

Typical parameters for such a wheelset are given in Table 2-1*.

TABLE 2-1. WHEELSET PARAMETERS

a	= 2.5 ft		
a_1	= 0.05 (new wheels)	δ_o	= 0.05 (new wheels)
f_{11}	= 3 X 10^6 lb	Δ_1	= 0.0 (new wheels)
f_{33}	= 3 X 10^6 lb	λ	= 0.05 (new wheels)
I_{wz}	= 360 slug-ft^2	F_{oy}	= 1,000 lb
M_w	= 90 slugs	K_y	= 10,000 lb/ft
r_o	= 1.75 ft	K_R	= 1 X 10^6 lb/ft
W	= 30,000 lb	K_ψ	= 105,630 ft-lb/radian
		δ_R	= 0.03 ft
		ψ_o	= 0.25°

* From Reference [14]

2.7.2 Single Wheelset with Nonlinear Wheel/Rail Geometry

A more realistic model for the single wheelset dynamic behavior incorporates the nonlinear wheel/rail constraint functions described earlier in this chapter. These nonlinear functions provide a better representation of the rolling radii difference for use in the lateral creep expression, and a better description of the contact angles for calculating the "gravitational" stiffness.

The creep forces may be also represented by the nonlinear function described earlier that accounts for saturation of the lateral and longitudinal creep forces separately.

The equations of motion for the single wheelset with the nonlinear suspension described in the preceding section and the nonlinear wheel/rail constraint functions and creep force relationship are as follows:

$$m_w\ddot{y}_w + F_{11}(\xi_y) + W[\phi(y_w - y_R) + \Delta(y_w - y_R)] + F_{ys}(y_w) = 0 \qquad (2\text{-}17)$$

$$I_{wz}\ddot{\psi}_w + \alpha F_{33}(\xi_x) - W\delta_o a\psi_w + M_{\psi s}(\psi_w) = 0 \qquad (2\text{-}18)$$

Where: $\xi_y = \frac{\dot{y}_w}{V} - \psi_w$

$$F_{11}(\xi_y) = \begin{cases} f_{11}\,\xi & |\xi_y| \le \frac{\mu N}{f_{11}} \\ \mu N & |\xi_y| > \frac{\mu N}{f_{11}} \end{cases}$$

$$\xi_x = \frac{a\dot{\psi}_w}{V} + \Lambda(y_w - y_R)$$

$$F_{33}(\xi_x) = \begin{cases} f_{33}\,\xi_x & |\xi_x| \le \frac{\mu N}{f_{33}} \\ \mu N & |\xi_x| \ge \frac{\mu N}{f_{33}} \end{cases}$$

$$\Delta(y) = 1/2\ [\delta_L\ (y) - \delta_R\ (y)]$$

$\phi(y)$ = wheelset roll angle

$$\Lambda(y) = \frac{r_L\ (y) - r_R(y)}{2a}\ .$$

The nonlinear wheel/rail constraint functions $\Delta(y)$, $\phi(y)$, and $\Lambda(y)$ are obtained using the procedures and computer programs described in reference [19]. Examples of such functions are shown in that report.

When linear creep relationships are used, these equations take the following form:

$$M_w \ddot{Y}_w + \frac{2f_{11}}{V}\dot{Y}_w + W[\phi(Y_w - Y_R) + \Delta(Y_w - Y_R)] - 2f_{11}\psi + F_{ys}(Y_w) = 0 \qquad (2\text{-}17a)$$

$$I_{W_Z}\ddot{\psi}_w + \frac{2f_{33}a^2}{V}\dot{\psi}_w - W\delta_o a\psi_w + M_{\psi_s} + \frac{2f_{33}a^2}{r_o}\left[\frac{r_L(Y_w - Y_R) - r_R(Y_w - Y_R)}{2a}\right] = 0. \qquad (2\text{-}18a)$$

2.7.3 Freight Car Rock and Roll Model

The "rock and roll" behavior of freight cars has been a major source of problems for North American railroads [10]. The "rock and roll" phenomena is a mode of freight car dynamics response to cross-level track disturbances that involves lifting and succeeding impact at the car/truck bolster and wheel/rail interfaces. Very high forces are experienced during these impacts, at times approaching 2.5 times the static load at the interfaces [10]. Such forces can cause serious damage to track, vehicle and lading.

A half freight car model is illustrated in Figure 2-9 that can be used to illustrate this rock and roll behavior [10]. In this model the wheelset is subjected to a sinusoidal cross-level input, ϕ_R, transmitted through the rails that are modeled by stiff, nonlinear compression springs. The wheelset has two degrees of freedom: vertical translation, z_w , and roll rotation, ϕ_w . Because it is free to rotate for small angles about either rail, a constrained lateral motion, y_w, may also occur. The bolster has two degrees of freedom; vertical translation, z_b and a roll rotation, ϕ_b . Small lateral displacements, y_b may occur when the bolster rotates. The car body also has two degrees of freedom: vertical translation, z_c , and roll rotation, ϕ_c . Small lateral displacements, y_c , occur when the car body rocks on either the centerplate or the sidebearing.

The bolster/sideframe suspension group is modeled in the vertical and lateral directions by the parallel spring and coulomb friction combination described earlier. The car body/bolster behavior is represented by the piecewise linear springs shown in Figure 2-10.

The equations describing the half car body motion have been derived [10] directly from force and moment balance conditions as well as kinematic constraints. The vertical force balance equations on the car body, bolster, and wheelset are:

$$M_c \ddot{z}_c = F_1 + F_2 + F_3 + F_4 - M_c g \qquad (2\text{-}19)$$

$$M_b \ddot{z}_b = F_5 + F_6 - F_1 - F_2 - F_3 - F_4 - M_b g \qquad (2\text{-}20)$$

$$M_w \ddot{z}_w = F_7 + F_8 - F_5 - F_6 - M_w g, \qquad (2\text{-}21)$$

where F_1 through F_8 are the forces acting at points 1 through 8 in Figure 2-9 and are the nonlinear spring forces defined in Figure 2-10.

The moment balance equations are:

$$I_c' \ddot{\phi}_c + \ell_2 F_{y_c} = \ell_1(F_2 - F_1) - \ell_4(F_4 - F_3)$$

$$I_b' \ddot{\phi}_b + \ell_6 F_{y_b} = \ell_1(F_1 - F_2) + \ell_4(F_4 - F_3) - \ell_3(F_6 - F_5)$$

$$I_w' \ddot{\phi}_w + \ell_8 F_{y_w} = \ell_3(F_6 - F_5) - \ell_5(F_8 - F_7),$$

where the forces F_{y_c}, F_{y_b}, and F_{y_w} are the lateral forces exerted on the car body, bolster and wheelset respectively. If it is assumed that the angles of rotation are small and that no relative lateral motion can occur between the bolster and wheelset the following kinematic constraints exist:

$$y_c \approx \ell_2\phi_c + \ell_6\phi_b + y_b$$

$$y_b \approx \ell_8\phi_w$$

$$y_w \approx \ell_7\phi_w .$$

Using these relationships in the moment balance equations yields:

$$I_c \ddot{\phi}_c + M_c \ell_2\ell_8 \ddot{\phi}_w + M_c \ell_2\ell_6 \ddot{\phi}_B = - \ell_1(F_2 - F_1) - \ell_4(F_4 - F_3) \qquad (2\text{-}22)$$

$$I_b \ddot{\phi}_B + M_c \ell_2\ell_6 \ddot{\phi}_c + M_c \ell_8\ell_6 \ddot{\phi}_w = \ell_1(F_1 - F_2) + \ell_4(F_4 - F_3) + \ell_3(F_6 - F_5) \qquad (2\text{-}23)$$

$$I_w \ddot{\phi}_w + M_c \ell_2\ell_8 \ddot{\phi}_c + M_c \ell_6\ell_8 \ddot{\phi}_B = \ell_3(F_6 - F_5) - \ell_5(F_8 - F_7). \qquad (2\text{-}24)$$

The track input to the dynamic equations occurs through F_7 and F_8 which are functions of $\ell_5(\phi_w - \phi_i)$ where ϕ_i is the track angular displacement.

Where:

F_i - Nonlinear spring force acting at point i in Figure 2-9.

ℓ_i - Dimensions defined in Figure 2-9.

M_b - Bolster mass

M_c - Car body mass

M_w - Wheelset mass

$I_b = I_b^1 + M_c \ell_6^2$

$I_c = I_c^1 + M_c \ell_2^2$

$I_w = I_w^1 + M_w \ell_7^2 + (M_c + M_b) \ell_8^2$

I_b^1 - Bolster moment of inertia in roll

I_c^1 - Car body moment of inertia in roll

I_w^1 - Wheelset roll moment of inertia

Typical values of the parameters used in this rock and roll model are given in Table 2-2.

TABLE 2-2. PARAMETERS USED IN SIMULATIONS OF 70 AND 100 TON CARS

Car Parameters	70 Ton
Weight of Car Body and Two Bolsters for Loaded Car [lbs]	172,650
Empty Car [lbs]	66,000
Weight of Each Wheelset [lbs]	6,380
Roll Moment of Inertia of Car Body for Loaded Car [lb-in-sec^2]	1,288,800
Empty Car [lb-in-sec^2]	346,000
Suspension Spring Vertical Rate [lb/in]	20,840
Suspension Spring Lateral Rate [lb/in]	8,850
Gib Stop Lateral Spring Rate at One End of Bolster [lb/in]	660,000
Bottoming Stiffness for Vertical Spring Group [lb/in]	660,000
Centerplate Stiffness [lb/in]	4,240,000
Sidebearing Stiffness [lb/in]	7,160,000
Rail Vertical Stiffness [lb/in]	420,000
Vertical Coulomb Friction Force Between Bolster and Side Frame at One End of Bolster [lbs]	4,000
Lateral Coulomb Friction Force Between Bolster and Side Frame at One End of Bolster [lbs]	4,000
Height of Car Body CG Above Center Plate for Loaded Car	72.5
Empty Car	35.0
Height of Center Plate Above Top of the Springs [in]	7.875
Side Bearings Spacing from Center Line [in]	25.0
Height of Side Bearing Above Top of the Springs [in]	12.1875
Height of Top of the Springs (Uncompressed) Above Rails [in]	20.125
Spring Group Spacing from Center Line [in]	39.0
Half of the Total Gib Clearance [in]	0.375
Spring Travel-From Free Height to Bottomed [in]	3.6875
Rail Gauge [in]	56.5
Rail Length [ft]	39.0

2.7.4 Rail Freight Car Lateral Dynamics Model

The lateral behavior of a complete rail freight car is of great practical interest to railway operating personnel. The North American freight truck has the following five major components, as shown in Figure 2-18: two wheelsets, two side frames, and one bolster. The side frames rest directly on bearing adapters that sit on the bearings. The bolster is connected to the side frames by a suspension system that allows relative vertical movement, relative lateral movement within limits, and relative angular motion about all axes. Very little relative longitudinal motion is possible between bolster and side frame.

As described in the preceding section, the freight car body rests directly on the truck bolster centerplate. Rotation about a vertical axis of the truck bolster relative to the car body is resisted by friction at the centerplate. Under the conditions previously discussed, the car body will rock on the centerplate, transferring the contact point to the edge of the centerplate, or, under more extreme conditions, shifting contact to a side bearing located toward the end of the bolster.

One model for the lateral dynamics of this freight car assumes that the side frames are attached to the wheelsets by the equivalent of a ball joint that allows relative angular rotation but precludes any relative translational motion. The additional assumption is also made that there is no relative longitudinal motion between the bolster and the side frames. Then, the lateral truck motions can be described by the following

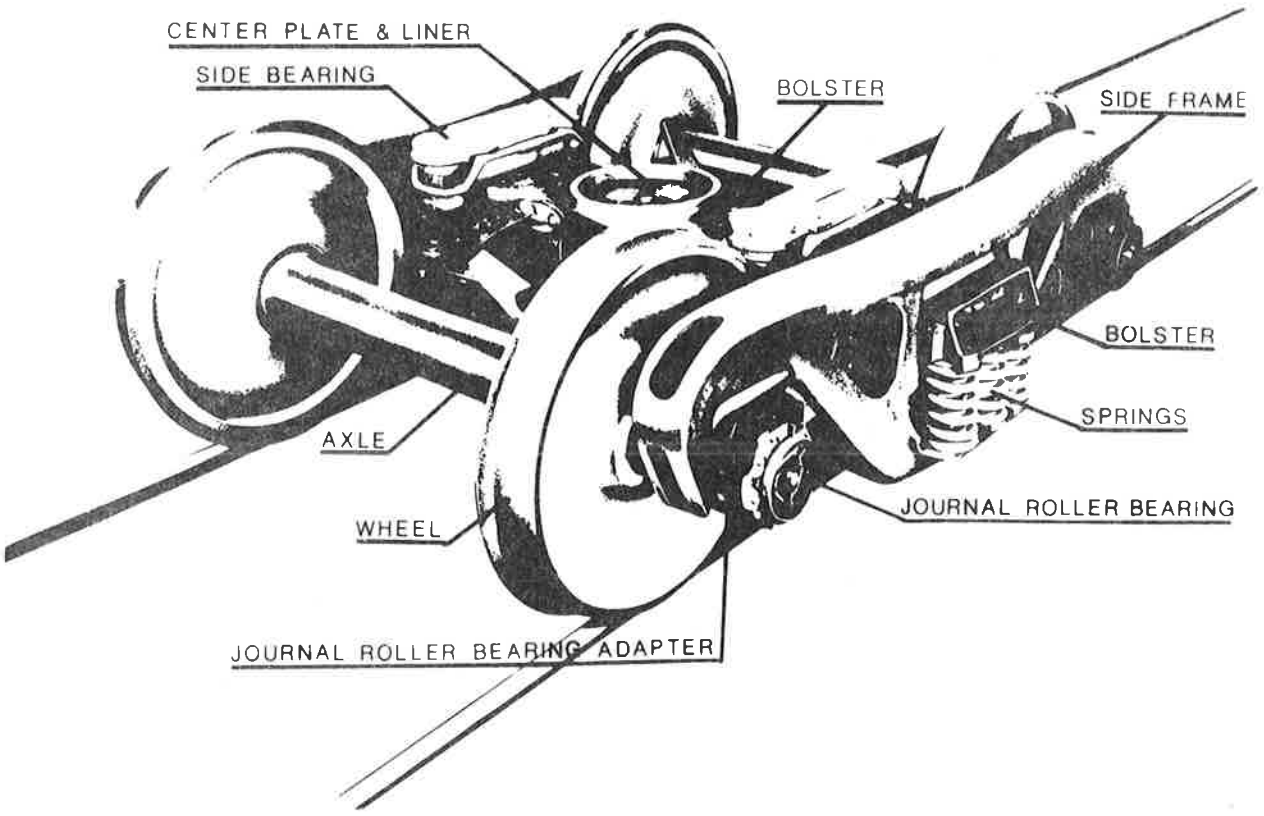

FIGURE 2-18. THREE PIECE FREIGHT TRUCK

three degrees of freedom:

Truck lateral displacement - y_{TF} (front truck)

y_{TR} (rear truck)

Truck yaw displacement - ψ_{TF} (front truck)

ψ_{TR} (rear truck)

Truck warp displacement - ψ_{WF} (front truck)

ψ_{WR} (rear truck).

These variables are illustrated in Figure 2-19. When the car body is relatively rigid it will have the following three degrees of freedom.

Lateral displacement - y_c

Yaw displacement - ψ_c

Roll displacement - ϕ_c

Note that this model neglects roll motions of the side frames, assumes that the bolster remains parallel to the wheelsets while translating laterally and vertically with the car body, and does not account for rocking of the car body on the centerplate.

All of the suspension connections in the freight car include dry friction. Within the truck itself, warp motion of the truck is resisted at the six connections between the side frames and bolster by friction and stiffness that can be modeled by a linear spring with stiffness $K_{\psi W}$, in parallel with Coulomb friction of magnitude T_{OW}. This composite torque is represented by the function $T_{\psi W}$. The characteristic is illustrated in Figure 2-20(a).

The suspension between the bolster and the sideframes also can be modeled in both the vertical and lateral directions by a linear spring

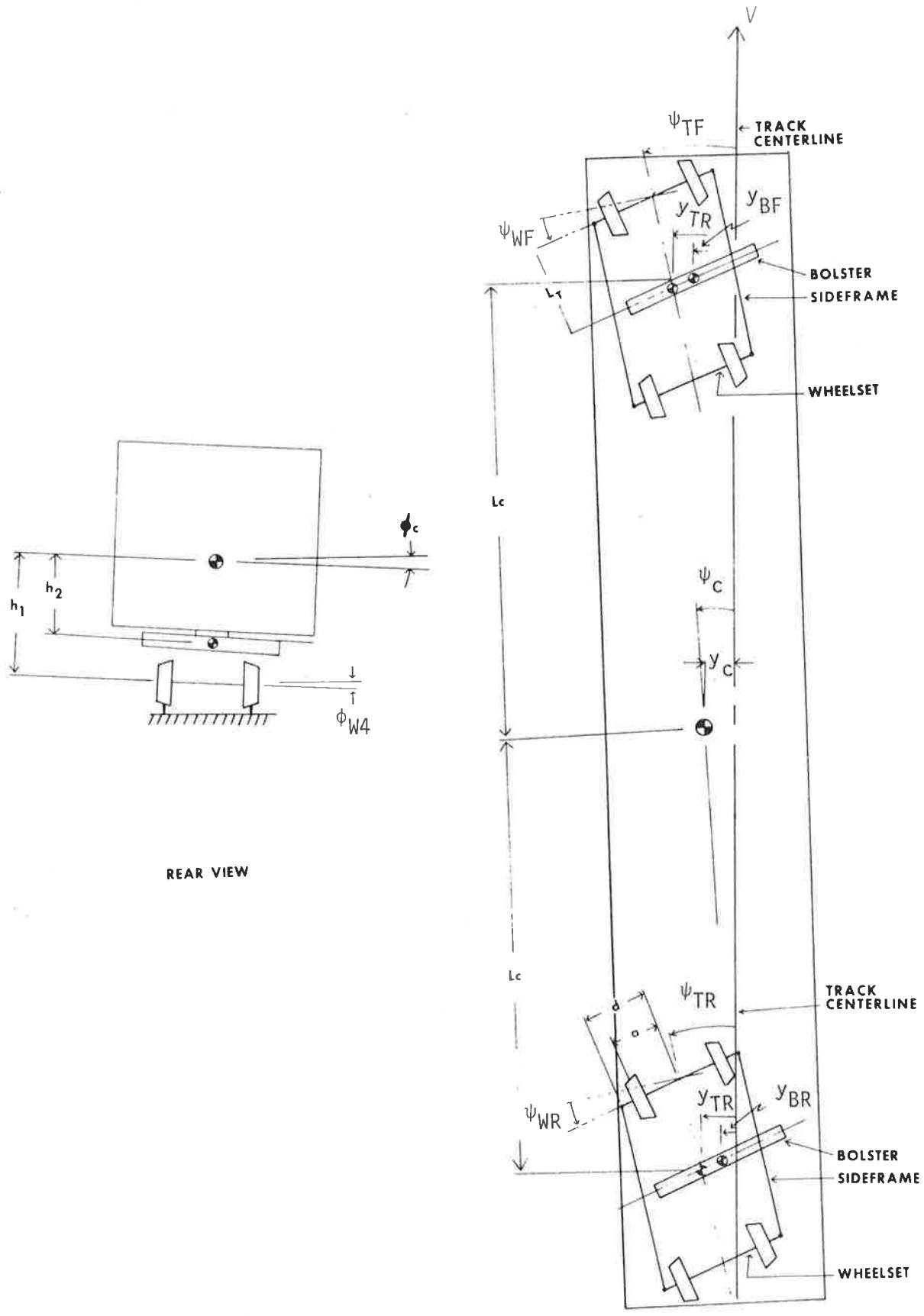

FIGURE 2-19. TYPICAL FREIGHT CAR MODEL

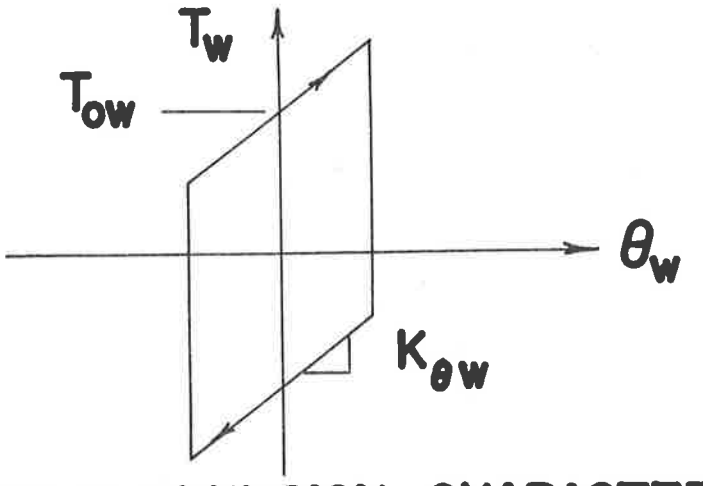

a.) WARP SUSPENSION CHARACTERISTIC

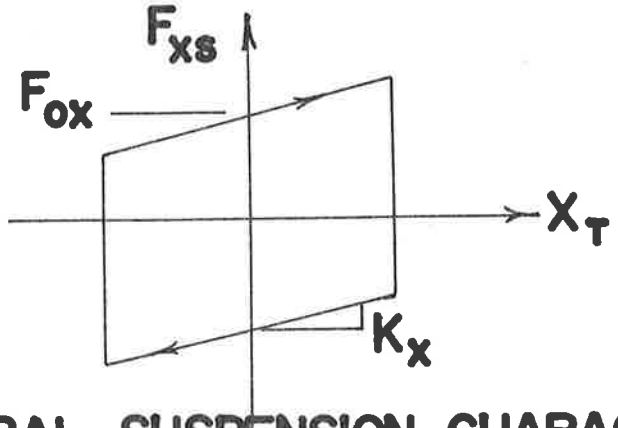

b.) LATERAL SUSPENSION CHARACTERISTIC

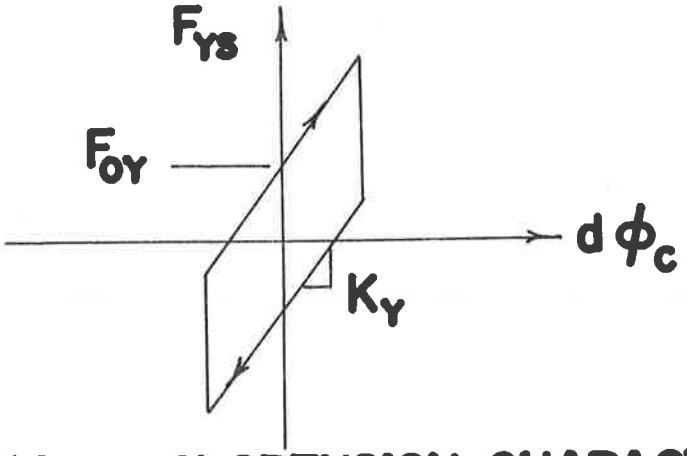

c.) VERTICAL SUSPENSION CHARACTERISTIC

FIGURE 2-20. FREIGHT CAR SUSPENSION NONLINEARITIES

parallel with dry friction. The spring rates and friction force levels in the two directions may be different.

Rotation of the truck bolster relative to the car body is resisted by friction at the centerplate. This resistance can be represented by dry friction with a breakout torque of $T_{\circ B}$.

Equations of motion for this freight car model with linear creep force expressions but nonlinear wheel/rail geometry are given below. The effects of spin creep, in addition to those of lateral and longitudinal creep, are represented in this model.

FRONT TRUCK LATERAL

$$2(M_F + M_W)\ddot{y}_{TF} + f_{11}(\xi_{YR1} + \xi_{YL1} + \xi_{YR2} + \xi_{YL2})$$

$$+ f_{12}(\xi_{\psi R1} + \xi_{\psi L1} + \xi_{\psi R2} + \xi_{\psi L2}) + 2F_{YSF}$$

$$+ W_F\left(\frac{\delta_{L1} - \delta_{R1}}{2} + \frac{\delta_{L2} - \delta_{R2}}{2}\right) + W_F(\phi_{W1} + \phi_{W2}) = 0 \qquad (2\text{-}25)$$

FRONT TRUCK YAW

$$(2I_W + 2I_{SF} + 2L_T^2 M_W + 2d^2 M_F + I_B)\ddot{\psi}_{TF}$$

$$+ (2I_W + 2d^2 M_F + I_B)\ddot{\psi}_{WF} + a^2 f_{33}(\xi_{XL1} - \xi_{XR1} + \xi_{XL2} - \xi_{XR2})$$

$$+ L_T^2 f_{11}(\xi_{YR1} + \xi_{YL1} - \xi_{YR2} - \xi_{YL2}) - f_{12}(\xi_{YR1} + \xi_{YL1} + \xi_{YR2} + \xi_{YL2})$$

$$+ f_{22}(\xi_{\psi R1} + \xi_{\psi L1} + \xi_{\psi R2} + \xi_{\psi L2}) + L_T W_F\left(\frac{\delta_{L1} - \delta_{R1}}{2} - \frac{\delta_{L2} - \delta_{R2}}{2}\right.$$

$$\left. + \phi_{W1} - \phi_{W2}\right) - 2aW_F\delta_\circ(\psi_{TF} + \psi_{WF}) + T_{BF} = 0 \qquad (2\text{-}26)$$

FRONT TRUCK WARP

$$(2I_W + 2d^2M_F + I_B)(\ddot{\psi}_{TF} + \ddot{\psi}_{WF})$$

$$+ a^2f_{33}(\xi_{XL1} - \xi_{XR1} + \xi_{XL2} - \xi_{XR2})$$

$$- f_{12}(\xi_{YR1} + \xi_{YL1} + \xi_{YR2} + \xi_{YL2}) + f_{22}(\xi_{\psi R1} + \xi_{\psi L1} + \xi_{\psi R2} + \xi_{\psi L2})$$

$$- 2aW_F\delta_o(\psi_{WF} + \psi_{TF}) + T_{4WF} + T_{BF} = 0 \qquad (2\text{-}27)$$

REAR TRUCK LATERAL

$$2(M_F + M_W)\ddot{y}_{TR} + f_{11}(\xi_{YR3} + \xi_{YL3} + \xi_{YR4} + \xi_{YL4})$$

$$+ f_{12}(\xi_{4R3} + \xi_{4L3} + \xi_{4R4} + \xi_{4L4}) + 2F_{YSR}$$

$$+ W_R\left(\frac{\delta_{L3} - \delta_{R3}}{2} + \frac{\delta_{L4} - \delta_{R4}}{2} + \phi_{W3} + \phi_{W4}\right) = 0 \qquad (2\text{-}28)$$

REAR TRUCK YAW

$$(2I_W + 2I_{SF} + 2L_T^2M_W + 2d^2M_F + I_B)\ddot{\psi}_{TR} + (2I_W + 2d^2M_F + I_B)\ddot{\psi}_{WR}$$

$$+ a^2f_{33}(\xi_{XL3} - \xi_{XR3} + \xi_{XL4} - \xi_{XR4}) + L_T^2f_{11}(\xi_{YR3} + \xi_{YL3} - \xi_{YR4} - \xi_{YL4})$$

$$-f_{12}(\xi_{YR3} + \xi_{YL3} + \xi_{YR4} + \xi_{YL4}) + f_{22}(\xi_{\psi R3} + \xi_{\psi L3} - \xi_{\psi YR4} - \xi_{\psi YL4})$$

$$+ L_TW_R\left(\frac{\delta_{L3} - \delta_{R3}}{2} - \frac{\delta_{L4} - \delta_{R4}}{2} + \phi_{W3} - \phi_{W4}\right) - 2aW_R\delta_o(\psi_{TR} + \psi_{WR}) + T_{BR} = 0$$

(2-29)

REAR TRUCK WARP

$$(2I_W + 2d^2M_F + I_B)(\ddot{\psi}_{TR} + \ddot{\psi}_{WR}) + a^2f_{33}(\xi_{XL3} - \xi_{XR3} + \xi_{XL4} - \xi_{XR4})$$

$$-f_{12}(\xi_{YR3} + \xi_{YL4} + \xi_{YR4} + \xi_{YL4}) + f_{22}(\xi_{4R3} + \xi_{4L3} + \xi_{4R4} + \xi_{4L4})$$

$$-2_aW_R\delta_o(\psi_{WR} + \psi_{TR}) + T_{\psi WR} + T_{BR} = 0 \qquad (2\text{-}30)$$

CAR BODY LATERAL

$$(m_C + 2m_B)\ddot{y}_C + 2h_2 m_B \ddot{\phi}_C = 2F_{YSF} + 2F_{YSR} \qquad (2\text{-}31)$$

CAR BODY YAW

$$(I_{CY} + 2L_C^2 m_B)\ddot{\psi}_C = 2L_C F_{YF} - 2L_C F_{YSR} + T_{BF} + T_{BR} \qquad (2\text{-}32)$$

CAR BODY ROLL

$$2h_2 m_B \ddot{y}_C + (I_{CZ} + 2I_{BZ} + 2h_2^2 m_B)\ddot{\phi}_C - h_2(m_C + 2m_B)\phi_C g = 2h_2 F_{YSF} +$$

$$2h_2 F_{YSR} - 2dF_{YSF} - 2dF_{YSR} \qquad (2\text{-}33)$$

The additional parameters appearing in these equations are defined as follows:

F_{YSF} - Lateral suspension force, front

F_{YSR} - Lateral suspension force, rear

F_{ZSF} - Vertical suspension force, front

F_{ZSR} - Vertical suspension force, rear

g - Gravitational constant = 32.2 slug-ft/sec^2

L_T - One half truck wheelbase

L_C - One half the truck spacing

I_W - Wheelset yaw moment of inertia

I_{SF} - Side frame yaw moment of inertia

I_{BX} - Bolster roll moment of inertia

I_{BZ} - Bolster yaw moment of inertia

I_{CX} - Car body rollment of inertia

I_{CZ} - Car body yaw moment of inertia

m_W - Wheelset mass

m_{SF} - Sideframe mass

m_B - Bolster mass

m_c - Car body mass

T_{BF} - Centerplate torque, front

T_{BR} - Centerplate torque, rear

T_{4WF} - Warp torque, front

T_{4WR} - Warp torque, rear

The following expressions describe the lateral, longitudinal, and spin creepages for the leading wheelset of the front truck in terms of the vehicle degrees of freedom and the vehicle parameters:

$$\xi_{YR} = \xi_{YL} = \frac{1}{V}(\dot{y}_{TF} + L_T \dot{\psi}_{TF}) - (\psi_{WF} + \psi_{TF}) \qquad (2\text{-}34)$$

$$\xi_{XR} = -\xi_{XL} = -\frac{a}{V}(\dot{\psi}_{TF} + \dot{\psi}_{WF})$$

$$\frac{-1}{2r_o}(r_L(y_{W1} - y_{R1}) - r_R(y_{W1} - y_{R1})) \qquad (2\text{-}35)$$

$$\xi 4_R = \frac{\delta_R}{r_o} + \frac{\dot{\psi}_{TF} + \dot{\psi}_{WF}}{V} \qquad (2\text{-}36)$$

$$\xi 4_L = \frac{\delta_L}{r_o} + \frac{\dot{\psi}_{TF} + \dot{\psi}_{WF}}{V} \qquad (2\text{-}37)$$

Where :

ξ_{YR}, ξ_{YL} - Lateral creepages

ξ_{XR}, ξ_{XL} - Longitudinal creepages

$\xi_{\psi R}$, $\xi_{\psi L}$ - Spin creepages

L_T - One half truck wheel base

$$y_{w1} = y_{TF} + L_T\psi_{TF}$$

Similar expressions can be written for the other wheelsets. Details of the derivation of these equations may be found in References [23 and 24]. The complete equations of motion for the freight vehicle subject to these forces are given in Figure 2-21.

Only track centerline alignment variations are accounted for in the equations above, although cross-level irregularities can be easily added to the equations.

Typical values for the parameters appearing in these equations are given in Table 2-3. These parameters are for a 80 ton hopper car on 70 ton, Ride Control trucks. Most of these values were obtained by tests conducted as part of the Government-Industry, Track-Train Dynamics Program administered by and reported in references [17] and [18].

2.7.5 Track Irregularities

Individual consideration of track centerline alignment or profile variations are easily handled by describing function methods. However, simultaneous consideration of several irregularities such as alignment and cross-level is a dual input problem that requires an extension of the quasi-linearization methods used here.

The track alignment irregularities enter the equations of motion through the wheel/rail geometric constraint functions. The argument of these functions becomes $y_W - y_R$. For the sinusoidal response studies, the track alignment was represented by a sinusoidal function of the following

FRONT TRUCK LATERAL

$$2(m_F + m_W)\ddot{x}_{TF} + 4\frac{f_{11}}{V}\dot{x}_{TF} + 4\frac{f_{12}}{V}\dot{\delta}_{TF} - 4f_{11}v_{TF} + 4\frac{f_{12}}{V}\dot{\theta}_{WF} - 4f_{11}r_{WF} + (W_F - \frac{2f_{12}}{r_o})(\frac{\delta_{L1} - \delta_{R1}}{2} + \frac{\delta_{L2} - \delta_{R2}}{2}) + W_F(\phi_{W1} + \phi_{W2}) + 2\frac{f_{11}r_o}{V}(\dot{\phi}_{W1} + \dot{\phi}_{W2}) = -2F_{XSF}$$

FRONT TRUCK YAW

$$-4\frac{f_{12}}{V}\dot{x}_{TF} + (2I_{WY} + 2I_{FY} + 2L_T^2m_W + 2d^2m_F + I_{BY})\ddot{\theta}_{TF} + (4\frac{f_{22}}{V} + 4a^2\frac{f_{33}}{V} + 4\frac{L_T^2f_{11}}{V})\dot{\delta}_{TF} + (4f_{12} - 2aW_F\delta_o)r_{TF} + (2I_{WY} + 2d^2m_F + I_{BY})\ddot{\theta}_{WF} + (4\frac{f_{22}}{V} + 4\frac{a^2f_{33}}{V})\dot{\delta}_{WF}$$
$$+ (4f_{12} - 2aW_F)\theta_{WF} + (L_TW_F - \frac{2L_Tf_{12}}{r_o})(\frac{\delta_{L1} - \delta_{R1}}{2} - \frac{\delta_{L2} - \delta_{R2}}{2}) + W_FL_T(\phi_{W1} - \phi_{W2}) + 2\frac{r_oL_Tf_{11}}{V}(\dot{\phi}_{W1} - \dot{\phi}_{W2}) - \frac{2r_of_{12}}{V}(\dot{\phi}_{W1} + \dot{\phi}_{W2})$$
$$- 2\frac{f_{22}}{r_o}(\frac{\delta_{L1} - \delta_{R1}}{2} + \frac{\delta_{L2} - \delta_{R2}}{2}) + 2a\,f_{33}(\frac{r_{L1} - r_{R1}}{2r_o} + \frac{r_{L2} - r_{R2}}{2r_o}) = -T_{BF}$$

FRONT TRUCK WARP

$$-4\frac{f_{12}}{V}\dot{x}_{TF} + (2I_{WY} + 2d^2m_F + I_{BY})\ddot{\theta}_{TF} + (4\frac{f_{22}}{V} + 4a^2\frac{f_{33}}{V})\dot{\delta}_{TF} + (4f_{12} - 2aW_F\delta_o)r_{TF} + (2I_{WY} + 2d^2m_F + I_{BY})\ddot{\theta}_{WF} + (4\frac{f_{22}}{V} + 4\frac{a^2f_{33}}{V})\dot{\delta}_{WF} + (4f_{12} - 2aW_F\delta_o)r_{WF}$$
$$- \frac{2f_{22}}{r_o}(\frac{\delta_{L1} - \delta_{R1}}{2} + \frac{\delta_{L2} - \delta_{R2}}{2}) - 2\frac{r_of_{12}}{V}(\dot{\phi}_{W1} + \dot{\phi}_{W2}) + 2a\,f_{33}(\frac{r_{L1} - r_{R1}}{2r_o} + \frac{r_{L2} - r_{R2}}{2r_o}) = -T_{\theta WF} - T_{BF}$$

REAR TRUCK LATERAL

$$2(m_F + m_W)\ddot{x}_{TR} + 4\frac{f_{11}}{V}\dot{x}_{TR} + 4\frac{f_{12}}{V}\dot{\delta}_{TR} - 4f_{11}v_{TR} + 4\frac{f_{12}}{V}\dot{\theta}_{WR} - 4f_{11}r_{WR} + (W_R - \frac{2f_{12}}{r_o})(\frac{\delta_{L3} - \delta_{R3}}{2} + \frac{\delta_{L4} - \delta_{R4}}{2}) + W_R(\phi_{W3} + \phi_{W4}) + 2\frac{f_{11}r_o}{V}(\dot{\phi}_{W3} + \dot{\phi}_{W4}) = -2F_{XSR}$$

REAR TRUCK YAW

$$-4\frac{f_{12}}{V}\dot{x}_{TR} + (2I_{WY} + 2I_{FY} + 2L_T^2m_W + 2d^2m_F + I_{BY})\ddot{\theta}_{TR} + (4\frac{f_{22}}{V} + 4a^2\frac{f_{33}}{V} + 2\frac{L_T^2f_{11}}{V})\dot{\delta}_{TR} + (4f_{12} - 2aW_R\delta_o)r_{TR} + (2I_{WY} + 2d^2m_F + I_{BY})\ddot{\theta}_{WR} + (4\frac{f_{22}}{V} + 4\frac{a^2f_{33}}{V})\dot{\delta}_{WR}$$
$$+ (4f_{12} - 2aW_F)\theta_{WR} + (L_TW_R - \frac{2L_Tf_{12}}{r_o})(\frac{\delta_{L3} - \delta_{R3}}{2} + \frac{\delta_{L4} - \delta_{R4}}{2}) + W_RL_T(\phi_{W3} - \phi_{W4}) + 2\frac{r_oL_Tf_{11}}{V}(\dot{\phi}_{W3} - \dot{\phi}_{W4}) - \frac{2r_of_{12}}{V}(\dot{\phi}_{W3} + \dot{\phi}_{W4})$$
$$- 2\frac{f_{22}}{r_o}(\frac{\delta_{L3} - \delta_{R3}}{2} + \frac{\delta_{L4} - \delta_{R4}}{2}) + 2a\,f_{33}(\frac{r_{L3} - r_{R3}}{2} + \frac{r_{L4} - r_{R4}}{2}) = -T_{BR}$$

REAR TRUCK WARP

$$-4\frac{f_{12}}{V}\dot{x}_{TR} + (2I_{WY} + 2d^2m_F + I_{BY})\ddot{\theta}_{TR} + (4\frac{f_{22}}{V} + 4a^2\frac{f_{33}}{V})\dot{\delta}_{TR} + (4f_{12} - 2aW_R\delta_o)r_{TR} + (2I_{WY} + 2d^2m_F + I_{BY})\ddot{\theta}_{WR} + (4\frac{f_{22}}{V} + 4\frac{a^2f_{33}}{V})\dot{\delta}_{WR} + (4f_{12} - 2aW_R\delta_o)\theta_{WR}$$
$$- 2\frac{f_{22}}{r_o}(\frac{\delta_{L3} - \delta_{R3}}{2} + \frac{\delta_{L4} - \delta_{R4}}{2}) - 2\frac{r_of_{12}}{V}(\dot{\phi}_{W3} + \dot{\phi}_{W4}) + 2a\,f_{33}(\frac{r_{L3} - r_{R3}}{2r_o} + \frac{r_{L4} - r_{R4}}{2r_o}) = -T_{\theta WR} - T_{BR}$$

CAR BODY LATERAL

$$(m_C + 2m_B)\ddot{x}_C - 2h_2m_B\ddot{\phi}_C = 2F_{XSF} + 2F_{XSR}$$

CAR BODY YAW

$$(I_{CY} + 2L_C^2m_B)\ddot{\theta}_C = 2L_CF_{XSF} - 2L_CF_{XSR} + T_{BF} + T_{BR}$$

CAR BODY ROLL

$$2h_2m_B\ddot{x}_C + (I_{CZ} + 2I_{BZ} + 2h_2^2m_B)\ddot{\phi}_C - h_2(m_C + 2m_B)g\phi_C = 2h_2F_{XSF} + 2h_2F_{XSR} - 2dF_{YSF} - 2dF_{YSR}$$

x_{TF} - FRONT TRUCK LATERAL DISPLACEMENT
x_{TR} - REAR TRUCK LATERAL DISPLACEMENT
x_C - CAR BODY LATERAL DISPLACEMENT
θ_{TF} - FRONT TRUCK YAW DISPLACEMENT
θ_{TR} - REAR TRUCK YAW DISPLACEMENT
θ_C - CAR BODY YAW DISPLACEMENT
θ_{WF} - FRONT TRUCK WARP DISPLACEMENT
θ_{WR} - REAR TRUCK WARP DISPLACEMENT
ϕ_C - CAR BODY ROLL DISPLACEMENT
ϕ_{Wi} - ith WHEELSET ROLL DISPLACEMENT

FIGURE 2-21. FREIGHT CAR LATERAL EQUATIONS OF MOTION

TABLE 2-3. TYPICAL PARAMETER VALUES FOR FREIGHT CAR

Dimensions		Light	Loaded	
a	(One half rail gauge)	2.48	2.48	ft
d	(One half side frame spacing)	3.25	3.25	ft
h_1	(Vertical distance, truck c.g. to car body c.g.)	2.99	4.62	ft
h_2	(Vertical distance, car body c.g. to bolster)	2.99	4.62	ft
L_c	(One half distance between truck centers)	16.9	16.9	ft
r_o	(Nominal wheel radius)	1.375	1.375	ft
Mass Properties				
I_{BY}	(Bolster yaw moment of inertia)	178.6	178.6	$slug\text{-}ft^2$
I_{BZ}	(Bolster roll moment of inertia)	178.6	178.6	$slug\text{-}ft^2$
I_{CY}	(Car body yaw moment of inertia)	2.34×10^5	1.07×10^6	$slug\text{-}ft^2$
I_{CZ}	(Car body roll moment of inertia)	1.3×10^4	8.77×10^4	$slug\text{-}ft^2$
I_{FY}	(Side frame yaw moment of inertia)	77.6	77.6	$slug\text{-}ft^2$
I_{WX}	(Wheelset spin moment of inertia)	53.1	53.1	$slug\text{-}ft^2$
I_{WY}	(Wheelset yaw moment of inertia)	448.5	448.5	$slug\text{-}ft^2$
M_B	(Bolster mass)	36.1	36.1	slugs

TABLE 2-3. (CONT.)

		Light	Loaded	
M_C	(Car body mass)	1102.	6282.	slugs
M_F	(Side frame mass)	24.	24.	slugs
M_W	(Wheelset mass)	76.6	76.6	slugs
Creep Coefficients (Full Kalker Values)				
f_{11}	(Lateral creep coefficient)	1.15×10^6	3.034×10^6	lb
f_{12}	(Lateral/spin creep coefficient)	6750.	28950.	ft-lb
f_{22}	(Spin creep coefficient)	42.1	293.	ft^2-lb
f_{33}	(Longitudinal creep coefficient)	$1.262\ NO^6$	3.3305×10^6	lb
Suspension Properties				
K_{xs}	(Lateral suspension stiffness, per side frame)	2.4×10^4	1.116×10^5	lb/ft
K_{ys}	(Vertical suspension stiffness, per side frame)	2.658×10^5	2.658×10^5	lb/ft
$K_{\theta Y}$	(Yaw suspension stiffness, per truck)	0.0	0.0	ft-lb/rad
K_θ	(Warp stiffness, per truck)	3.81×10^6	4.61×10^6	ft-lb/rad
F_{xso}	(Lateral friction force, per side frame)	5200.	5200.	lb
F_{Yso}	(Vertical friction force, per side frame)	3120.	3120.	lb
T_{BO}	(Friction torque at centerplate, per truck)	606.	3456.	ft lb
T_{wo}	(Warp friction torque, per truck)	4271.	17084.	ft lb
D_{xso}	(Lateral equivalent viscous damping coefficient, per side frame)	9520.	9520.	$\frac{\text{lb sec}}{\text{ft}}$

TABLE 2-3. (CONT.)

		Light	Loaded	
D_{yso}	(Vertical equivalent viscous damping coefficient, per side frame)	3035.	3035.	$\frac{lb\ sec}{ft}$
D_{BO}	(Yaw equivalent viscous damping coefficient at centerplate, per truck)	2220.	1.27×10^4	ft lb sec
D_{wo}	(Warp equivalent viscous damping coefficient, per truck)	1.322×10^4	5.29×10^4	ft lb sec

form:

$$y_{Ri} = A_R \cos (\omega (t + L_i/V)) ,$$

where A_R is the magnitude of the irregularity and L_i is the distance along the track from the leading wheelset to the ith wheelset.

Cross-level and profile irregularities enter the equations of motion directly, causing motions of masses or suspension components. Continuous track gauge variations can be handled, but introduce numerical complexity that requires great effort. The difficulty with gauge variation is that the wheel/rail geometric constraint functions become functions of two variables, the wheelset position and the track gauge, and consequently the amount of stored data that is required increases geometrically. Simultaneous consideration of gauge and alignment variations is also a dual input problem. Track gauge can be introduced, however, as a discrete parameter as was done in the single wheelset limit cycle studies reported in Chapter 5.

2.8 SUMMARY

Nonlinearities for many characteristics found in rail vehicles have been described in this chapter. This discussion is not intended to be all inclusive, and other nonlinearities, particularly combinations of those discussed here, may be seen in rail car operation.

The examples of equations of motion presented in this chapter for typical rail vehicle models will be used in subsequent chapters to illustrate the quasi-linearization techniques.

3. THE QUASI-LINEARIZATION TECHNIQUE

3.1 INTRODUCTION

This chapter presents analytical techniques that may be used to predict the response of rail vehicles that contain significant nonlinearities. Traditionally, the rail vehicle analyst has had two options for computing nonlinear response: 1) linearize the nonlinearities and use well established linear analytical techniques such as frequency domain methods or 2) simulate the nonlinear system using numerical integration methods. The first method, although convenient and relatively inexpensive, is not accurate enough for problems where there is essential nonlinear behavior. The second method, although accurate, leads to very little physical insight and can be extremely expensive, especially for parametric studies.

The describing function (D.F) or "quasi-linearization" method is an attempt to combine the computational efficiency of linear analysis with the accuracy of numerical simulation. References [25, 26, 27, 28] provide a theoretical background for quasi-linearization.

Figure 3-1 is a schematic diagram of a nonlinear element, $y = f(x)$, and an approximate signal, $y_a = K(\cdot)x$. The notation $K(\cdot)$ implies that the gain, K, is a function in some sense, of the input $x(t)$. In general the functional dependence will depend upon the specific signal form that $x(t)$ takes. In fact one drawback of the D.F. method is that the form of the signal must be assumed before the gain, $K(\cdot)$, is computed. In order to approximate the nonlinearity with a signal $y_a = Kx$, the error, or difference between the nonlinear output, $y(x)$, and the approximate output, y_a, is defined to be the error signal ε, i.e.:

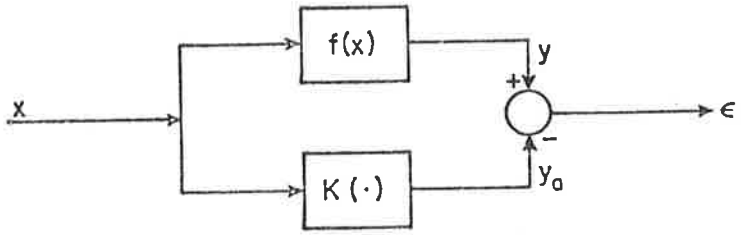

FIGURE 3-1. NONLINEAR ELEMENT AND ITS QUASI-LINEAR APPROXIMATOR

$$\varepsilon = y - y_a = f(x) - Kx . \tag{3-1}$$

If K is required to be a constant, independent of x, then the well known linear approximation is $K = \frac{\partial f}{\partial x}\Big|_{x_o}$, where x_o is the nominal value of x. In many rail applications, assuming that K remains constant is an invalid assumption and leads to incorrect predictions of dynamic behavior.

The basic method for developing a quasi-linear approximator for the nonlinear element is to choose K so that the error, ε, between the nonlinear element and its quasi-linear approximation is minimized. The precise criterion is to choose K so that the average square error, $\overline{\varepsilon^2}^*$, is minimized, i.e.,

$$\begin{aligned} \overline{\varepsilon^2} &= \overline{(f(x) - Kx)^2} \\ &= \overline{f(x)^2} - 2K\overline{xf(x)} + K^2\overline{x^2} . \end{aligned} \tag{3-2}$$

The K which minimizes $\overline{\varepsilon^2}$ can be found by differentiating $\overline{\varepsilon^2}$ with respect to K, i.e.,

$$-2\,\overline{xf(x)} + 2K\overline{x^2} = 0$$

or

$$K = \frac{\overline{xf(x)}}{\overline{x^2}} \tag{3-3}$$

Equation (3-3) expresses the quasi-linear gain, K, as a function of both

* The notation $\overline{(\ )}$ denotes the average value of ( ), i.e. $\lim_{T\to\infty} \frac{1}{T}\int_{-T}^{T} (\ )\, dt$.

the input, x, and the nonlinearity, f(x). It is important to note that the quantities on the right side of equation (3-3) cannot be computed unless the form of the input is known.

In general the nonlinearity, f(x), is part of a dynamic system containing either internal or external (control) feedback paths; thus the output, y, passes through the rest of the system on its way back to the input, x. If we assume that the signal x(t) has a certain form, then in order for the D.F. approach to be useful, the signal form should not change significantly after it has passed through the nonlinearity and the rest of the system. Signals that pass through linear systems essentially unchanged are biases, sinusoids, exponentials, and Gaussian random variables. Therefore, if x(t) has one of these signal forms, and if the system is "predominantly" linear, the D.F. approach is quite powerful. Stated in feedback control terms, the system must possess "sufficient low pass filtering" after the nonlinearities in order to assure good results. In almost every case where the D.F. approach fails it can be shown that insufficient filtering existed. Unfortunately a quantitative description of how much filtering (or integration) is required is not currently available.

This section illustrates how the D.F. can be used to predict the dynamic response of nonlinear systems that have this property of "sufficient filtering". Computational algorithms to predict the response to sinusoids and Gaussian random variables are described and illustrated by practical examples.

A theoretical framework for quasi-linearization that includes general multiple inputs of any wave form is described in Gelb and Vander Velde [25]. Figure 3-2, adapted from [25], shows the signal $x(t)$ that is composed of $x_1 \ldots x_n$, i.e., $x(t) = x_1(t)+\ldots+x_n(t)$. This is a generalization of figure 3-1, where the quasi-linear operator is described by its impulse response, $w_i(t)$. There will be a "filter" $w_i(t)$ for each input signal $x_i(t)$.

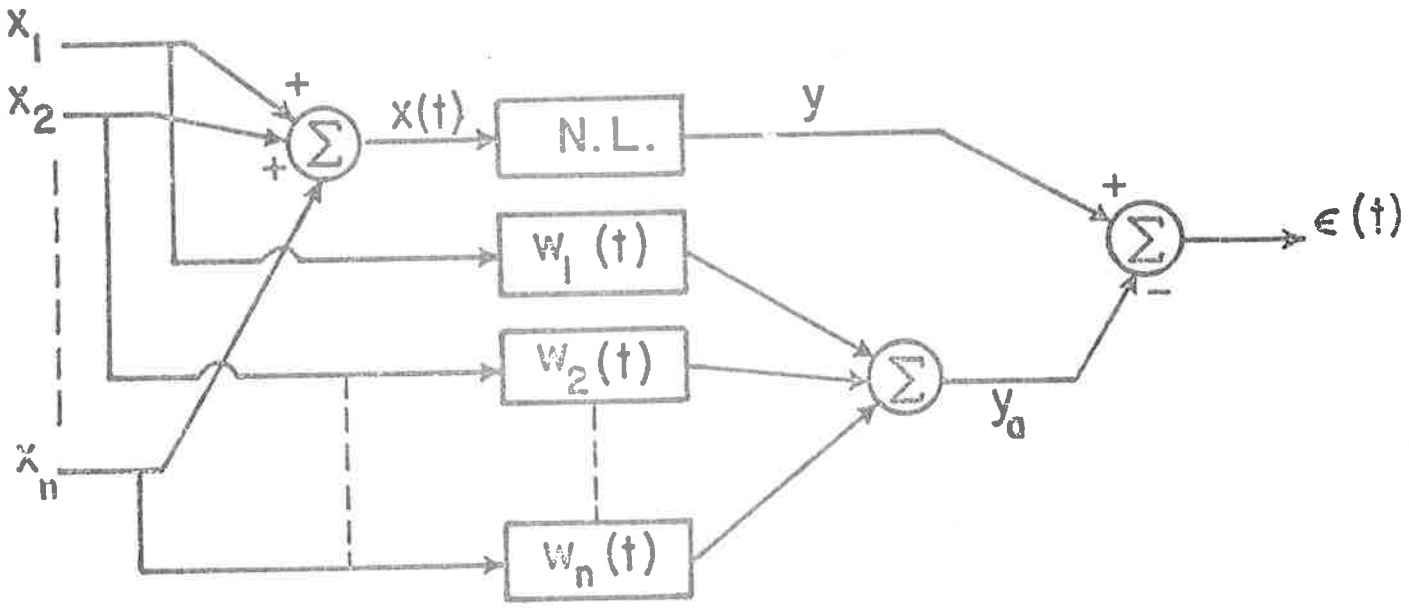

FIGURE 3-2. A GENERAL REPRESENTATION OF THE QUASI-LINEAR APPROXIMATION

The optimum quasi-linear impulse response functions, $w_1(t) \ldots w_n(t)$, are found by choosing them to minimize the mean square error between the actual signal, $y(t)$, and the approximate signal, $y_a(t)$, i.e., to minimize the following integral:

$$\lim_{T\to\infty} \frac{1}{T} \int_{-T}^{T} (y(t) - y_a(t))^2 \, dt . \qquad (3\text{-}4)$$

The derivation of the solution for the optimum $w_i(t)$'s is found in [25, 26]. In general the solution will involve a difficult set of n coupled integral equations, known as Wiener-Höpf integral equations. The assumptions necessary to simplify these integral equations, such as statistical independence of the inputs, stationarity, symmetric single valued nonlinearities, etc., are outlined in [25]. Equation 3-3 represents the solution of the Wiener-Höpf equation for the very practical case of static nonlinearities.

With this general theoretical framework, the various combinations of input signals can be considered and describing functions computed. It should be clear, from this formulation, that the quasi-linear approach requires that the form of the input signal be known and that this wave form remain essentially unchanged as it propagates through the system. For this reason, the most commonly considered signals are sinusoids, biases, and aussian random variables, although some useful results have been achieved by considering damped exponentials. In the following sections some of the more useful input combinations are considered.

3.2 DESCRIBING FUNCTIONS FOR RAIL VEHICLE NONLINEARITIES

Section 2 describes the common suspension and wheel/rail profile nonlinearities of rail vehicles. In this section the sinusoidal and random input describing functions are presented.

3.2.1 Sinusoidal Describing Functions

If we assume that x(t) in Figure 3-1 is a sine wave, $x = A \sin\omega t$, then the describing function gain given by equation 3-3 can be averaged over one period yielding:

$$K = \frac{\int_0^{2\pi/\omega} A \sin\omega t \, f(a \sin\omega t) \, dt}{\int_0^{2\pi/\omega} A \sin^2 \omega t \, dt}$$

$$K = \frac{1}{\pi A} \int_0^{2\pi} f(A \sin\omega t) \sin\omega t \, d(\omega t) \qquad (3\text{-}5)$$

Equation (3-5) is used to compute the sinusoidal describing function for any single input-single output nonlinearity whose input is sinusoidal. Tables of most common describing functions are found in references [25, 26, 27].

3.2.2 Deadband Spring

As described in Section 2, the deadband spring is commonly used in the nonlinear modeling of rail vehicles. Figure 2-2 shows the force-displacement relationship for a deadband spring. The Sinusoidal Input Describing Function (SIDF) is found by using (3-5) or by referring to the appendices of well known texts. The result is:

$$f_{D.B.}(x) \approx K_{D.B.} x \qquad (3\text{-}6)$$

$$K_{D.B.} = K_R[1 - f^*(\delta_o/A)] .$$

Where

$$f^*(\gamma) \begin{cases} = -1 & \gamma < -1 \\ = \frac{2}{\pi}(\sin^{-1}\gamma + \gamma\sqrt{(1-\gamma^2)} & |\gamma| < 1 \\ = 1 & \gamma > 1 \end{cases} \qquad (3\text{-}7)$$

Figure 3-3 shows equation (3-6) graphically

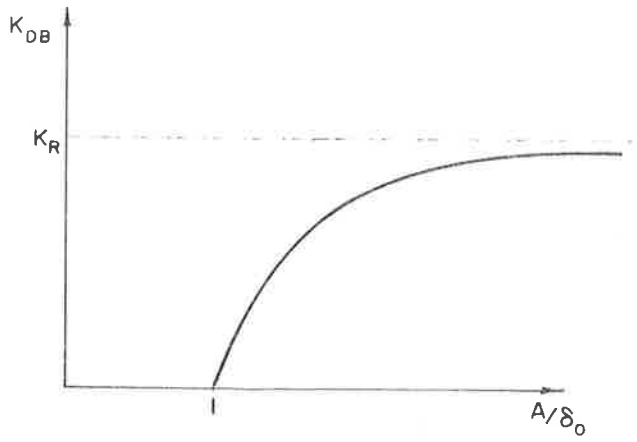

FIGURE 3-3. DEAD BAND SPRING DESCRIBING FUNCTION

3.2.3 Hardening or Softening Springs

Figure 2-3 shows the force-displacement relationship for

hardening and softening springs where a linear hardening and softening effect is modeled. The D.F. approximation for this nonlinearity is:

$$f_{H/S}(x) \approx K_{H/S}\, X \tag{3-8}$$

$$k_{H/S} = (K_1 - K_2)\, f^*(\delta_1/A) + K_2$$

where $f^*(\gamma)$ is given by equation (3-7). Figure 3-4 shows equation (3-8) graphically.

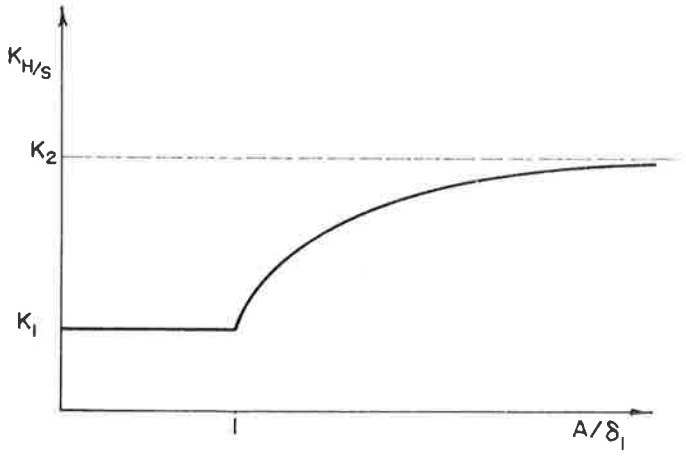

FIGURE 3-4. D.F. FOR LINEAR HARDENING/SOFTENING SPRINGS

3.2.4 Coulomb or Dry Friction

Figure 2-4 shows the force-velocity relationship for dry friction. Since $x = A \sin\omega t$, we have $\dot{x} = A\omega\cos\omega t$ and $A_v = A\omega$ where A_v is the amplitude of the velocity across the friction damper. The D.F. approximation for this nonlinearity is:

$$f_c(\dot{x}) \approx C_c \dot{x} \tag{3-9}$$

where $$C_c = \frac{4 F_o}{\pi A_v} = \frac{4 F_o}{\pi A\omega},$$

Figure 3-5 shows equation (3-9) graphically.

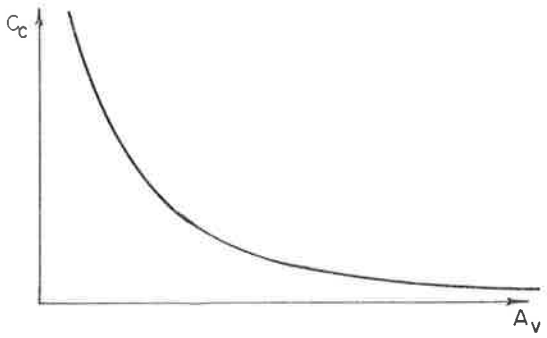

FIGURE 3-5. D.F. GAIN FOR COULOMB FRICTION

3.2.5 Parallel Spring-Dry Friction Combination

As mentioned in Section 2 a commonly used suspension grouping is a parallel combination of a linear spring and coulomb damper. The total force through the suspension can be expressed as:

$$F_s = K_s x + F_o \operatorname{sgn}(\dot{x}).$$

The quasi-linear approximation, if $x = A \sin\omega t$, is:

$$F_s \approx K_s x + \frac{4 F_o}{\pi A \omega} \dot{x} \qquad (3\text{-}10)$$

3.2.6 Series Spring-Dry Friction Combination

As mentioned in Section 2 a series spring-dry friction combination is commonly used to model suspension elements where for small deflections the suspension is linear but for larger deflections the contacting surfaces break away. Figure 2-17a shows a schematic representation as well as the force displacement characteristic.

The D. F. formulation for this nonlinearity is:

$$M_s \approx K_s \psi + C_s \dot{\psi} \qquad (3\text{-}11a)$$

where

$$K_s = \frac{K\psi}{2} [1 + f^*(-\beta)] \qquad (3\text{-}11b)$$

and

$$C_s = \begin{cases} 0 , & B \leq \psi_o \\ \frac{K\psi}{\omega\pi}(1-\beta^2) , & B > \psi_o \end{cases} \qquad (3\text{-}11c)$$

and

$$\beta = \frac{B - 2\psi_o}{B},$$

and ψ was assumed to be $B \sin\omega t$.

3.2.7 Wheel/Rail Geometry Nonlinearities

Section 2 described the wheel/rail geometric constraint functions. The important functions are:

1. The difference in wheel rolling radii at the contact point $(r_L - r_R)$
2. The difference in contact angles at the contact point $(\delta_L - \delta_R)$
3. The wheelset roll angle (ϕ).

The describing function approximations for these geometric constraint functions are:

$$\frac{r_L - r_R}{2a} \approx \lambda\, y/a \qquad (3\text{-}12)$$

$$\frac{\delta_L - \delta_R}{2} \approx \Delta_1\, y/a \qquad (3\text{-}13)$$

$$\phi \approx a_1\, y/a \qquad (3\text{-}14)$$

where $\lambda(A)$, $\Delta_1(A)$, and $a_1(A)$ are the describing function gains and are computed by minimizing the following integrals:

$$\int_0^{2\pi/\omega} \left(\frac{r_L - r_R}{2} - \lambda y\right)^2 dt$$

$$\int_0^{2\pi/\omega} \left(\frac{\delta_L - \delta_R}{2} - \Delta_1\, y/a\right)^2 dt$$

$$\int_0^{2\pi/\omega} (\phi - a_1\, y/a)^2 \; dt\,.$$

The minimization of these integrals leads to the following equations (equation 3-5), if we let $y = A\sin\omega t$, and let $\omega t = \psi$:

$$\lambda(A) \triangleq \frac{1}{\pi A} \int_0^{2\pi} \left(\frac{r_L\,(A\sin\psi) - r_R\,(A\sin\psi)}{2}\right) \sin\psi d\psi \qquad (3\text{-}15)$$

$$\Delta_1(A) \triangleq \frac{a}{\pi A} \int_0^{2\pi} \left(\delta_L\,\frac{(A\sin\psi) - \delta_R\,(A\sin\psi)}{2}\right) \sin\psi d\psi \qquad (3\text{-}16)$$

$$a_1(A) \triangleq \frac{a}{\pi A} \int_0^{2\pi} \phi(A\sin\psi) \sin\psi d\psi \qquad (3\text{-}17)$$

The integrals defined by equations (3-15 → 3-17) have been numerically integrated using the data from new, worn, and Heumann profiles (such as Figure 2-13). Some examples of these describing function gains as a function of amplitude are shown in Figures 3-6 to 3-8.

$\lambda(A)$ is called the "effective" conicity while Δ_1 and a_1 are generally combined to form what is commonly called the "gravitational" stiffness term, i.e.,

$$w\left[\phi + \frac{\delta_L - \delta_R}{2}\right] \approx w\left[\frac{a_1}{a} + \frac{\Delta_1}{a}\right] y \qquad (3\text{-}18)$$

$$\approx K_g(A)\, y$$

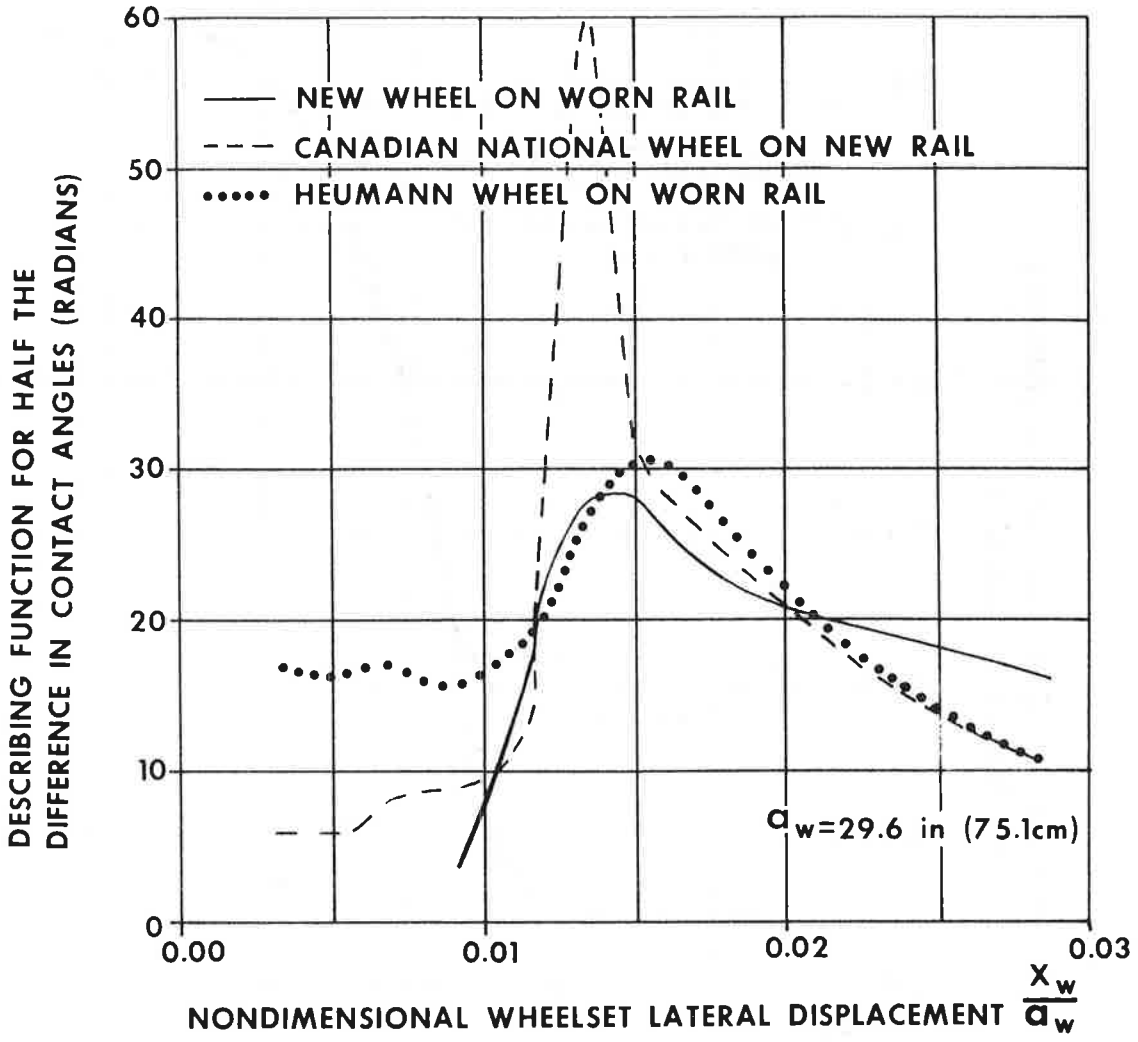

FIGURE 3-6. D.F. FOR HALF THE DIFFERENCE IN CONTACT ANGLES

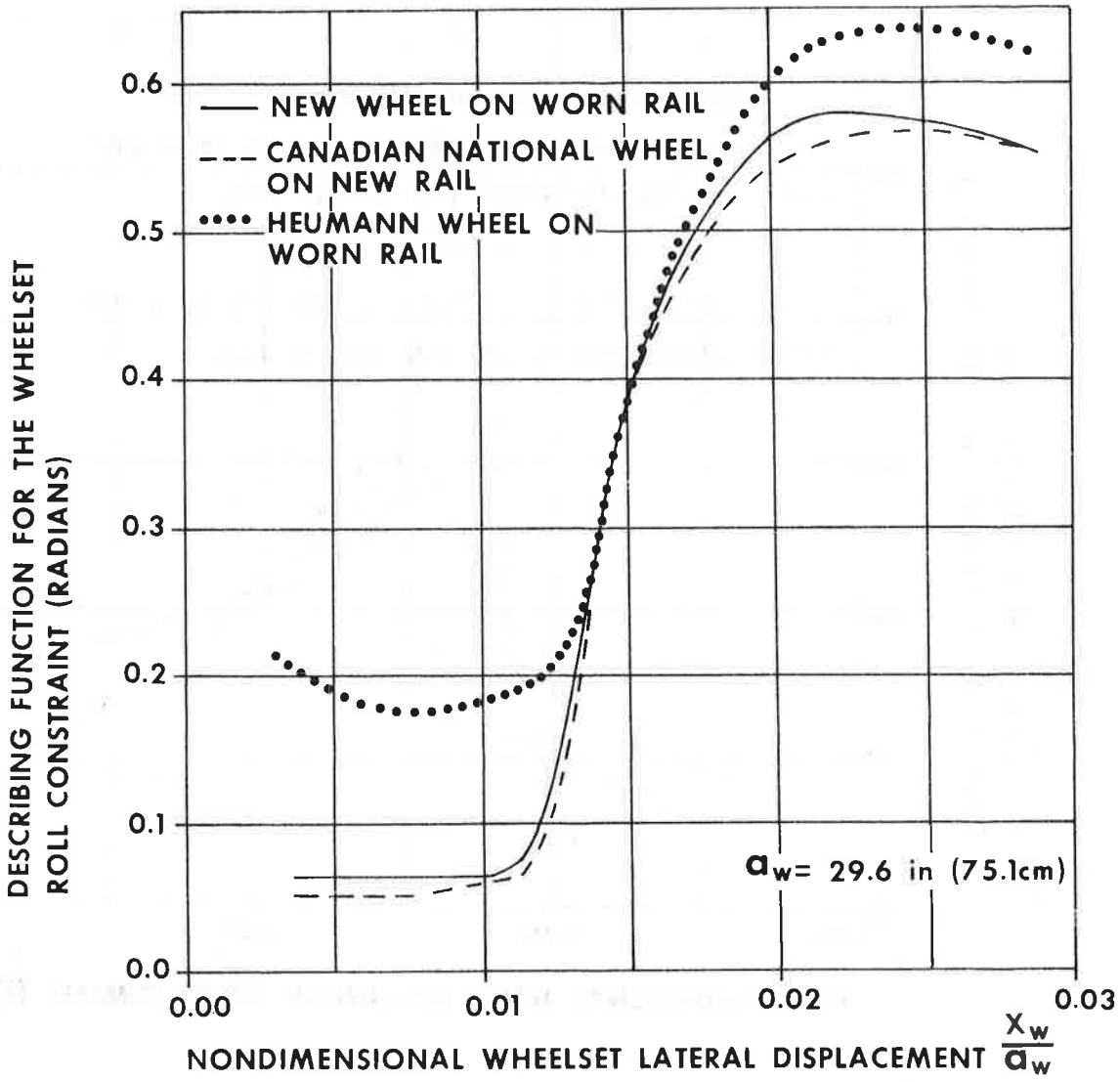

FIGURE 3-7. D.F. FOR THE WHEELSET ROLL CONTRAINT

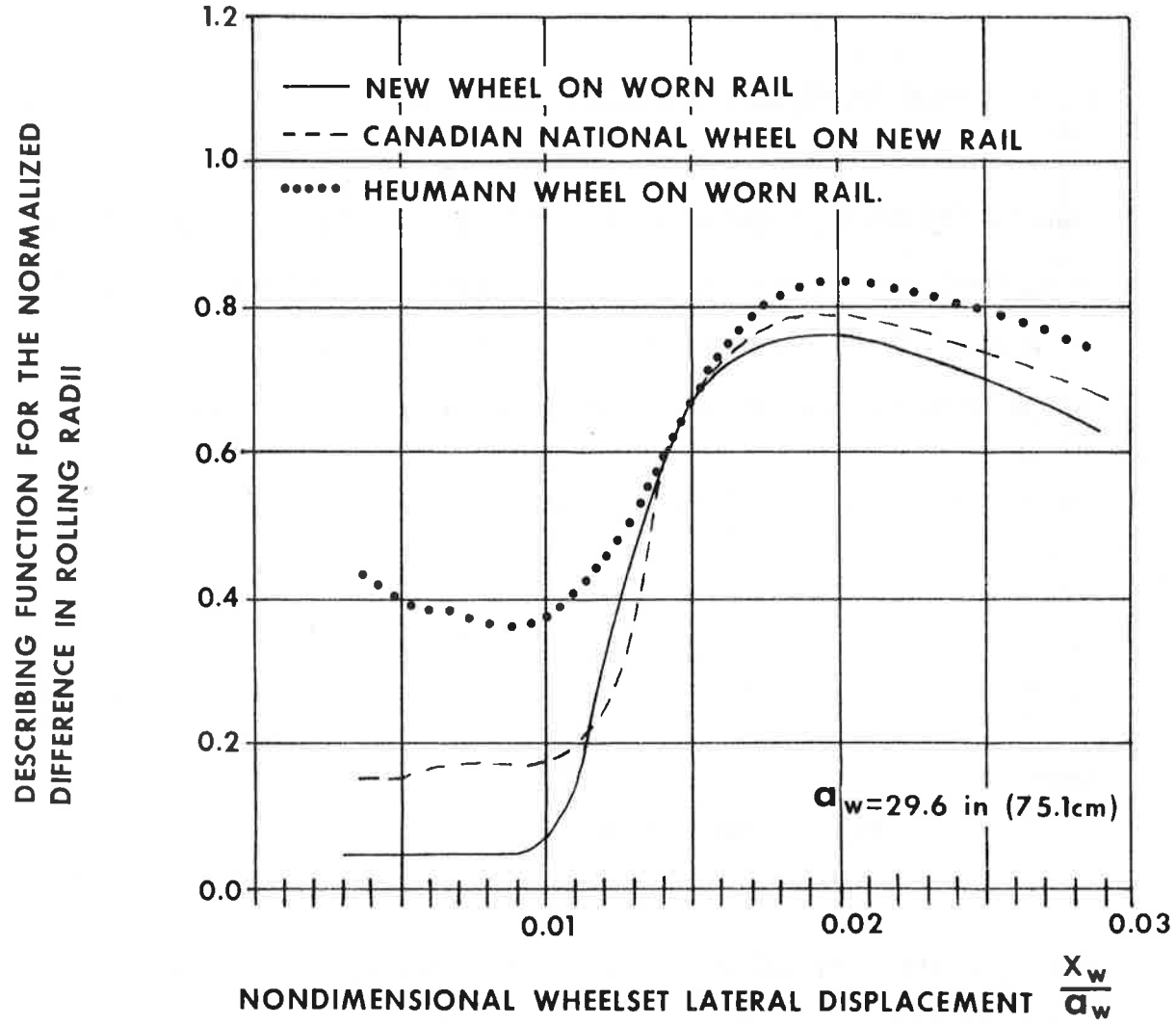

FIGURE 3-8. D.F. FOR THE NORMALIZED DIFFERENCE IN ROLLING RADII

or

$$K_g(A) \triangleq \frac{W}{a}[a_1(A) + \Delta_1(A)]. \qquad (3\text{-}19)$$

3.2.8 Random Input Describing Functions

Track irregularities such as surface, cross-level, and alignment are typically modeled as statistical variables. In general these irregularities are modeled [29] as stationary Gaussian processes. If we assume that x(t) in Figure 3-1 is a Gaussian random variable then the describing function gain given by equation (3-3) becomes:

$$K = \frac{\overline{xf(x)}}{\overline{x^2}}$$

$$\overline{xf(x)} = \int_{-\infty}^{\infty} xf(x)p(x)\,dx \qquad (3\text{-}20)$$

where

$$p(\ ) = \frac{1}{\sqrt{2\pi}\,\sigma_x}\, e^{\frac{-x^2}{2\sigma_x^2}}$$

and σ_x is the standard deviation of the Gaussian distribution. The averaging process defined by equation (3-20) becomes:

$$\overline{x\ f(x)} = \int_{-\infty}^{\infty} x\ f(x)\ p(x)\ dx = \int_{-\infty}^{\infty} \frac{x\ f(x)\ e^{\frac{-x^2}{2\sigma_x^2}}}{\sqrt{\pi 2}\ \sigma_x} \qquad (3\text{-}21)$$

$$\overline{x^2} = \int_{-\infty}^{\infty} \frac{x^2 \, e^{-x^2/2\sigma_x^2}}{\sqrt{2\pi}\ \sigma_x} \, dx = \sigma_x^2 \qquad (3\text{-}22)$$

Thus equation (3-3) becomes

$$K = \frac{1}{\sqrt{2\pi}\ \sigma_x} \int_{-\infty}^{\infty} x\, f(x)\, e^{-x^2/2\sigma_x^2} \, dx \qquad (3\text{-}23)$$

Equation (3-23) defines the statistical describing function gain for any single input-single output nonlinearity whose input is a zero mean Gaussian random variable. References [25, 26, 27, 28] establish the theoretical foundations for statistical describing functions and derive numerous examples using equation (3-23). Equation (3-23) can be used to calculate the random input describing function gains as a function of the input standard deviation for the common nonlinearities that appear in rail vehicle dynamics.

3.2.9 Deadband Spring (Figure 2-2)

$$f_{D.B.}(x) \approx K_{D.B.}\ x \qquad (3\text{-}24)$$

$$K_{D.B.} = K_R \left[1 - \text{erf}\left(\frac{\delta}{\sqrt{2}\ \sigma_x}\right)\right] \qquad (3\text{-}25)$$

where erf( ) is the well known error function and is tabulated in most mathematical handbooks.

Figure 3-9 shows equation (3-25) graphically.

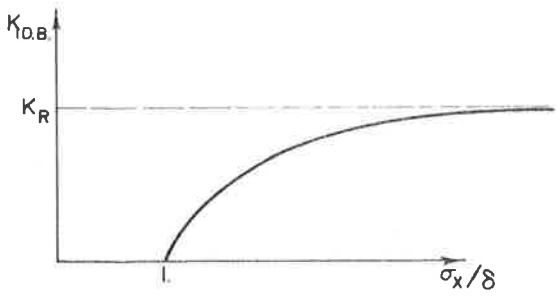

FIGURE 3-9. D.F. FOR A DEADBAND RAIL SPRING

3.2.10 Hardening or Softening Springs (Figure 2-3)

$$f_{H/S}(x) \approx K_{H/S}\, X \tag{3-26}$$

$$K_{H/S} = K_1 + (K_2 - K_1)\left[1 - \text{erf}\left(\frac{\delta}{\sqrt{2}\,\sigma_x}\right)\right] \tag{3-27}$$

Figure 3-10 shows equation (3-27) graphically.

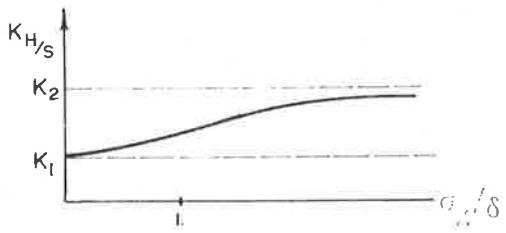

FIGURE 3-10. D.F. FOR A HARDENING/SOFTENING SPRING

3.2.11 Coulomb or Dry Friction (Figure 2-4)

$$f_c(\dot{x}) \approx C_c \dot{x} \tag{3-28}$$

where $C_c = \dfrac{\sqrt{2/\pi}\ F_o}{\sigma_{\dot{x}}}$, as shown in Figure 3-11.

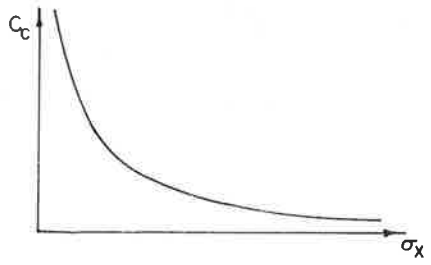

FIGURE 3-11. D.F. GAIN FOR COULOMB FRICTION

3.2.12 Parallel Spring-Dry Friction Combination

$$F_s = K_s x + F_o \operatorname{sgn}(\dot{x}) \tag{3-29}$$

$$F_s \approx K_s x + \frac{\sqrt{2/\pi}\ F_o}{\sigma_{\dot{x}}} \dot{x} . \tag{3-30}$$

3.2.13 Series Spring-Dry Friction Combination (Figure 2-6)

The series spring-dry friction combination is more difficult to describe for a random input describing function due to its hysteretic force-displacement relationship (Figure 2-6). This hysteresis

effect can be eliminated by employing an additional coordinate as shown in Figure 3-12 where the yaw suspension has been modeled with $_{o}$ the breakaway angle and K the rotational stiffness.

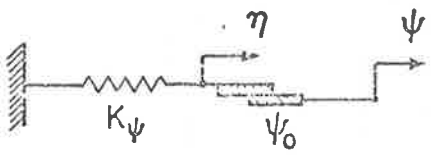

FIGURE 3-12. SERIES SPRING-DRY FRICTION ELEMENT

$$M_{\psi s} = K_{\psi} (\psi - \eta) \tag{3-31}$$

By equating this to the moment across the coulomb element we have:

$$M_{\psi s} = K_{\psi} \psi_o \text{ sgn } (\dot{\eta}) \tag{3-32}$$

Eliminating η from (3-31) and (3-32) one obtains:

$$M_{\psi s} = K_{\psi} \psi_o \text{ sgn}(\dot{\psi}_w - \frac{\dot{M}_{\psi s}}{K_{\psi}}) \cdot \tag{3-33}$$

It is extremely important to take account of <u>casuality</u> <u>before</u> we quasi-linearize equation (3-33), i.e., the moment across the spring determines the velocity across the damper, thus we need to express (3-33) as,

$$\dot{\psi} - \frac{M_{\psi s}}{K_{\psi}} = \text{sgn}^{-1} \left(\frac{M_{\psi s}}{K_{\psi}\psi_o}\right) \tag{3-34}$$

where sgn^{-1} is the inverse sgn function shown in Figure 3-13.

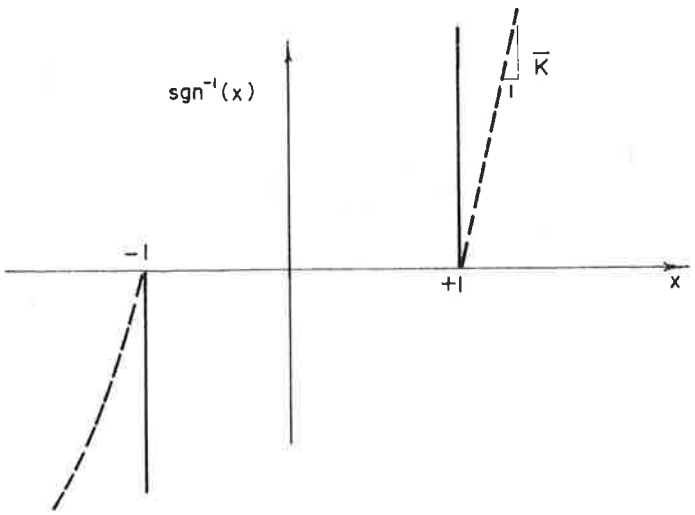

FIGURE 3-13. sgn^{-1} FUNCTION AND ITS APPROXIMATION

The slope of the $sgn^{-1}(x)$ function should be infinite at $x = \pm 1$ but can be approximated numerically by a finite $\bar{K}$. The approximate sgn^{-1} function has the same form as a deadband spring and its statistical describing function can be found in many standard texts [25]., i.e.,

$$sgn^{-1}\left(\frac{M_{\psi s}}{K_{\psi}\psi_o}\right) \approx \bar{K}\left[1 - \text{erf}\left(\frac{K_{\psi}\psi_o}{\sqrt{2}\,\sigma_{M_{\psi s}}}\right)\right] \cdot \frac{M_{\psi s}}{K_{\psi}\psi_o} \qquad (3\text{-}35)$$

where $\bar{K} \approx 2$, erf is the "error function" and is tabulated [25], and

$\sigma_{M\psi_s}$ is the rms value of $M\psi_s$. Thus (2-36) can be quasi-linearized as

$$\dot{\psi} - \frac{\dot{M}_{\psi s}}{K_\psi} \approx \bar{K}\left[1 - \operatorname{erf}\left(\frac{K_\psi \psi_o}{\sqrt{2}\,\sigma_{M_{\psi s}}}\right)\right] \cdot \frac{M_{\psi s}}{K_\psi \psi_o} \quad (3\text{-}36)$$

Summarizing, the yaw moment, $M_{\psi s}$, is defined by a quasi-linear differential equation:

$$\dot{M}_{\psi s} + \frac{\bar{K}}{\psi_o}\left[1 - \operatorname{erf}\left(\frac{K_\psi \psi_o}{\sqrt{2}\,\sigma_{M_{\psi s}}}\right)\right] M_{\psi s} = K_\psi \dot{\psi}. \quad (3\text{-}37)$$

3.2.14 Wheel/Rail Geometry Nonlinearities

The same approach to finding the random input describing function gains as was used for the sinusoidal input case can be used by changing equations (3-15 to 3-17) to:

$$\lambda(\sigma_x) = \frac{1}{\sqrt{2\pi}\,\sigma_x} \int_{-\infty}^{\infty} x \frac{(r(x) - r_R(x))}{2} e^{\frac{-x^2}{2\sigma_x^2}} dx \quad (3\text{-}38)$$

$$\Delta(\sigma_x) = \frac{1\,a}{\sqrt{2\pi}\,\sigma_x} \int_{-\infty}^{\infty} x \frac{(\delta_L(x) - \delta_R(x))}{2} e^{\frac{-x^2}{2\sigma_x^2}} dx \quad (3\text{-}39)$$

$$a_1(\sigma_x) = \frac{a}{\sqrt{2\pi}\,\sigma_x} \int_{-\infty}^{\infty} x\,\phi(x)\, e^{\frac{-x^2}{2\sigma_x^2}} dx. \quad (3\text{-}40)$$

The gravitational stiffness is defined by:

$$K_g(\sigma_x) = \frac{W}{a}\left[a_1(\sigma_x) + \Delta_1(\sigma_x)\right] . \qquad (3\text{-}41)$$

An example of these describing function gains are shown in Figures 3-14 and 3-15.

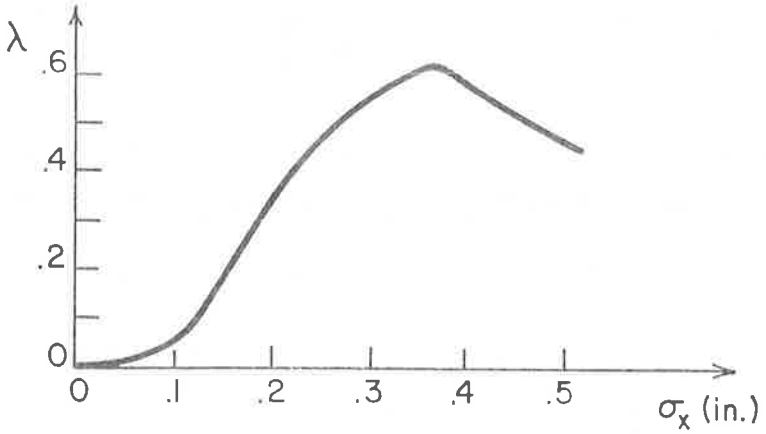

FIGURE 3-14. EFFECTIVE CONICITY D.F. FOR A NEW WHEEL ON WORN RAIL

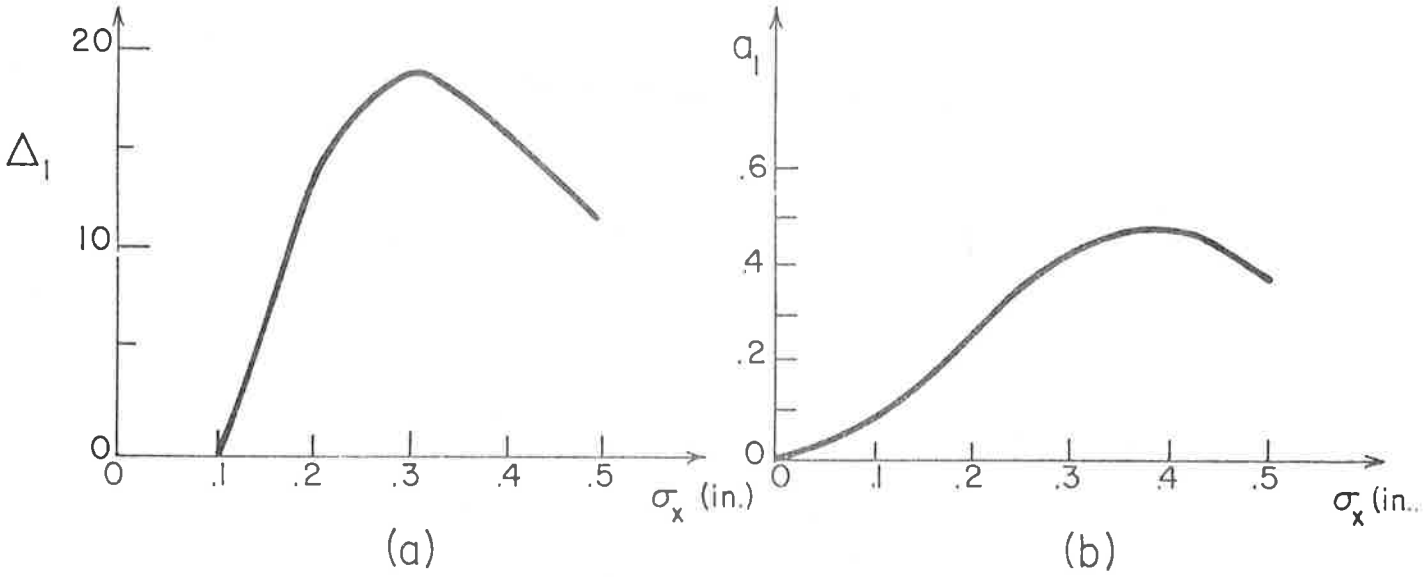

FIGURE 3-15. D.F.'s FOR HALF THE DIFFERENCE IN CONTACT ANGLES AND THE WHEELSET ROLL ANGLE

3.3 THE SINUSOIDAL SINGLE-INPUT DESCRIBING FUNCTION (SIDF) METHOD

Historically, the original and most popular input is the single sinusoid. The work of Krylov and Bogoliubov [30], and Bogoluibov and Mitropolsky [31] introduced the method of averaging and form the basis for the

widely used K & B method. Although extremely useful for low order systems the K & B method does not lend itself to the analysis of higher order systems.

Around 1950 the concept of harmonic linearization was introduced by numerous people. Koehenburger [32] in the U.S. and Goldfarb [33] in Russia are generally given credit for the concept. The concept of harmonic linearization has evolved into what is commonly called the SIDF method, i.e., using the fundamental harmonic of the nonlinearity and neglecting the higher harmonics. Figure 3-16a shows a linear systems response to a sine wave input while Figure 3-16b shows the response of a nonlinear system.*

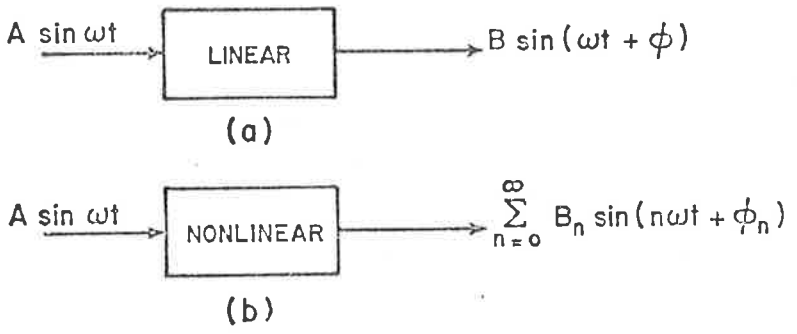

FIGURE 3-16. LINEAR AND NONLINEAR SINUSOIDAL RESPONSE

Figure 3-16b is the Fourier series representation of the periodic output.. If the nonlinearity is symmetric then the bias term, B_0, will be zero. The signal will then be composed of the fundamental harmonic, $B_1 \sin(\omega t+\phi_1)$, plus the higher harmonics, $B_2 \sin(2\omega t+\phi_2) +\ldots$. The single input describing function (SIDF) is defined to be the amplitude and phase of the first harmonic, i.e.,

* This assumes that the nonlinearity is such that the output is periodic and that subharmonics are not generated.

$$N \triangleq \frac{\text{Fundamental Harmonic}}{\text{Input Amplitude}} = \frac{B_1 e^{j\phi_1}}{A} . \qquad (3\text{-}42)$$

The complex describing function, N, can be evaluated by the single complex Fourier integral for the first harmonic [25],

$$N = \frac{1}{A} \int_{-\pi}^{\pi} f(\theta) e^{-j\theta} \, d\theta . \qquad (3\text{-}43)$$

In general N will be a function of A, the input amplitude, and ω, the input frequency. Figure 3-17 shows the quasi-linear system that is used to replace figure 3-16b. Note that the effect of the higher harmonics can be included by the remnant term.

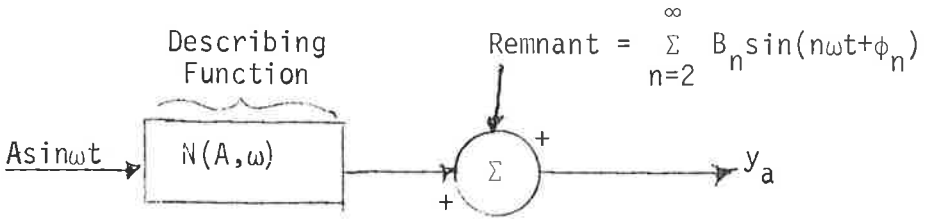

FIGURE 3-17. QUASI-LINEAR APPROXIMATOR PLUS REMNANT

If the rest of the system, of which figure 3-16b is part, is "predominantly" linear, i.e., there exists a great deal of filtering in the feedback path between the output of the nonlinearity and the input, then the remnant terms will be attenuated and "filtered out". Thus in general, the more filtering that occurs in the system the more the input signal will look like a sinusoid, Asinωt.

The SIDF can be used to predict the occurrence of free oscillation or limit cycles and also the forced sinusoidal response of nonlinear

systems in which all of the system variables are responding at a single frequency. Therefore, it is necessary that:

a) All transients have died out

b) There is no bias term in input or output

c) Any higher or lower harmonics generated by the

d) System nonlinearities are filtered out.

System conditions that help to insure that these requirements are satisfied are:

a) Symmetric nonlinearities

b) A "predominantly" linear system

c) No "sharp" resonant peaks in the linear portion

It is interesting to note that, as pointed out in [25], the minimum mean square error and fundamental harmonic approach yields precisely the same describing function, i.e.,

$$N = K = \frac{1}{A}\int_{-\pi}^{\pi} f(A\sin\theta)\sin\theta\, d\theta . \qquad (3\text{-}44)$$

Thus, the optimum quasi-linear gain is just the ratio of the fundamental harmonic to the input amplitude.

3.4 LIMIT CYCLE DETERMINATION

Nonlinear systems exhibit many phenomena [26] that do not occur in linear systems and which are of concern to the analyst. One of the most important of these phenomena is the limit cycle, a periodic self-sustained oscillation of fixed frequency and amplitude. Note that

this differs from an undamped linear oscillation whose amplitude is dependent on initial conditions. Limit cycles are usually undesirable and the control engineer designs the system so that they do not occur in the normal operating range. There are a few instances when limit cycles are used intentionally, e.g., in detector and oscillator circuits.

The sinusoidal SIDF is a very convenient analytical tool for predicting the amplitude and frequency of limit cycles for many systems. A first example of this method is the well known Rayleigh equation:

$$\ddot{y} - 2\zeta(1 - \alpha\dot{y}^2)\,\dot{y} + y = 0$$

or

$$\ddot{y} + 2\zeta\,\dot{y} - 2\zeta\alpha\,\dot{y}^3 + y = 0\,. \tag{3-45}$$

The sinusoidal SIDF for a cubic nonlinearity can be calculated using (3-44) or it can be found in numerous texts [25]:

$$\dot{y}^3 \approx \frac{3}{4} A^2\,\dot{y} \tag{3-46}$$

The right side of equation (3-46) is the describing function approximation for $\dot{y}^3$ when $\dot{y} = A\cos\omega t$. Substituting (3-46) into (3-47) yields:

$$\ddot{y} + 2\zeta\left(1 - \frac{\alpha 3A^2}{4}\right)\dot{y} + y = 0\,. \tag{3-47}$$

If it is assumed that $\dot{y} = A\cos\omega t$, equation (3-47) demands that:

$$\omega = 1$$
$$A = \sqrt{\frac{4}{3\alpha}}\,. \tag{3-48}$$

Therefore the SIDF modified predicts a limit cycle at a frequency of $\omega = 1$ and an amplitude of $A = \sqrt{\frac{4}{3\alpha}}$. Ref [28] shows that (3-48) is an excellent approximation for small ζ.

A limit cycle that occurs in a rail vehicle system is commonly called hunting. The forward speed of the vehicle at which hunting first occurs is commonly called the critical speed. SIDF method is a particularly useful tool for predicting the critical speed and the amplitude and frequency of the hunting motion.

Section 2 derived the equations of motion for the simple wheelset suspended from a fixed truck, moving at constant forward speed. It is easily shown from the linearized equations that if the wheelset were not suspended it would exhibit an undamped oscillation at all forward speeds at the kinematic frequency,

$$\omega = V \sqrt{\frac{\lambda}{a\, r_o}} \quad . \tag{3-49}$$

When the wheelset is suspended, the oscillations will damp out disturbances for forward speeds below a critical forward speed V_c, and oscillate at speeds above this value. The calculation of this critical speed at which "hunting" occurs is of paramount importance to the truck designer. In real rail vehicles there exist significant nonlinearities such as variations in the wheel/rail profile geometry, and coulomb friction in the suspension which complicate the analytical prediction of the critical speed.

First consider the nonlinear model of the wheelset with a stiff deadband spring to describe the effect of flanging (equations (2-15) - (2-16)) and the parallel and series spring/dry friction suspension.

The quasi-linear version of these equations obtained by substituting the appropriate describing functions in place of the nonlinearities are:

$$
\begin{aligned}
&M_w \ddot{y}_w + \frac{2f_{11}}{V}\dot{y}_w + \frac{w(\Delta_1 + a_1)}{a} y_w - 2 f_{11}\psi \\
&+ K_y y_w + \frac{4 F_o}{A\omega\pi}\dot{y}_w + K_{D.B.}(A) y_w = 0 \\
&I_w \ddot{\psi} + \frac{2 f_{33} a^2}{V}\dot{\psi} - w\delta_o a \psi + \frac{2 f_{33} a}{r_o}\lambda_o y_w \\
&+ K_s(B)\psi + C_s(B)\dot{\psi} = 0
\end{aligned}
\qquad (3\text{-}50)
$$

where the describing function gains $K_{D.B.}$, K_s, and C_s are defined by equations (3-6), (3-11b), and (3-11c) for a solution of the form, $y_\omega = A\sin\omega t$, $\theta_\omega = B\sin(\omega t + \phi_1)$. The quasi-linear equations (3-50), are placed in "state" form by defining the state vector,

$$
\underset{\sim}{x} = \begin{bmatrix} x_1 \\ x_2 \\ x_3 \\ x_4 \end{bmatrix}
$$

where $x_1 = y_w$, $x_2 = \dot{y}_w$, $x_3 = \psi$, $x_4 = \dot{\psi}$.

The state form of equations (3-50) is:

$$
\dot{\underset{\sim}{x}} = \tilde{\underset{\sim}{N}}\,\underset{\sim}{x} \qquad (3\text{-}51)
$$

where the 4x4 $\tilde{\underset{\sim}{N}}$ matrix contains various constants and D.F. gains.

The condition for an undamped oscillation to occur is:

$$
\underset{\sim}{x} = \underset{\sim}{X}\, e^{j\omega t} \qquad (3\text{-}52)
$$

where $\underset{\sim}{X}$ is a complex eigenvector corresponding to the undamped eigenvalue, ω. Substituting (3-52) into (3-51) yields:

$$\{j \underset{\sim}{\tilde{I}} - \underset{\sim}{\tilde{N}}\} \underset{\sim}{X} = 0 . \qquad (3\text{-}53)$$

A necessary condition for a nontrivial solution of (3-53) to exist is:

$$|j \underset{\sim}{\tilde{I}} - \underset{\sim}{\tilde{N}}| = 0 \qquad (3\text{-}54)$$

Equation (3-54) represents 2 nonlinear algebraic equations (real and imaginary parts) in terms of ω, A, and B since $\underset{\sim}{\tilde{N}}$ is a function of ω, A, and B. An additional independent equation can be obtained from equation (3-53). There are several numerical techniques that can be used to solve these nonlinear algebraic equations. A particularly efficient routine called LIMCY will be described in Section 4.

Typical numerical results for a wheelset based upon these computations are shown in Figure 3-18. Curve 1 represents the solution for a purely linear model, i.e., there exists a critical speed, independent of amplitude, below which oscillations decay and above which oscillations grow. Curve 2 represents the model described by equation (3-50) and clearly indicates the importance of including nonlinearities in the analysis. Notice that the speed at which hunting can occur is substantially below that predicted by the linear analysis and that the amplitude of the oscillation is a function of the forward speed. Curve 3 represents the results of a model that includes the realistic wheel/rail profile geometries described earlier. Note that the results of the realistic profile model are similar to the deadband spring

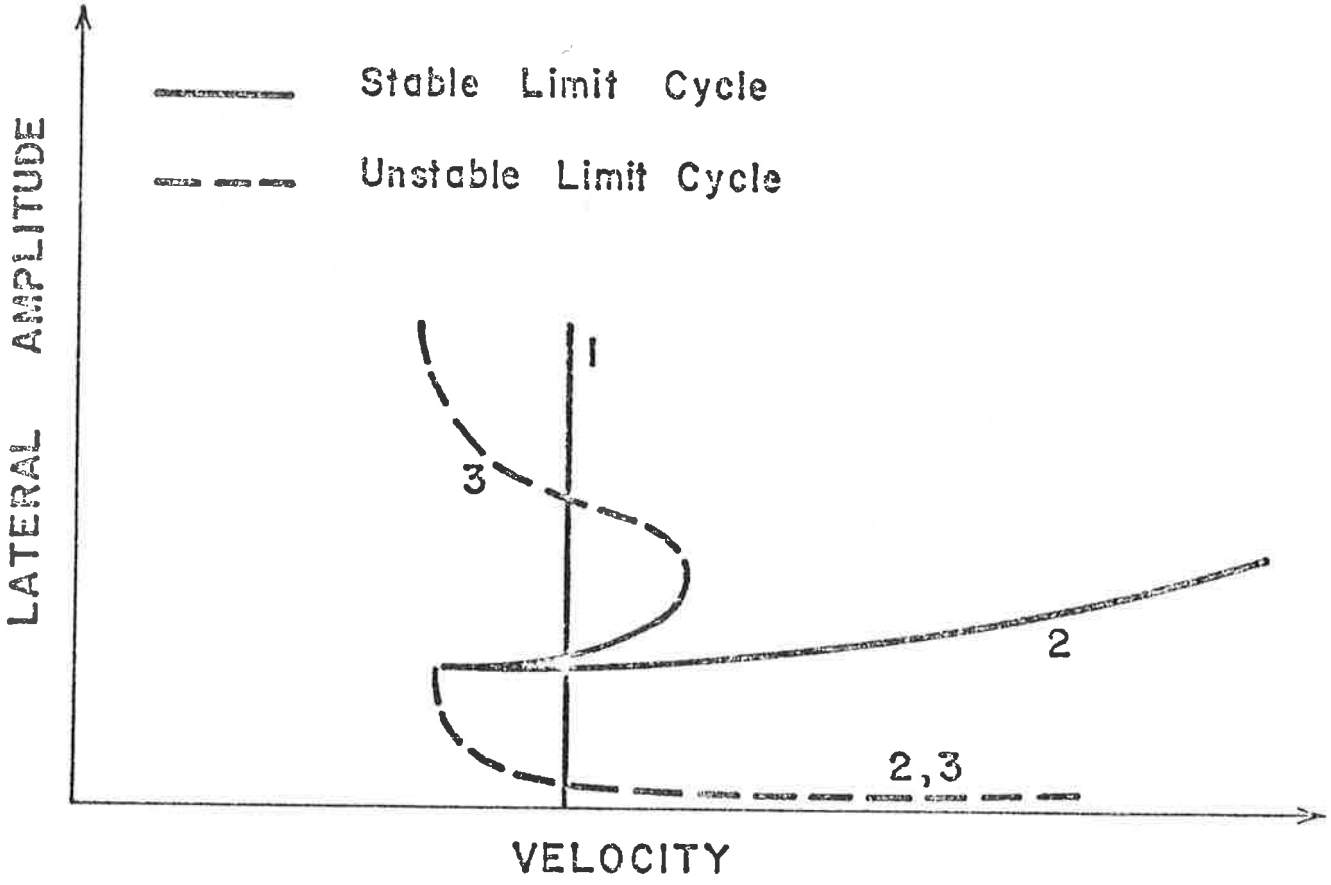

FIGURE 3-18. WHEELSET HUNTING BEHAVIOR

model at low amplitudes. However, at higher amplitudes (close to wheel climb) the flange cannot supply the required restoring force that the deadband spring model does.

It is clear from Figure 3-18 that the effect of the nonlinearities is very significant and must be included in rail vehicle hunting predictions.

3.5 FORCED RESPONSE USING THE SIDF

The SIDF is also a very useful analytical tool for predicting the forced sinusoidal response of a nonlinear system where subharmonics are substantially filtered out. The procedure outlined in [25,26,27,28] is basically to replace the nonlinearity with its SIDF and to proceed as if the system was linear. The added computation will involve an iterative solution at each frequency since the "transfer function" will be a function of the unknown amplitude. This procedure is best illustrated by a simple example. The equation of motion for a single degree of freedom mass with a linear viscous damper and a nonlinear spring forced by a sinusoidal applied force is:

$$m\ddot{x} + c\dot{x} + f(x) = F_o \sin\omega t \qquad (3\text{-}55)$$

where we will let $f(x) = Kx + \beta x^3$, $\beta > 0$ represents a "hardening" spring and $\beta < 0$ represents a "softening" spring.

The SIDF for a cubic nonlinearity is:

$$x^3 \approx \frac{3}{4} A^2 x \qquad (3\text{-}56)$$

where we have assumed that $x = A\sin(\omega t + \phi)$. Substituting (3-56) into (3-55) and computing the transfer function between the input and output yields:

$$|H(j\omega)| = \frac{A}{F_o} \quad \sqrt{\frac{1}{(K + \frac{3}{4} A^2 \beta - m\omega^2)^2 + \omega^2 c^2}} \quad . \qquad (3\text{-}57)$$

Equation (3-57) represents a nonlinear algebraic equation for A as a function of F_o, i.e., the amplitude ratio $\frac{A}{F_o}$ is a function of F_o. Typical results for a softening spring ($\beta<0$) are shown in Figure 3-19.

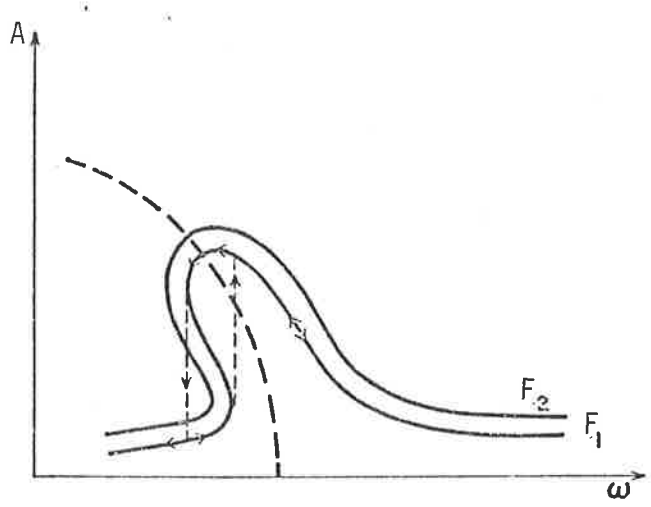

FIGURE 3-19. SOFTENING SPRING-MASS-DAMPER FREQUENCY RESPONSE

Figure 3-19 also illustrates a nonlinear phenomena known as "jump resonance" [28]. The first curve in Figure 3-19 was computed for an input value of F_{o_1}; if we follow this curve starting at low frequencies and gradually increase the forcing frequency, ω, we proceed to the right until we reach the point of infinite slope at which point there occurs a sudden jump in output amplitude. If we had started at high frequencies and had reduced the forcing frequencies gradually we would have proceeded to the left until the infinite slope point was reached and the response would have jumped down discontinuously.

The accuracy of the SIDF approach in computing the forced sinusoidal response is strongly dependent upon the nature and location of the nonlinearities. A rigorous and quantitative description of the amount of filtering required is not available at present.

The application of the SIDF to predict the forced sinusoidal response of rail vehicles is discussed in detail in Section 6. A simple wheelset example will be discussed here to illustrate the technique.

The quasi-linearized equation of motion of a rail vehicle can be placed in the following form:

$$\dot{\underset{\sim}{x}} = \tilde{\underset{\sim}{N}}_1 \, x + \underset{\sim}{N}_2 \, u \qquad (3\text{-}58)$$

where x is an nxl vector, $\tilde{\underset{\sim}{N}}_1$ is a nxn D.F. matrix and $\underset{\sim}{N}_2$ is a 4xl D.F. vector. u has been assumed for simplicity to be a scalar. Since we are looking for the steady-state sinusoidal response we let, $u = \bar{u}\, e^{j\omega t}$, and $\underset{\sim}{x} = \underset{\sim}{X}\, e^{j\omega t}$ where $\bar{u}$ is the input amplitude, $\underset{\sim}{X}$ is the complex response vector, and ω is the forcing frequency. Substituting these expressions into (3-58) yields:

$$\underset{\sim}{X} = (j\omega I - \tilde{\underset{\sim}{N}}_1)^{-1} \, \underset{\sim}{N}_2 \, \bar{u} \qquad (3\text{-}59)$$

Equation (3-62)represents a set of nonlinear algebraic equations (since $\tilde{\underset{\sim}{N}}_1$, and $\tilde{\underset{\sim}{N}}_2$ are both functions of ω, and X) that can be solved numerically. Typical results for a two degree of freedom wheelset with nonlinear contact geometry and nonlinear suspension (equations (2-17) - 2-18)) are shown for a wheelset with the Heumann wheel profile in figure 3-20.

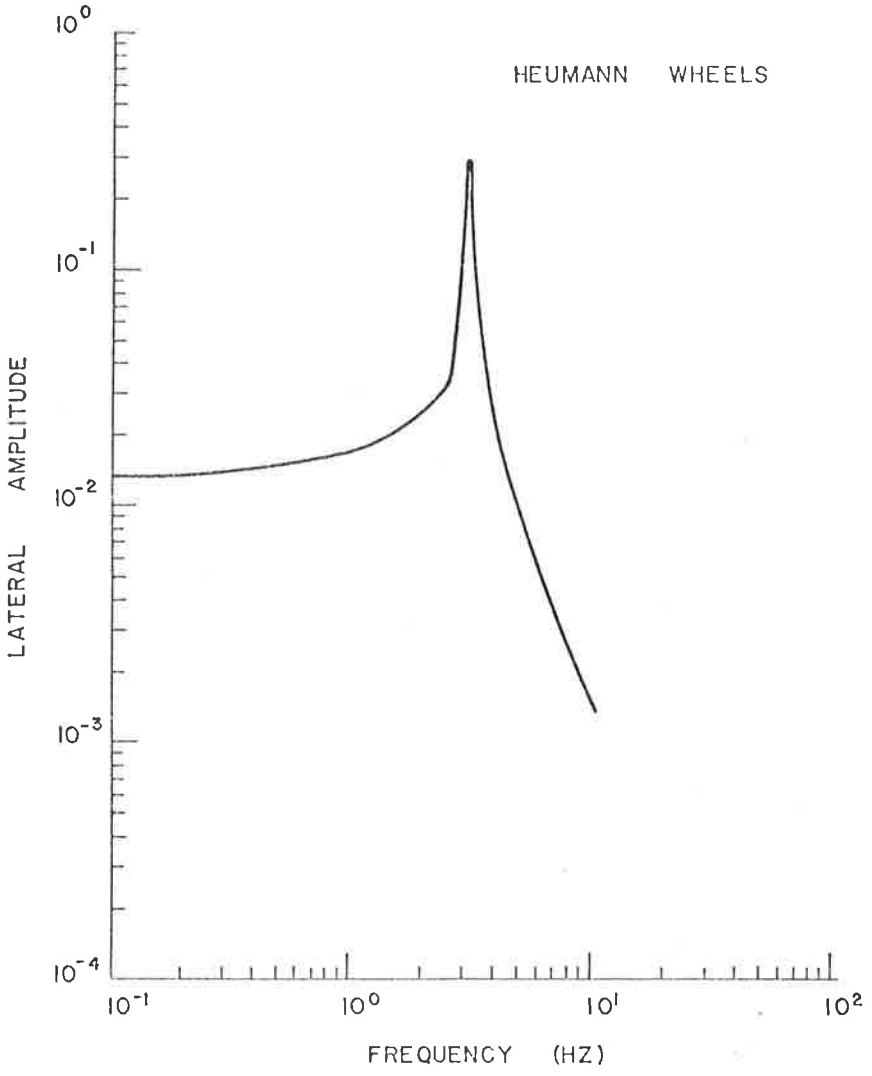

FIGURE 3-20. WHEELSET SINUSOIDAL RESPONSE USING D.F.'S

3.6 A GENERAL METHOD FOR SINGLY PERIODIC SYSTEMS

The describing function approach is not limited to the SIDF method. Fig. 3.20 shows that the input signal to the nonlinearity can be a sum of input signals. Some of the multi-input describing functions that have been described in the literature [25,26,27,28] are the dual input describing function (bias + sinusoid) and the two sinusoid

describing function. This section describes a general approach for an arbitrary number of sinusoids that are harmonically related, i.e., singly periodic systems.

We will assume that the nonlinear equations of motion can be expressed as:

$$\ddot{\underset{\sim}{x}} = g(\underset{\sim}{x}, \dot{\underset{\sim}{x}}, u(t)) \tag{3-60}$$

where $u(t)$ is a scalar, $u_o \sin\omega t$. If we assume that the system responds with a single period, T, then the Fourier expansion of $x(t)$ can be expressed as:

$$\underset{\sim}{x}(t) = \sum_{n=0}^{\infty} \underset{\sim}{X}_n e^{jn\omega t} \tag{3-61}$$

and $\underset{\sim}{g}(t)$ can be expressed as:

$$\underset{\sim}{g}(t) = \sum_{n=0}^{\infty} \underset{\sim}{G}_n e^{jn\omega t} \tag{3-62}$$

where $\underset{\sim}{X}_n$ and $\underset{\sim}{G}_n$ are complex Fourier coefficients and $\omega = 2\pi/T$. The Fourier coefficients of $\underset{\sim}{g}(t)$ can be expressed as:

$$\underset{\sim}{G}_n = \frac{1}{2\pi} \int_0^{2\pi} \underset{\sim}{g}(\omega t) e^{jn\omega t} \, d(\omega t) \, . \tag{3-63}$$

If we substitute (3-61) and (3-62) into (3-60) we have:

$$\sum_{n=0}^{\infty} - (n\omega)^2 \underset{\sim}{X}_n = \sum_{n=0}^{\infty} \underset{\sim}{G}_n \, . \tag{3-64}$$

Taking advantage of the orthogonality property of a Fourier series we can write:

$$
\begin{aligned}
\underset{\sim}{G}_o &= 0 \\
\underset{\sim}{G}_1 &= -\omega^2 \underset{\sim}{X}_1 \\
\underset{\sim}{G}_2 &= -(2\omega)^2 \underset{\sim}{X}_2 \\
&\vdots \\
\underset{\sim}{G}_n &= -(n\omega)^2 \underset{\sim}{X}_n
\end{aligned}
\qquad (3\text{-}65)
$$

In any particular problem the analyst must decide how many terms of the Fourier series he needs for the desired accuracy, i.e., how large should n be. If the amplitudes of the position variables are sought then rearranging the last equation yields:

$$
\underset{\sim}{X}_n = -\frac{1}{(n\omega)^2} \underset{\sim}{G}_n \; . \qquad (3\text{-}66)
$$

Thus the consecutive harmonic amplitudes are decreased by a factor of $\frac{1}{(n\omega)^2}$; if an estimate of $\underset{\sim}{G}_n$ is made, then the importance of $\underset{\sim}{X}_n$ can be determined.

The ease of this method is determined by the computation of the describing functions (equation (3-63)) and the algebraic solution of equations (3-65). The first expression represents n algebraic equations for the bias terms while each succeeding expression represents 2n algebraic equations since $\underset{\sim}{G}_n$ and $\underset{\sim}{X}_n$ are complex.

It is interesting to note that the SIDF is just n=1 with the implicit assumption that $\underset{\sim}{X}_o = 0$. The dual input describing function is n=1 with $\underset{\sim}{X}_o \neq 0$, and the two sinusoid input describing function is any two of equation (3-65) as long as the periods of the two sinusoids are integrally related.*

* The case of two non-integrally related sinusoids is treated in [25]

3.7 Freight Car Rock and Roll

As in the previous cases this method is best illustrated by a practical example. Figure 2-8 shows a cross-section of a typical freight car. The freight car responds to periodic cross-level (difference in elevation between the rails) inputs, as might be induced by the staggered 39 feet rail joints, with a periodic 'rock and roll' motion. At certain critical or resonant speeds the motion can become dangerous with high roll amplitude, and wheel lift. Nonlinear digital simulations [10, 8] have been used but are costly to run parametric studies with.

The general describing function approach was applied to this problem to take advantage of the "quasi-linear" computational advantages. Figure 2-9 shows the simplified model used in this study [10] which included nonlinear springs to model the center plate, side bearings, and rail spring as well as coulomb friction. These nonlinear force expressions are shown in Figure 2-10. The centerplate is modeled as a very stiff compression spring with no tension; the rail is modeled similarily; the side bearings are similar except that a deadzone is required to account for the clearance at equilibrium.

The number of harmonics needed (number of terms in equation (3-65)) was determined by observing a few digital simulations and noticing that a bias, the fundamental frequency, and the second harmonic were clearly evident. Thus the first three terms (n=2) were used in this analysis, i.e.,

$$\begin{aligned} \underset{\sim}{G}_0 &= 0 \\ \underset{\sim}{G}_1 &= -\omega^2 \underset{\sim}{X}_1 \\ \underset{\sim}{G}_2 &= -(2\omega)^2 \underset{\sim}{X}_2 \end{aligned} \qquad (3\text{-}67)$$

The model employed had six degrees of freedom; thus equations (3-67) represents thirty (6+12+12) nonlinear algebraic equations. In order to reduce this number, the symmetry properties of the freight car were exploited, i.e., all of the nonlinearities occur in symmetric pairs about a vertical centerline; thus the thirty equations can be reduced to fifteen. The fifteen independent scalar equations require the first three Fourier coefficients for each force. All of the nonlinearities are piecewise linear, hence the required integrations to compute the coefficients can be performed analytically once the zero crossings are known. Thus the solution of the freight car steady state rock and roll response to sinusoidal cross level inputs involves two major subtasks:

1) Evaluation of appropriate Fourier coefficients for the nonlinear forces.
2) Solution of a set of fifteen nonlinear algebraic equations.

A particularly efficient root solving algorithm developed by Powell [39] was used to solve the nonlinear equations.

Figure (3-21) shows the numerical results for three values of rail cross-level input amplitude. Note how the jump resonance phenomena is present. This can be very important from a safety point of view.

The utility of this quasi-linear approach depends upon a comparison between numerical integration and the solution of nonlinear algebraic equations. Experience to date indicates that the quasi-linear methods allows greater computer time saving in the generation of parametric steady-state solutions. The numerical procedures required converge extremely rapidly when a good initial guess is available, as is the case when a parameter variation is being made.

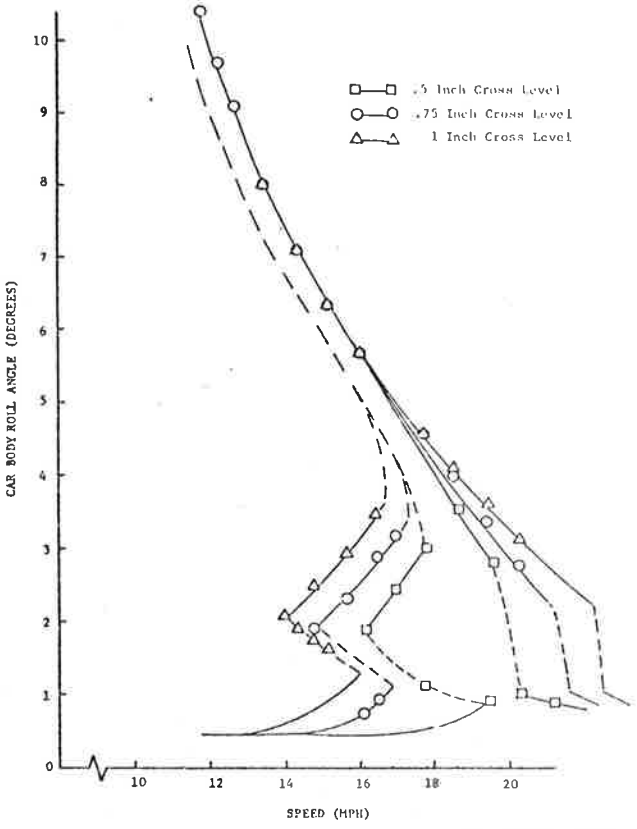

FIGURE 3-21. CAR BODY ROLL ANGLE FOR 70 TON CAR OBTAINED FROM A DESCRIBING FUNCTION ANALYSIS

3.8 FORCED RANDOM RESPONSE ANALYSIS

This section describes the application of quasi-linearization to predict the statistical response of nonlinear systems. The concept of statistical linearization was approached by several investigators in the early 1950's (Booton [40], West [41], Kazakov [42] and Sawaragi [44]). There were a number of different techniques proposed for the selection of the quasi-linear gain. The most popular technique is to minimize the mean squared error between the nonlinearity and its approximator as was outlined earlier (equation (3-2)). Two different approaches to this task are: 1) equate the mean square value of the nonlinearity with the output of its approximator, and 2) match as closely as possible the two autocorrelation functions. Smith's study [43] comparing these different approaches concluded that all of the methods were very similar in their accuracy. The minimum mean squared error approach is in general computationally easier and has been used more frequently.

As was stated earlier, when quasi-linearization is used the form of the signal at the input to the nonlinearity must be known or assumed. Some authors [45,46] have proposed using the exact probability density function rather than an assumed Gaussian one. This has been shown to yield more accurate results for those systems where the statistics of the input to the nonlinearity can be computed. However, for high order systems with multiple nonlinearities this is a very difficult task.

Statistical linearization has been used to predict the response of nonlinear systems to stationary and non-stationary Gaussian inputs. In stationary systems the quantities desired are, in general, the variances

and spectral densities of the output variables. In non-stationary systems the time-varying rms values are sought. For stationary systems both time domain [48] and frequency domain methods [25,26,27,44] have been used while time domain methods [47 , 48] are used for non-stationary systems. This report will concentrate on the stationary response of nonlinear systems.*

3.8.1 Frequency Domain Methods

A few simple examples will help to illustrate this method of analysis. The normalized equation of motion for a mass, viscous damper, and nonlinear spring is given by equation (3-68), where the forcing function is a stationary Gaussian white noise process:

$$\ddot{x} + 2\xi\dot{x} + x(1 + \mu x^2) = w(t) \qquad (3\text{-}68)$$

where,

$$E[w(t)] = 0,\ E[w(t)w(t-\tau)] = q\delta(\tau). \qquad (3\text{-}69)$$

Ref. [49] provides a very nice comparison of three methods of determining the rms value of x. The first is the Fokker-Planck-Kolmogorov method that yields, for this simple problem, the exact solution since the probability density function of x can be found. The second is the statistical linearization and the third is the method of Wiener.

The statistical describing function for a cubic nonlinearity can be found from equation (3-23) or from standard texts [25,26,27]; the result is:

$$x^3 \approx 3\sigma_x^2\, x\ . \qquad (3\text{-}70)$$

*Ref. [47] provides a tutorial paper on the use of describing functions for nonstationary nonlinear systems.

Substituting (3-70) into (3-69) yields:

$$\ddot{x} + 2\xi\dot{x} + (1 + \mu 3\sigma_x^2)x = w(t) \qquad (3\text{-}71)$$

The transfer function between x and w is:

$$H(j\omega) = \frac{1}{(1 + 3\mu\sigma_x^2 - \omega^2) + j2\xi\omega} \qquad (3\text{-}72)$$

The rms value of a stationary random process can be found by integrating the power spectral density function, i.e.,

$$S_x(\omega) = |H(j\omega)|^2 \frac{q}{2\pi} \qquad (3\text{-}73)$$

$$\sigma_x^2 = \frac{q}{2\pi} \int_0^\infty |H(j\omega)|^2 \, d\omega \, . \qquad (3\text{-}74)$$

Tables of integrals for equation (3-74) for typical $H(j\omega)$ are available [25], The result is :

$$\sigma_x^2 = \frac{q}{4\xi(1 + 3\mu\sigma_x^2)} \, . \qquad (3\text{-}75)$$

Solving for σ_x^2 ($\mu \neq 0$) yields:

$$\sigma_x^2 = \frac{-1 + \sqrt{1 + \frac{3\mu q}{\xi}}}{6\mu} \qquad (3\text{-}76)$$

Reference [49] shows a plot of how the statistical linearization result compares with the exact solution. Figure 3-22 is adapted from this reference.

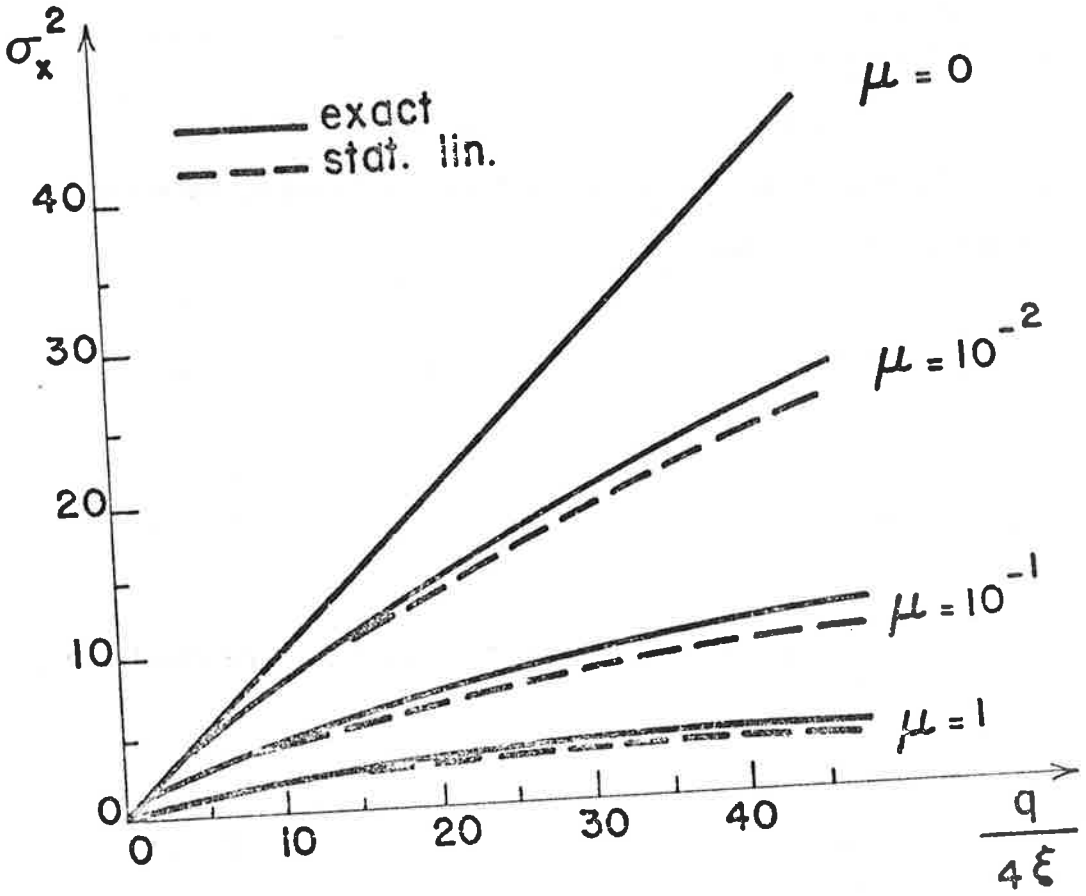

FIGURE 3-22. A COMPARISON OF STATISTICAL LINEARIZATION WITH AN EXACT SOLUTION

Figure 3-22 shows that the error increases as the relative strength of the nonlinearity increases (μ), as the white noise signals strength increases (q), and as the damping decreases. It is surprising how good the results are even for the worst cases, e.g., for $\mu = .1$ and $q/4\xi = 45$. The error is about 10 percent. Thus, even for a second order system that has very little filtering the results are quite good.

3.8.2 State Space Method

The rms values for this system cam also be comptued using state variable methods [48]. A linear system forced with white noise can be placed in the following form:

$$\dot{\underset{\sim}{x}} = \tilde{\underset{\sim}{A}}\, \underset{\sim}{x} + \tilde{\underset{\sim}{\Gamma}}\, \underset{\sim}{w}(t) \tag{3-77}$$

where, $E[\underset{\sim}{w}(t)\underset{\sim}{w}^T(t-\tau)] = \tilde{\underset{\sim}{Q}}\, \delta(\tau)$

$E[\underset{\sim}{w}(t)] = 0.$

The covariance matrix is defined to be, $\bar{\underset{\sim}{X}} \triangleq E[\underset{\sim}{x}\, \underset{\sim}{x}^T]$. The diagonal elements of the covariance matrix are the variances of the state variables. If $\underset{\sim}{w}(t)$ is a stationary Gaussian random vector, the steady state covariance matrix can be found from the following linear matrix equation [48]:

$$0 = \tilde{\underset{\sim}{A}}\, \bar{\underset{\sim}{X}} + \bar{\underset{\sim}{X}}\, \tilde{\underset{\sim}{A}}^T + \tilde{\underset{\sim}{\Gamma}}\, \tilde{\underset{\sim}{Q}}\, \tilde{\underset{\sim}{\Gamma}}^T. \tag{3-78}$$

Thus the mean square values of the state variables can be found by solving for the diagonal elements of (3-78).

For a nonlinear system forced with Gaussian white noise the quasi-linearized equations can be placed in a form similar to (3-77):

$$\dot{\underset{\sim}{x}} = \tilde{\underset{\sim}{N}}\, \underset{\sim}{x} + \tilde{\underset{\sim}{\Gamma}}\, \underset{\sim}{w}\,(t) \tag{3-79}$$

where $\tilde{\underset{\sim}{N}}$, and $\tilde{\underset{\sim}{\Gamma}}$ matrices may contain describing function gains. Since the D.F. gains are a function of the rms values of the states, we have that $\tilde{\underset{\sim}{N}} = \tilde{\underset{\sim}{N}}(\underline{\bar{X}})$, and $\tilde{\underset{\sim}{\Gamma}} = \tilde{\underset{\sim}{\Gamma}}(\underline{\bar{X}})$. Using the same approach that we did for the linear system the steady-state covariance matrix of the quasi-linear system can be found from:

$$0 = \tilde{\underset{\sim}{N}}\, \underline{\bar{X}} + \underline{\bar{X}}\, \tilde{\underset{\sim}{N}}^T + \tilde{\underset{\sim}{\Gamma}}\, \tilde{\underset{\sim}{Q}}\, \tilde{\underset{\sim}{\Gamma}}^T \tag{3-80}$$

Equation (3-80) is now a nonlinear algebraic matrix equation due to the functional dependence of $\tilde{\underset{\sim}{N}}$ and $\tilde{\underset{\sim}{\Gamma}}$ matrices on the state variances. Applying this method to the nonlinear spring system (equation (3-68)) yields:

$$\underset{\sim}{x} = \begin{bmatrix} x \\ \dot{x} \end{bmatrix}, \quad \tilde{\underset{\sim}{N}} = \begin{bmatrix} 0 & , & 1 \\ -(1+3\mu\sigma_x^2) & , & -2\xi \end{bmatrix}$$

$$\tilde{\underset{\sim}{\Gamma}} = \begin{bmatrix} 0 \\ 1 \end{bmatrix}, \quad Q = q, \qquad \underline{\bar{X}} = \begin{bmatrix} \sigma_x^2 & , & E[x\,\dot{x}] \\ E[x\,\dot{x}], & & \sigma_{\dot{x}}^2 \end{bmatrix}$$

Equation (3-80) yields:

$$E[x\,\dot{x}] = 0 \tag{3-81}$$

$$\sigma_{\dot{x}}^2 = \frac{q}{4\xi} \tag{3-82}$$

$$\sigma_x^2 = \frac{q}{4\xi(1+3\mu\sigma_x^2)} \quad . \tag{3-83}$$

Thus the state variable approach (equation (3-83)) yields the same result as the frequency domain method (equation 3-75)). The preferred approach depends upon whether, in a given problem, the integral equations of the frequency domain approach or the algebraic equations of the state variable approach are easier to solve.

The statistical response of the simple rail vehicle wheelset described in equations (63, 50) provides a good practical illustration of the statistical linearization method.

The first task as always is to replace the nonlinearities with the appropriate describing functions. The statistical describing function for the deadband rail spring, lateral and yaw suspensions are given by equations 3-24, 3-30, and 3-37, substituting these expressions into 3-50 yields:

$$m_w\ddot{y}_w + \frac{2f_{11}}{V}\dot{y}_w + \frac{Wa_1}{a_o}\,y_w - 2f_{11}\psi + k_y y_w + F_o\sqrt{2/\pi}\,\frac{\dot{y}_w}{\sigma_{\dot{y}_w}}$$

$$+ K_R\left[1 - \operatorname{erf}\left(\frac{\delta_c}{\sqrt{2}\,\sigma_\Delta}\right)\right] y_w = K_R\left[1 - \operatorname{erf}\left(\frac{\delta_c}{\sqrt{2}\,\sigma_\Delta}\right)\right] y_r + \frac{Wa_1}{a_o}\,y_R \tag{3-84}$$

$$I_w\ddot{\psi} + \frac{2f_{33}a^2}{V}\dot{\psi} - W\delta_o a\psi + \frac{2f_{33}a\lambda_o}{r_o}\,y_w$$

$$+ M_\psi = \frac{2f_{33}a\lambda_o}{r_o}\,y_r \tag{3-85}$$

$$\dot{M}_\psi + \frac{\bar{K}}{\psi_o}\left[1 - \operatorname{erf}\left(\frac{K_\psi\,\psi_o}{\sqrt{2}\,\sigma_{M_\psi}}\right)\right]M_\psi - K_\psi\,\dot{\psi} = 0 \tag{3-86}$$

where $\sigma_\Delta^2 = E[(y_w - y_r)^2]$.

A commonly used form to model [37] the spectral density of rail alignment variations as the vehicle travels at a constant forward speed, V, is:

$$S_{y_r}(\omega) = \frac{KV}{\omega_o^2 + \omega^2} \tag{3-87}$$

Either the frequency domain or state variable approach can be used to compute the statistical response of the wheelset, using equations (3-51) - (3-53). If the state space method is chosen equation (3-54) must be placed in the form of white noise into a first order filter, i.e.,

$$\dot{y}_r = \omega_o y_r + w(t) \tag{3-88}$$

$$E[w(t)] = 0,\ E[w(t)w(t-\tau)] = \pi KV\delta(\tau)$$

3.9 SUMMARY

This section on quasi-linearization was intended to describe and illustrate by simple and practical problems a very useful analytical technique. The fundamental contribution of the quasi-linearization (or D.F.) method is that the convenient and powerful analytical procedures developed for linear systems such as frequency domain and state variable methods can be applied to nonlinear systems. It should be recognized that these linear methods must be applied in an iterative fashion since the D.F. matrices are functions of the unknown response variables. Therefore, an iterative procedure that initially guesses the unknown response variables that are required to compute the D.F. matrices is used. The linear methods are then used to compute the response variables which

are then compared to the guessed values. The cycle is repeated until satisfactory convergence is obtained.

In general the D.F. method converts a set of nonlinear differential equations into a set of nonlinear algebraic equations. The advantages of the D.F. method over numerical integration depends upon the complexity of the describing function (e.g. how many harmonics are required) and the efficiency of the algebraic equation solver.

An important prerequisite to using the D.F. method is that the form of the signal at the input to the nonlinearity must be known. This requirement has led to the use of sinusoids, biases, Gaussian random variables, exponentials,* and linear combinations of all four forms.

The SIDF has been the most widely used wave form and can be used to predict either unforced oscillations (limit cycles) or forced steady state sinusoidal response. The SIDF method works quite well in systems where subharmonics are not generated and higher harmonics are filtered; thus the systems respond predominantly at the fundamental frequency.

For systems where the assumption described above is not true other D.F. techniques can be used. The Dual Input Describing Function (DIDF, bias plus sinusoid) and the Two Sinusoid Input Describing Function (TSIDF, two sinusoids of different frequencies) methods have been successfully applied to many practical problems and extensive tables of these D.F.'s for most common nonlinearities exist in standard texts [25].

A general method for analyzing singly periodic systems using harmonic linearization was presented in this section. The method was illustrated on a six degree of freedom system with multiple nonlinearities.

*Some success has been achieved by the use of exponential D.F.'s to compute the transient response of nonlinear systems [25, 27].

Finally the random input describing function method was described and both frequency domain and state variable methods were illustrated via practical examples.

4. ALGORITHMS FOR STABILITY ANALYSIS

4.1 INTRODUCTION

The hunting behavior of rail vehicles, as explained earlier, is a matter of great practical interest in the railroad community. Actual derailment is obviously a matter of even greater interest. Both of these situations, hunting and derailment, bring into play the non-linear mechanisms described in previous chapters, and can be studied by the quasi-linearization techniques discussed in Section 3.

Rail vehicle hunting is a stable limit cycle. In studying this phenomenon, one is interested in determining the conditions for the existence of such limit cycles. For a rail vehicle, the vehicle speeds and corresponding amplitudes of the stable limit cycles are of particular interest.

Unstable limit cycles are also of practical interest because they describe boundaries between stable and unstable performance. Derailment, for example, occurs when the vehicle motion exceeds the amplitude of an unstable limit cycle that marks the boundary between bounded and divergent motion.

Techniques of applying quasi-linearization to find rail vehicle limit cycles are discussed in this chapter. Two approaches were developed: a technique based on optimization methods and a technique that employs eigenvalue/eigenvector solutions. Both techniques are described and results for a typical rail vehicle problem presented.

4.2 LIMIT CYCLE PREDICTION USING AN OPTIMIZATION ALGORITHM

The discussion of quasi-linearization presented in Section 3 can be integrated to construct an algorithm capable of predicting hunting of nonlinear rail vehicles. The essential steps are:

1) Develop sinusoidal describing functions for the nonlinear elements
2) Solve the nonlinear algebraic equations that determine an undamped oscillation (equations 3-56 and 3-57)
3) Check for physical significance of the solution (examine eigenvector relationships)
4) Determine the limit cycle stability or instability.

In a limit cycling system the describing function technique assumes all states to be sinusoidally oscillating with frequency, ω. For example, the wheelset, the state vector, $\underline{x}$, can be defined

$$\underline{x} = \begin{Bmatrix} y_w \\ \psi \\ \dot{y}_w \\ \dot{\psi} \end{Bmatrix} = \begin{Bmatrix} A\sin \omega t \\ B\sin(\omega t + \phi) \\ \omega A\cos \omega t \\ \omega B\cos(\omega t + \phi) \end{Bmatrix}$$

Actually,

$$\dot{\underline{x}} = \underline{f}(x) \qquad (4\text{-}1)$$

where $\underline{f}(x)$ represents the nonlinear wheelset equations that may include the effects of nonlinear creep, contact geometry, and suspension elements as qualitatively discussed earlier. To investigate the stability of this nonlinear wheelset, the four above steps are then

followed.

The describing function matrix $[\underline{N}(A, B, \omega, V)]$ is computed by replacing each nonlinear term of $\underline{f}(x)$* with its describing function approximation. This produces the following quasi-linear description of the vehicle behavior:

$$\dot{\underline{x}} \simeq [\underline{\bar{N}}(B, \omega, V)]\, \underline{x} \,. \qquad (4\text{-}2)$$

Note that the describing functions depends only on A,B, and ω. However, since the limit cycle condition also depends upon the wheelset forward velocity, V, it too is included as an unknown in (4-2). The actual determination of the individual elements of $[\underline{\bar{N}}(A,B, \omega, V)]$ is is detailed later.

The necessary condition for limit cycle existence is given by equation (3-56). Solving that equation is the second step in solving the limit cycle problem. For the wheelset, equation (3-57) is written as follows:

$$|j\omega\underline{\bar{I}} - [\underline{\bar{N}}(A,B, \omega,V)]| = 0 \qquad (4\text{-}3)$$

This characteristic equation will, in general, have both real and imaginary parts. Obtaining a solution to (4-3) requires satisfying both the real and imaginary parts of the equation. One approach to this is to minimize the function OBJ where

$$OBJ = ABS[Re(|j\omega\underline{\bar{I}} - [\underline{\bar{N}}(A,B,\omega,V)]|)] + ABS[Im(|J\omega\underline{\bar{I}} - [\underline{\bar{N}}(A,B,\omega,V)]|)] \qquad (4\text{-}4)$$

and thus obtain values for A,B,ω, and V.

*This step is more complex when nonlinear creep as well as nonlinear wheel/rail geometry is modeled.

The solution of (4-3) is not necessarily unique due to an excess of unknowns. A means of determining whether the solution of (4-3) actually depicts a limit cycle is required. To do this, the third solution step involves examining the eigenvectors of $[\underline{\overline{N}}(A,B,\omega,V)]$. For the wheelset, the complex eigenvector $\underline{X}$ corresponding to an eigenvalue, $j\omega$, will satisfy

$$[j\ I - [\underline{\overline{N}}(A,B,\omega,V)]\ ]\ \underline{X} = 0 \qquad (4\text{-}5)$$

where $$\underline{X} = \begin{bmatrix} X_{y_w} \\ X_{\psi} \\ X_{\dot{y}_w} \\ X_{\dot{\psi}} \end{bmatrix} .$$

Thus for a physically meaningful solution to (4-3) the solution must also satisfy the following eigenvector relationships

$$\begin{aligned} |\ X_{y_w}\ | &= A \\ |\ X_{\psi}\ | &= B \\ |\ X_{\dot{y}_w}\ | &= \omega A \\ |\ X_{\dot{\psi}}\ | &= \omega B \quad . \end{aligned} \qquad (4\text{-}6)$$

Values of A,B,ω,V satisfying (4-3) but not (4-6) are not valid descriptions of the limit cycle, i.e., the combination of (4-3) and (4-6) are necessary and sufficient limit cycle criteria.

Assuming successful completion of the first three steps, all that remains to be addressed is the question of limit cycle stability. The following procedure is employed to ascertain whether the limit cycle described by A,B,ω, and V that satisfies both (4-3) and (4-6) is stable or unstable. There exists a purely imaginary pair of eigenvalues, i.e., $j\omega$ for this solution. If the lateral amplitude is changed by an amount ξ then the dominant eigenvalues of the perturbed system, i.e., $[\underline{\bar{N}}(A + \xi, B, , V)]$, can be examined for changes in their real parts. Table 4-1 summarizes the possibilities.

TABLE 4-1. LIMIT CYCLE STABILITY DETERMINATION

	DOMINANT EIGENVALUE REAL PART			
	$=0$	>0	<0	
$\bar{N}(A,\omega)$ (unperturbed)	x			Limit cycle condition
$\bar{N}^+(A,\omega)$ $(\xi>0)$		x		Unstable limit cycle
$\bar{N}^+(A,\omega)$ $(\xi>0)$			x	Stable limit cycle
$\bar{N}^-(A,\omega)$ $(\xi<0)$		x		Stable limit cycle
$\bar{N}^-(A,\omega)$ $(\xi<0)$			x	Unstable limit cycle

Although heuristic, it is believed that this is a reasonable approach to the stability investigation as long as the original assumption (sinusoidal oscillation) is not violated. Keeping ξ small will usually insure that the eigenvalue real parts do not wander far off the imaginary axis.

4.2.1 LIMCY Program

LIMCY*, a program for investigating the nonlinear stability of the wheelset, was formulated based on the preceding discussion. Its basic structure is discussed in this section. A flow chart has been included as Figure 4-1.

Values of the wheelset physical constants are read into the program MAIN. The quasi-linear form of the wheelset equations, as given by equation (4-2) are placed in subroutine DFMAT with the values of A,B,ω, and V left as unknowns in the expression for the describing function matrix elements.

The first goal of the program is to minimize (4-4), a function of four variables. However, if one of these parameters is held fixed, i.e., read into MAIN as a constant, the unknowns are reduced to three. Since a reasonable range of limit cycle lateral amplitudes is known, i.e., A < 1.2 in., A will be held constant and values of B, ω, and V that satisfy the limit cycle criteria will be sought. Various optimization techniques are available for minimizing equations such as (4-4). Some require gradient computation, some do not. The technique used here to minimize (4-4) is a pattern search method proposed by Hooke and Jeeves [50]. Its attributes include no need for gradient computation, coding simplicity, and fast solution speed. Simply put, given an initial guess for B,ω, and V the method searches the variable space computing (4-4) until a minimum OBJ is found. One

---

* A user's manual for LIMCY was prepared as a separate document under this contract.

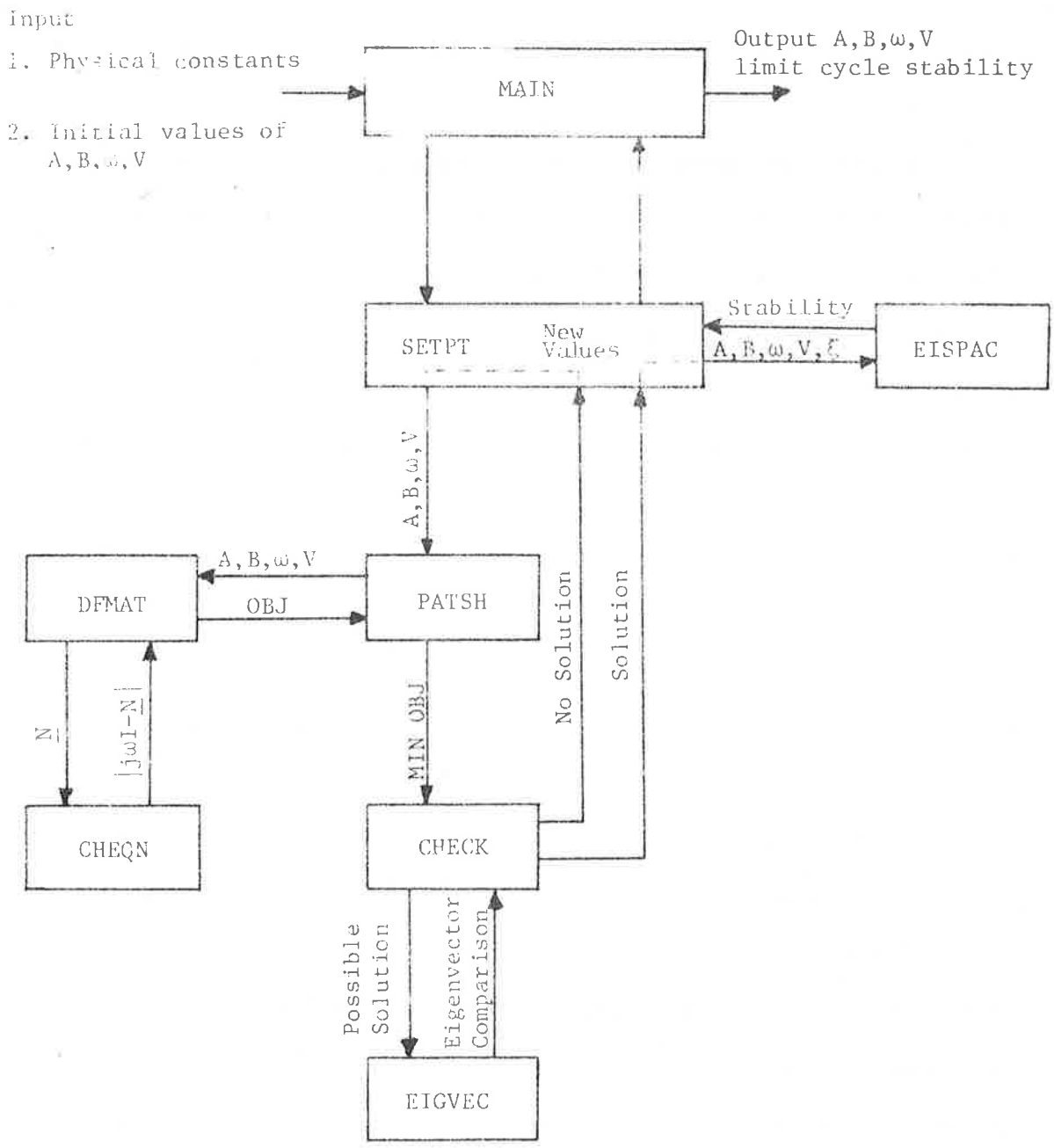

FIGURE 4-1. LIMCY FLOWCHART

drawback to the pattern search algorithm is that it may find only local minima. Hence, if the value of OBJ returned is not "sufficiently small" then the search must be restarted with a new set of initial values. Subroutine PATSH performs the pattern search in LIMCY.

Since PATSH requires evaluation of (4-4) for every variable change, an efficient method of computing the characteristic polynomial of $[\underline{\overline{N}}(A,B,\omega,V)]$ is needed. The method of A.M. Danilevsky [51] was chosen to perform this function. Based on successive similarity transformations of $\underline{\overline{N}}(A,B,\omega,V)$, the technique is easily coded for digital computation and is one of the most efficient schemes for obtaining the characteristic polynomial. Furthermore, the method retains information that allows easy computation of the system eigenvectors when needed. Subroutine CHEQN computes the characteristic polynomial.

When PATSH returns values of B,ω,V, subroutine CHECK determines if the value of OBJ is "sufficiently small" to qualify A,B,ω, and V as a possible limit cycle condition. If it does not qualify subroutine SETPT changes the initial values of B,ω,V and the pattern search is restarted. If the values do qualify as a possible limit cycle description, subroutine EIGVEC is called to evaluate the system eigenvectors using the most recent similarity transformations of CHEQN. The eigenvector magnitudes are returned to CHECK for comparison with A,B, and ω; good agreement indicates satisfaction of (4-6) and signifies that a valid limit cycle condition described by A,B,ω, and V has been found. If the eigenvector magnitudes do not agree with A,B, and ω, then

return is made to SETPT where new initial values are chosen.

After (4-3) and (4-6) have been satisfied, the value of A is perturbed by an amount ξ, the limit cycle values of B,ω, and V retained, and the eigenvalues of $[\overline{N}(A,B,\omega,V)^{-}]$ computed in order to determine the stability of the limit cycle. Subroutine EISPAC performs this function.

All subroutines used in LIMCY were written specifically for it with the exception of PATSH and EISPAC which are available in disc libraries at the Joint Civil-Mechanical Engineering Computing Center at M.I.T.

4.2.2. The Wheelset Example Using LIMCY

The quasi-linearized equations for the wheelset including the describing functions for the nonlinear wheel/rail profile and nonlinear suspension elements described in Section 3 (equations 3-10, 3-11a, 3-12, 3-13, and 3-14) are:

$$m_w \ddot{y}_w + \left(\frac{2 f_{11}}{V} + \frac{4 F_o}{A\omega\pi}\right) \dot{y}_w + [K_g(A) + k_y] y_w - 2 f_{11} \psi = 0 \qquad (4\text{-}7)$$

$$I \ddot{\psi} + \left[\frac{2 f_{33} a^2}{V} + \frac{k_\psi}{\omega\pi}(1 - \beta^2)\right] \dot{\psi} + \left[\frac{k_\psi}{2}(1 + f^{*}(-\beta)) - w\delta_o a\right]\psi + \frac{2 f_{33} a}{r_o} \lambda(A) y_w = 0 \qquad (4\text{-}8)$$

Figure 4-2 shows the effective conicity and gravitational stiffness describing functions used in this example that are illustrative

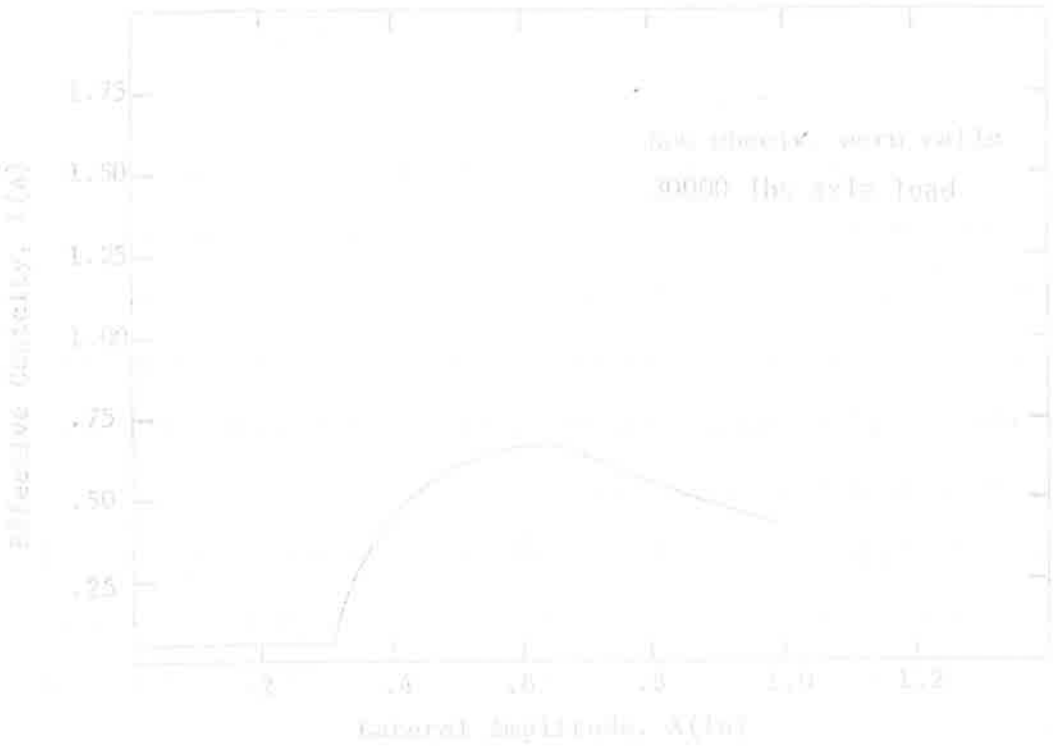

a. Effective Conicity vs. Lateral Amplitude

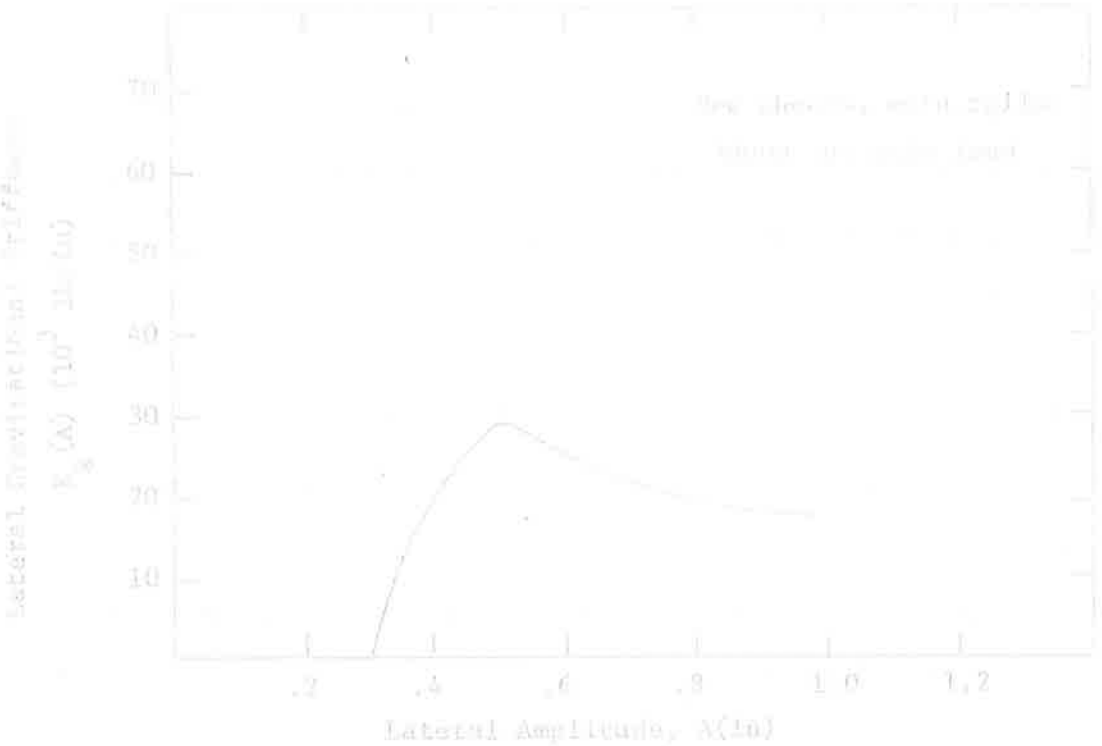

b. Lateral Gravitational Stiffness vs. Lateral Amplitude

FIGURE 4-2. NEW WHEEL CONTACT CONIC BY DESIGN TRUCK CONDITION

of new wheels on worn rail. These figures represent a new wheel on worn rails at standard gauge (56.5"). Note how the functions increase sharply at a lateral amplitude of .3 in. where flange contact is made, and then decrease as the amplitude increases. Recall that an increased effective conicity $\lambda(A)$ is generally considered a destabilizing effect while large $k_g(A)$ is known to be a stabilizing influence. Physical constants used in this model were:

M_w	= 90 slugs	k_ψ	= 105,630 ft-lb/rad	r_o	= 1.75 ft
I_{w_t}	= 360 slug-ft^2	$f_{11} = f_{33}$	= 3×10^6 lb/wheel	δ	= .024 ft
W	= 30000 lb	a	= 2.5 ft	F_o	= 4000 lb
k_R	= 10^6lb/ft	λ_o	= .05	ψ_o	= .125°
k_y	= 10000 lb/ft	δ_o	= .05		

Equations (4-7) and (4-8) were placed in the form of equations (4-2) and LIMCY was used to compute the hunting behavior. Numerical results are shown in Figure 4-3. The region to the left of the A(or B) vs. V plots can be considered stable and that to the right unstable. The significance of the contact geometry describing functions is easily seen, i.e., stable limit cycles (hunting oscillations) will only occur over a limited speed range. If such an oscillation is encountered it will be maintained at an ever increasing amplitude as speed is increased until the speed indicated by the right extreme of the stable limit cycle is reached. Beyond that speed the response will become unstable possibly indicating derailment. Note that this limited range of stable limit cycles is due to the decrease in the restoring force of

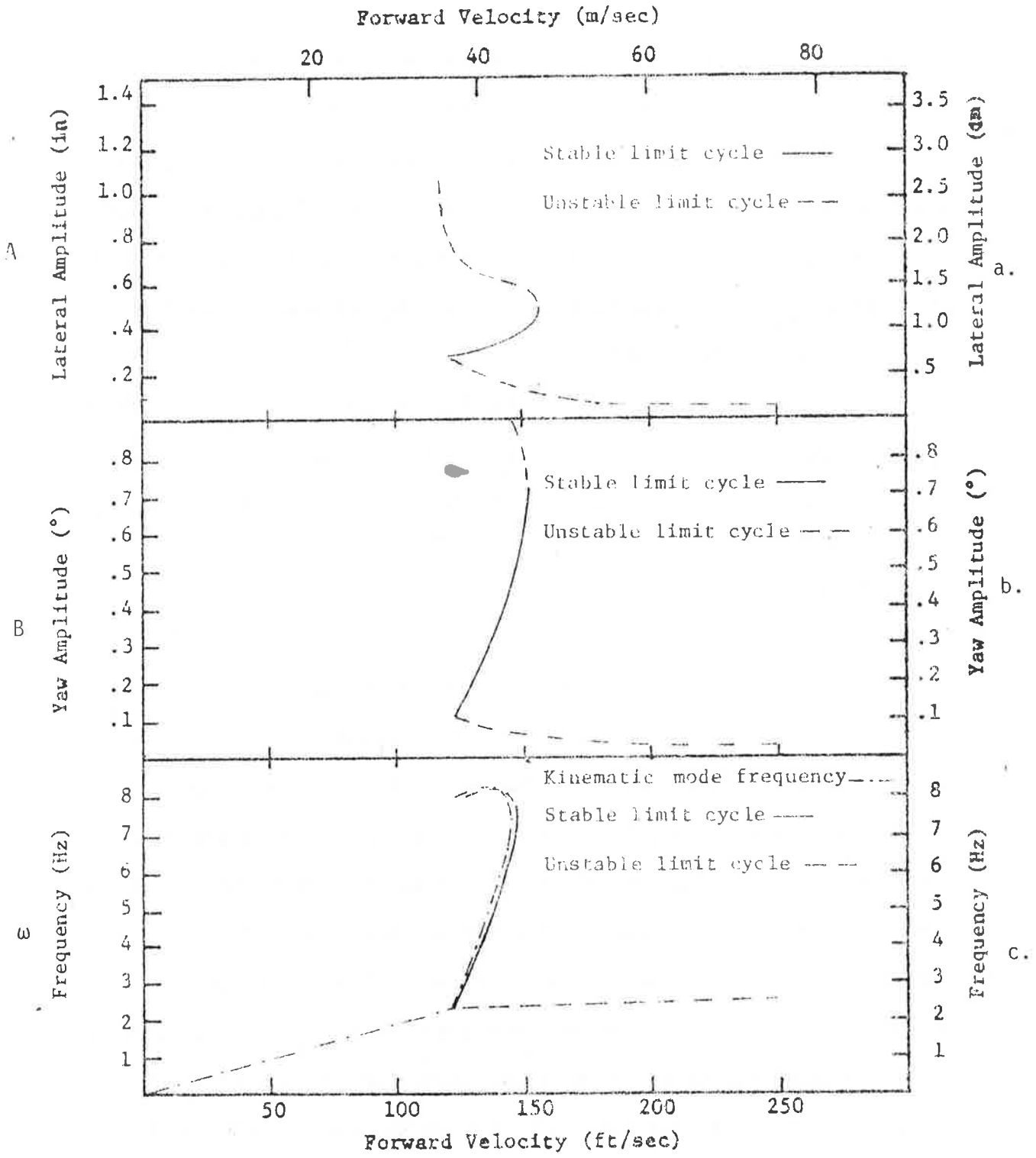

FIGURE 4-3. WHEELSET LIMIT CYCLES WITH NONLINEAR CONTACT GEOMETRY AND SUSPENSION FRICTION

the gravitational stiffness at higher amplitudes. Also, these plots point out the nature of the low amplitude/high speed stable region. If irregularities are sufficient to excite the unstable limit cycle locus, the system will either hunt or, if the velocity is high enough, derailment may result. Finally note the kinematic mode frequency, (Figure 4-3c) now given by

$$\omega_k = V\sqrt{\frac{\lambda(0)}{d\tau_0}} \tag{4-9}$$

4.3 An Alternative Approach

An alternative approach to finding limit cycles employs well developed eigenvalue/eigenvector numerical techniques.

The quasi-linear rail vehicle dynamic model for limit cycle investigations can be expressed in the following form.

$$\dot{x} = \bar{N}(A,\omega)x \tag{4-10}$$

Where A = Amplitudes of the state variables
ω = Frequency of the limit cycle
$\bar{N}(A,\omega)$ = Describing function matrix
x = State vector

The existence of a limit cycle in (4-10) requires that $\bar{N}(A,\omega)$ have a pair of purely imaginary eigenvalues. Additionally, the amplitude and frequency of the limit cycle must satisfy the relationships of the eigenvector and frequency associated with the purely imaginary

eigenvalue as well as the condition that $\underline{\bar{N}}(\underline{A},\omega)$ have such a pair of imaginary eigenvalues.

The limit cycle conditions may be determined by investigating, in an iterative fashion, the eigenvalues of the linear problem that corresponds to a motion at a given amplitude. Limit cycles are found, in this approach, by employing information in one of the least damped eigenvalues of the describing function matrix, $\underline{\bar{N}}(\underline{A},\omega)$, to lead iteratively to the values of amplitude and frequency that correspond to purely imaginary eigenvalues.

In this iterative technique, the amplitude of one state, A_i, is chosen, and the remaining amplitudes and the system frequency are found from the eigenvalue with the smallest real part and its associated eigenvector. At each step, initial values for evaluating the describing function matrix are found by employing the frequency and eigenvector of the preceding step. The eigenvalue/eigenvector computation is repeated to improve the correspondence between the amplitudes and frequency used in computing the describing functions, and those that result from the eigenvalue/eigenvector computation. New values for one of the system parameters, such as the vehicle speed, are chosen to move in a direction that drives the real part of the eigenvalue with the smallest real part toward zero.

Information about the stability of the limit cycles is a side product of this technique. The limit cycle stability is found by varying the amplitude of the limit cycle a small amount. If the limit cycle is stable, slightly smaller amplitudes should result in the corresponding

eigenvalue having a positive real part, and larger amplitudes should produce a negative real part. The opposite situation should prevail for an unstable limit cycle [51].

The approach described above was implemented in the form of computer algorithms written in FORTRAN for computation on a digital computer. The basic procedures and analytical expressions are given here.

A flow chart of the computer algorithms used to find the limit cycles is shown in Figure 4-4. In the procedure, the first value of the maximum* wheelset lateral displacement amplitude is specified, and estimates of the critical velocity, state vector and frequency are made. In an inner loop describing functions are obtained corresponding to these estimates, and eigenvalues and eigenvectors calculated. Repeated estimates of the frequency and the state vector are made until the estimates are consistent with the least damped eigenvalue and eigenvector computed. An outer loop iteratively estimates velocity to find the critical velocity at which the limit cycle occurs. The process is repeated for the next value of maximum wheelset lateral displacement.

New estimates for the frequency and state vector in the inner loop are made by choosing, as improved guesses, the frequency and the eigenvector relationship of one of the least damped modes. Generally, the iteration procedure will then converge to a frequency and state vector

---

* "Maximum" means the maximum value for any of the four wheelsets. Each wheelset generally has a different amplitude.

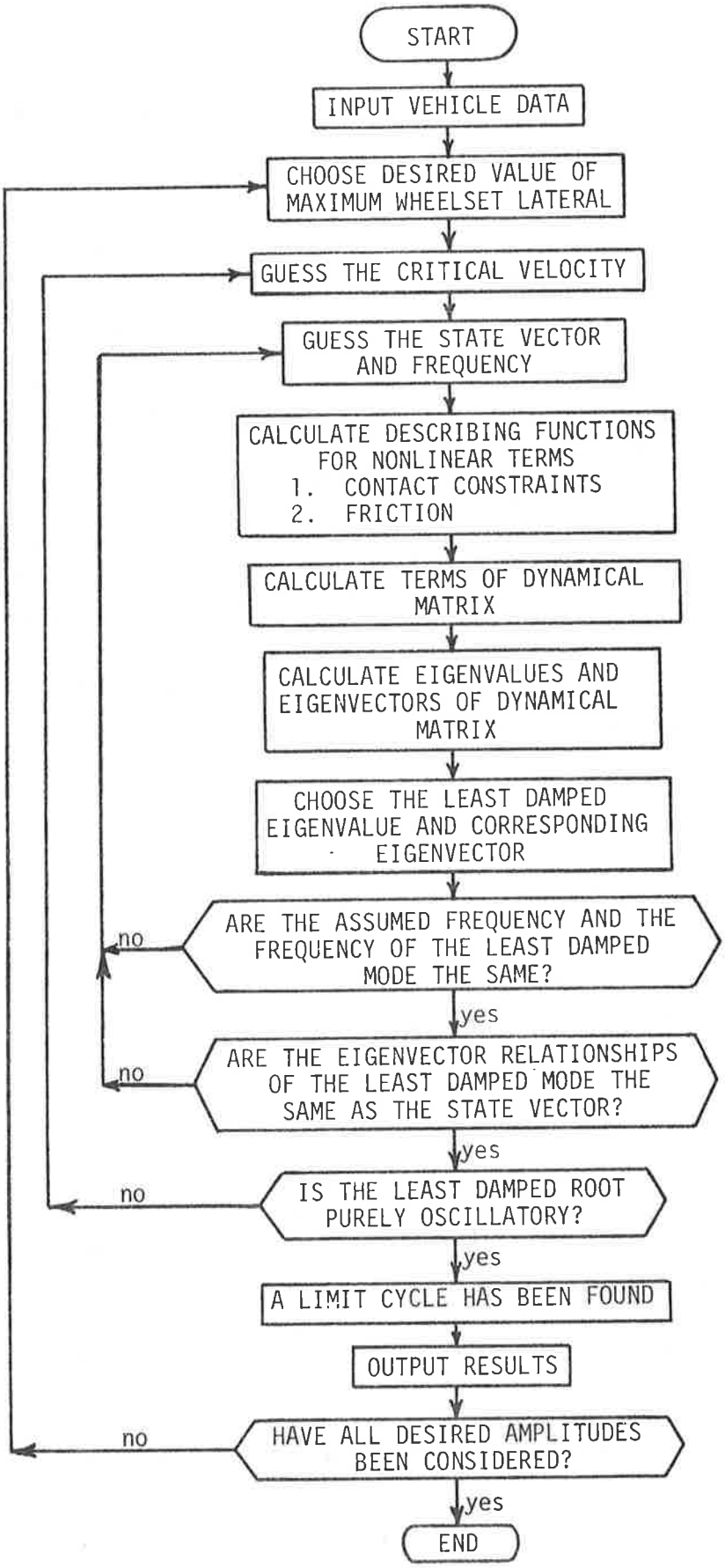

FIGURE 4-4. EIGENVALUE/EIGENVECTOR ALGORITHM FLOWCHART

that are consistent with the frequency and eigenvector of the chosen mode.

An Example Using the Eigenvalue/Eigenvector Method

The eigenvalue/eigenvector technique was used to determine the hunting stability of a nine degree of freedom representation of a North American rail freight car. This freight car model, as described in Section 2 and shown in Figure 2-19, includes nonlinearities in the suspension and at the wheel/rail contact. The suspension nonlinearities involve Coulomb friction in the warp, yaw, lateral and vertical motions. These nonlinear characteristics are discussed in Section 2 and their describing functions given in Section 3. In this application those describing functions take the following form:

Lateral Suspension

$$F_{ySF} = K_{yS}(y_{TF} - y_C - h_2\phi_C - L_C\psi_C + \frac{4F_{ySO}}{\pi A_5}(\dot{y}_{TF} - \dot{y}_C - h_2\dot{\phi}_C - L_C\dot{\psi}_C) \quad (4\text{-}11)$$

$$F_{ySR} = K_{yS}(y_{TR} - y_C - h_2\phi_C + L_C\psi_C) + \frac{4F_{ySO}}{\pi A_6}(\dot{y}_{TR} - \dot{y}_C - h_2\dot{\phi}_C + L_C\dot{\psi}_C) \quad (4\text{-}12)$$

where A_5 = Amplitude of $(\dot{y}_{TF} - \dot{y}_C - h_2\dot{\phi}_C - L_C\dot{\psi}_C)$

A_6 = Amplitude of $(\dot{y}_{TR} - \dot{y}_C - h_2\dot{\phi}_C + L_C\dot{\psi}_C)$

Vertical Suspension

$$F_{ZSF} = F_{ZSR} = K_{ZS}(d\phi_C) + \frac{4F_{ZSO}}{\pi A_7}(\dot{d\phi_C})$$

where: A_7 = Amplitude of $(\dot{d\phi_C})$

Warp Suspension

$$T_{\psi WF} = K_W(\psi_{WF}) + \frac{4T_{WO}}{\pi A_8}(\dot{\psi}_{WF})$$

$$T_{\psi WR} = K_W(\psi_{WR}) + \frac{4T_{WO}}{\pi A_9}(\dot{\psi}_{WR})$$

where: A_8 = Amplitude of $(\dot{\psi}_{WF})$

A_9 = Amplitude of $(\dot{\psi}_{WR})$

Yaw Suspension

$$T_{BF} = \frac{4T_{BO}}{\pi A_{10}}(\dot{\psi}_{WF} + \dot{\psi}_{TF} - \dot{\psi}_C)$$

$$T_{BR} = \frac{4T_{BO}}{\pi A_{11}}(\dot{\psi}_{WR} + \dot{\psi}_{TR} - \dot{\psi}_C)$$

where: A_{10} = Amplitude of $(\dot{\psi}_{WF} + \dot{\psi}_{TF} - \dot{\psi}_C)$

A_{11} = Amplitude of $(\dot{\psi}_{WR} + \dot{\psi}_{TR} - \dot{\psi}_C)$

The nonlinearities in the wheel/rail contact geometry required to describe the nature of the wheel/rail contact forces are also discussed in Section 2 and their describing functions given in Section 3. As

explained previously, the suspension describing functions are represented analytically while the wheel/rail geometry describing functions are defined in tabular form.

The amplitude of the largest lateral wheelset motion at any of the four wheelsets was chosen as the independent variable in the eigenvalue/eigenvector algorithm for this example. This meant that at times during the iteration process the independent variable would shift from one wheelset to another. The computer program began with a small lateral amplitude value and proceeded in small increments to larger values of the lateral wheelset amplitude.

Results for this freight car example showing the largest wheelset lateral amplitude as a function of vehicle speed at limit cycle conditions are presented in igure 4-5. These results are for a freight car with linear viscous damping that is independent of the motion amplitude and frequency, and nonlinear wheel/rail geometry representing a new wheel on worn rail.

This example model behaves like a linear system at amplitudes below flange contact. In this range, the wheel/rail geometric constraint functions are nearly linear and thus the system is effectively linear. The stability of vehicle motion, in this linear region, does not depend on the motion amplitude as indicated by the vertical line depicting unstable limit cycles at a speed of 144 ft/sec.

In this figure the region to the right and above the unstable limit cycles may be regarded as an unstable region while the region

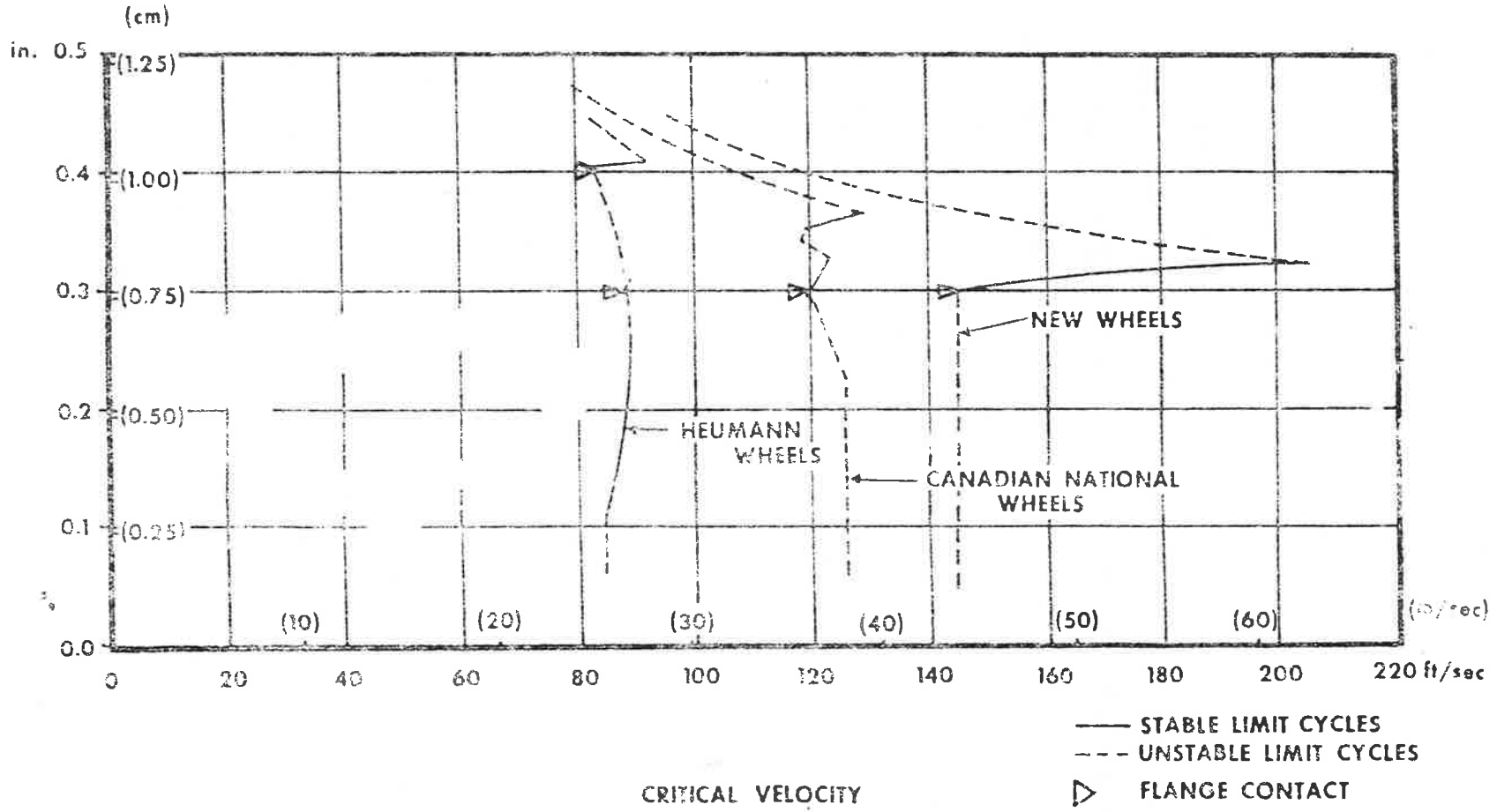

FIGURE 4-5. LIMIT CYCLE AMPLITUDES VERSUS VELOCITY FOR FREIGHT CAR WITH NONLINEAR WHEEL/RAIL GEOMETRY AND LINEAR VISCOUS DAMPING

below and to the right is stable. Thus, at any speed below 144 ft/sec. the vehicle response to disturbances with amplitudes less than the upper unstable limit cycle will damp out. At these speeds, amplitudes above the unstable limit cycle will diverge, presumably representing derailment. These results indicate that the stable limit cycles, representing vehicle hunting, only exist at speeds between 144 and 204 ft/sec. In this range, disturbances with amplitudes up to the upper unstable limit cycle will settle into a limit cycle or hunting behavior. Larger disturbances will result in divergent motion.

4.4 SUMMARY

This chapter has illustrated two numerical methods that can be used to predict the nonlinear hunting phenomena of rail vehicles using the describing function method.

The first method was the optimization technique that directly seeks a solution of equation (3-56), i.e.,

$$\{j\,\omega\,\underline{\underline{I}} - \underline{\underline{N}}\}\quad \underline{X} = 0\ .$$

The necessary condition for a non-trivial solution is:

$$/j\,\omega\,\underline{\underline{I}} - \underline{\underline{N}}/ = 0\ .$$

This determent contains a real and imaginary part, both of which must be zero. In order to find values of the amplitudes and frequency that satisfy this equation an objective function of the form,

$$OBJ = \text{Re}\ \{/j\omega \underline{\bar{I}} - \underline{\bar{N}}/\} + \text{Im}\ \{/j\omega \underline{\bar{I}} - \underline{\bar{N}}/\}.$$

A parameter search method is employed Ref. [50] to minimize this objective function. The program developed using this method is called LIMCY and has been used successfully to investigate the hunting of a nonlinear wheelset.

The second method was the eigenvector/eigenvalue method that seeks to drive the real part of the eigenvalue closest to the imaginary axis to zero. The eigenvector corresponding to this particular eigenvalue is used to improve the subsequent iterations. This method was successfully used to investigate the hunting of a nine degree of freedom freight car model.

The relative efficiency of these two methods was not investigated but will be the subject of future research.

5. APPLICATIONS OF STABILITY ANALYSIS ALGORITHMS

5.1 INTRODUCTION

The two nonlinear stability analysis programs described in Section 4 were applied to the prediction of rail vehicle hunting for different vehicle models. A parametric study of the influence of suspension parameters, axle-load, gauge, and wheel profile on the critical speed of a simple nonlinear wheelset was performed using the optimization algorithm. The eigenvector/eigenvalue method was applied to a nine degree of freedom freight car model to determine the influence of nonlinear wheel/rail contact geometry on vehicle stability.

5.2 WHEELSET STABILITY RESULTS WITH LIMCY

It is well known that track gauge, axle loading, and wheel profile greatly influence wheelset stability. However, the methods used throughout the literature have only considered idealizations of these effects. In this section many of these idealizations are replaced by more realistic quasi-linear modeling techniques.

Modeling flange contact as a dead band rail spring can indirectly account for track gauge by changing the dead band (flange clearance) size. Increasing axle load is generally thought to be a stabilizing effect because of its impact on the gravitational stiffness term in the wheelset equations of motion. However, it has been determined by measurement [20] that changing axle load also changes some of the

suspension characteristics as well as the creep coefficients. Previous investigators have considered wheel profile effects by varying a constant taper ratio (conicity) [8, 9]. Nonlinear profiles have been considered [2, 11] to a limited extent on models that were otherwise linear. With the methods developed in this report actual profiles can be included in the describing function analysis of the wheelset without compromising the wheelset geometry.

The model that will be used in this study is defined by equations (2-17b) and (2-18). However, the values of the constants will be changed from those used in the previous section. The new values chosen to model the wheelset of a 70 ton freight truck are:

$$M_w = 76.6 \text{ slugs} \qquad r_o = 1.375 \text{ ft}$$

$$I_{wz} = 448 \text{ slug-ft}^2, \qquad F_o = 5200 \text{ lbs}$$

All of the other parameters depend upon the gauge, profile, or axle-loading used.

All combinations of three axle loadings (15000 lbs, 35000 lbs, 70000 lbs), three track gauges (tight, $a = \frac{56.0"}{2}$; standard, $a = \frac{56.6"}{2}$; and wide, $a = \frac{57.5"}{2}$), and three profiles (new, slightly worn, and Heumann) were considered. Note that the gauge variation spans the allowable range for Class 5 track or better. The contact geometry describing functions are functions both of profile and gauge and were computed by the method described in Section 3. All were made for slightly worn rail profiles. Typical dependence on these parameters is shown in Figures 5-1 and 5-2.

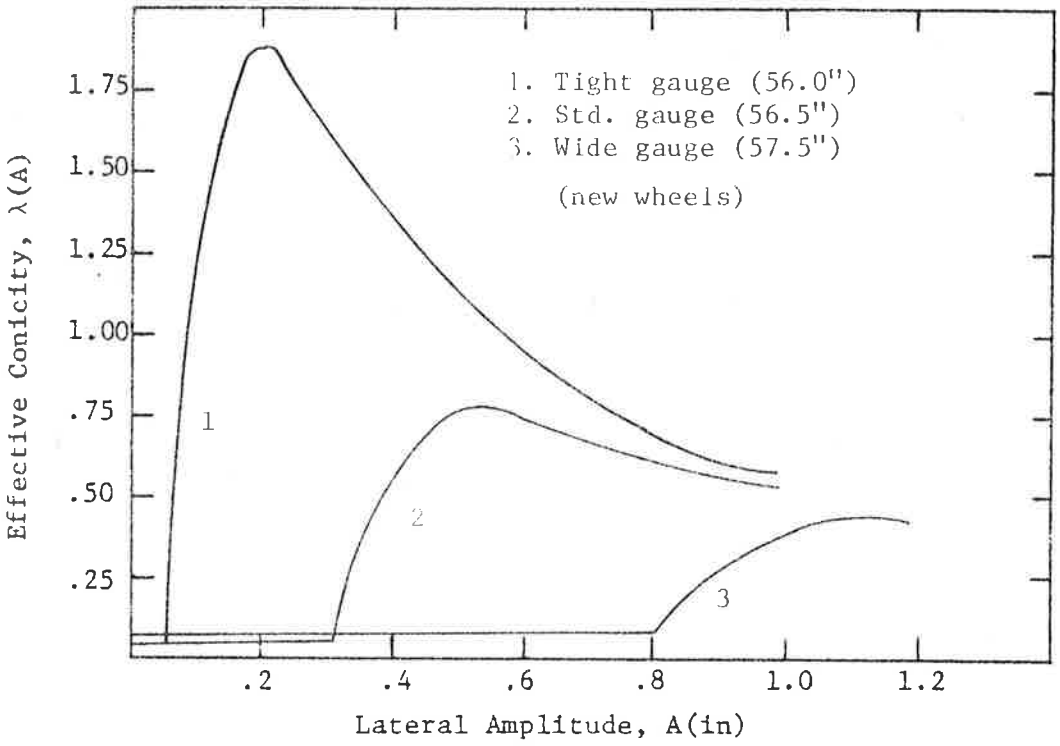

a. Effective Conicity vs. Lateral Amplitude

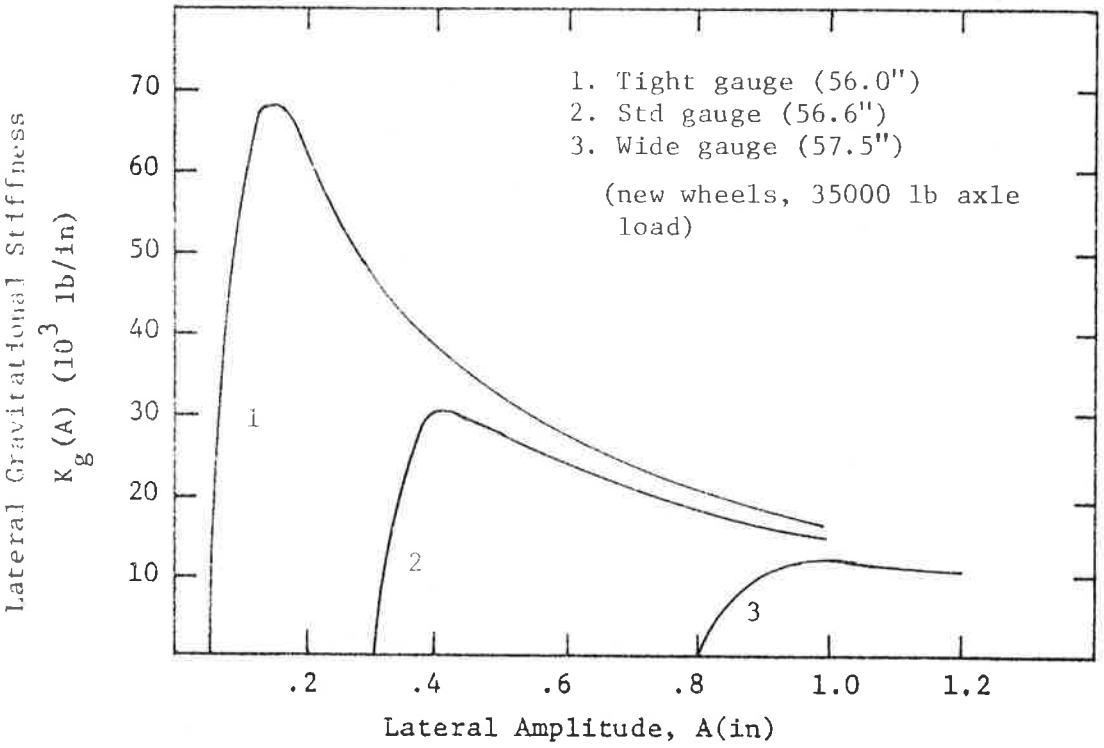

b. Lateral Gravitational Stiffness vs. Lateral Amplitude

FIGURE 5-1. CONTACT GEOMETRY DESCRIBING FUNCTION DEPENDENCE UPON TRACK GAUGE

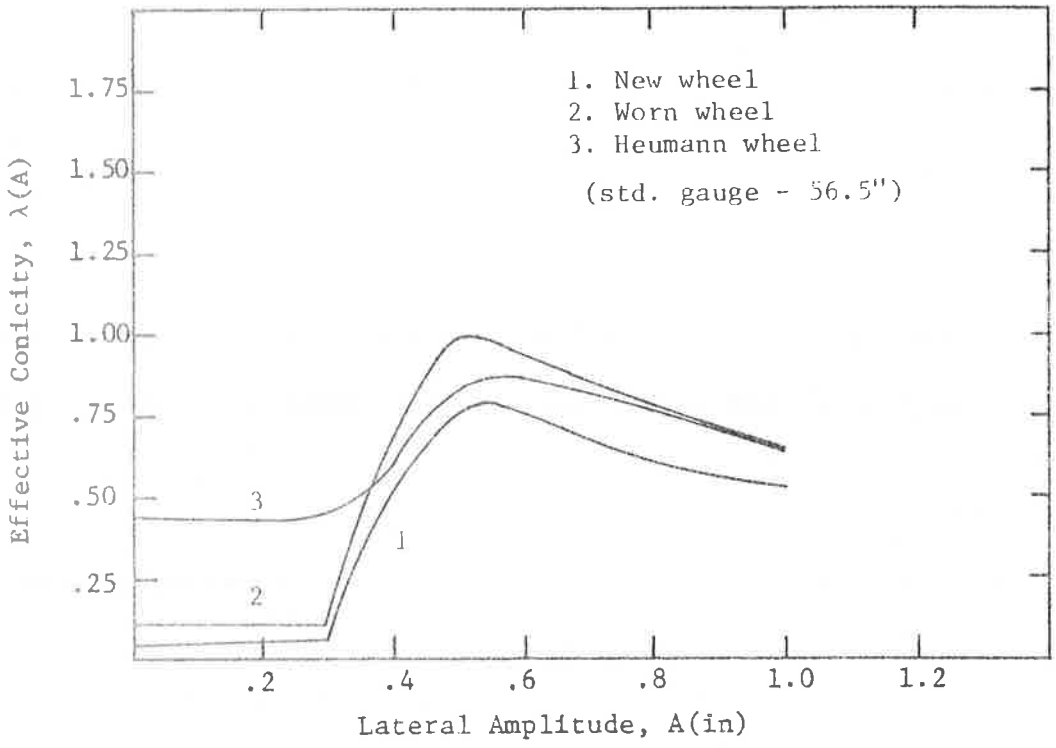

a. Effective Conicity vs. Lateral Amplitude

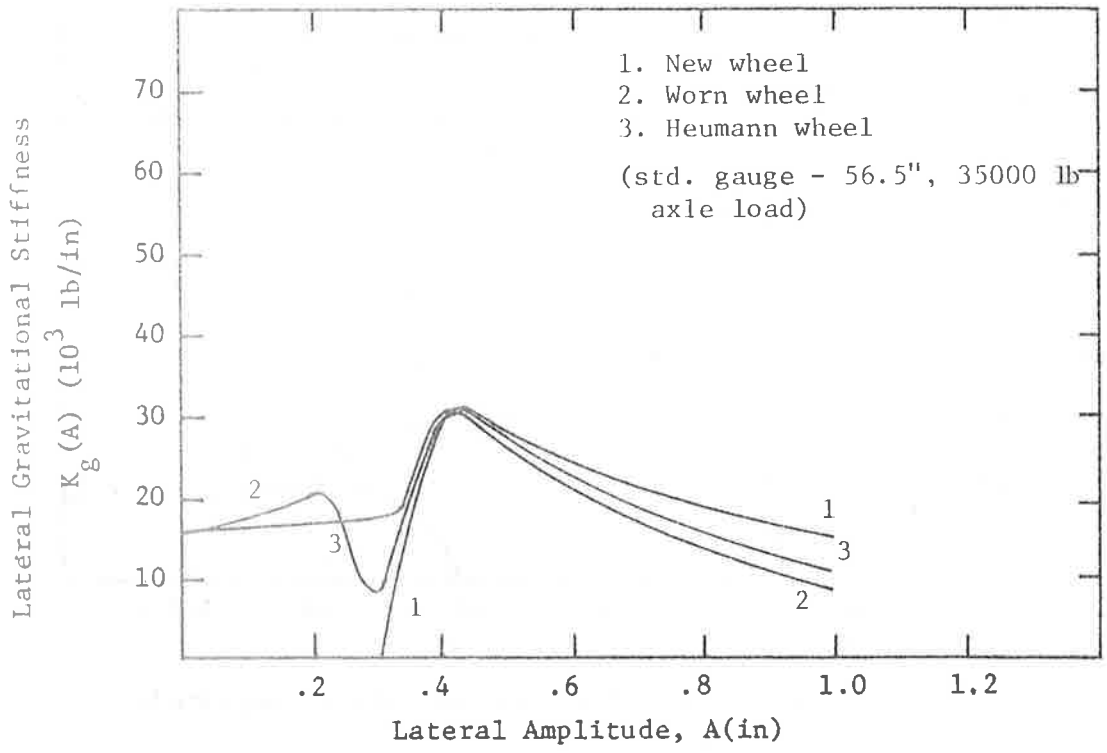

b. Lateral Gravitational Stiffness vs. Lateral Amplitude

FIGURE 5-2. CONTACT GEOMETRY DESCRIBING FUNCTION DEPENDENCE UPON WHEEL PROFILE

The steep rises of these functions in Figure 5-1 are due to flange contact and hence occur at different amplitudes. In Figure 5-2 the variations are due to different design profiles (new standard AAR, and Heumann wheels) as well as wheel tread and flange wear (worn AAR wheel).

The dependence of suspension characteristics and creep coefficients upon axle loading and track gauge is shown in Table 5-1, 5-2, and 5-3.

Generally, the creep coefficients, f_{11} and f_{33}, are proportional to $W^{2/3}$ [21].

5.2.1 Parametric Study Results

The results of the parametric studies are presented in Figures 5-3 to 5-11. These results are arranged so that one may choose any combination (of the possible 27) of wheel profile, track gauge, and axle loading and, by consulting the proper figure, determine the effects of varying any one of those parameters.

All plots are of limit cycle lateral amplitude vs. velocity, and are interpreted in the same manner as those shown earlier, i.e., the space to the left of the curve indicates that all of the system eigenvalues have negative real parts (stable system), while that to the right indicates that one pair of eigenvalues has positive real parts (unstable system). Note, though, that for these plots all limit cycles (stable and unstable) are shown as solid lines. The determination of limit cycle stability will be discussed later in this section.

TABLE 5-1. NEW WHEEL CONSTANTS

AXLE LOAD	GAUGE	f_{11} 10^6 lbs/wheel	f_{33} 10^6 lbs/wheel	k_y 10^4 lbs/ft	k_ψ 10^6 ft-lbs/rad	ψ_o (rad)
15000 lbs	56.0"	1.361	1.471	1.379	1.916	.00122
	56.5"	"	"	"	"	"
	57.5"	"	"	"	"	"
35000 lbs	56.0"	2.394	2.587	3.490	2.108	.00248
	56.5"	"	"	"	"	"
	57.5"	"	"	"	"	"
70000 lbs	56.0"	3.801	4.107	7.187	2.444	.00463
	56.5"	"	"	"	"	"
	57.5"	"	"	"	"	"

TABLE 5-2. WORN WHEEL CONSTANTS

AXLE LOAD	GAUGE	f_{11} 10^6 lbs/wheel	f_{33} 10^6 lbs/wheel	k_y 10^4 lbs/ft	k_ψ 10^6 ft-lbs/rad	ψ_o (rad)
15000 lbs	56.0"	1.283	1.294	1.379	1.916	.00122
	56.5"	1.263	1.260	"	"	"
	57.5"	1.498	1.809	"	"	"
35000 lbs	56.0"	2.257	2.277	3.490	2.108	.00248
	56.5"	2.222	2.217	"	"	"
	57.5"	2.636	3.182	"	"	"
70000 lbs	56.0"	3.583	2.888	7.187	2.444	.00463
	56.5"	3.527	3.519	"	"	"
	57.5"	4.184	5.051	"	"	"

TABLE 5-3. HEUMANN WHEEL CONSTANTS

AXLE LOAD	GAUGE	f_{11} 10^6 lbs/wheel	f_{33} 10^6 lbs/wheel	k_y 10^4 lbs/ft	k_ψ 10^6 ft-lbs/rad	ψ_o (rad)
15000 lbs	56.0"	1.222	1.711	1.379	1.916	.00122
	56.5"	1.249	1.230	"	"	"
	57.5"	1.310	1.400	"	"	"
35000 lbs	56.0"	2.146	2.060	3.490	2.108	.00248
	56.5"	2.193	2.164	"	"	"
	57.5"	2.325	2.460	"	"	"
70000 lbs	56.0"	3.407	3.270	7.187	2.444	.00463
	56.5"	3.482	3.435	"	"	"
	57.5"	3.715	3.900	"	"	"

5.2.2 Effects of Track Gauge Variations

In Figures 5-3 to 5-5 it is seen that, for any wheel profile and axle loading, increasing track gauge increases the stable regime to the left of the curves. This implies that, at a given velocity, larger track irregularities can be tolerated on wide gauge than on tight. This effect is directly related to flange contact occurring sooner at tighter gauges. Figure 5-3 indicates that the minimum velocity below which all response is guaranteed stable is changed little by varying gauge. However, for worn and Heumann profiles this minimum velocity is more dependent upon gauge.

All curves in Figures 5-3 and 5-4 possess a high speed, low amplitude stable region that can be attributed to the high effective lateral suspension damping for these small displacements. In addition, this effect is reinforced in the new wheel, standard gauge plots by using values of effective conicity lower than the design value of .05. This may be the result of the worn rail profile and/or of difficulty in gathering low amplitude data for the describing function program discussed earlier. Thus the destabilizing effect of increasing conicity is seen.

Note that, using the stability argument developed earlier, there are few instances of stable limit cycles in these plots. Only when the amplitude locus increases with velocity can the curve be interpreted as a stable limit cycle (Figure 5-3a, wide gauge; Figure 5-5 a-c, wide gauge). Hence, most of the curves represent unstable limit cycles and are interpreted as stability boundaries rather than observable hunting oscillations.

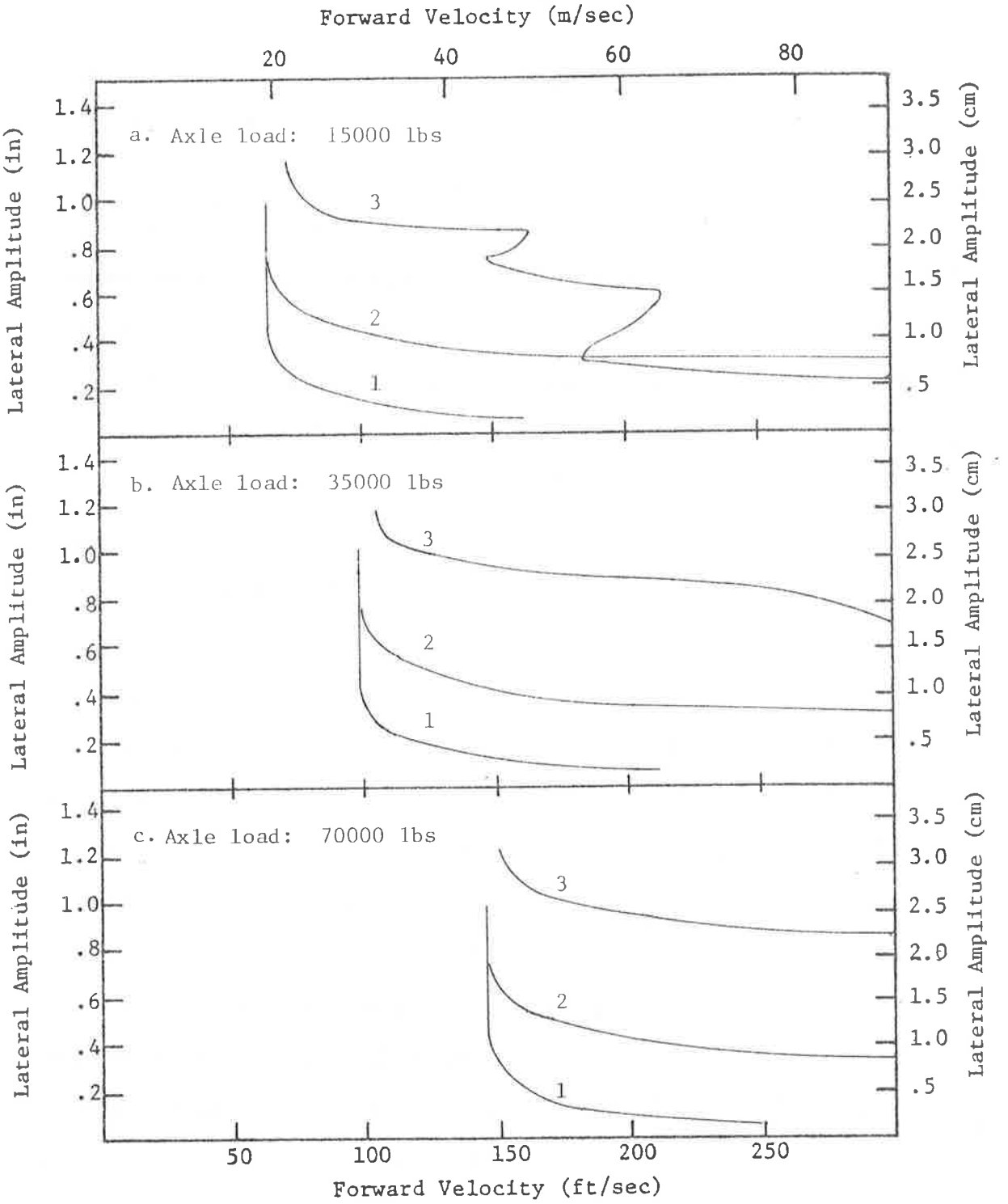

Gauge variation key: 1. Tight (56.0") 2. Std. (56.5") 3. Wide (57.5")

FIGURE 5-3. EFFECTS OF TRACK GAUGE: NEW WHEEL PROFILE

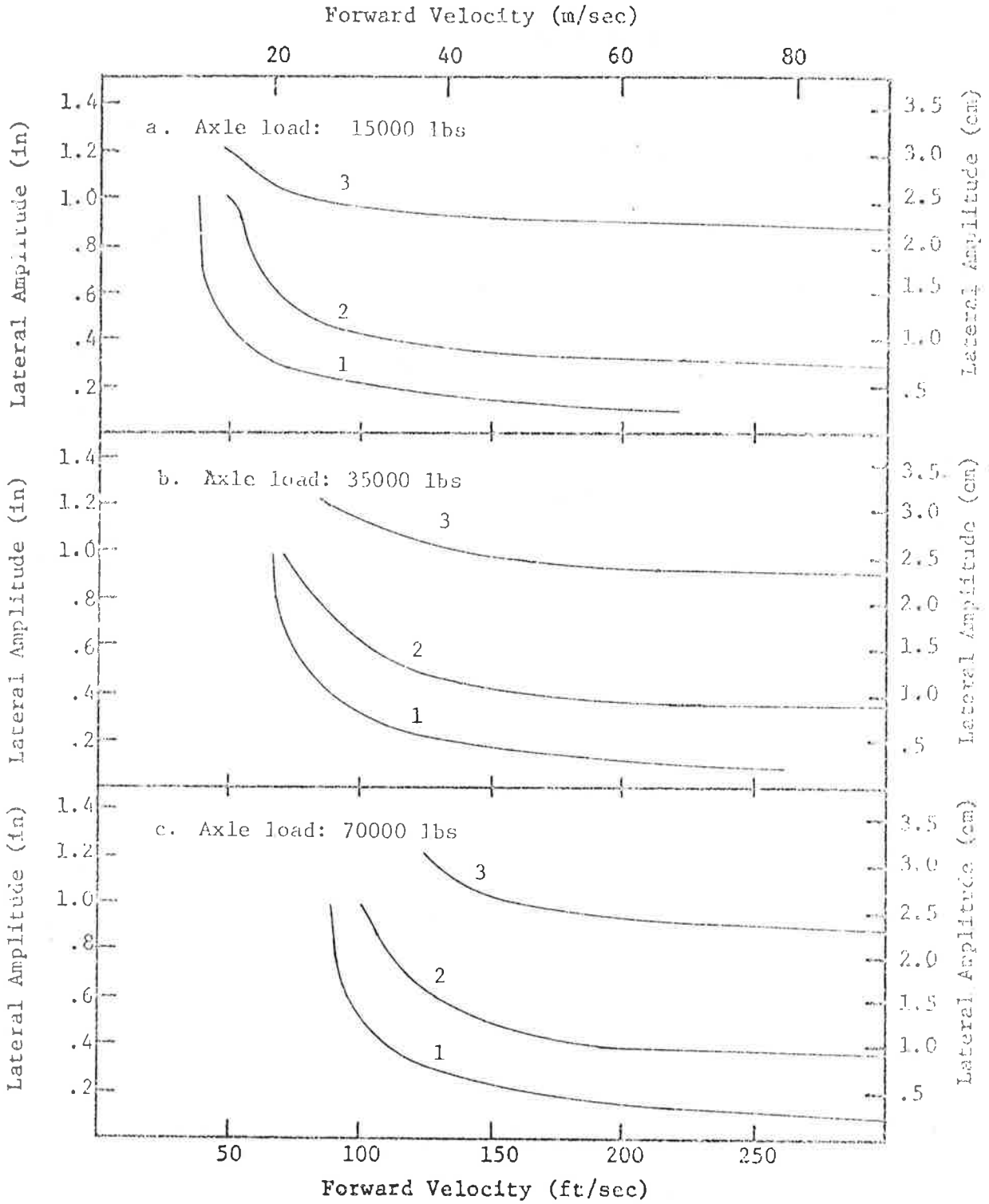

Gauge variation key: 1. Tight (56.0") 2. Std.(56.5") 3. Wide (57.5")

FIGURE 5-4. EFFECTS OF TRACK GAUGE: WORN WHEEL PROFILE

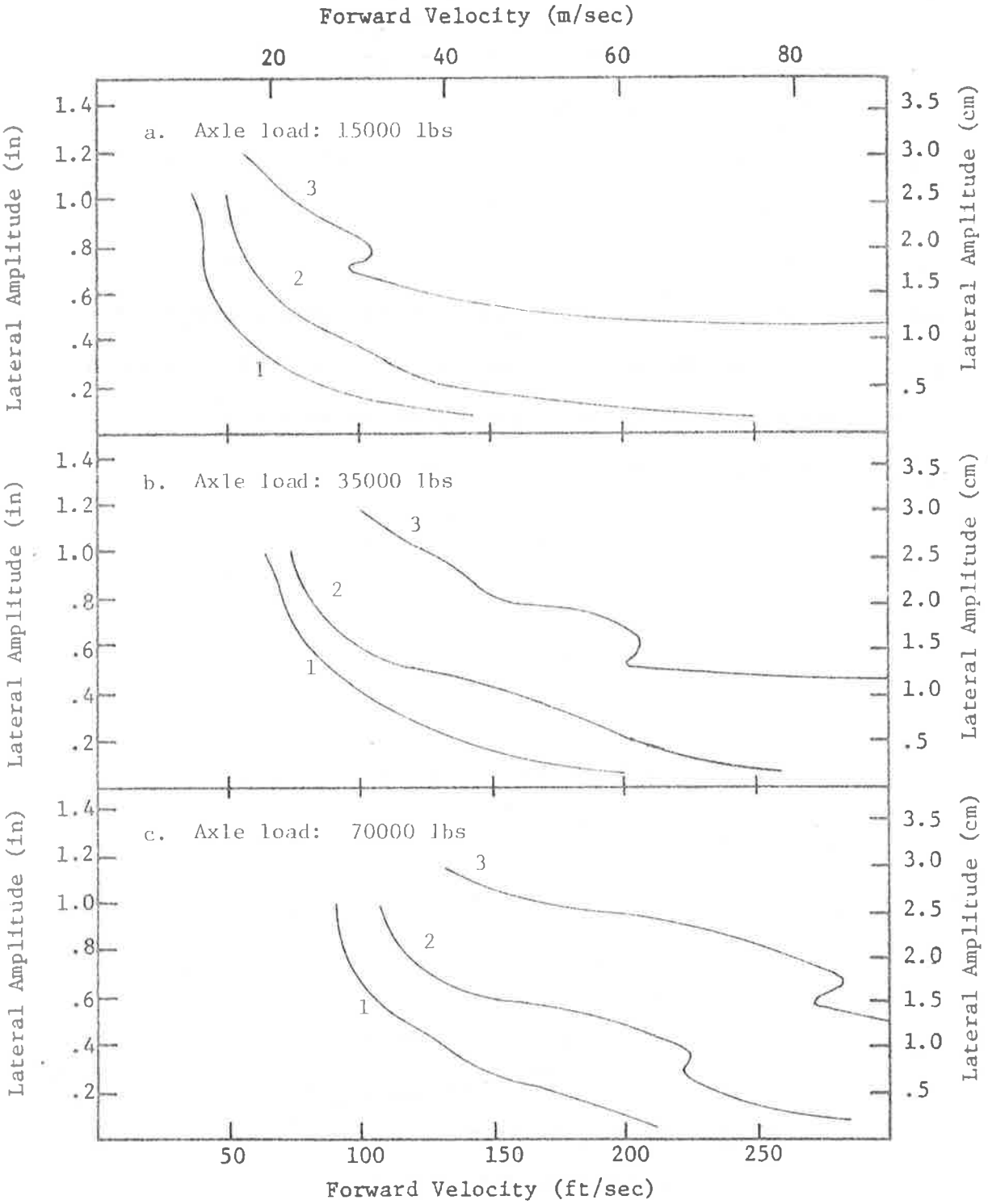

Gauge variation key: 1. Tight (56.0") 2. Std. (56.5") 3. Wide (57.5")

FIGURE 5-5. EFFECTS OF TRACK GAUGE: HEUMANN WHEEL PROFILE

5.2.3 Effects of Axle Load Variations

Figures 5-6 to 5-8 indicate that for any guage and wheel profile, increasing axle load has a definite stabilizing effect especially at the higher amplitudes, i.e., for a given velocity, increasing axle load permits larger track irregularities to be encountered before the onset of instability. Also, the velocity range for guaranteed stable response is improved by increasing axle load. Axle load is found in the gravitational stiffness term, thus explaining this stabilizing influence. Note that for most of the Figures, the results for a given gauge and profile with various axle loads are similar at low amplitudes. Again, this trend is attributed to the wheelset being influenced primarily by the suspension elements (rather than the conicity or gravitational stiffness terms) at low amplitudes.

5.2.4 Effects of Wheel Profile Variations

Figures 5-8 to 5-11 examine the stability differences between wheel profiles for fixed combinations of axle load and gauge. Nearly all the figures exhibit identical traits. For instance, for a given speed at low amplitudes, the worn wheel may provide a slightly more stable response that the new wheel. For these amplitudes, the effective conicities of the worn wheel is generally a bit larger than those of the new but its gravitational stiffness contributions are considerably greater. Thus the gravitational stiffness counteracts the effective conicity at least in the new wheel/worn wheel comparisons for low amplitudes. The

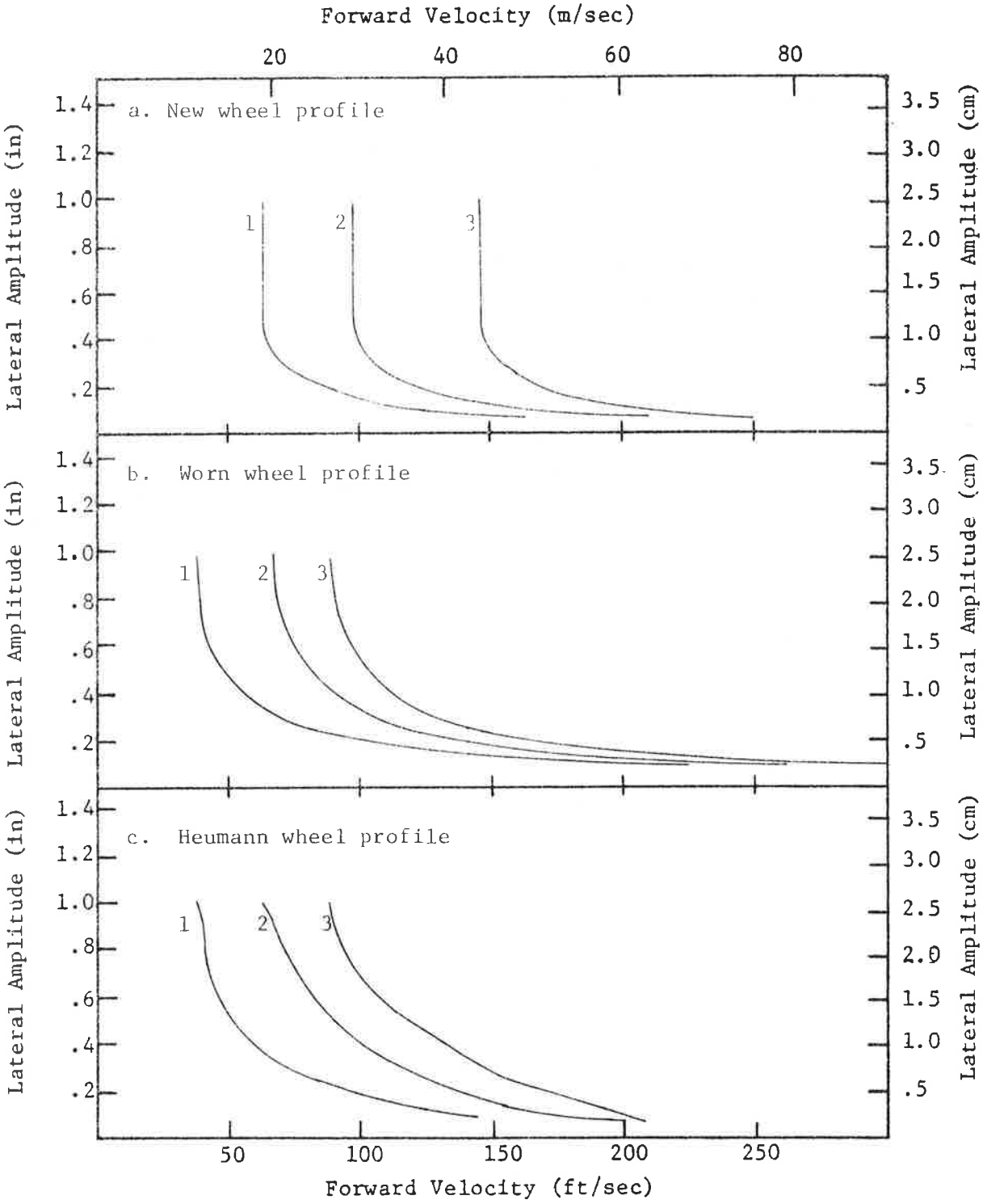

Axle load variation key: 1. 15000 lbs 2. 35000 lbs 3. 70000 lbs

FIGURE 5-6. EFFECTS OF AXLE LOAD: TIGHT GAUGE (56.0")

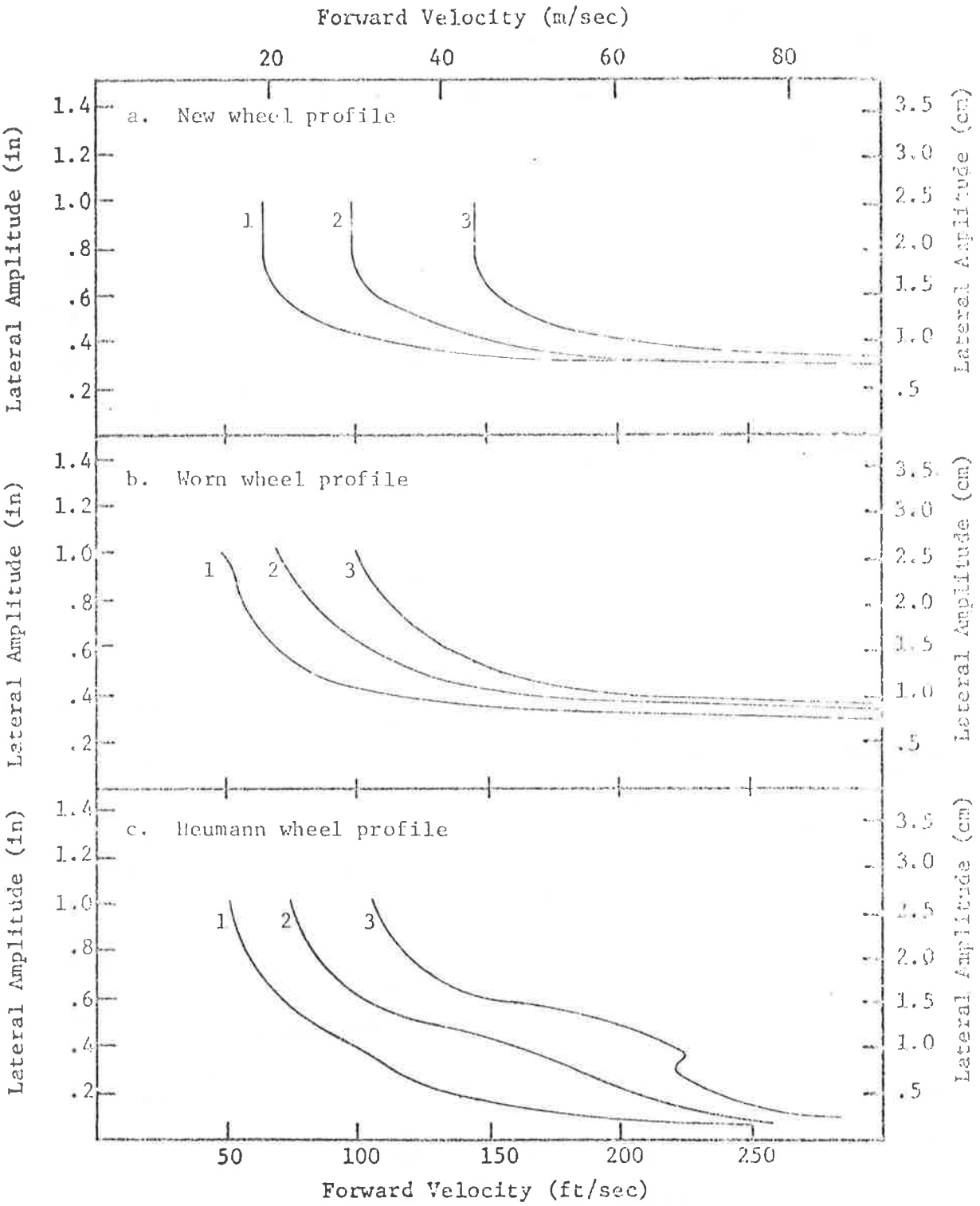

Axle load variation key: 1. 15000 lbs 2. 35000 lbs 3. 70000 lbs

FIGURE 5-7. EFFECTS OF AXLE LOAD: STANDARD GAUGE (56.5")

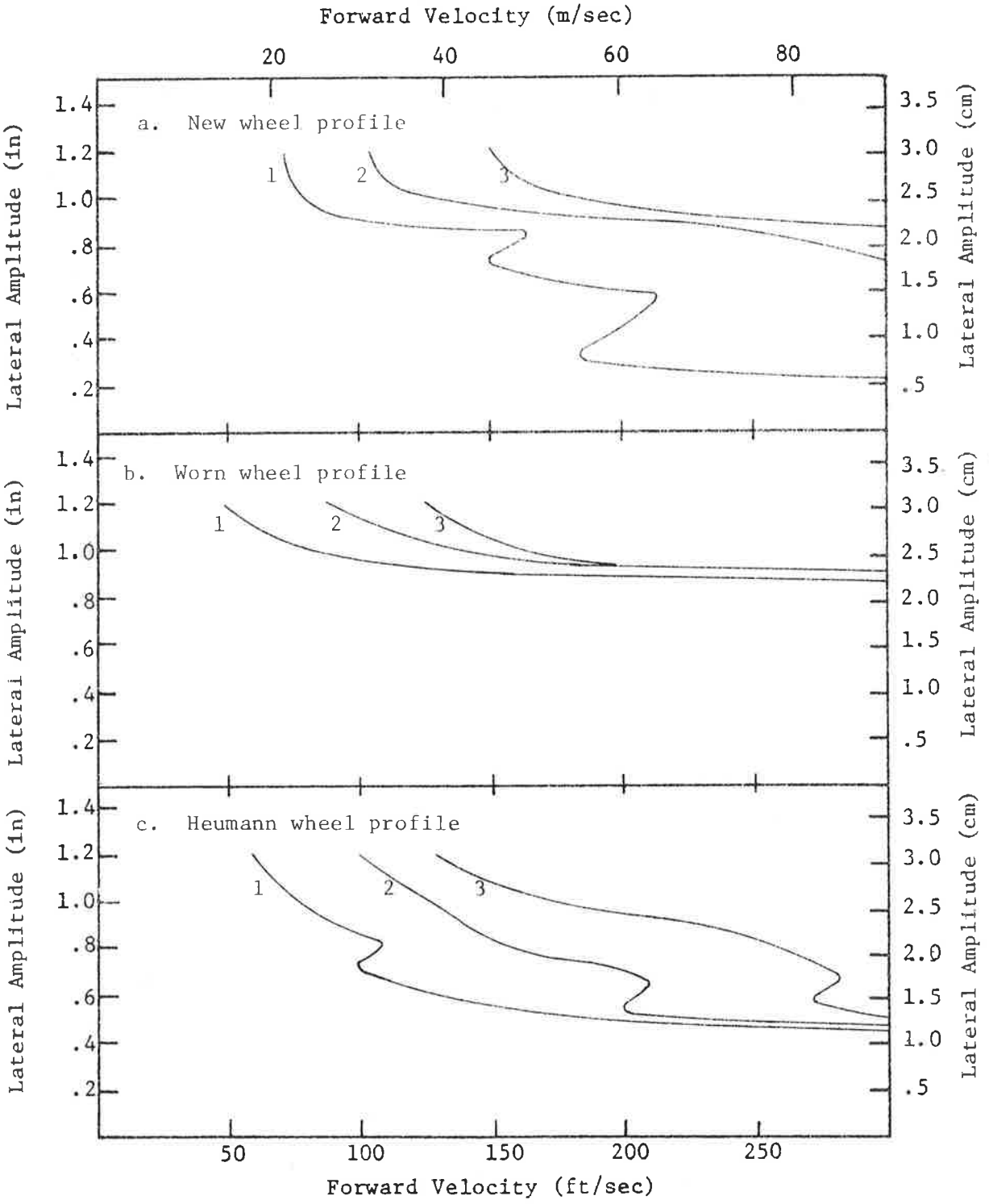

Axle load variation key: 1. 15000 lbs 2. 35000 lbs 3. 70000 lbs

FIGURE 5-8. EFFECTS OF AXLE LOAD: WIDE GAUGE (57.5")

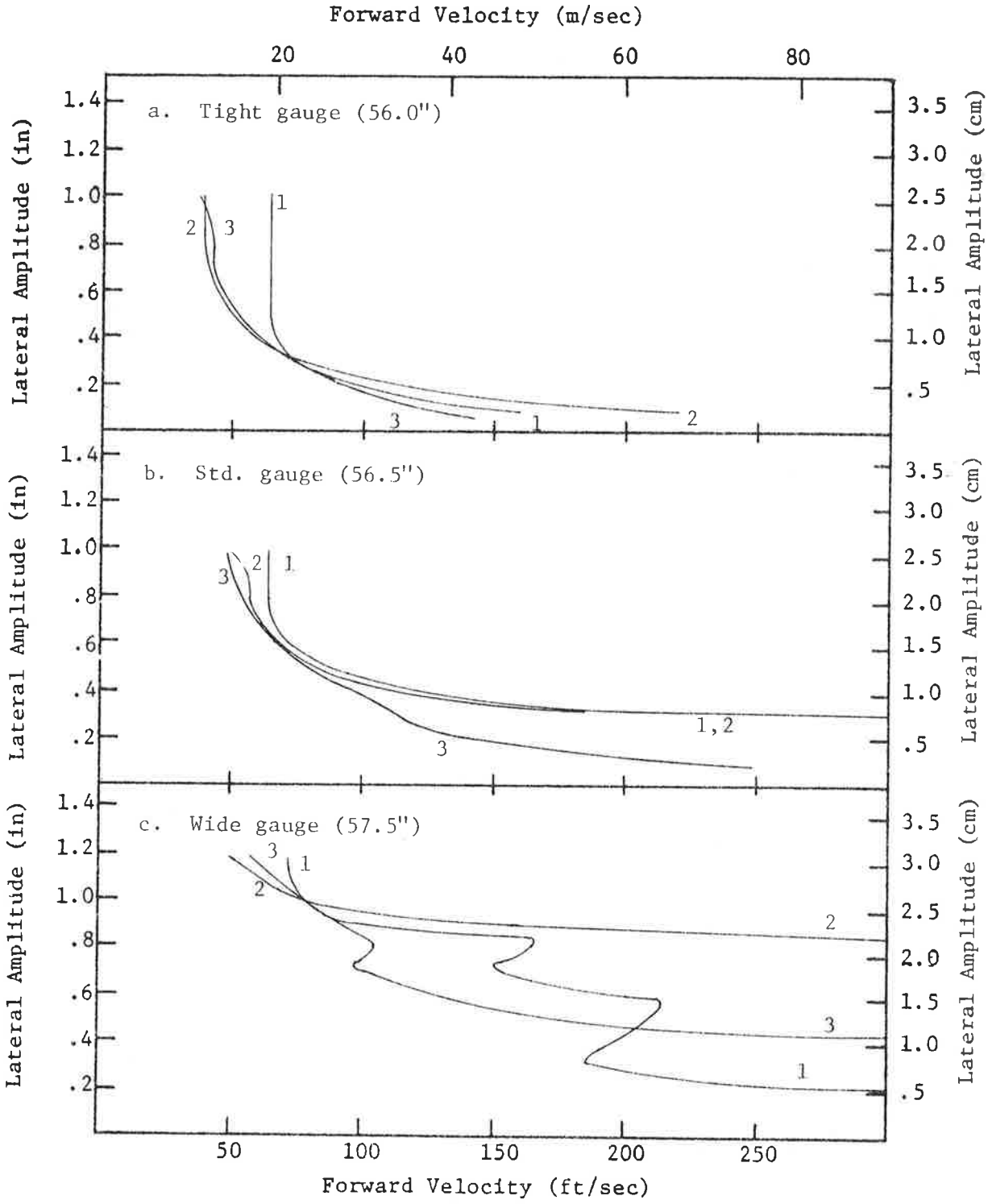

Wheel profile variation key: 1. New wheel 2. Worn wheel 3. Heumann wheel

FIGURE 5-9. EFFECTS OF WHEEL PROFILE: 15000 lb AXLE LOAD

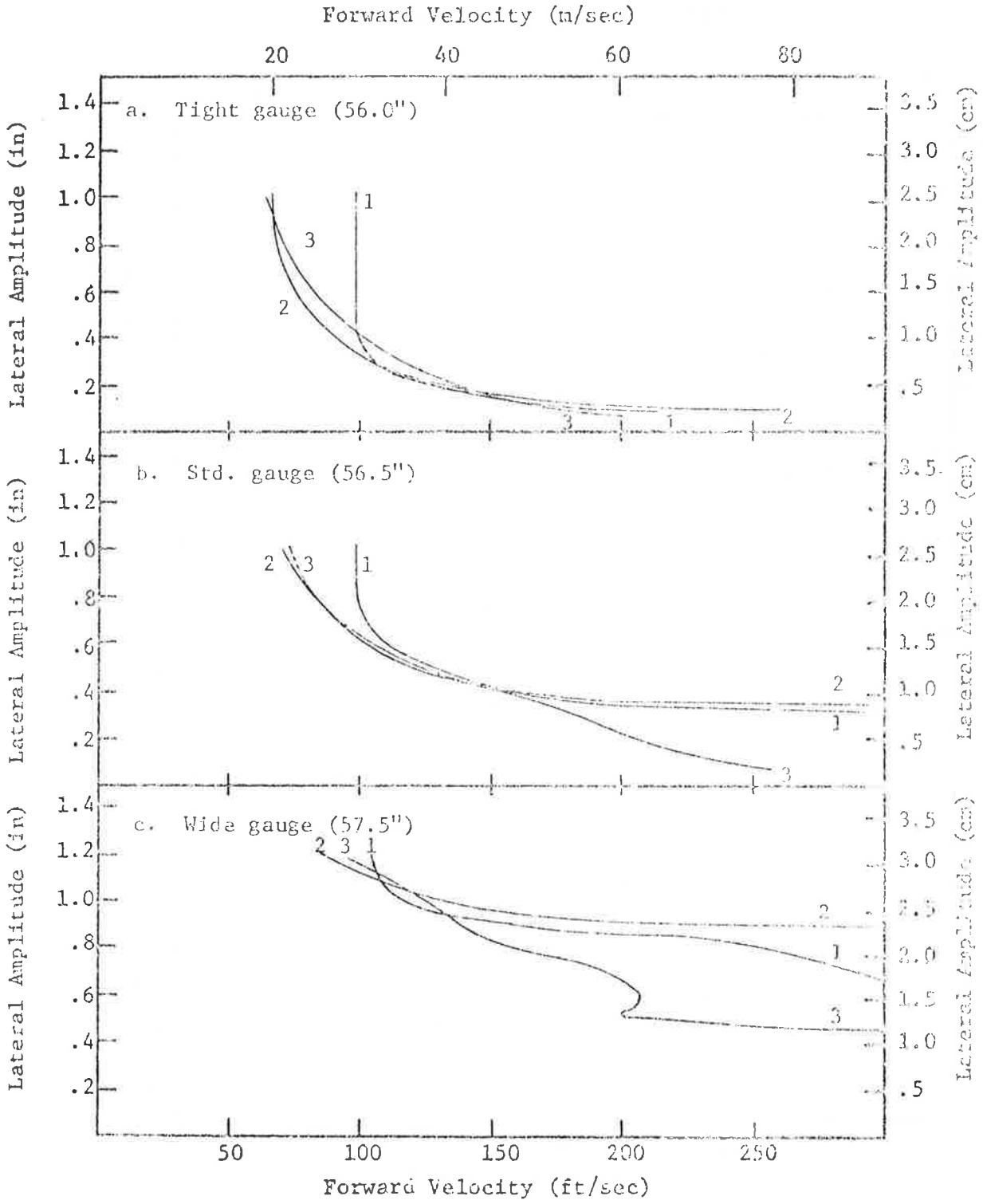

Wheel profile variation key: 1. New wheel 2. Worn wheel 3. Heumann wheel

FIGURE 5-10. EFFECTS OF WHEEL PROFILE: 35000 lb AXLE LOAD

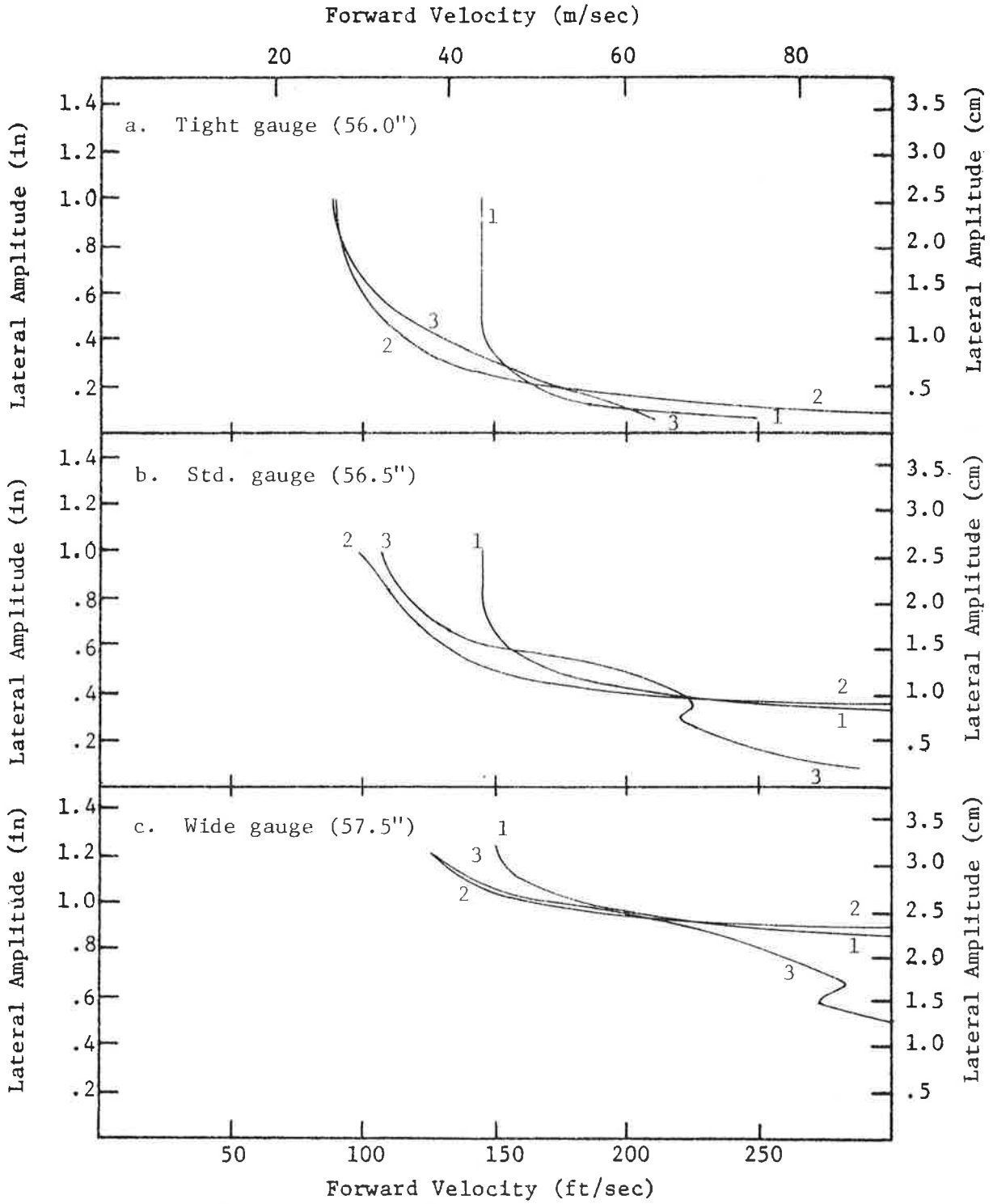

Wheel profile variation key: 1. New wheel 2. Worn wheel 3. Heumann wheel

FIGURE 5-11. EFFECTS OF WHEEL PROFILE: 70000 lb AXLE LOAD

Heumann profile clearly exhibits poorer stability at low amplitudes, an effect owed to its high conicities in this range.

At higher amplitudes the new wheel clearly allows the highest speeds to be attained. The velocity locus given at the high amplitude is probably a more important design consideration than that at the lower amplitudes since, as mentioned earlier, the low amplitude, high stability region cannot be counted on for absolute wheelset stability.

Also, at these higher amplitudes the Heumann wheel exhibits slightly better stability than does the worn wheel. However, the real benefit from Heumann wheels may be in their tendency to wear more evenly and thus maintain their original stability locus. In contrast the geometry of the standard AAR profile will change unpredictably with wear making it difficult to design for long term use.

5.2.5 Further Explanation of the Exhibited Trends

It can be seen that Figures 5-3 to 5-11 do not, in general, possess characteristics similar to the earlier lateral amplitude vs. velocity plot of Figure 3-18. In this plot, stable limit cycles were encountered at flange contact whereas the plots of Figures 5-3 to 5-11 generally do not show these trends. The describing functions are not that much different for the comparable new wheel/rail standard gauge cases of these sections However, the suspension elements have very different constants for the two models examined. The much higher yaw suspension stiffness and lateral coulomb force act as stablizing terms in this new model. Thus the loci are located at very high velocities for some of

the amplitude range. As a result, the describing function terms are overshadowed by the suspension terms in the amplitude ranges where the geometry changes considerably with displacement.

5.2.6 Possible Errors Due to Violation of Small Contact Angle Approximation

The describing function for contact angle difference, $\Delta(A)$, (equation 3-16) was obtained after making small contact angle assumptions. However, when flange contact is first made, these angles can be of the order of 60°, thus violating that assumption. The resulting error in the small contact angle assumption (Figure 5-12) can cause errors of the same magnitude in the gravitational stiffness term. New describing functions that included the contact geometry trigonometric terms were computed and some of the cases rerun. A typical result, as shown in Figure 5-13, (new wheel, standard gauge, 35000 lb axle load) proved to be qualitatively similar to the original locus (i.e., the shape of the locus did not change) although all of the plots were shifted slightly to higher velocities. Thus, apparently, the conicity and suspension terms were predominant in affecting stability in these parametric studies.

5.3 FREIGHT CAR STABILITY EXAMPLE USING EIGENVALUE METHOD

The application of quasi-linearization techniques to the problem of determining the hunting stability of a more complex rail vehicle model is discussed in this section. The nine degree of freedom

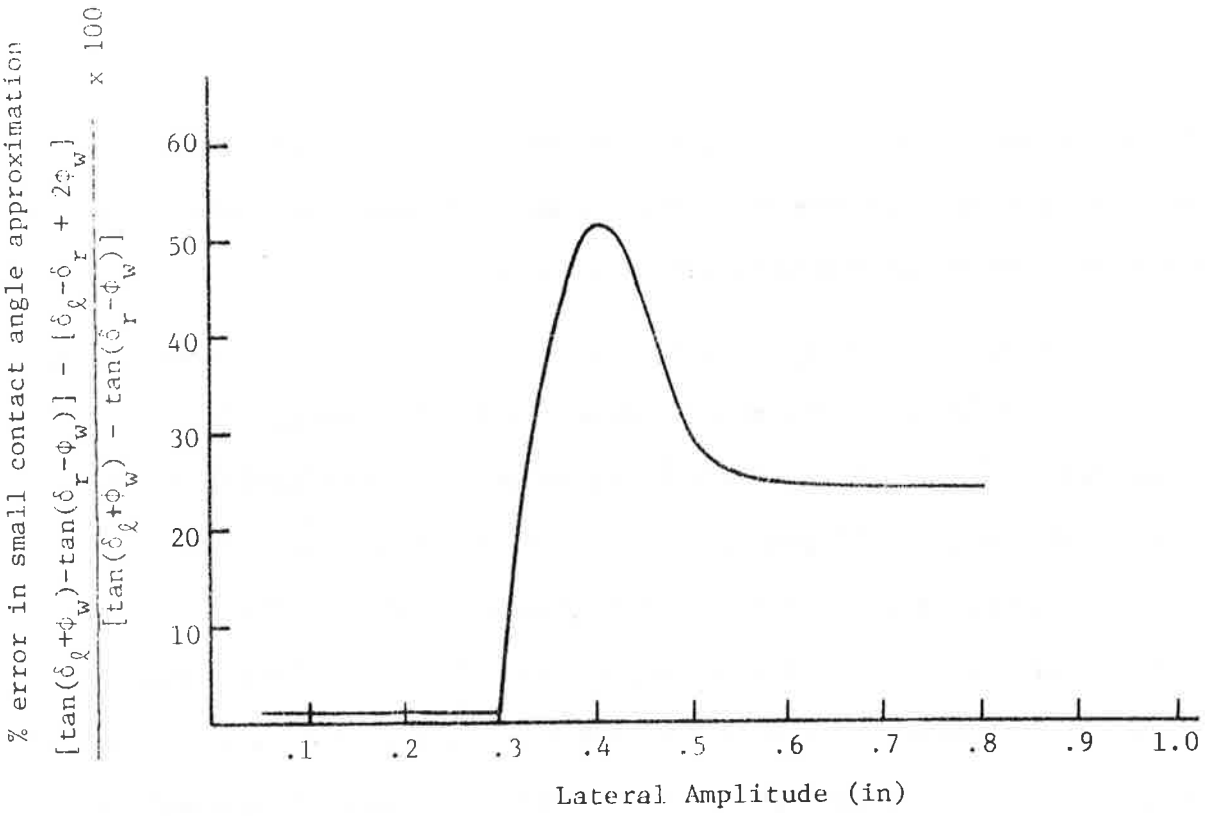

FIGURE 5-12. ERROR IN SMALL CONTACT ANGLE APPROXIMATION

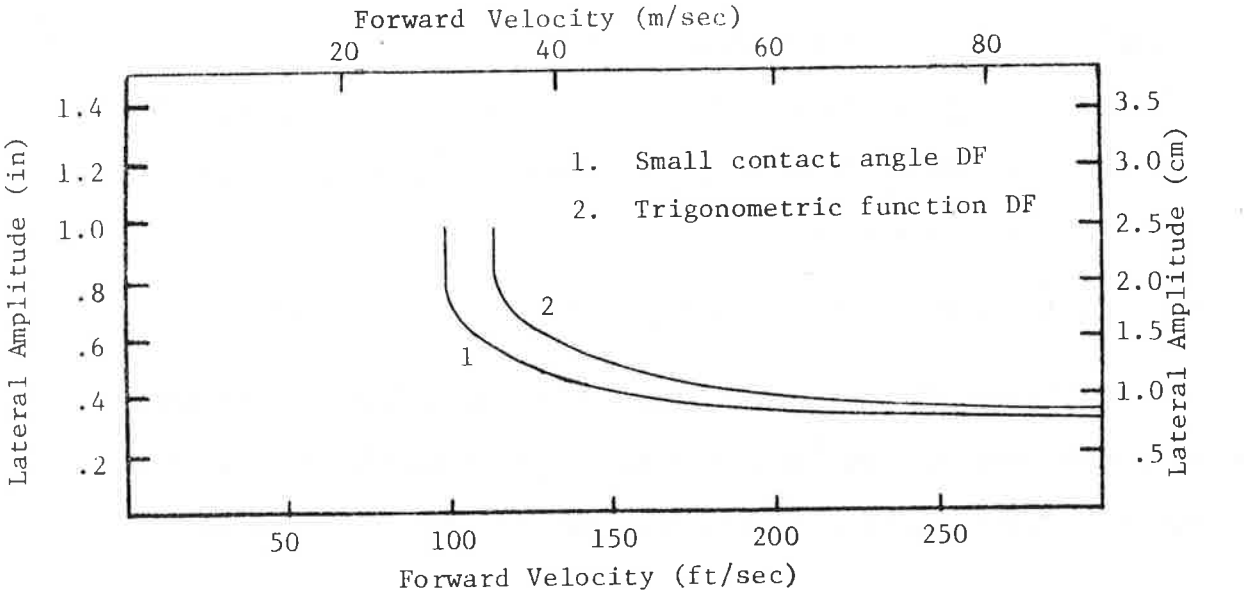

FIGURE 5-13. EFFECT OF ERROR DUE TO SMALL CONTACT ANGLE APPROXIMATION

representation of a North American rail freight car described in Section 2 was used with the nominal parameters given in Table 2-4. Results were obtained with the eigenvalue/eigenvector algorithm described in the preceding Section.

Stable and unstable limit cycle wheelset lateral amplitudes as a function of speed for three wheel profiles are shown for a vehicle with linear viscous damping in Figure 4-5 and for a vehicle with nonlinear, Coulomb suspension friction in Figure 5-14. The linear damping descriptions were computed by the describing function method, assuming constant amplitudes and frequencies. The wheelset lateral amplitude in these figures is the maximum lateral amplitude of any of the four wheelsets. The four wheelsets do not generally have the same amplitude of lateral displacement. Stable limit cycles (hunting) are again indicated by solid lines and unstable limit cycles (stability boundaries) by dashed lines.

When linear, viscous suspension damping is used, the critical velocity, shown in Figure 4-5, is almost independent of amplitude until flange contact is reached. For the new, "conical", wheel the unstable limit cycle curve is vertical until flange contact. This same result was found with the single wheelset model.

The first occurence of flange contact is characterized by a stable limit cycle that extends to a high velocity. The velocity is quite

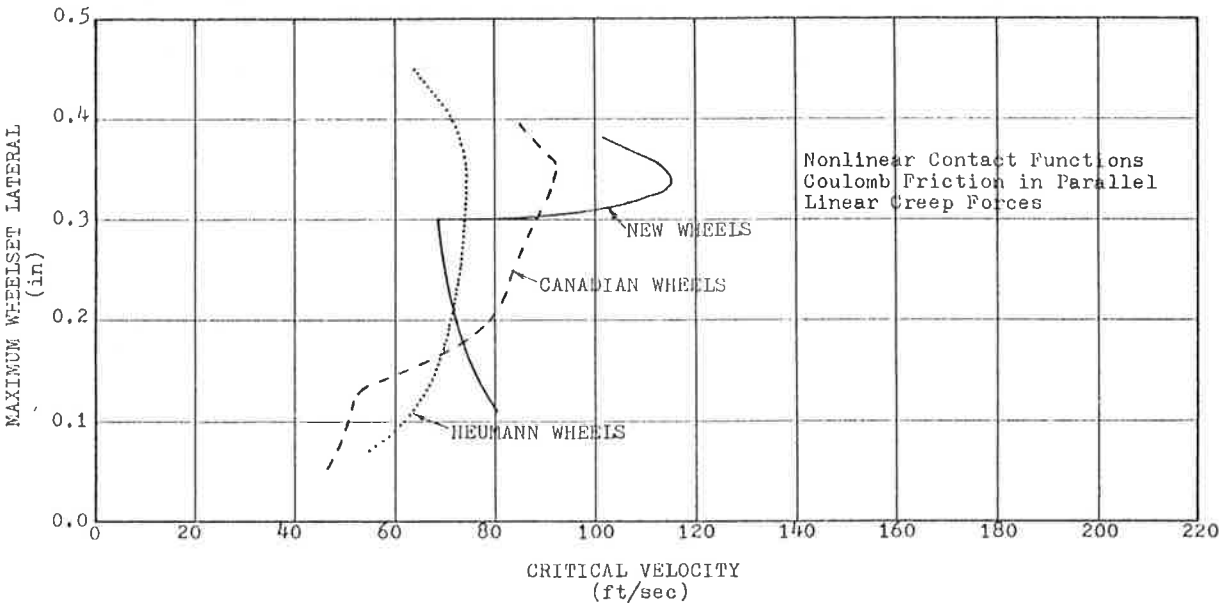

FIGURE 5-14. FREIGHT CAR LIMIT CYCLE AMPLITUDES NONLINEAR SUSPENSION

large for the new wheel case. The hunting phenomenon, that has been observed for actual rail vehicles, is described by such stable limit cycles.

The stabilizing effect of flange contact was also observed in the single wheelset results, except for the light vehicle configuration with new wheels, as was discussed.

In Figure 4-5 the freight car running on new wheels is the most stable. The freight vehicle on wheels with modified Heumann profiles, which are representative of severely worn wheels, is least stable and the stability of the freight vehicle on wheels with Canadian National wheel profiles, which are representative of slightly worn wheels, falls in between.

Stable limit cycles occur at two distinct regions of flange contact for the Canadian National wheel profile. The indication is that two distinct modes of hunting are possible here. In the lower mode, only a wheelset of the rear truck contacts the flange. In the higher one, a wheelset of each truck experiences flange contact.

The modified Heumann profile configuration experiences hunting over a limited range of speeds at low amplitudes that do not include flange contact. This probably occurs because the "conicity", or describing function for the difference in wheel radii, decreases with amplitude in this range. The effect is a result of the extreme nonlinearity of the contact geometry.

The effects of nonlinear friction on the critical velocity are shown in Figure 5-14. Note that at low amplitudes the stability was drastically

reduced. Although stable limit cycles are predicted at low speeds, these have very low amplitudes. Stable limit cycles are also found at large amplitudes. The stable limit cycles, or hunting, in which flange contact is present occur at higher speeds, closer to, but still below, that which has been found in linear analyses [3].

The low critical speeds found with nonlinear damping at low amplitudes are the result of the vehicle tending to perform as a rigid body. This is because the forces at low amplitudes due to dry friction are relatively large. At larger amplitudes the initial "breakaway" force of the dry friction is easily overcome and the vehicle acts more as a system of separate elements that allows large amount of relative motion. In fact, after flange contact, the wheelset and truck become essentially uncoupled from the car body. This is discussed further on the following pages.

In the computer algorithm, in order to prevent the dynamical matrix from becoming singular when the vehicle model tended to perform as a rigid body at low amplitudes, lower limits were placed on the magnitudes of the relative motions across the dry friction contacts. The lower limits on the motions imposed upper limits on the values of the friction force describing functions. In retrospect, it appears that this limiting effect would be better modeled by a stiff spring in series with the friction element. In this case, the spring would be the dominant suspension element at small amplitudes of relative suspension motion.

The dry friction results for low amplitude limit cycles are contrary to those found with the single wheelset model. See igures 4-7 and 4-8. In those cases dry friction was found to be very stabilizing at lower amplitudes. This difference occurs because the single wheelset model was assumed sprung to a reference body. As discussed in the previous section, the large force provided by the friction elements at small amplitudes stabilized the wheelset against the reference. The friction elements at low amplitudes forced the complete vehicle to behave as a large, rigid body which would have a low critical hunting speed.

Examination of recent freight car test data indicates that quite frequently there is little or no motion across friction elements such as the snubbers or centerplate. Consequently, this small amplitude behavior should receive closer attention in future studies.

Figure 5-14 also shows the effects of varying the friction level. The freight car running on wheels with Canadian National profiles was more stable when the friction levels were reduced by one half than when the full friction forces were used.

Eigenvector relationships, or mode shapes, for the limit cycles found for the new wheel case are shown in Figure 5-15. The abrupt change in mode shape upon flange contact is quite apparent here. Before flange

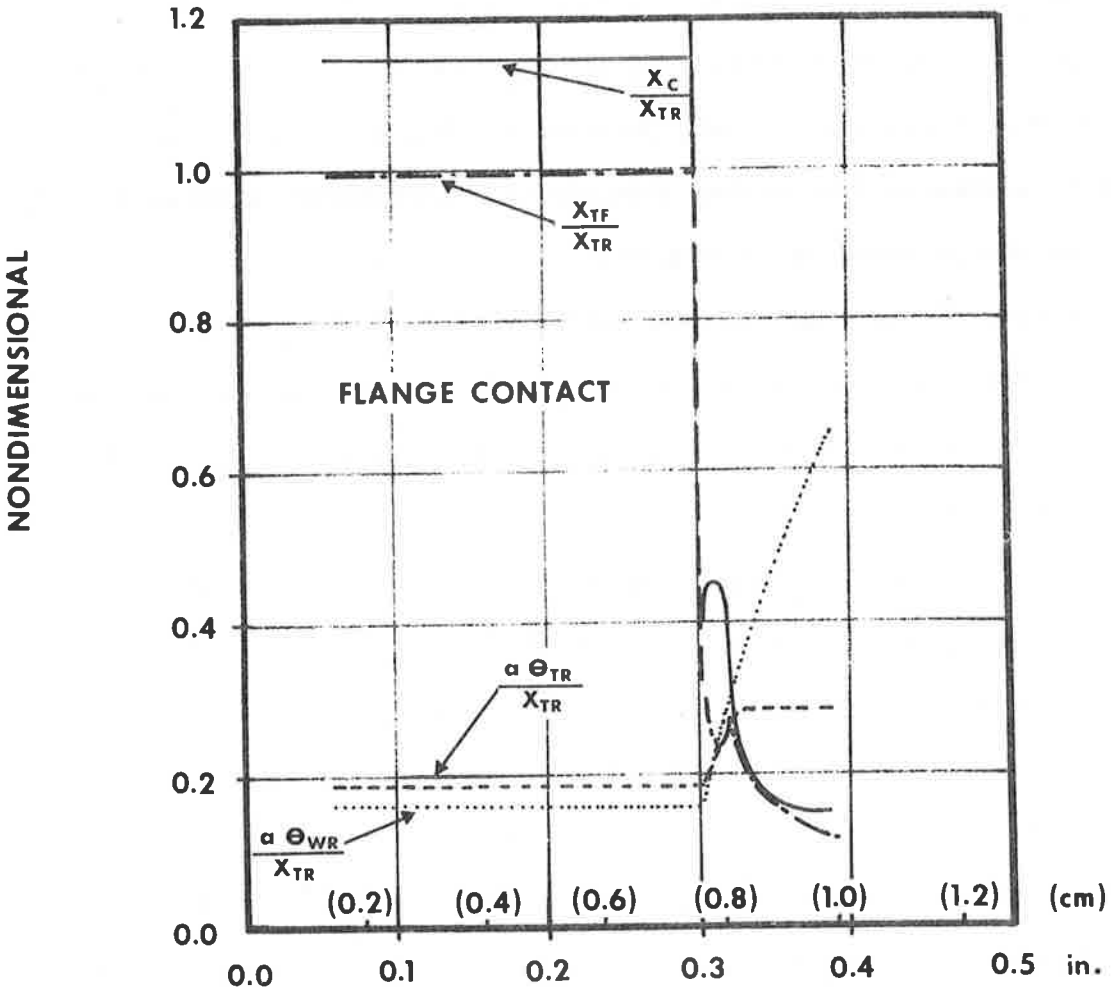

FIGURE 5-15. LIMIT CYCLE MODE SHAPES FOR NEW WHEEL

contact the mode shape is characterized by approximately equal front and rear truck lateral displacements, and the vehicle components essentially move as a unit. This shape is constant until flange contact. After flange contact the rear wheelset and truck become essentially uncoupled from the car body. The mode shape can be described as "fishtailing". The frequency is much higher than when the components moved as a unit; 30 rad/sec compared to 12 rad/sec.

Tread contact for all three wheel profile cases was characterized by the front and rear trucks having approximately equal, and out of phase, lateral amplitudes. In the worn wheel cases, though, there was negligible car body motion. This can be explained by the higher frequency of the limit cycles in the worn wheel cases, as shown in figure 5-16. The frequency was probably below the resonant frequency for car body motion in the new wheel case, and above it in the worn wheel cases.

After flange contact, the worn wheel configurations experienced "fishtailing" limit cycles similar to those of the new wheel case.

It should also be noted here that the limit cycles shown plotted in figures 4-5 , 5-14 and 5-15 were not the only limit cycles found. Limit cycles for speeds higher than the critical speeds could be found. These secondary limit cycles had different mode shapes than the primary limit cycles occurring at lower speeds. During flange contact these secondary limit cycles could be described as "nosing" modes, while the primary limit cycles would be "fishtailing" modes. It would be expected that the limit cycles occurring in practice would depend on the initial conditions and inputs to the vehicle. In the study of rail vehicle dynamics,

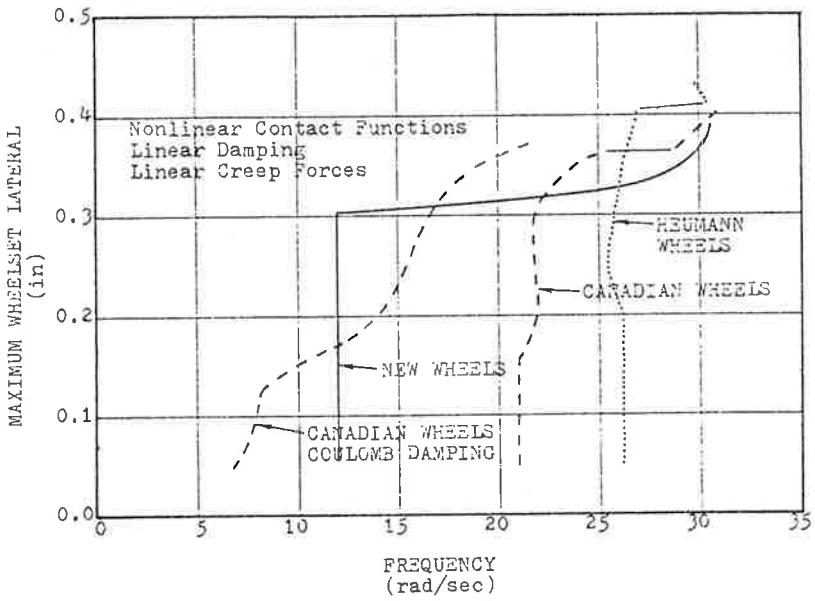

FIGURE 5-16. FREIGHT CAR LIMIT CYCLE FREQUENCY

the greatest interest is in the lowest speeds at which the rail vehicle might become unstable. Consequently, only the primary limit cycles need to be found.

Some of the results found here correlate with rail vehicle operating experience. Reynolds [33] mentions observing a fishtailing mode where a rail vehicle started to yaw and then to fishtail. The yawing could have been the low amplitude limit cycling found here that changed to the high amplitude fishtailing upon flange contact.

Reynolds and others have found that reducing the yaw friction level can induce hunting, while increasing it stabilizes hunting. The results found here showed that halving the friction forces in all of the suspension elements at one time made the vehicle more stable. This implies that a full parametric study, varying the friction elements one at a time rather than all together should be performed to understand the contribution of each friction element.

5.4 SUMMARY

The results of this study indicate that nonlinear wheel/rail contact geometry and dry friction should be considered in rail vehicle analysis because they significantly influence the hunting behavior of such vehicles. Nonlinear contact geometry must be considered to study the limit cycle motion that can occur when the wheelset lateral motion exceeds the flange contact boundary. It appears that linear descriptions of the wheel/rail contact geometry may be sufficient for studying small amplitude motions, although the critical hunting speed for small motions varies widely with different wheel/rail geometry.

Stable limit cycles, representing vehicle hunting behavior, were found to exist above certain speed ranges that were determined, in part, by the wheel/rail geometry. The speed ranges associated with flange contact were generally among these. The large gravitational forces at flange contact produced stable limit cycles, or hunting.

The parametric variations of axle loading, track gauge, and wheel profile presented in this section indicate that increasing gauge allows larger track irregularities to be tolerated while still insuring a stable response. However, Cooperrider [10] has shown that wide gauge may also cause more violent and potentially destructive wheel/rail forces to arise during flange contact. Hence, another design compromise is necessary.

Increasing axle load was shown to be a definite stabilizing influence because of its effect in the gravitational stiffness term. Design compromise here though may need to consider realistic limits imposed by the structural properties of the rolling stock and track.

New wheels were shown to possess the most desirable stability characteristics since they exhibited the highest velocities below which a stable response is guaranteed. Heumann wheels generally provided a smaller stability regime at low amplitudes (due to their high conicities at small displacement) than new and worn wheels but were comparable to worn wheels at higher amplitudes. It is noted though that since all wheelsets will wear differently the worn wheel trends may change with each specific wheelset. Also the Heumann profile may be counted on to wear more evenly (because of its single contact point design for all

amplitudes) and thus retain its stability locus longer than the standard AAR profile.

In the freight car example, limit cycles for motions not exceeding the flange contact boundary were symmetric, with similar front and rear truck lateral motions. After flange contact the limit cycles were asymmetric, fishtailing modes. Nosing shaped limit cycles could be found at slightly higher velocities than the primary limit cycles.

The freight car results gave different critical speeds with dry friction than with linear damping. This indicates that dry friction must be considered in rail vehicle analysis. For small motions, friction causes the full vehicle to tend to perform as one rigid body, which results in low amplitude limit cycles at low speeds. However, with the single wheelset, friction has a similar, stabilizing effect at low amplitudes. It is probable that the single wheelset results are of questionable practical importance because the car body, represented by the reference, would follow the wheelset in an actual vehicle. Because the small motion case appears to be of practical importance, additional study of this regime should be made.

At large amplitudes the dry friction caused the limit cycles to occur at speeds lower than predicted with equivalent linear damping. This indicates that the amplitudes and frequencies used to obtain the equivalent linear values were too large, and points out the importance of the quasi-linear techniques for handling such nonlinearities.

Qualitative results about the effects of such variables as wheel profile design, and vehicle load found with the single wheelset, were similar to the freight vehicle results, but the numerical values for such results as the critical speeds differed. Part of the difference can be explained by the difficulty in choosing representative data for the suspension parameters on the single wheelset. Also friction has a different effect on the wheelset at low amplitudes than on the freight vehicle.

The results obtained from the describing function quasi-linearization and eigenvalue/eigenvector procedure are more general than could have been obtained with conventional numerical integration which would have given results pertaining only to the specific initial conditions and inputs considered. The results indicate that nonlinear wheel/rail contact geometry and dry friction should be considered. Thus linear analysis would not be sufficient.

Future work on the present algorithms should entail improving the iteration procedures to make the consideration of creep saturation possible and to make convergence to the correct mode in the full vehicle routine more efficient. Describing functions for the tangent of the contact angles and wheelset roll angle should be used as input to the limit cycle programs to make the modeling of gravitational stiffness forces more accurate. The effects of this change on the results found with flange contact should be investigated. Additionally, more data points should be input for the contact describing functions so that the result curves would be smoother.

After the improvements described above, the quasi-linear procedure should be validated by comparison with numerical integration and experimental results.

6. FORCED SINUSOIDAL RESPONSE

6.1 INTRODUCTION

In this chapter, we discuss the use of quasi-linearization to solve for the response of rail vehicles to sinusoidal forcing introduced through the rail alignment irregularities. The discussion in Section 3 illustrated that the forced sinusoidal response problem involves solution of coupled, simultaneous, nonlinear algebraic equations. The techniques available for numerically solving such equations vary widely in complexity and in their ability to converge on a solution to the nonlinear equations. The feasibility of quasi-linearization for solving rail vehicle response problems depends on finding a simple algorithm that has good convergence properties when applied to rail vehicle problems.

The two numerical techniques used in this study are described and discussed in the following section. Results of applying these algorithms to the single wheelset model and the freight car model are presented in the succeeding sections.

6.2 SOLUTION TECHNIQUES

The quasi-linear equations of motion of a railway vehicle with sinusoidal forcing can be expressed in the following form:

$$M\ddot{\underline{x}} + N_c\dot{\underline{x}} + N_k\underline{x} = N_u\underline{u} + N_{\dot{u}}\dot{\underline{u}} \qquad (6\text{-}1)$$

where: M - Mass matrix

N_c - Describing function matrix for damping

N_k - Describing function matrix for stiffness

N_u - Describing function matrix for input vector

$N_{\dot{u}}$ - Describing function matrix for derivative of input vector

$\underline{x}$ - State vector

$\underline{u}$ - Input vector

The mass matrix terms are constants for most rail vehicle problems, but the damping and stiffness matrices contain terms that may depend on the amplitude and phase of the system response, and the amplitude and frequency of the forcing function.

When the only input to the vehicle is variation in centerline alignment, then the forcing terms, which enter through the wheel/rail constraint functions at each axle, are related by time delays. The input to the second axle, for example, is the input to the leading axle delayed by the time the vehicle takes to travel the distance between the axles. Thus, the input terms can be reduced to a scalar term, y_R, and a vector of time delays, $\underline{U}$, that depend on the vehicle speed and the distance between the axles.

In the quasi-linear sinusoidal response problem, we assume that, if the scalar input, y_R, has the form

$$y_R = A_R \cos \omega t, \tag{6-2}$$

then the system response is also sinusoidal,

$$x_i = A_i \cos (\omega t + \phi_i). \tag{6-3}$$

If expressions (6-2) and (6-3) are substituted into equation (6-1) the following set of equations is obtained:

$$[-\omega^2 M + i\omega N_c\ (\underline{A},\ A_R,\ \omega) + N_k\ (\underline{A},\ \dot{A_R},\ \omega)]\ \underline{A}$$

$$= [N_u\ (\underline{A},\ A_R,\ \omega) + i\omega N_{\dot{u}}\ (\underline{A},\ A_R,\ \omega)]\ \underline{U}\ A_R\ . \qquad (6\text{-}4)$$

Complex notation has been used to represent the in phase and out of phase components of the system response. The symbols in this equation are defined as follows:

$i \equiv \sqrt{-1}$

$\underline{A} \equiv$ Complex vector of state amplitudes.

Thus, our quasi-linear sinusoidal response problem involves solving this coupled set of 2n nonlinear algebraic equations.

One promising solution approach utilizes the special form of the above equations to employ readily available techniques for solving linear algebraic equations. This approach is shown in the flow chart of Figure 6-1. For a specified input amplitude and frequency, an initial guess is made for the amplitude and phase of the state variables, $\underline{A}_o^E$, ϕ_o^E. This information is used to compute the elements of the describing function matrices. The linear response problem with these describing functions is then solved to obtain new values for the amplitude and phase of the state variables, $\underline{A}_o^C$, ϕ_o^C. The computed values are compared with the estimates used to obtain the describing function values, and new estimates are made if the comparisons do not agree as closely as desired. The new amplitude and phase estimates are based on the previous estimates and computed responses. The process is repeated until the desired agreement is obtained. The entire process can be repeated for as many input amplitudes and frequencies as desired.

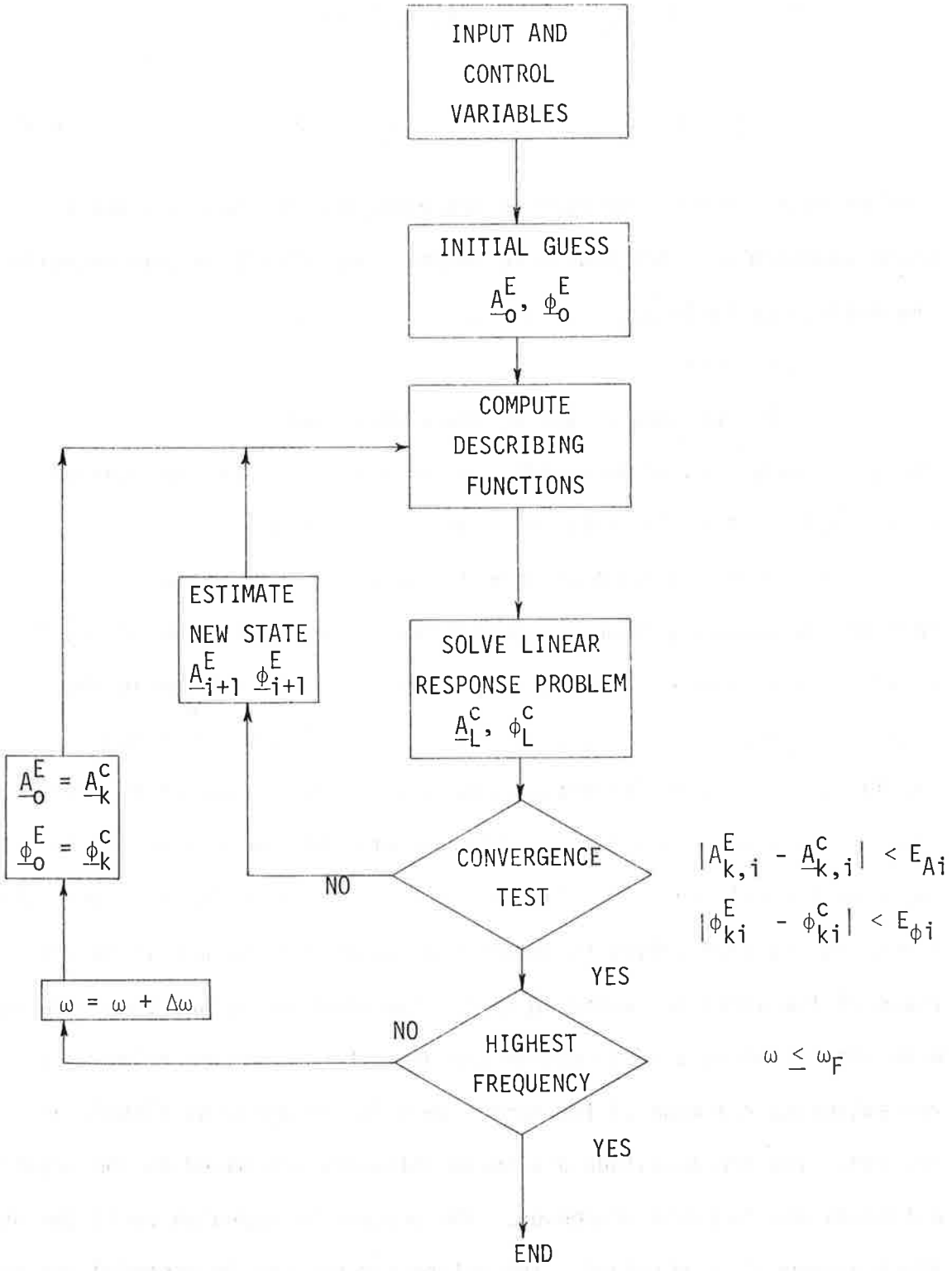

FIGURE 6-1. FLOWCHART FOR SINUSOIDAL RESPONSE ALGORITHMS

The success of the approach described above depends in part on the initial guess, A^E_o and ϕ^E_o, for the amplitude and phase of the state variables. Previous knowledge obtained from linear response studies can be used to estimate the initial state for a given input amplitude. After converging on a solution at a low frequency, this solution can be used as an initial guess for an increased frequency. This process is repeated until the highest desired frequency is reached. The ability of some iterative algorithms to converge on a solution to equation (6-4) depends on the proximity of the initial guess to the final solution.

Convergence was particularly touchy near the first resonance of the system response. It proved helpful to limit the frequency step between solution points when the phase of the variables changed rapidly with frequency. A check was made in the computer programs to cut back the frequency step when the phase change for any state between the two previous frequency values exceeded a limit, such as 10 degrees.

The success of such an approach depends most strongly on the algorithm used to estimate new state conditions from the previous estimates and computed responses. Two techniques for the forced sinusoidal response problem were used in this study. The first approach was to simply base the new estimates on the difference between the most recent computed values and the values computed in the previous iteration, i.e. for the ith state, the estimated value for the k+1 interation is given by

$$A^E_{k+1,i} = A^c_{k+1,i} + p\,(A^c_{k,i} - A^c_{k-1,i}), \qquad (6\text{-}5)$$

where p is set between 0 and 1. A similar equation defines the new estimate of the phases. The parameter p is selected to obtain numerical stability, and can be varied during the iteration process. In general, the range of stability is greater for smaller values of p, but convergence speed is better with larger values of p.

A second iterative algorithm, loosely based on the Newton-Rapheson search technique, was also used in this study because the techniques described above did not converge under certain conditions. This technique involved numerically estimating the rate of change of the computed response to changes in the estimated state, and using this estimate to linearly extrapolate to a point where the two are equal. If we regard the computed response as a function of the estimate, i.e.

$$\underline{A}_i^c = \underline{f}_A (\underline{A}_i^E , \underline{\phi}_i^E)$$

$$\underline{\phi}_i^c = \underline{f}_\phi (\underline{A}_i^E , \underline{\phi}_i^E) , \qquad (6\text{-}6)$$

and ignore the coupling between the estimate for one state and the response of another, so that

$$A_{i,k}^c = f_{Ak} (A_{i,k}^E)$$

$$\phi_{i,k}^c = f_{\phi i} (\phi_{i,k}^E) , \qquad (6\text{-}7)$$

then we want to find $A_{k,i}$ and $\phi_{i,k}$ such that

$$A^{c}_{i,k} = A^{E}_{i,k}$$

$$\phi^{c}_{i,k} = \phi^{E}_{i,k} \quad , \tag{6-8}$$

Define the function,

$$F_{Ak}\ (A^{E}_{i,k}) = f_{Ak,}\ (A^{E}_{i,k}) - A^{E}_{i,k} \tag{6-9}$$

Then, if we apply the Newton-Rapheson procedure to find the zeros of this function we require that

$$\frac{dF_{Ak}}{dA^{E}_{i,k}} \Delta A^{E}_{i,k} = - F_{Ak}\ (A^{E}_{i,k}) \tag{6-10}$$

If we use a two point estimate for

$$\frac{dF_{Ak}}{dA^{E}_{i,k}} = \frac{F_{Ak}(A^{E}_{i,k}) - F_{Ak}\ (A^{E}_{i,k-1})}{A^{E}_{i,k} - A^{E}_{i,k-1}} \quad , \tag{6-11}$$

then we obtain the following expression for iterative algorithm,

$$A^{E}_{i+1,k} = A^{E}_{i,k} - p \frac{F_{A}\ (A^{E}_{i,k})}{\frac{dF_{Ai}}{dA^{E}_{i,k}}} \tag{6-12}$$

where: p - parameter between 0 and 1 that controls the size of the change in step.

Because this algorithm ignores the coupling between equations there is no apriori reason to expect it to converge. However, this approach had better convergence properties for the problems studied here than the algorithm described earlier. Additional logic was needed in the computer programs to avoid overflow problems when the $\frac{dF_{Ak}}{dA^{E}_{i,k}}$ or $F_{Ak}(A^{E}_{i,k})$ expressions approached zero.

As mentioned earlier, convergence of the iteration procedure often failed at frequencies near the first resonance of the system response. At this position small changes in the estimated state amplitudes and phases caused large changes in the computed state amplitudes and phases. As expected, the numerical stability was poor in this situation with a high gain between the input and output of the process. The second technique described above was more stable in this situation than the simpler technique described first. Reducing the change in estimated state and phase at each iteration, by using a smaller value of the parameter p, also improves numerical stability at the expense of convergence time. In order to improve stability when needed without increasing computation time when the improved stability was not needed, the parameter p was made a function of the number of iterations. The following relationship between p and the number of iterations, I, was found to work well:

I	p
1 - 10	1.0
11 - 20	0.50
21 - 30	0.25
31 - 40	0.125
41 - 50	0.0625

6.3 TYPICAL WHEELSET RESULTS

6.3.1 Computational Considerations

The behavior of the algorithms described in the previous section is most easily illustrated by a simple example. The two algorithms built around linear system analysis techniques were applied to the equations describing the response of a single wheelset with nonlinear wheel/rail geometry and Coulomb friction in the suspension connection to a sinusoidal track alignment input. The equations of motion for this example are developed in Section 2, and the sinusoidal input describing functions for these nonlinearities are given in Section 3. A normalized form of the equations with the nominal parameters given in Table 2-1 was used to develop the results discussed below.

The forced sinusoidal response of the single wheelset with new wheels and nominal values for friction is illustrated in Figures 6-2 and 6-3. Figure 6-2 shows lateral wheelset amplitude as a function of frequency, while the amplitude of the yaw motion is shown in Figure 6-3. Neither of the two algorithms converged reliably in the region from 1 Hz to 2 Hz.

It appears that the convergence difficulty is due to the fact that, in the wheelset amplitude region near flange contact, very small changes in amplitude cause large changes in the describing function values. This can be seen in the steep slopes of the describing functions for the wheel/rail geometry functions shown in Figures 3-14 and 3-15. These steep slopes mean a high gain in the feedback of the iteration process, which

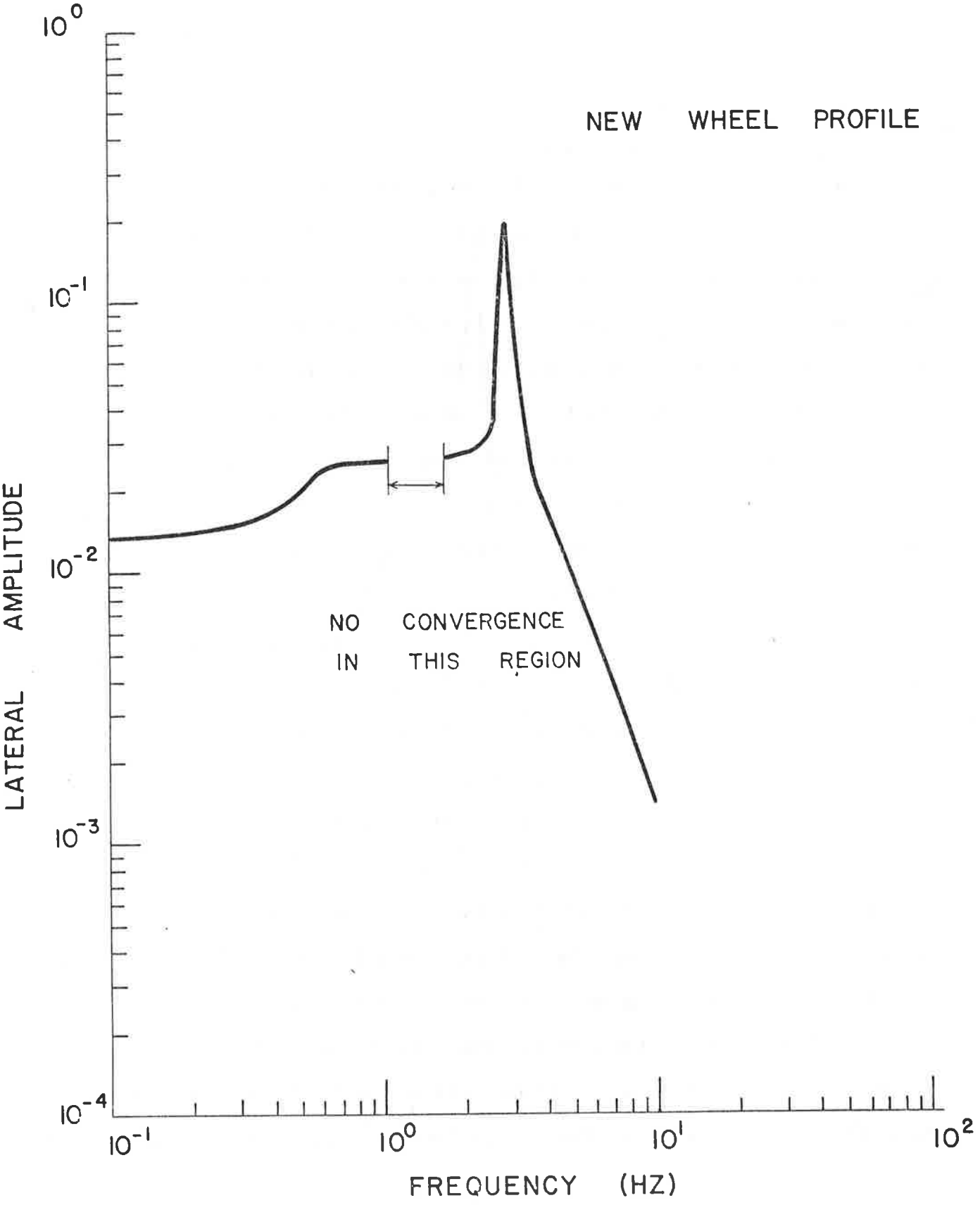

FIGURE 6-2. WHEELSET LATERAL RESPONSE WITH NEW WHEELS

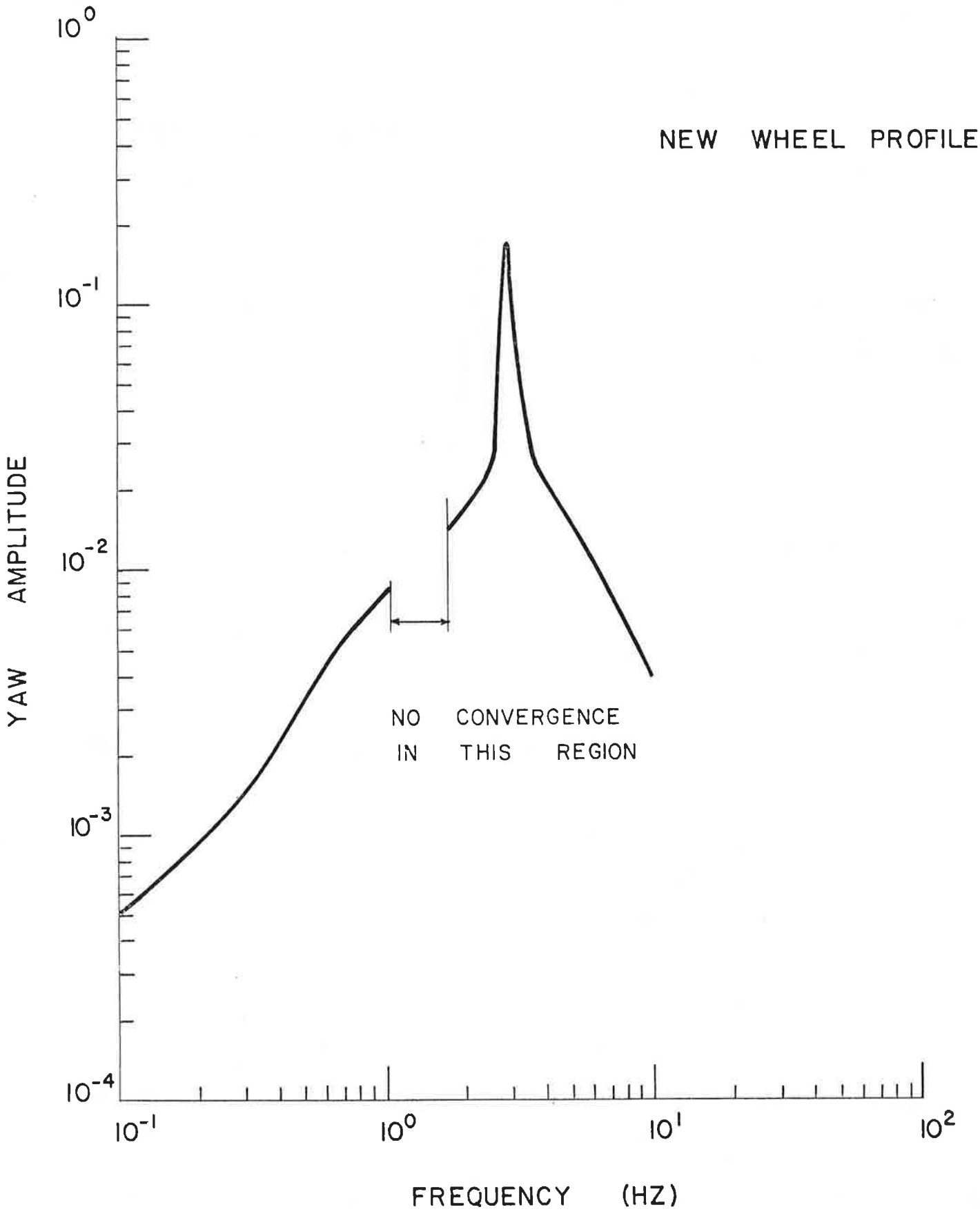

FIGURE 6-3. WHEELSET YAW RESPONSE WITH NEW WHEELS

leads to numerical stability problems. The convergence difficulty with this example occurred at frequencies near the "kinematic" mode of the new wheel frequency where amplitudes large enough to cause flange contact occur. At other frequencies flange contact did not occur, and there the algorithm converged within 3 or 4 iterations.

Several approaches were tried to improve numerical stability in this region. In the direct substitution algorithm, the percentage of the difference between new and old values was reduced. At small percentages, near 1 percent, the range of stability increased, but did not provide convergence at all frequencies. The stability of the technique appears to be strongly dependent on initial conditions. Convergence will occur at some frequencies when the initial guess is close to the final solution, but will diverge for large differences between initial guess and solution. To improve convergence smaller frequency steps were tried. This provided a better initial estimate at each new frequency, and increased the region of stable solutions. However, even frequency steps as small as 0.001 Hz were not sufficient to converge throughout the frequency range of interest.

The approximate Newton-Rapheson technique was more reliable than the direct substitution method. To improve its numerical stability the change in the independent variable was limited to a percentage of the estimated value. Again, this improved convergence at the expense of computation time but did not provide convergence at all frequencies. The most successful technique found for applying the approximate Newton-Rapheson

method was to initially use the full estimated value of the independent variable, and if convergence was not obtained after a given number of iterations to cut the step size of the independent variable to one-half the estimate. This process was continued, cutting the step size by 50 percent after running through a fixed number of iterations until the solution converged, or a limit on the number of iterations was reached. This approach was considerably more reliable than the direct substitution algorithms.

If one desires the quasi-linear response of a system with a "stiff" nonlinearity as is found in the model of a wheelset with new wheels used here, then a more sophisticated numerical iteration algorithm should be considered. However, in some cases it may be possible to soften the nonlinearity without compromising the integrity of the model. In the wheelset, for example, the rail structure itself has some flexibility that will reduce the effective stiffness. The small angle assumptions used for the contact angle describing functions should also be replaced with the trigonometric functions, a change that may increase the effective stiffness.

The lateral wheelset amplitude vs. frequency relationship found for a single wheelset with Heumann profile wheels by the approximate Newton-Rapheson algorithm is shown in Figure 6-4. Better convergence is obtained for this problem because the wheel/rail geometry functions for the Heumann wheel profile are not as "stiff" as those for the new wheel profile.

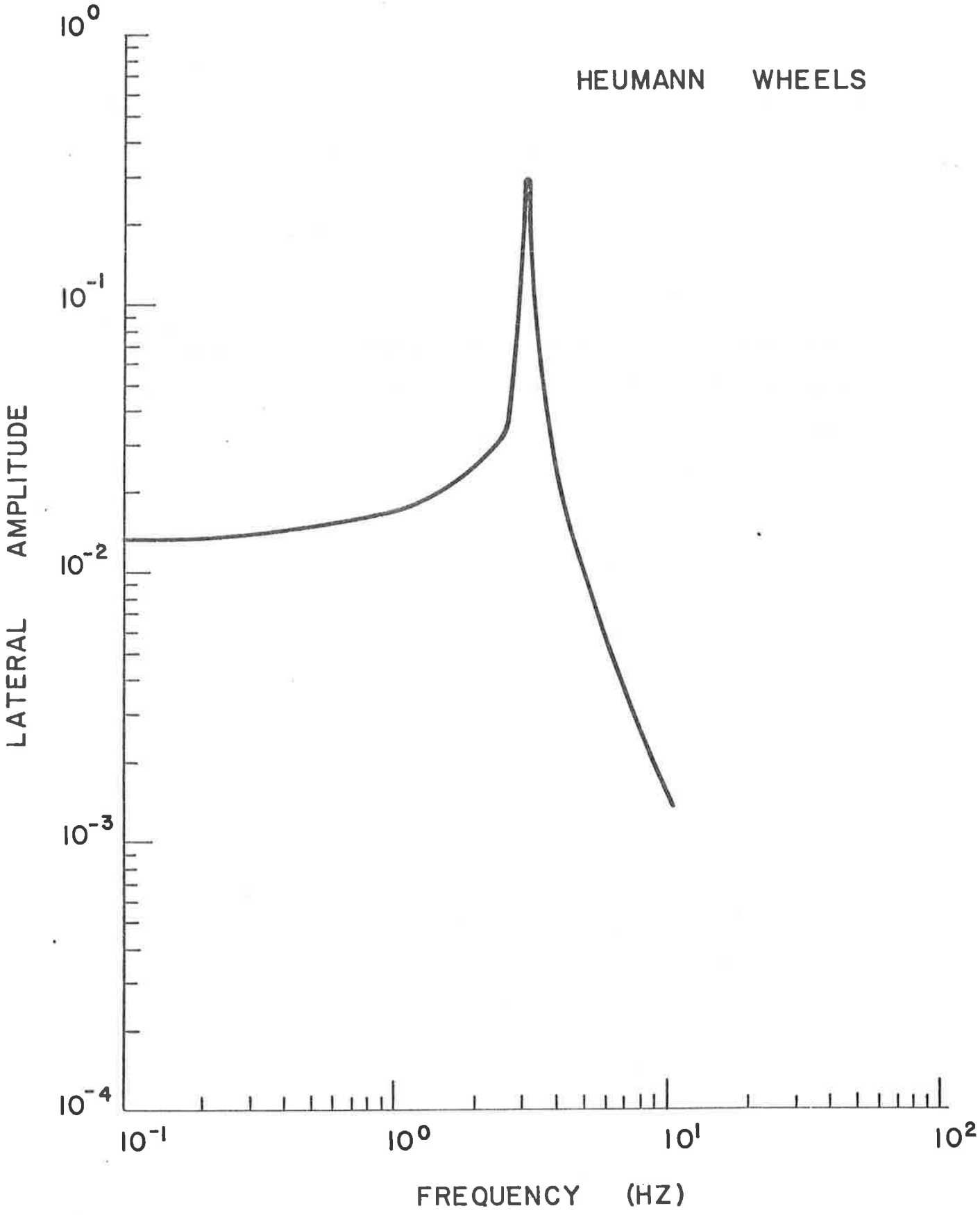

FIGURE 6-4. WHEELSET LATERAL RESPONSE WITH HEUMANN WHEEL PROFILES

6.3.2 Parametric Variations

The nonlinear sinusoidal response computed for the single wheelset revealed several interesting, and somewhat unexpected, characteristics. In the new wheel response curves shown in Figures 6-2 and 6-3, the second peak at about 3.5 Hz is well above the kinematic frequency for this wheelset. It appears that this higher frequency resonance is a large amplitude oscillation dominated by the contact of the flange on the rail. One might think of this as analogous to the wheelset mass oscillating on a stiff spring that represents the gravitational stiffness of the rail. The high conicity at large amplitudes no doubt also influences this mode. This interpretation of the high frequency peak is borne out by the results of varying the rail alignment amplitude discussed later in this section. At low input amplitudes, flange contact does not occur at the higher frequencies, and the response drops off rapidly, as one would expect in a linear system.

The sinusoidal response for the wheelset with Heumann wheel profiles shown in igures 5-20 and 6-4 demonstrate the nonlinear character of the system a bit more directly. The dips in this response curve directly reflect the corresponding dips in the numerically computed wheel/rail geometric constraint functions. Perhaps the most interesting aspect of the Heumann response curve is that the single peak occurs at about 3.5 Hz, the same frequency as the high frequency peak found with new wheels. This is not so surprising if we recall that both the Heumann and new wheels have the same wheel/rail geometry describing functions at large

amplitudes. Thus, this peak also corresponds to a flange contact oscillation of the wheelset.

The variation in wheelset response to changes in sinusoidal alignment amplitude revealed several characteristics typical of nonlinear systems. Figure 6-5 depicts the wheelset lateral amplitude as a function of frequency for new wheels at two additional input amplitudes. As mentioned above, the response at low input amplitudes is quite similar to that of a linear system, as expected. At high amplitudes, however, a jump resonance is seen at higher frequencies. This jump resonance, similar to that seen in a simple mass - hardening spring system, is probably due to the hardening character of the gravitational stiffness.

The wheelset lateral response to different input amplitudes with Heumann profile wheels, shown in Figure 6-6, indicates similar results to those found for the new wheel. At very high amplitudes the jump resonance behavior does not appear, but it is evident at smaller input amplitudes.

The friction levels in the parallel and series suspension connections were varied independently over wide ranges for the new and Heumann wheel profiles. For these conditions, the variation in friction levels had no perceptible influence on the response curves. Thus, it appears that the wheelset response is dominated by the wheel/rail geometry nonlinearities.

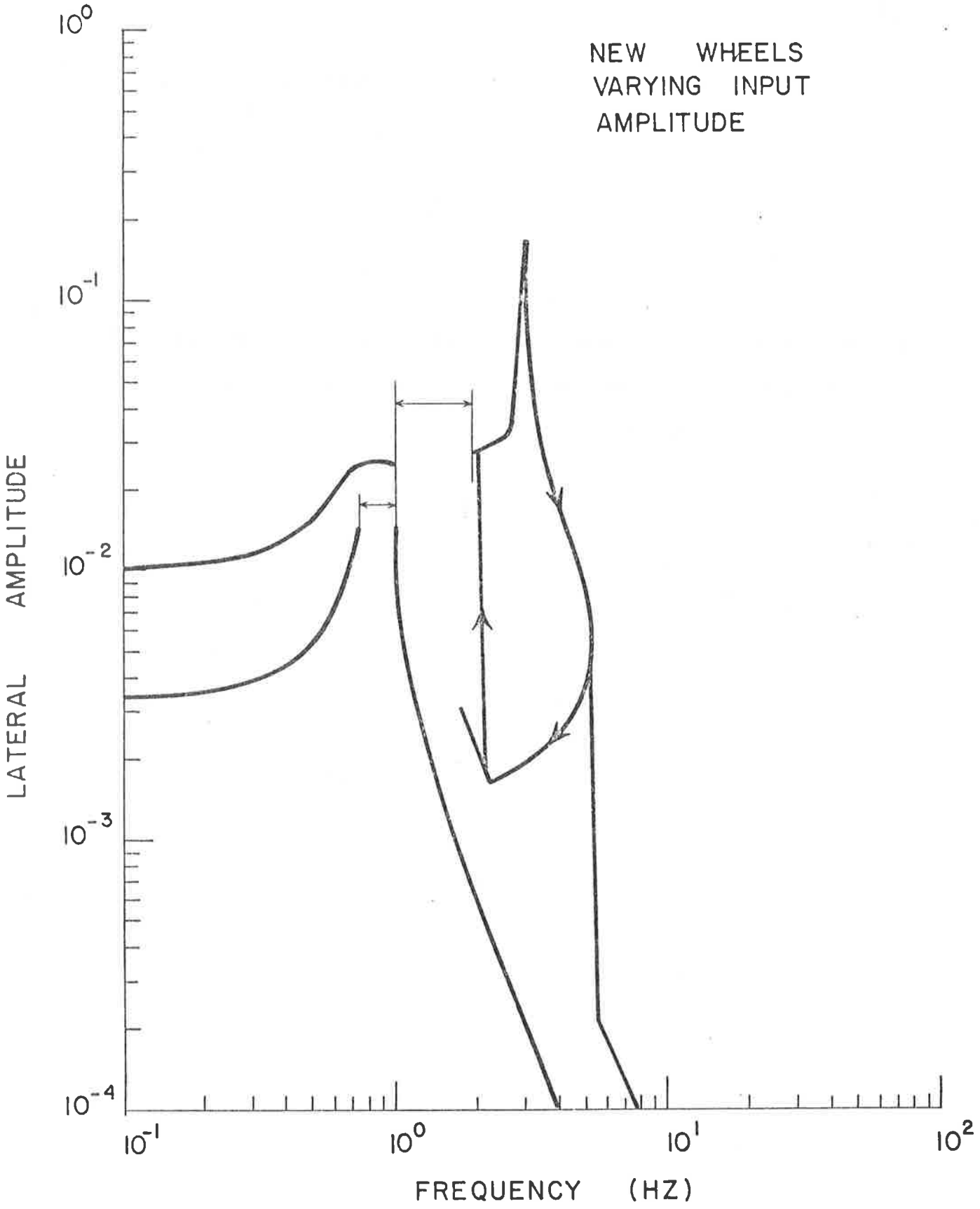

FIGURE 6-5. WHEELSET LATERAL RESPONSE WITH NEW WHEELS FOR TWO INPUT AMPLITUDES

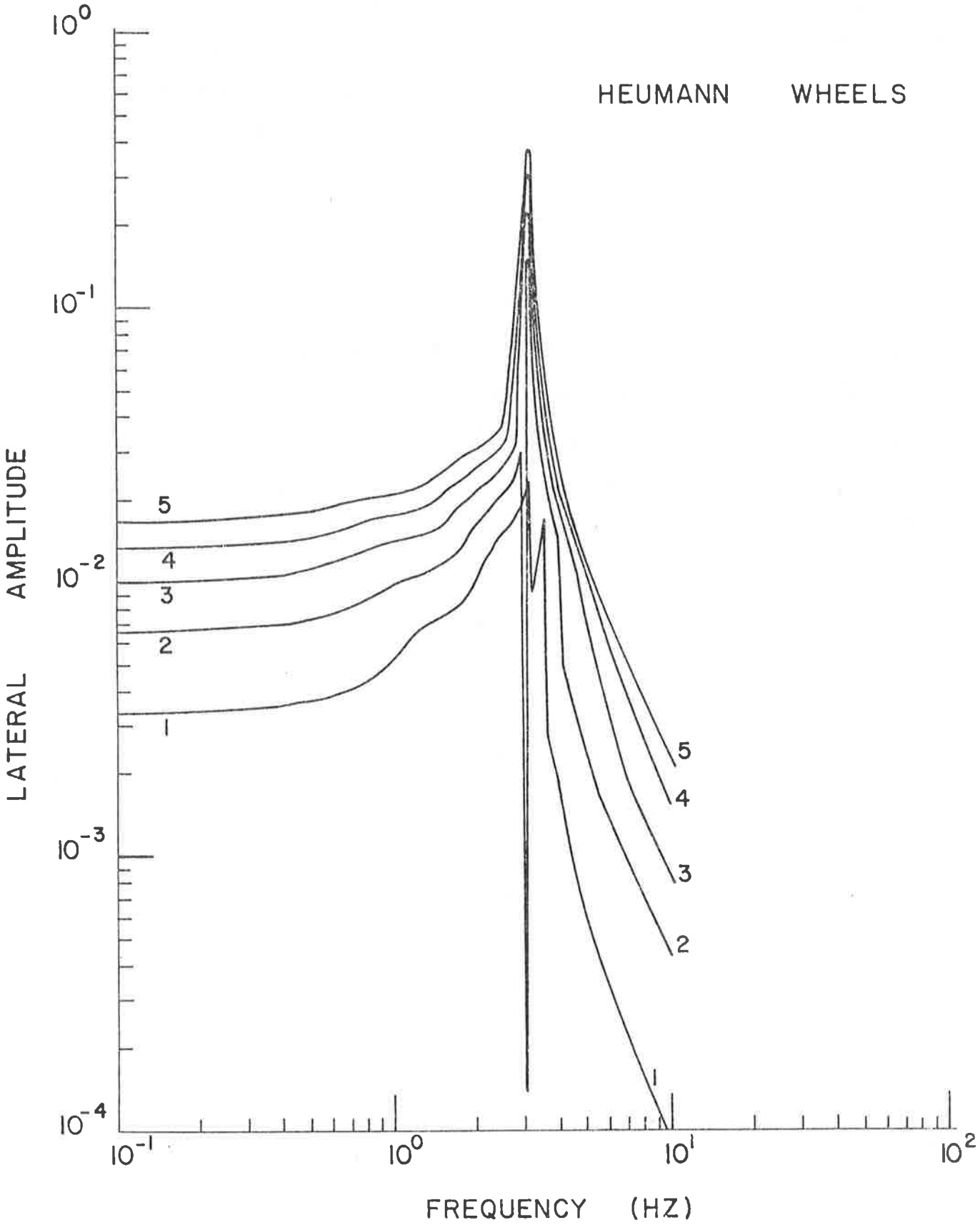

FIGURE 6-6. WHEELSET LATERAL AMPLITUDE IN RESPONSE TO SINUSOIDAL INPUTS AT DIFFERENT AMPLITUDES WITH HEUMANN WHEEL PROFILES

6.4 FREIGHT CAR EXAMPLE

The response of the nonlinear nine degree of freedom freight car model described in Section 2 to sinusoidal roadbed alignment irregularities was computed with the modified Newton-Rapheson algorithm. The baseline values for vehicle characteristics in this study are given in Table 2-3. In general, the algorithm converged more reliably for this example than it did for the single wheelset. This may be due to the greater filtering of the outputs from the nonlinear elements in this larger system. Some convergence problems were encountered, however, always near the system resonances.

The results for the freight car with new wheel profiles, shown in Figures 6-7, 6-8, 6-9 and 6-10, are similar to the wheelset results described earlier. Figures 6-7 and 6-8 illustrate the front, rear, and car body lateral amplitudes as functions of frequency when the suspension friction level is reduced to zero, the rail alignment amplitude is 0.0133 feet (0.16 inches), and the vehicle speed is 50 ft/sec. The only nonlinearities in this case, are the wheel/rail geometric functions. The dropout in the truck response at about 5 Hz is due to the filtering effect of the truck wheelbase on a response measured at the truck center. The dropout at about 1.3 Hz is another matter. It appears, based on results for other cases, that this dropout is really a jump from the upper to the lower branch of the nonlinear response curve. The actual response curve probably appears as shown in the dashed line on this illustration.

The car body response shown in Figure 6-8 appears quite similar to

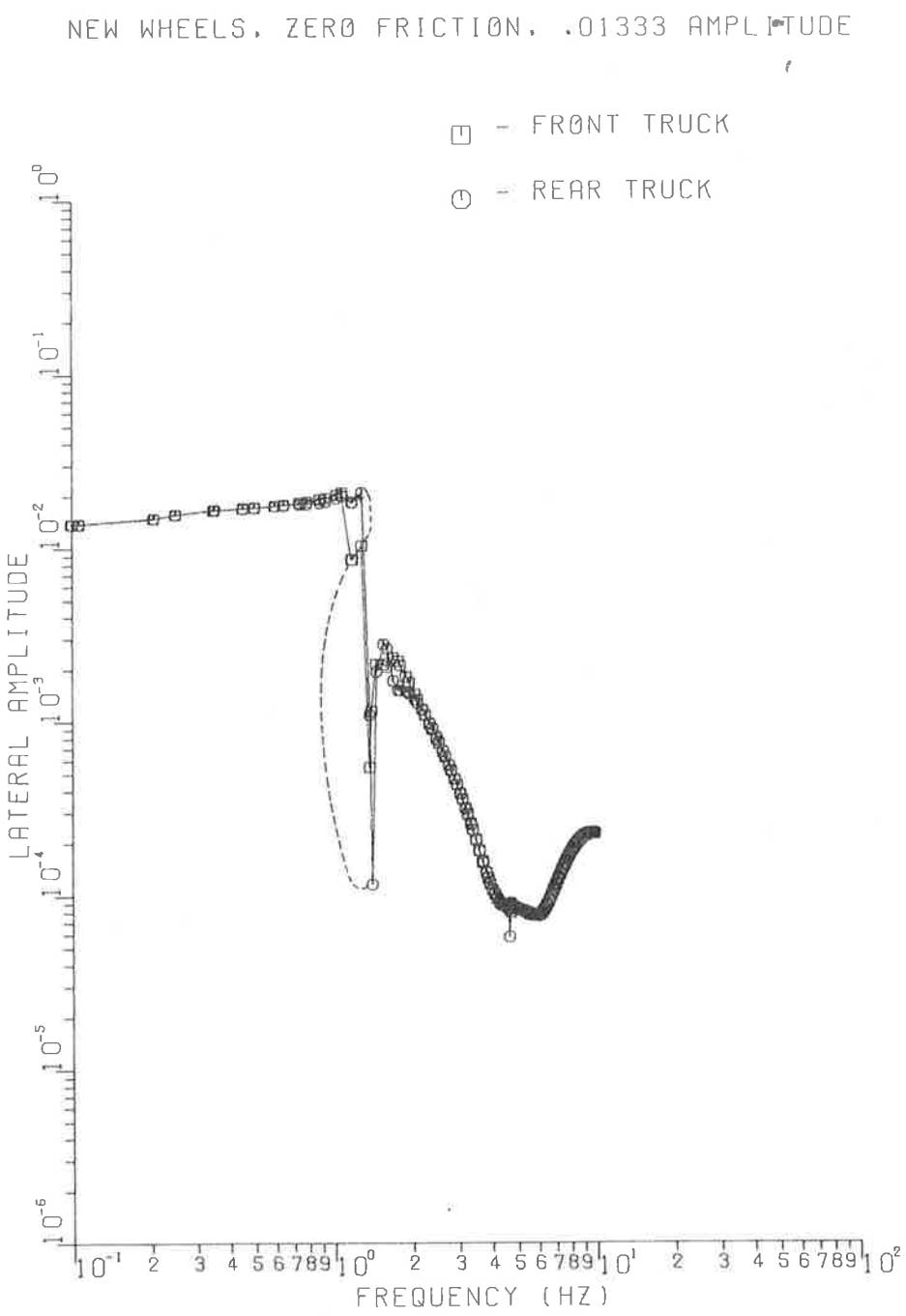

FIGURE 6-7. FREIGHT CAR TRUCK RESPONSE: NEW WHEELS WITHOUT SUSPENSION FRICTION

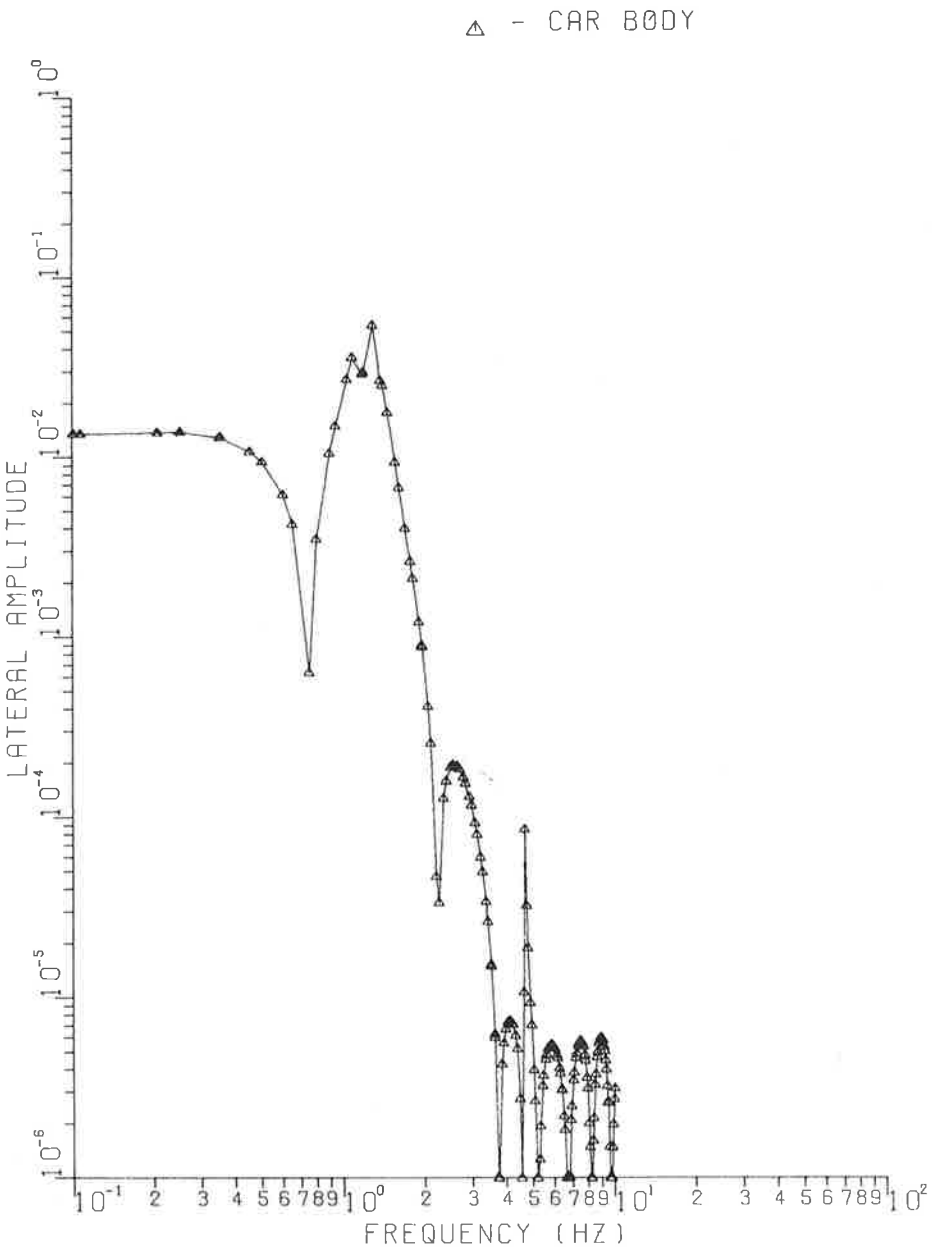

FIGURE 6-8. FREIGHT CAR BODY LATERAL RESPONSE FOR NEW WHEELS WITHOUT SUSPENSION FRICTION

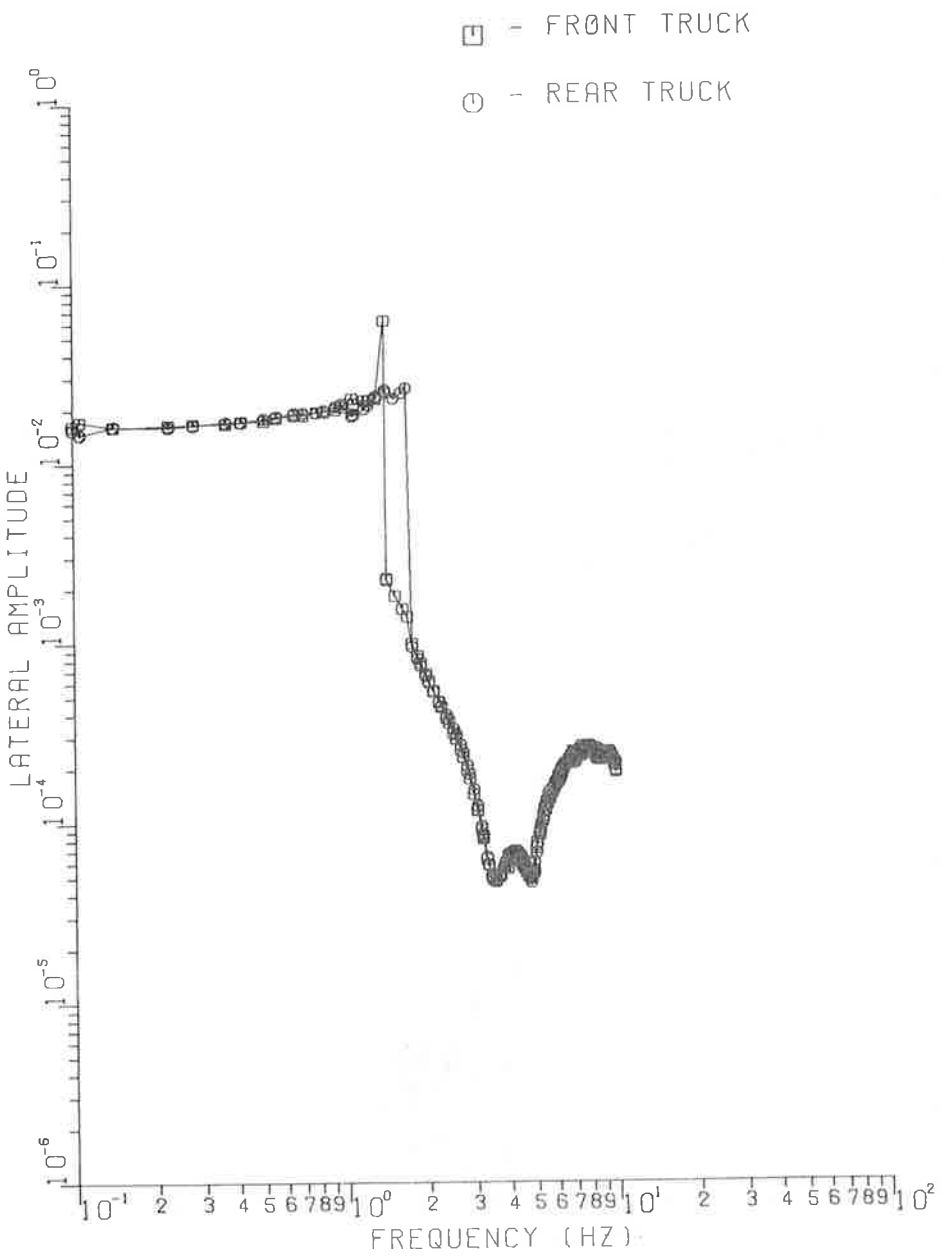

FIGURE 6-9. FREIGHT CAR TRUCK RESPONSE FOR NEW WHEELS WITH NOMINAL SUSPENSION FRICTION

those found in a linear analysis. The numerous dropouts seen in this figure are due to filtering at wavelengths corresponding to twice the truck center distance and its multiples. The first resonance at about 2 Hz corresponds to one of the lateral/roll modes of the car body on the truck suspension.

The freight car response at the same speed and alignment amplitude with nominal values for the friction in the suspension is shown in Figures 6-9 and 6-10. The truck response, shown in Figure 6-9, differs from the case without friction in that the jump behavior near 1.5 Hz is more evident. Keep in mind that the algorithm does not necessarily seek the most physically realizable branch of the response curve at each frequency. Consequently the jumps in the calculations from one branch to another may not occur at the same frequency that would be seen for the actual vehicle. For example, the response might continue on the upper branch beyond the frequencies shown in this figure.

The car body lateral response shown in Figure 6-11 differs from the response without friction in that jumps are quite evident at about 1.4 and 2.0 Hz, and the response at high frequencies, above 4 Hz, is nearly a couple of orders of magnitudes higher. The latter behavior is to be expected. Increased frequency increases the high frequency transmissibility. The two jumps correspond identically to the jumps in the response of the front and rear truck. A close inspection of the truck and car body response reveals that with, the nominal friction in the suspension, the car body follows the trucks nearly identically except for the dropouts

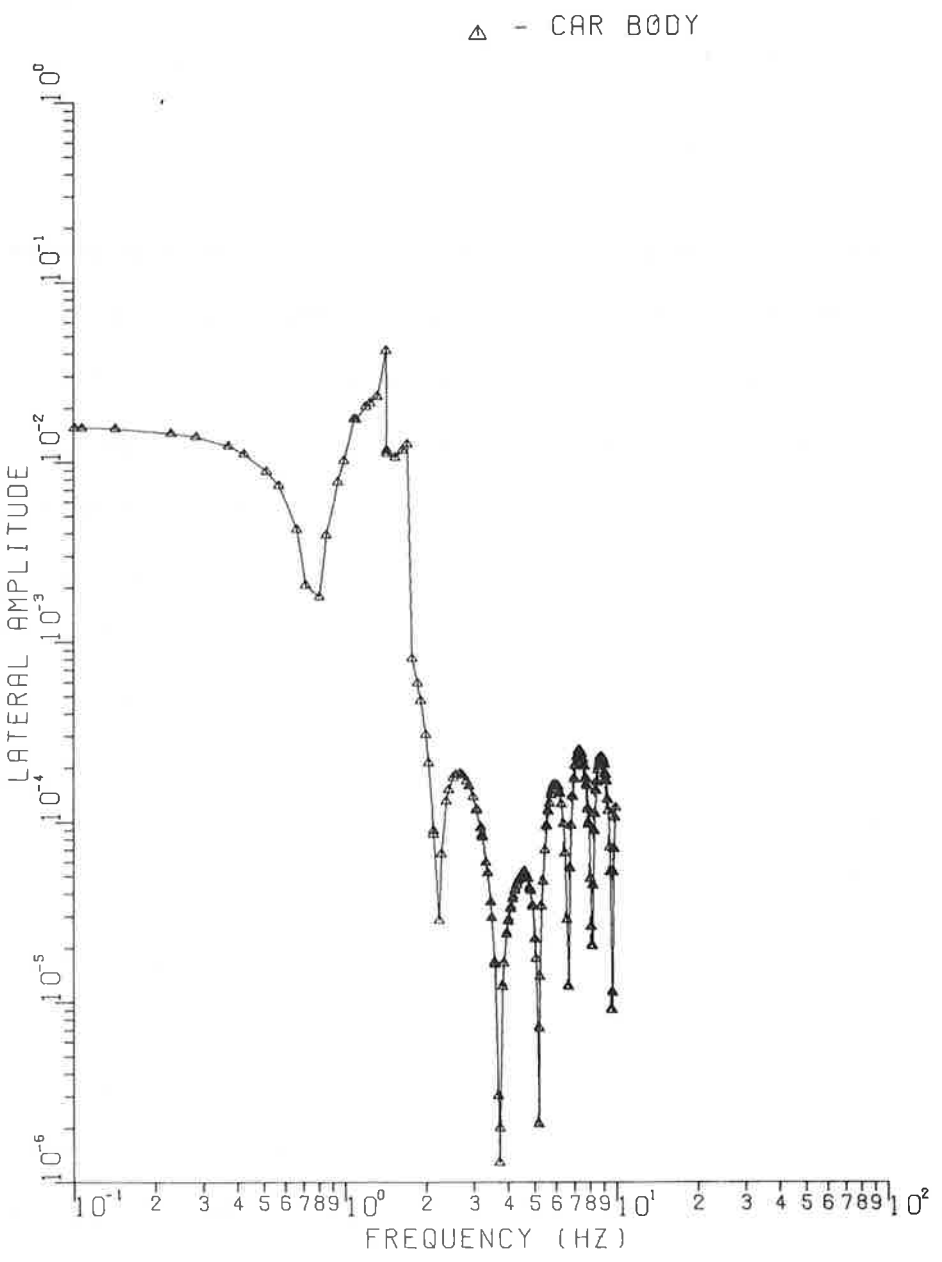

FIGURE 6-10. FREIGHT CAR BODY LATERAL RESPONSE FOR NEW WHEELS WITH NOMINAL SUSPENSION FRICTION

due to geometric filtering.

Results computed for smaller amplitudes showed, as one would expect, less tendency to jump. The truck response to an input amplitude of 0.00667 feet, for example, dropped off smoothly and continuously from about 0.7 Hz.

The freight car response to sinusoidal alignment inputs when the wheels have a Heumann profile is shown in Figures 6-11 and 6-12. This response, computed for the vehicle with nominal friction in the suspension and an alignment amplitude of 0.00667 feet (0.080 inches), is similar to the response computed for the single wheelset with Heumann wheel profiles. The peak frequency here is somewhat lower than that for the single wheelset, due to differences in the vehicle characteristics. However, jump resonance is evident here that did not show up in the particular cases studied for the single wheelset. As expected, the track response with Heumann profiles remains flat to a higher frequency than with new wheels, due to the fact that the kinematic mode has a higher frequency with the Heumann profile. Interestingly, the high frequency response for the two cases is nearly identical.

6.5 SUMMARY

The computational feasibility of the quasi-linearization method for determining nonlinear rail car response has been demonstrated. However, additional work is needed to improve its reliability when the vehicle contains hard nonlinearities. Methods that warrant investigation for

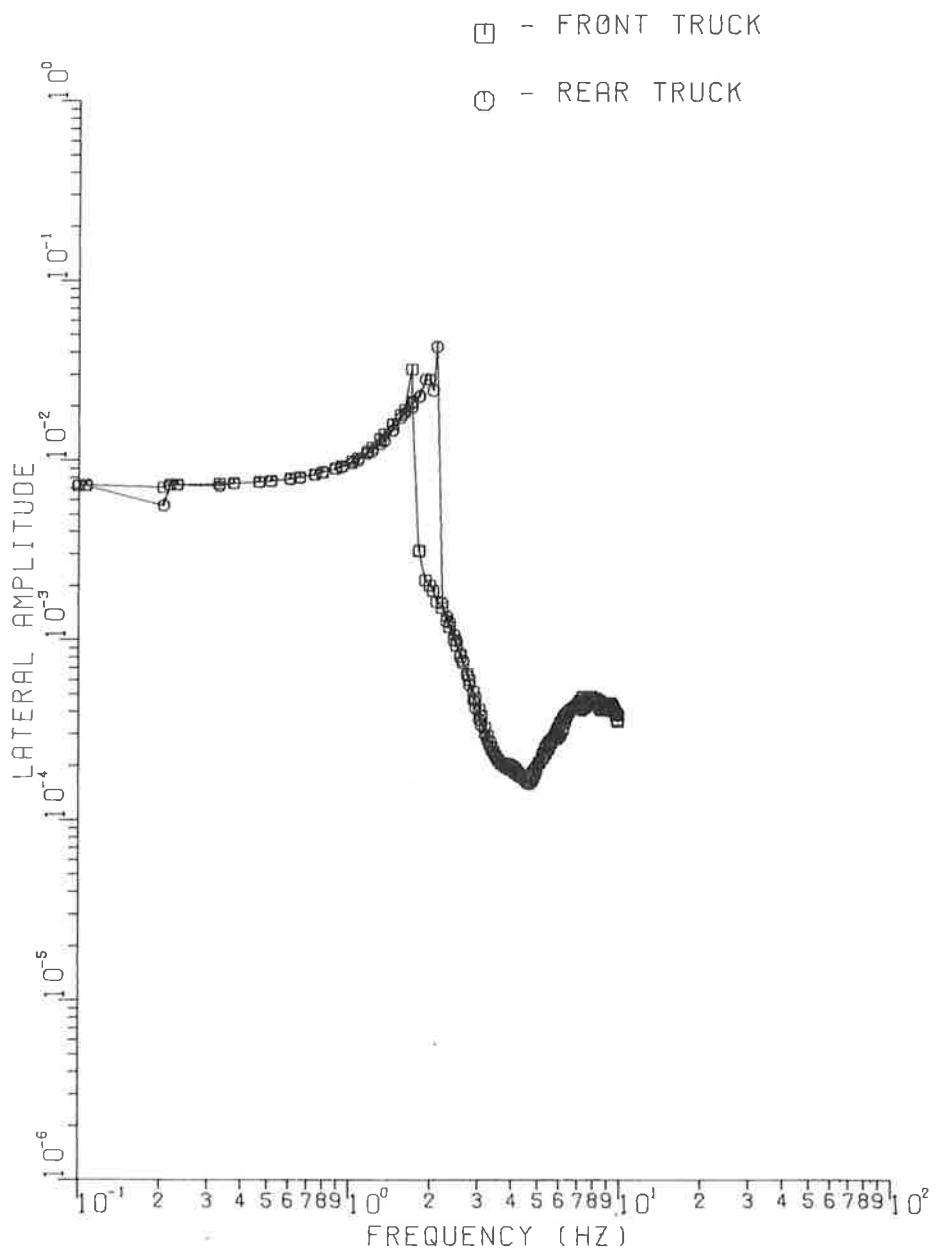

FIGURE 6-11. FREIGHT CAR TRUCK RESPONSE FOR HEUMANN WHEELS WITH NOMINAL SUSPENSION FRICTION

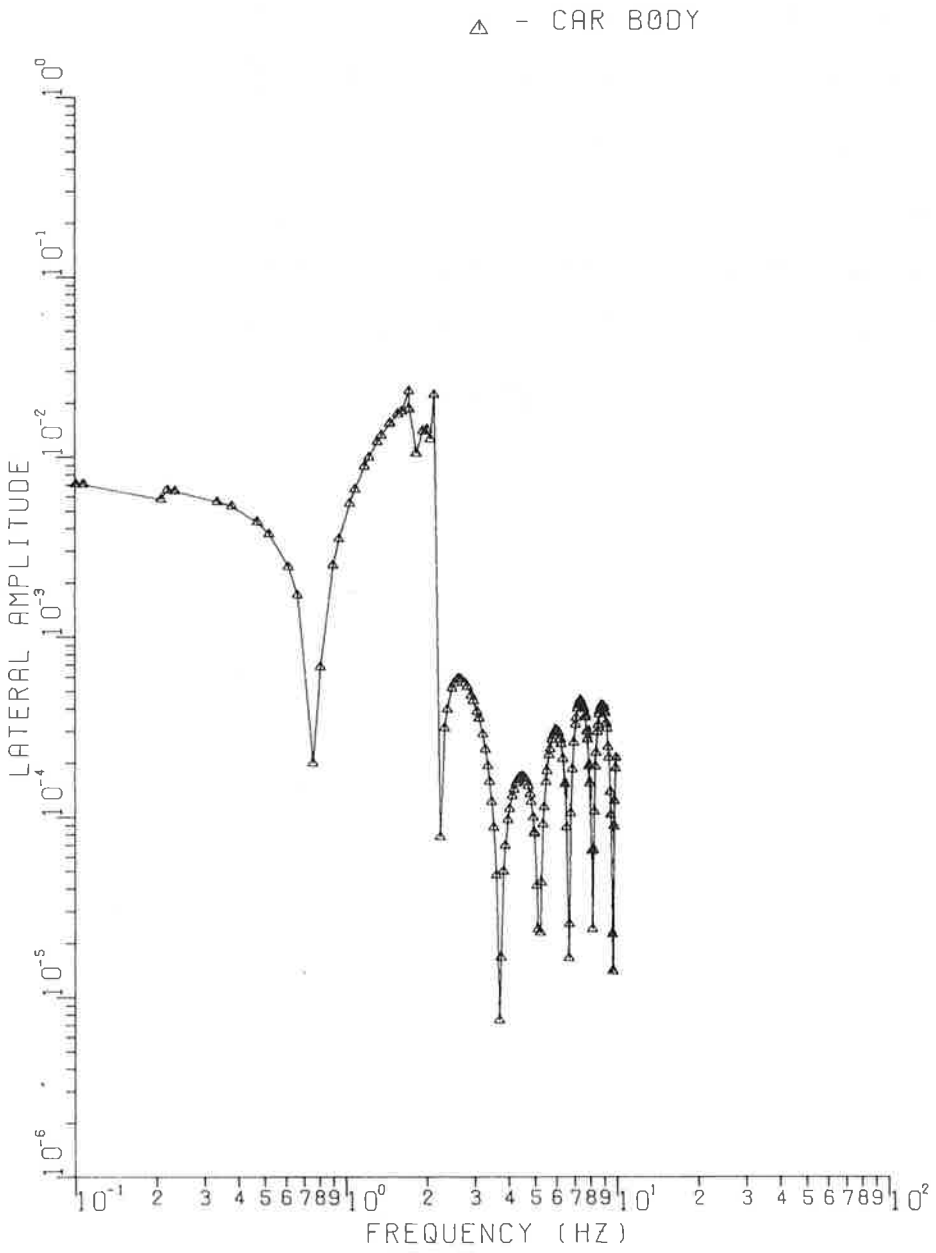

FIGURE 6-12. FREIGHT CAR BODY LATERAL RESPONSE FOR HEUMANN WHEELS WITH NOMINAL SUSPENSION FRICTION

this application include the many optimization search routines, the false position method, and an improved Newton-Rapheson approximation that includes cross-derivatives of the search variables. As noted in Section 3, the S-roots algorithm has been used with success for the freight car rock and roll problem.

The example results calculated here illustrate the jump resonance phenomena characteristic of certain nonlinear systems. These jumps might account for the bursts of activity often seen in rail car test data.

7. ALGORITHMS FOR FORCED RANDOM RESPONSE

7.1 INTRODUCTION

Chapter 3 discussed the use of statistical describing functions to predict the response of a nonlinear system subject to Gaussian random inputs. Equation (3-23) defines the quasi-linear gain for any memory-less single input-single output nonlinearity. Several examples of typical rail vehicle nonlinearities (deadband spring, hardening/softening spring, dry friction, parallel spring/dry friction, series spring/dry friction, and wheel/rail nonlinearities) were defined and their quasi-linearized approximation derived.

A sample example of a mass-damper-nonlinear spring subjected to Gaussian white noise was analyzed to compute the spectral density and r.m.s. value of the position variable. The r.m.s value was computed using both frequency domain and time domain methods.

Finally, in Section 3, the nonlinear wheelset subject to Gaussian random alignment inputs was analyzed by means of describing functions. Equations (3-87 to 3-89) are the quasi-linearized equations for the wheelset with nonlinear suspensions and a deadband spring to model flange contact. Equation (3-90) is a standard spectral density that is often used to model typical random alignment irregularities.

The purpose of this chapter is to illustrate how statistical describing functions can be applied to analyze a nine degree of freedom freight car subject to Gaussian random alignment irregularities.

7.2 STATISTICAL RESPONSE ALGORITHM

This section describes an algorithm that was developed to compute the statistical response of the full freight car model defined in Table 2-2. This nine degree of freedom model is described in detail in Section 2. Either the time domain or frequency domain approach could be used. However, it was decided to use the frequency domain method outlined in Section 3 becuase:

1) The size of the matrices in the time domain method are 2n x 2n where n is the number of degrees of freedom whereas the frequency domain matrices are nxn. For n=9 the difference is appreciable.

2) The alignment inputs to the 4-axle vehicle appear as time delays to the trailing wheelsets. Time delays are handled more easily in the frequency domain.

3) Most descriptions of the irregularity inputs are in experimental spectral density form. Although they can be modeled in the time domain for rational spectra they are handled easier in the frequency domain

4) The state space approach yields only the mean square values, the spectral density has to be computed separately.

5) The algorithms for frequency response and statistical response can use the same basic input-output programs if the statistical response is done in the frequency domain thus eliminating unnecessary duplication.

7.2.1 Rail Vehicle Quasi-Linear Equations

The quasi-linear equations of motion for the lateral behavior of a rail vehicle may be expressed in the following form.

$$[M]\,\ddot{\underline{y}} + [D]_{D.F.}\,\dot{\underline{y}} + [K]_{D.F.}\,\underline{y} = [B_1]_{D.F.}\,\dot{\underline{u}} + [B_2]_{D.F.}\,\underline{u} \qquad (7\text{-}1)$$

where $[D]_{D.F.}$, $[K]_{D.F.}$, $[B_1]_{D.F.}$, $[B_2]_{D.F.}$ matrices contain constants and describing function gains. The alignment input enters the equations of motion through the wheelsets. If a single car is considered there are four wheelsets and thus four inputs to be considered. The input to each trailing wheelset is just the input to the leading wheelset delayed by the time it takes for each wheelset to reach the same point

in the rail. Thus the four inputs to the rail vehicle can be expressed as:

$$\underline{u}(t) = \begin{bmatrix} u_1(t) \\ u_1(t - \tau_1) \\ u_1(t - \tau_2) \\ u_1(t - \tau_3) \end{bmatrix}$$

or using Laplace transforms with $s = j\omega$:

$$\underline{u}(s) = \begin{bmatrix} 1 \\ e^{-\tau_1 j\omega} \\ e^{-\tau_2 j\omega} \\ e^{-\tau_3 j\omega} \end{bmatrix} u_1(j\omega) \triangleq \underline{B}_3 \, u_1(j\omega) \qquad (7\text{-}2)$$

where τ_1, τ_2, τ_3 are the time delays between successive wheelsets and $\underline{u}$ is the 4x1 vector of rail alignment inputs. If we take the Laplace transform of (7-1) using (7-2):

$$\underline{y}(j\omega) = \left[[K]_{D.F.} - \omega^2[M] + j\omega[D]_{D.F.} \right]^{-1} \left[[B_2]_{D.F.} + j\omega[B_1]_{D.F.} \quad \underline{B}_3 u_1(j\omega) \right]$$

$$= \underline{H}(j\omega) \, u_1(j\omega) \qquad (7\text{-}3)$$

where $\underline{H}(j\omega)$ is the transfer function vector.

The describing function gains within $\underline{H}(j\omega)$ are functions of the rms values of the inputs to each nonlinearity. For the freight car model used there are twelve rms values that must be computed in order to determine the D.F. gains. These variables can be expressed as a linear combination of the position vector, $\underline{y}$, and the velocity vector, $\dot{\underline{y}}$, i.e.,

$$Z_i(j\omega) = [c(j\omega)]_i \, \underline{y}(j\omega), \quad i = 1, \ldots, 12 \tag{7-4}$$

where Z_i is an input to a nonlinearity and $[c(j\omega)]_i$ is a 1x9 complex vector that relates Z_i to $\underline{y}$. Using (7-3) and (7-4) yields:

$$\begin{aligned} Z_i(j\omega) &= [c]_i \, \underline{H} \, U_1(j\omega) \\ &= H_{Z_i}(j\omega) \, U_1(j\omega) . \end{aligned} \tag{7-5}$$

Thus $H_{Z_i}(j\omega)$ is the complex scalar transfer function that relates the inputs to the nonlinearities to the rail alignment input. The relationship between the output spectral density, $\phi_{Z_i}(\omega)$, and the input spectral density is:

$$\phi_{Z_i}(\omega) = |H_{Z_i}(j\omega)|^2 \, \phi_{u_1}(\omega). \tag{7-6}$$

The r.m.s. value of z_i can be found from:

$$\sigma_{Z_i} = \sqrt{\int_0^\infty \phi_{Z_i}(\omega) d\omega} . \tag{7-7}$$

A typical form for $\phi_{u_i}(\omega)$ was given by equation (3-90):

$$\phi_{u_1}(\omega) = \frac{KV}{\omega_o^2 + \omega^2} \tag{7-8}$$

where K and ω_o are determined experimentally for class 1-6 track [37].

7.2.2 Solution Procedure

The following algorithm can be used to solve for the system rms response and spectral densities:

1. Guess the values of $\sigma_{z_1}, \ldots \sigma_{z_{12}}$. i.e., those rms values that required to compute [D], [K], $[B_1]$ and $[B_2]$.

2. By computing $\underline{H}(j\omega)$ and thus $H_{z_i}(j\omega)$ over a range of frequencies, compute $\sigma_{z_1}, \ldots \sigma_{z_{12}}$ using (7-7)

3. Compare the computed values of σ_{z_i} to the guessed values, and iterate until a consistent of σ_{z_i} is obtained.

Figure 7-1 is a flow chart of this procedure.

7.3 FREIGHT CAR EXAMPLE

The procedure described above was applied to the nine degree of freedom freight car model described in Section 2. The nonlinearities included in this model are the wheel/rail contact forces (gravitational stiffness, effective conicity) of each of the four wheels as well as coulomb friction resistance to truck warp, lateral, and vertical motion. The rotation of the truck bolster relative to the car body is modeled also as dry friction.

The numerical values for the North American Freight car are given in Section 2 (Table 2-4). These values were used along with the statistical describing functions for the wheel/profile geometry (Figures 3-14, 3-15) of a new AAR wheel on a typical worn rail.

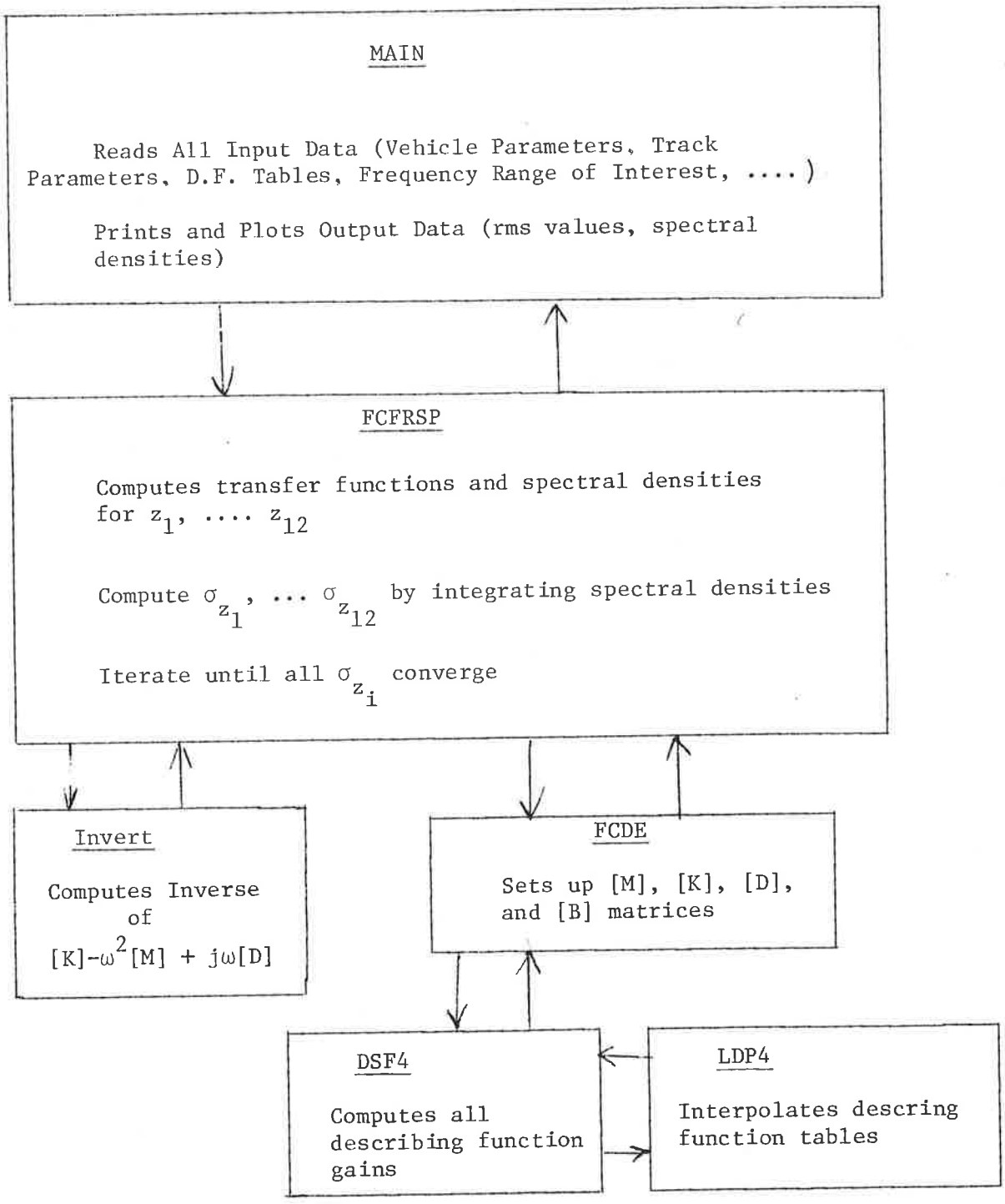

FIGURE 7-1. FLOW DIAGRAM AND SUBROUTINES USED IN STATISTICAL RESPONSE COMPUTER PROGRAM

The nine degrees of freedom for this model are:

$y_1 = y_{TF}$ = Lateral displacement of front truck

$y_2 = \theta_{TF}$ = Yaw angle of front truck

$y_3 = \theta_{WF}$ = Warp angle of front truck

$y_4 = y_{TR}$ = Lateral displacement of rear truck

$y_5 = \theta_{TR}$ = Yaw angle of rear truck

$y_6 = \theta_{WR}$ = Warp angle of rear truck

$y_7 = y_c$ = Lateral displacement of car body

$y_8 = \theta_c$ = Yaw angle of car body

$y_9 = \phi_c$ = Roll angle of car body.

In order to evaluate the describing functions for the nonlinearities we need to compute 12 r.m.s. values. They are:

$Z_1 = y_{TF} + L_1 \theta_{TF} - y_{R1}$ = Wheelset displacement

$Z_2 = y_{TF} - L_1 \theta_{TF} - y_{R2}$ = Wheelset displacement

$Z_3 = y_{TR} + L_1 \theta_{TR} - y_{R3}$ = Wheelset displacement

$Z_4 = y_{TR} + L_1 \theta_{TR} - y_{R4}$ = Wheelset displacement

$Z_5 = \dot{y}_c + h_z \dot{\phi}_c + L_z \dot{\theta}_c - \dot{y}_{TF}$ = Velocity across friction damper

$Z_6 = d\dot{\phi}_c$ = Velocity across friction damper

$Z_7 = -\dot{\theta}_{\omega F}$ = Velocity across friction damper

$Z_8 = \dot{\theta}_c - \dot{\theta}_{TF} - \dot{\theta}_{\omega F}$ = Velocity across friction damper

$Z_9 = \dot{y}_c + h_z \dot{\phi}_c - L_3 \dot{\theta}_c - \dot{y}_{TR}$ = Velocity across friction damper

$Z_{10} = d\dot{\phi}_c$ = Velocity across friction damper

$Z_{11} = -\dot{\theta}_{\omega R}$ = Velocity across friction damper

$Z_{12} = \dot{\theta}_c - \dot{\theta}_{TR} - \dot{\theta}_{\omega R}$ = Velocity across friction damper

As described in the previous section the r.m.s. values of these 12 quantities were guessed and then evaluated by equation (7-7). This process was continued until convergence was obtained, i.e.,

$(\sigma_{z_i})_{guessed} \approx (\sigma_{z_i})_{computed}$.

The following approximate track alignment spectral density inputs were used (equation 7-8):

Class 4 track: $K = 9.9 \times 10^{-5}$ rad. ft.

Class 5 track: $K = 2.47 \times 10^{-5}$ rad. ft.

Class 6 track: $K = 1.1 \times 10^{-5}$ rad. ft.

It was assumed that the vehicle was traveling at a constant forward speed of V = 50 ft/sec, and that the break frequency (ω_o in eqn. 7-8) is approximately zero. Figure 7-2 shows the lateral acceleration spectral densities for the car body c.g. for the class 4, 5, and 6 inputs. Table 7-1 shows some of the r.m.s. values of the freight car,

TABLE 7-1. NUMERICAL RESULTS FOR FREIGHT CAR R.M.S. VALUES

r.m.s. Value	Track Class 4	5	6
y_c(g's)	.09	.04	.03
Z_1(in.)	.21	.14	.12
Z_2(in.)	.80	.42	.29

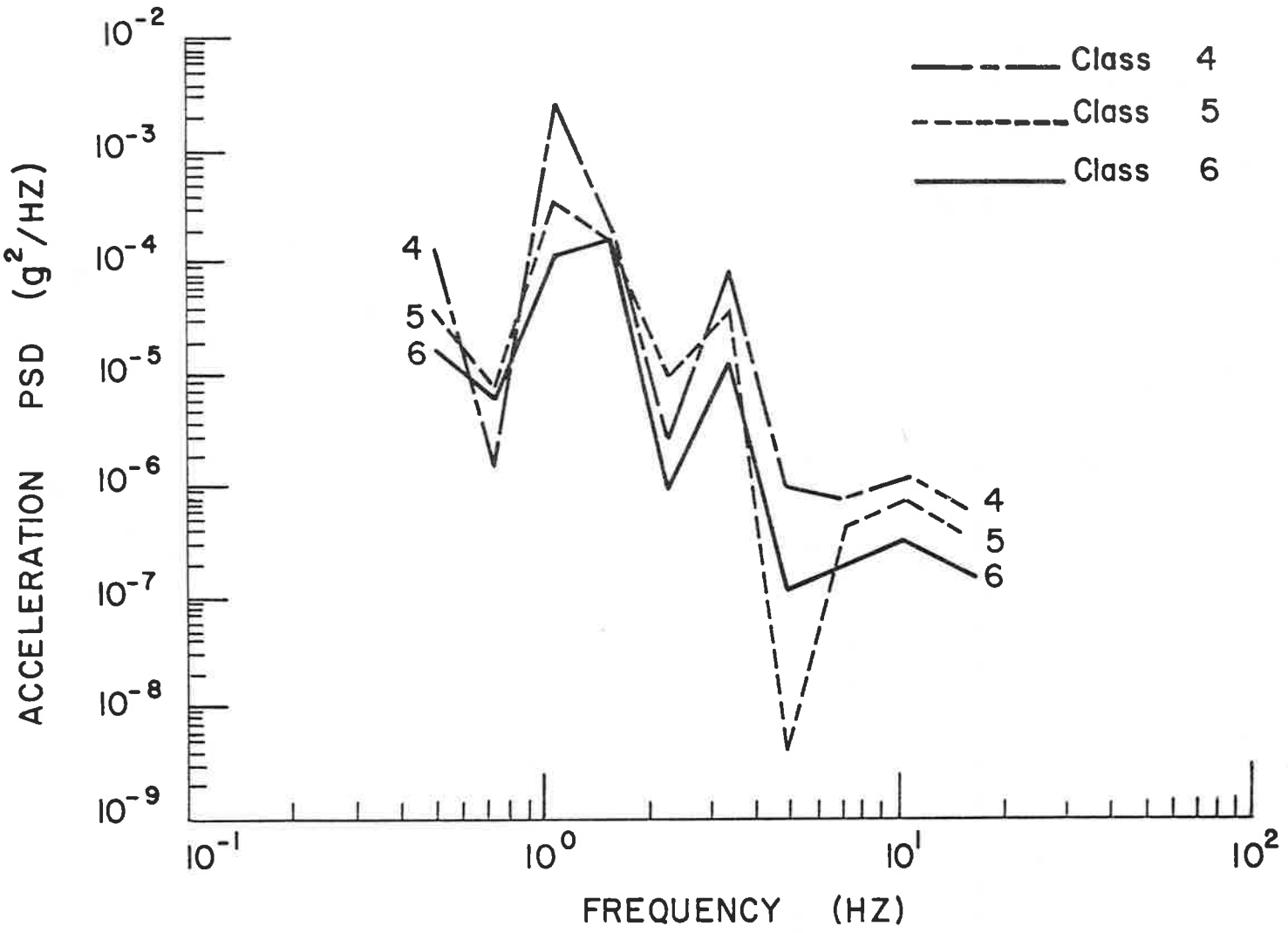

FIGURE 7-2. ACCELERATION SPECTRAL DENSITY OF FREIGHT CAR C.G. FOR CLASS 4, 5, AND 6 TRACK (ALIGNMENT INPUTS)

where Z_1 is the leading wheelset relative displacement and Z_2 is the second wheelset relative displacement. Note that in the rough track case (Class 4) that the second wheelset's r.m.s. value is extremely large. It is clear from these r.m.s. displacements that a nonlinear analysis is required.

7.4 SUMMARY

An algorithm for computing the statistical response of a nonlinear rail vehicle subject to random track inputs was demonstrated. The algorithm was applied to a nine degree of freedom freight car model and rapid convergence was obtained.

8. SUMMARY AND CONCLUSIONS

This report has demonstrated that describing function analysis can be successfully applied to rail vehicle analysis and design. The results have indicated that:

1 Quasi-linearization permits application of linear frequency domain, eigenvalue/vector, and state space methods to nonlinear rail system dynamics problems.

2 There are significant computational advantages to be gained using quasi-linearizations both for simple (e.g. wheelset) and higher order (e.g. nine D.O.F. Freight Car) dynamic models.

3 The parametric studies indicate that the wheel/rail profile and suspension nonlinearities must be included for analyzing medium to large amplitude rail vehicle performance.

4 Quasi-linearization computational algorithms for predicting rail vehicle hunting, forced sinusoidal response, and forced statistical response can be formulated and applied both for simple and higher order rail vehicle dynamic models.

Section 2 described typical rail vehicle nonlinearities including suspension, wheel/rail geometry, wheel contact forces, as well as the nonlinear differential equations of motion for a suspended wheelset and a nine degree of freedom freight car model.

Section 3 presented the fundamentals of quasi-linearization including sinusoidal input describing functions and random input describing functions. The single input describing function (SIDF) was used to calculate the critical speed (speed at which hunting occurs) of the wheelset and also to predict the forced sinusoidal response of the

wheelset. The method was extended to include all singly periodic systems. The response of a freight car to periodic cross-level inputs was computed via a multiple input describing function. Finally, the response of the nonlinear wheelset to a random alignment input was computed by use of the Gaussian statistical describing function.

Section 4 discussed two algorithms for computing the hunting behavior of rail vehicles. The first was an optimization algorithm that was presented and applied to the nonlinear wheelset. The second was the eigenvalue/eigenvector method that was presented and applied to the nine degree of freedom model.

Section 5 used these two algorithms to parametrically study the wheelset and freight car model. The optimization algorithm was used to study the influence of axle load, track gauge, suspension parameters, and wheel profile on the hunting behavior of the nonlinear wheelset. The eigenvector/eigenvalue algorithm was used to study the influence of wheel/rail profile geometry on the hunting behavior of the nine degree of freedom freight car model.

Section 6 presented a numerical algorithm using sinusoidal describing functions to predict the forced sinusoidal response of the nine degree of freedom freight car model. The algorithm was discussed and numerical results presented.

Section 7 presented a numerical algorithm using Gaussian random input describing functions to predict the spectral density and r.m.s. response of the nine degree of freedom model. The algorithm was discussed

and numerical results presented.

The quasi-linearization method appears to be a very powerful analytical technique for predicting the response of rail vehicles. In their present form the computational algorithms appear to offer significant advantages over nonlinear digital simulation for the computation of:

1) Unforced oscillatory motion, e.g. primary and secondary hunting.

2) Forced periodic motion, e.g. freight car rock and roll.

3) Forced statistical motion, e.g. response to random alignment, cross-level, and surface irregularities.

Quasi-linearization is not intended to replace nonlinear digital simulation, but rather to complement it during parametric analysis. It should also be pointed out that digital simulation is appropriate when transient dynamic phenomena, such as the response to frogs and switches, is to be predicted.

The success of these preliminary investigations points to the need for further research and development in the following areas:

1) Improve the coding of these algorithms and package them in a form that would be convenient to a wide range of industrial users.

2) Further validation and definition of the range of application of the quasi-linearization results by a direct comparison with nonlinear digital simulations of rail vehicle hunting, forced sinusoidal, and statistical response.

3) The application of parametric studies on higher order dynamic models to determine the influence of wheel profile, axle-load, gauge, and suspension parameters on general primary and secondary suspension design.

9. REFERENCES

1. Law, E.H., and Cooperrider, N.K., "Literature Survey of Railway Vehicle Dynamics Research," Journal of Dynamic Systems, Measurement and Control, Transactions of the ASME, Series G, Vol. 96, No. 2, June 1974, pp. 132-164.

2. Matsudaira, T., "Hunting Problem of High Speed Railway Vehicles with Special Reference to Bogie Design for the New Tokaido Line," Interaction Between Vehicle and Track, Proceedings of the Institution of Mechanical Engineers, London, Vol. 180, Part 3F, 1966, pp. 58-66.

3. Cooperrider, N.K., "The Hunting Behavior of Conventional Railway Trucks," Journal of Engineering for Industry, Transactions of the ASME, Series B, Vol. 94, May 1972, pp. 752-762.

4. Gilchrist, A.O., Hobbs, A.E.W., King, B.L., and Wasby, V., "The Riding of Two Particular Designs of Four Wheeled Railway Vehicles," Interaction Between Vehicle and Track, Proc. Institution of Mechanical Engineers, Vol. 180, Part 3F, 1966, p. 99-113.

5. Law, E.H., "Nonlinear Wheelset Dynamic Response to Random Rail Irregularities," Journal of Engineering for Industry, Transactions of the ASME, Series B, Vol. 96, No. 2, November 1974.

6. Sauvage, G., "Nonlinear Model for the Study of Rail Vehicle Dynamics," Proc. IUTAM Symposium, Delft, August 1975, pp. 326-344.

7. Tse, Y.H. and Martin, G.C., "User's Manual, Flexible Body Railroad Freight Car," AAR Publication, 1975.

8. Healey, M.J., "A Computer Method for Calculating Dynamic Responses of Nonlinear Flexible Rail Vehicles," Wyle Laboratories Report, 1976.

9. Weibe, D., "The Effects of Lateral Instability of High Center of Gravity Cars," Transactions of the ASME, Vol. 90-B, No. 4, November 1968, pp. 462.

10. Platin, B.E., Beaman, J.J., Hedrick, J.K. and Wormley, D.N., Computational Methods to Predict Railcar Response to Track Cross-Level Variations, Report No. FRA-OR&D-76-293, Final Report prepared for U.S. D.O.T., FRA., September 1976.

11. DePater, A.D., "The Approximate Determination of the Hunting Movement of a Railway Vehicle by Aid of the Method of Krylov and Bogoliubov," Applied Scientific Research. Section A, Vol. 10, 1961, pp. 205-228.

12. van Bommel, P., "Application of the Theory of Non-linear Vibrations on the Problem of Vehicle Motion on the Railway". "Doctoral thesis, Technical University of Delft. The Netherlands, 1964.

13. Stassen, H.G., "Random Lateral Motions of Railway Vehicles," doctoral dissertation, Technische-Hogeschool, Delft. The Netherlands, 1967.

14. Law, E.H., "Analysis of the Nonlinear Dynamics of a Railway Vehicle Wheelset," Ph.D. thesis, Department of Mechanical Engineering, University of Connecticut, Storrs, Conn., 1971.

15. Law, E.H., and Brand, R.S., "Analysis of the Nonlinear Dynamics of a Railway Vehicle Wheelset," Journal of Dynamics, Measurement, and Control, TRANS. ASME, Series G, Vol. 95, No. 1, March 1973, pp. 28-35.

16. Garg, D.P., "Describing Function Techniques for Nonlinear Analysis of the Dynamics of a Rail Vehicle Wheelset," Report No. FRA-OR&D-75-83, Final Report prepared for U.S. D.O.T., July 1975.

17. Abbott, P.W., Morosow, G., and Macpherson, J., "Track-Train Dynamics," SAE Paper 751058, November 1975.

18. "70 Ton Truck Component Data Physical Restraints, Mechanical Properties Damping Characteristics," Truck-Train Dynamics Harmonic Roll Series, Vol. 2, 1974.

19. Cooperrider, N.K., Law, E.H., Hull, R., Kadala, P.S. and Tuten, J.M., "Analytical and Experimental Determination of Nonlinear Wheel/Rail Geometric Constraints," Report No. FRA-OR&D-76-244/PB252290), December 1975.

20. Kalker, J.J., "Simplified Theory of Rolling Contact," Delft, Progress Report, Series C: Mechanical and Aeronautical and Shipbuilding, 1973, pp. 1010.

21. Kalker, J.J., "On the Rolling Contact of Two Elastic Bodies in the Presence of Dry Friction," doctoral dissertation, Technische Hogeschool, Delft, The Netherlands, 1967.

22. Vermeulen, P.J. and Johnson, K.L., "Contact of Nonspherical Elastic Bodies Transmitting, Tangential Forces," Transactions of the ASME, June 1964, pp. 338-340.

23. Hadden, J.A., "The Effects of Truck Design and Component Flexibility on the Lateral Stability of Railway Freight Vehicles," M.S. Thesis, Clemson University, December 1976.

24. Law, E.H., Hadden, J.A. and Cooperrider, N.K., "General Models for Lateral Stability Analyses of Railway Freight Vehicles," FRA-OR&D-77-36 (PB 272371), June 1977.

25. Gelb, A., and VanderVelde, W.E., Multiple-Input Describing Functions and Nonlinear System Design, McGraw-Hill, New York, 1968.

26. Graham, D. and McRuer, D., Analysis of Nonlinear Control Systems, Dover Publications, Inc., New York 1961.

27. Atherton, D.P., Nonlinear Control Engineering, Van Nostrand Reinhold, London, 1975.

28. Hsu, J.C. and Meyer, A.U., Modern Control Principles and Applications, McGraw-Hill, New York 1968.

29. Corbin, J. and Kaufman, W.M., "Classifying Track by Power Spectral Density," Mechanics of Transportation Suspension Systems, AMD-Vol. 15, 1975.

30. Kryloff, N. and Bogoliubov, N., Introduction to Non-Linear Mechanics, (Translations by S. Lefschetz) Princeton University Press, 1947.

31. Bogoliubov, N., and Mitropolsky, Y.A., Asymptotic Methods in the Theory of Nonlinear Oscillations, Gordon and Breach, N.Y., 1961.

32. Kocenburger, R.J., "Limiting in Feedback Control Systems," Transactions of the AIEE, Part II, App. Ind., Vol. 22, July 1953, pp. 180-194.

33. Goldfarb, L.C., "On Some Nonlinear Phenomena in Regulatory Systems," Frequency Response, The Macmillan Company, New York, 1956.

34. Meyer, A.U., "Nonlinear System Fundamentals," presented at 1976, ASME Winter Annual Meeting, New York, December 5-10, 1976.

35. Cooperrider, N.K., Hedrick, J.K., Law, E.H., and Malstrom, C., "The Application of Quasi-linearization Techniques to the Prediction of Nonlinear Railway Vehicle Response," Vehicle System Dynamics, Vol. 4, No. 2-3, July 1975, pp. 141-148.

36. Hannebrink, D.N., Lee, H.S.H., Weinstock, H. and Hedrick, J.K., "Influence of Axle Load, Track Gauge, and Wheel Profile on Rail-Vehicle Hunting," Transactions of the ASME, Journal of Engineering for Industry, Series B, Vol. 99, No. 1, February 1977, pp. 186-195.

37. Cooperrider, N.K., Cox, J.J. and Hedrick, J.K., "Lateral Dynamics Optimization of a Conventional Railcar," Transactions of the ASME Journal of Dynamic Systems, Measurement, and Control, Vol. 97, Series G, No. 3, September 1975.

38. Tse, Y.H., "Methods of Analysis for the Dynamic Behavior of a Flexible Body Railroad Freight Car," M.S. Thesis, Department of Mechanical Engineering, Illinois Institute of Technology, Chicago, 1974.

39. Rabinowitz, P., Numerical Methods for Nonlinear Algebraic Equations, Gordon and Breach Pub., London, 1970, pp. 115.

40. Booton, R.C., "Nonlinear Control Systems with Random Inputs," IRE Trans. Circuit Theory, Vol. CT-1, No. 1, March 1954, pp. 9-17.

41. West, J.C. and Nikiforuk, P.N., "The Response of Remote-Position Control Systems with Hard Spring Nonlinear Characteristics to Step Function and Random Inputs; Proc. IEE, Vol. B-102, No. 5, October 1954, pp. 575-593.

42. Kazakov, I.Y., "Approximate Probabilistic Analysis of the Operational Accuracy of Essentially Nonlinear Automatic Systematics," Automation and Remote Control, Vol. 17, No. 5, 1956, pp. 385-409.

43. Smith, H.W., "The Applicability of Quasi-linear Methods to Nonlinear Feedback Systems with Random Inputs," Proc. Second IFAC Congr.,Basel, Switzerland, August 1963.

44. Sawaragi, Y., Sugai, N., and Sunahara, Y., Statistical Studies on Nonlinear Control Systems, Nipon Printing and Publishing Co., LTD., OSAKA, Japan, 1962.

45. Crandall, S.H., "On Statistical Linearization for Nonlinear Oscillators," Department of Mechanical Engineering, M.I.T., Cambridge, Massachusetts 1976.

46. Krishna, M.B., and Hullender, D., "An Alternate Approach for Using the Random Input Describing Function in Modeling Random Processes," presented at the ASME Winter Annual Meeting, New York, 1976.

47. Taylor, J.H., Price, C.F., Siegel, J., and Gelb, A., "Statistical Analysis of Nonlinear Stochastic Systems via Cadet," presented at the ASME Winter Annual Meeting, New York, 1976.

48. Gelb, A., Editor, Applied Optimal Estimation, the M.I.T. Press, Cambridge, Mass., 1974.

49. Hyynh, H.T., Moreau, N., and Paquet, J.G., "Comparative Studies of Methods of Non-Linear Systems Undergoing Hazardous Entries". Ann. Telecommun. (France), Vol. 27, No. 11-12, November-December 1974, pp. 518-525.

50. Kuester, J. and Mize, J., Optimization Techniques with Fortran, McGraw-Hill, New York, 1973.

51. Hannebrink, D.N., "The Application of Describing Functions to the Nonlinear Stability Analysis of a Railcar Wheelset," M.S. Thesis, Massachusetts Institute of Technology, Cambridge, Mass., 02139, May 1976.

APPENDIX

REPORT OF INVENTIONS

The material presented in this report has been thoroughly reviewed and does not contain patentable or copyrightable material. The innovations reported in this document are of both an analytical and a computational nature. The analytical innovations are described in Sections 2 and 3 and concern the modeling of important rail vehicle nonlinearities and their describing function representations.

The computational innovations are described in Sections 4, 5, 6, and 7 and concern numerical algorithms that are used to compute limit cycles, forced sinusoidal, and forced statistical response of nonlinear rail vehicle systems. These algorithms can be used to analyze and design rail vehicles including the effects of significant nonlinearities.